THE
PHYSICAL REVIEW

A journal of experimental and theoretical physics established by E. L. Nichols in 1893

SECOND SERIES, VOL. 74, No. 8 OCTOBER 15, 1948

Theory of Oscillating Absorber in a Chain Reactor*

A. M. WEINBERG AND H. C. SCHWEINLER
*Oak Ridge National Laboratory, Oak Ridge, Tennessee***

(Received July 9, 1948)

The response of a critical chain-reacting pile to a thermal neutron absorber which is oscillated back and forth inside the pile is calculated. It is shown that at frequencies which are low compared to the periods of delayed neutrons, the neutron intensity in the pile rises and falls as a whole, the shape of the stationary distribution always being maintained. As the frequency of the oscillation increases, the nature of the neutron response changes from the over-all fluctuation characteristic at low frequency to a propagated and attenuated neutron wave which emanates from the neighborhood of the oscillator. These neutron waves set up at high frequencies are entirely analogous to the familiar thermal waves which are established in Angstrom's method of measuring thermal conductivities. It is pointed out that since the pile equations are linear, the amplitude of the oscillating response is proportional to the total neutron absorption of the oscillated absorber, and therefore a known and an unknown absorber can be compared by observing the magnitude of the neutron oscillations caused by each.

1. INTRODUCTION

IF a chain-reacting pile is modulated, i.e., if its reactivity is subjected to periodic fluctuations about critical, the neutron flux in the reactor will undergo oscillations of the same period. Qualitatively this is evident since the flux waxes while the reactor is super-critical and wanes while the reactor is sub-critical.

If the reactivity modulation is effected by periodically moving a neutron absorber between regions of high and low flux, then, since the pile equations are linear, the amplitude of the resulting neutron fluctuation must be proportional to the magnitude of the absorber. Thus a known absorber can be compared with an unknown by measuring the amplitudes of the neutron responses when each of the absorbers is oscillated in the same way, inside the pile.

In addition to reducing the reactivity of the pile, a localized absorber introduced into a chain reactor also lowers the neutron flux in its immediate vicinity. If the absorber is moved back and forth, this local neutron depression will move with the absorber, and the response in a nearby neutron-sensitive chamber will fluctuate with the same frequency as that of the oscillating absorber. This local response, like the over-all response which arose from the reactivity modulation, is also proportional to the size of the absorber, and hence can also be used to compare two neutron absorbers. Both methods have been used for neutron absorption cross-section measurements, the reactivity response by A. Langs-

* Declassified June 7, 1948.
** Work performed under Contract No. W35-058, eng. 71, with the Atomic Energy Commission, and the information contained herein will appear in the National Nuclear Energy Series as a contribution of the Oak Ridge National Laboratory.

dorf[1] and the local response by Pomerance, Hoover *et al.*[2]

The character of the response to an oscillating absorber depends on the frequency of the oscillation. At low frequencies the reactivity change predominates and the pile response is adiabatic: the neutron intensity rises and falls, always keeping essentially the shape it had before the absorber was oscillated. At high frequencies the positive and negative reactivity changes tend to cancel and what remains is the local depression. This depression in neutron intensity is propagated away from the absorber as a damped wave which is reflected at the pile boundary. The wave-length, velocity, and attenuation length of the waves depend on the properties of the chain-reacting medium. These "neutron waves" are analogous to the thermal waves set up in a conducting medium in which is placed a localized heat source whose strength varies periodically.

In the present paper we calculate the response of a pile to a periodically varying absorber. In particular we trace how the neutron response changes from an over-all fluctuation at low frequencies to a propagated wave which appears at high frequencies. The considerations reported here are a generalization of results first obtained by Cahn, Monk, and Weinberg[3] (for a reactor in which slowing down was ignored) and then extended to age theory slowing down by Wigner.[4] The method used bears considerable resemblance to that employed by Placzek and Volkoff[5] in discussing the response of a sub-critical pile to a stationary neutron source.

2. THE PILE EQUATION

We consider a non-reflected, homogeneous, uniform chain-reacting pile which is just critical. We suppose that the extrapolation distance is independent of the energy so that the density of neutrons of all energies extrapolates to zero at the same distance beyond the pile boundary; this assumption simplifies the analysis enormously without introducing any important error so long as the pile is large compared to the extrapolation distance. The pile equation, which describes the slowing down, diffusion, and multiplication of neutrons, is

$$D\Delta n_0-\sigma_p n_0+\frac{k}{p}(1-\beta)\sigma_p\int_\infty n_0(\mathbf{r}')P(|\mathbf{r}-\mathbf{r}'|)d\mathbf{r}'$$

$$+\sum_j\int_\infty\frac{c_{j0}(\mathbf{r}')}{\tau_j}P_j(|\mathbf{r}-\mathbf{r}'|)d\mathbf{r}'=0, \quad (1a)$$

$$(k/p)\beta_j\sigma_p n_0-(c_{j0}/\tau_j)=0, \quad (1b)$$

where

$n_0(\mathbf{r})$ = thermal neutron flux at $\mathbf{r}$, i.e., number of neutrons/cc × average velocity, v.

D = thermal neutron diffusion coefficient ÷ v.

σ_p = thermal neutron absorption cross section of pile per cc.

k = multiplication constant; i.e., average number of neutrons produced per neutron absorbed.

p = resonance escape probability; k/p is the average number of neutrons produced per *slow* neutron absorbed.

β_j = fraction of neutrons produced per fission which are delayed with a mean life τ_j. Each delayed neutron comes from a delayed neutron emitting fission fragment.

$\beta=\Sigma\beta_j$.

$P(|\mathbf{r}-\mathbf{r}'|)$ = the prompt neutron slowing down function, i.e., number of neutrons becoming slow at $\mathbf{r}'$ due to a prompt fission neutron produced at $\mathbf{r}$ in an infinite chain-reacting medium having the same slowing down and resonance absorption characteristics as the actual pile. Since the resonance escape probability is p,

$$\int_\infty P(|\mathbf{r}-\mathbf{r}'|)d\mathbf{r}'=p.$$

$c_{j0}(\mathbf{r})$ = density of fission fragment nuclei at $\mathbf{r}$ which will emit a delayed neutron with mean life τ_j.

$P_j(|\mathbf{r}-\mathbf{r}'|)$ = jth delayed neutron slowing-down function, i.e., number of neutrons becoming slow at $\mathbf{r}'$ due to a jth-type delayed fission neutron produced at $\mathbf{r}$ in an infinite chain-reacting medium. $P_j(|\mathbf{r}-\mathbf{r}'|)$ may differ from $P(|\mathbf{r}-\mathbf{r}'|)$ because the energy of the delayed and prompt neutrons may not be the same.

In Eq. (1a), $D\Delta n_0$ is the net diffusion flow of neutrons into a cubic centimeter, $\sigma_p n_0$ is the number of thermal neutrons absorbed per cc per second, while the two integrals represent the number of neutrons which become thermal per cc per second at $\mathbf{r}$ after birth as prompt or delayed fission neutrons, respectively.

[1] Alexander Langsdorf, Jr., Bull. Am. Phys. Soc. **23**, No. 3, 20 (1948).

[2] H. Pomerance and J. I. Hoover, Phys. Rev. **73**, 1265 (1948); also J. I. Hoover, W. H. Jordan, C. D. Moak, L. A. Pardue, H. Pomerance, J. Strong, and E. O. Wollan, Phys. Rev. **73**, 1259 (1948).

[3] A. Cahn, Jr., A. T. Monk, and A. M. Weinberg, Metallurgical Project Report, CP-2907.

[4] E. P. Wigner, Metallurgical Project Report, CP-3066.

[5] G. Placzek and G. Volkoff, Can. J. Research **A25**, 276 (1947).

The integrals in (1a), as indicated by subscripts ∞, are to be extended over all space. At first sight this would appear incorrect since the reactor is finite. However, as is well known in pile theory, $n_0(\mathbf{r})$, and therefore c_{j0}, satisfy

$$\Delta n_0(\mathbf{r})+\kappa_0^2 n_0(\mathbf{r})=0, \tag{2}$$

κ_0^2 being a constant; hence, as will be shown below, the integrals

$$q(\mathbf{r})=(k/p)(1-\beta)\sigma_p\int_\infty n_0(\mathbf{r}')P(|\mathbf{r}-\mathbf{r}'|)d\mathbf{r}', \tag{3}$$

and

$$q_j(\mathbf{r})=\int_\infty \frac{c_{j0}(\mathbf{r}')}{\tau_j}P_j(|\mathbf{r}-\mathbf{r}'|)d\mathbf{r}', \tag{4}$$

which represent the number of prompt and delayed neutrons becoming slow at $\mathbf{r}$, satisfy the same boundary conditions as $n_0(\mathbf{r})$. Thus the slow neutron production density $q(\mathbf{r})$ [and $q_j(\mathbf{r})$] is a linear superposition of infinite system slowing-down functions which satisfies the same boundary conditions as the thermal neutron density. Since we assume the density of neutrons of all energies extrapolates to zero at the same distance beyond the pile boundary, $q(\mathbf{r})$ and $q_j(\mathbf{r})$ are the proper production densities for a finite pile, i.e., it is correct to extend the integrals in (1) over all space.

The physical meaning of the preceding remarks, which are fundamental in pile theory, is the following:

The neutron distribution in a finite pile (in which the extrapolation distance is energy independent) can be calculated by extending the pile to infinity and finding the asymptotic neutron distribution in this infinite system. This solution oscillates, positive neutron densities alternating with negative ones *ad infinitum*. The positive and negative densities are so distributed that on the extrapolated pile boundary their superposed effect vanishes. In particular, the production density $q(\mathbf{r})$ in a finite pile is the same as that in an infinite system in which the neutron density $n(\mathbf{r})$ is the analytic continuation of the density appropriate to the finite system.

The regions in which the neutron density is negative may be called "negative" piles. The positive and negative piles constitute a system of images of the sort commonly used to solve ordinary boundary-value problems. In problems ordinarily encountered, which lead to non-homogeneous differential equations, e.g., the potential of a pre-assigned source distribution, the system of images can be constructed easily only if the bounding surface has sufficient symmetry. In the pile case, however, even if the boundary is arbitrarily shaped, the proper intensity and distribution of the image piles are automatically given by the analytic continuation of the asymptotic neutron distribution defined by (2) outside the pile.

It remains to show that q, q_j, and n_0 all satisfy the same boundary conditions (actually it will be shown that these functions are everywhere proportional). We represent $n_0(\mathbf{r})$ as a Fourier integral:

$$n_0(\mathbf{r})=\int_\infty A(\boldsymbol{\alpha})e^{i\boldsymbol{\alpha}\cdot\mathbf{r}}d\boldsymbol{\alpha},$$

where $\boldsymbol{\alpha}=\alpha_x\mathbf{i}+\alpha_y\mathbf{j}+\alpha_z\mathbf{k}$ is a vector integration variable. Since $n_0(\mathbf{r})$ satisfies (2), the function $A(\boldsymbol{\alpha})$ must vanish unless $\alpha^2=\kappa_0^2$; i.e., it is proportional to a δ-function on the surface of a sphere of radius κ_0. Now

$$\begin{aligned}q(\mathbf{r})&=\frac{k}{p}(1-\beta)\sigma_p\int_\infty n_0(\mathbf{r}')P(|\mathbf{r}-\mathbf{r}'|)d\mathbf{r}'\\&=\frac{k}{p}(1-\beta)\sigma_p\int_\infty\int_\infty A(\boldsymbol{\alpha})e^{i\boldsymbol{\alpha}\cdot\mathbf{r}'}P(|\mathbf{r}-\mathbf{r}'|)d\mathbf{r}'d\boldsymbol{\alpha}\\&=\frac{k}{p}(1-\beta)\sigma_p\int_\infty A(\boldsymbol{\alpha})e^{i\boldsymbol{\alpha}\cdot\mathbf{r}}d\boldsymbol{\alpha}\\&\qquad\times\int_\infty e^{i\boldsymbol{\alpha}\cdot(\mathbf{r}'-\mathbf{r})}P(|\mathbf{r}-\mathbf{r}'|)d(\mathbf{r}'-\mathbf{r}),\end{aligned}$$

or, since $A(\boldsymbol{\alpha})$ is a delta-function, i.e., since $A(\boldsymbol{\alpha})=0$ for $\alpha^2\neq\kappa_0^2$, $A(\boldsymbol{\alpha})=\infty$ for $\alpha^2=\kappa_0^2$,

$$q(\mathbf{r})=\frac{k}{p}(1-\beta)\sigma_p\bar{P}(\kappa_0^2)n_0(\mathbf{r}), \tag{5}$$

where $\bar{P}(\kappa_0^2)$ is the three-dimensional Fourier transform of $P(|\mathbf{r}-\mathbf{r}'|)$:

$$\bar{P}(\kappa_0^2)=4\pi\int_0^\infty P(r)\frac{\sin\kappa_0 r}{\kappa_0 r}r^2dr. \tag{6}$$

An exactly similar argument shows that q_j is also proportional to $n_0(\mathbf{r})$:

$$q_j(\mathbf{r})=\frac{c_{j0}(\mathbf{r})}{\tau_j}\bar{P}_j(\kappa_0^2)=\frac{k}{p}\sigma_p\beta_j n_0(\mathbf{r})\bar{P}_j(\kappa_0^2), \quad (7)$$

where $\bar{P}_j(\kappa_0^2)$ is the Fourier transform of the jth delayed neutron slowing-down function.

The characteristic equation which κ_0 satisfies is found by substituting the expressions for $q(\mathbf{r})$ and $q_j(\mathbf{r})$ from (5) and (7) into (1). The result is

$$\frac{k}{p}\bar{P}_{Aw}(\kappa_0^2)-L^2\kappa_0^2-1=0, \quad (8)$$

where

$$\bar{P}_{Aw}(\kappa_0^2)=(1-\beta)\bar{P}(\kappa_0^2)+\sum_j \beta_j\bar{P}_j(\kappa_0^2).$$

Since κ_0^2 depends on the size of the pile—for example, $\kappa_0^2=\pi^2/R^2$ for a sphere of radius R—Eq. (8) serves to determine the critical size of a pile in terms of its microscopic properties.

We now suppose that an absorber, whose absorption cross section per cc at position $\mathbf{r}$ and time t is $\sigma_a(\mathbf{r}, t)$, is placed in the pile. We assume that introduction of the absorber does not alter the pile scattering cross section. Since the pile is critical before the absorber was introduced, it will not be so, on the average, after the absorber is in place unless the multiplication constant is increased (by moving a control rod out) to a new value $k'>k$. After this adjustment has been made the pile equation is

$$D\Delta n-[\sigma_p+\sigma_a(\mathbf{r}, t)]n$$
$$+\frac{k'}{p}(1-\beta)\sigma_p\int_\infty n(\mathbf{r}', t)P(|\mathbf{r}-\mathbf{r}'|)d\mathbf{r}'$$
$$+\sum_j\int_\infty\frac{c_j(\mathbf{r}', t)}{\tau_j}P_j(|\mathbf{r}-\mathbf{r}'|)d\mathbf{r}'=-\frac{1}{v}\frac{\partial n}{\partial t}, \quad (9a)$$

$$(k'/p)\beta_j\sigma_p n-(c_j/\tau_j)=\partial c_j/\partial t, \quad (9b)$$

where the subscripts of Eq. (1) have been dropped. To determine how much k' must differ from k in order that the pile remain critical, on the average, we multiply (1a) and (1b) by n, (9a) and (9b) by n_0, subtract, integrate over the pile, and integrate with respect to time from time 0 to ∞. The integrals involving $n_0\Delta n$ and $n\Delta n_0$ vanish by Green's theorem and the homogeneity of the boundary conditions. Now the integral in (9) of the form

$$\int_\infty n(\mathbf{r}', t)P(|\mathbf{r}-\mathbf{r}'|)d\mathbf{r}', \quad (10a)$$

where the integration is extended over all space and $P(|\mathbf{r}-\mathbf{r}'|)$ is the slowing-down function appropriate to an infinite system, is equivalent to

$$\int_\mathfrak{p} n(\mathbf{r}', t)P_\mathfrak{p}(\mathbf{r}, \mathbf{r}')d\mathbf{r}', \quad (10b)$$

where the integral extends over the pile ($\mathfrak{p}$), and $P_\mathfrak{p}(\mathbf{r}, \mathbf{r}')$, the slowing-down kernel in a finite pile, can be constructed from $P(|\mathbf{r}-\mathbf{r}'|)$ by a suitable superposition of images. The equivalence of the pile integral (10b) and the all-space integral (10a) follows from the fact that the all-space integral vanishes on the extrapolated pile boundary. This, therefore, insures that the linear superposition of infinite system slowing-down kernels represented by the all-space integral is exactly that superposition which satisfies the boundary conditions on the finite pile. To show that (10a) vanishes on the extrapolated boundary of the pile we express $n(\mathbf{r}, t)$ as a superposition of functions $Z_\nu(\mathbf{r})$ which vanish on the extrapolated pile boundary and satisfy the wave equation

$$\Delta Z_\nu(\mathbf{r})+\kappa_\nu^2 Z_\nu(\mathbf{r})=0;$$

that is,

$$n(\mathbf{r}, t)=\sum_\nu n_\nu(t)Z_\nu(\mathbf{r}),$$

$n_\nu(t)$ being expansion coefficients and ν being an index which orders the eigenfunctions. Upon substituting this expansion into (10a) we obtain

$$\int_\infty n(\mathbf{r}', t)P(|\mathbf{r}-\mathbf{r}'|)d\mathbf{r}'=\sum_\nu n_\nu(t)Z_\nu(\mathbf{r})\bar{P}(\kappa_\nu^2),$$

which vanishes on the boundary, even for arbitrary $n_\nu(t)$. The double integrals can therefore be transformed thus:

$$\int_\mathfrak{p}\int_\infty n_0(\mathbf{r})P(|\mathbf{r}-\mathbf{r}'|)n(\mathbf{r}', t)d\mathbf{r}'d\mathbf{r}$$
$$=\int_\mathfrak{p}\int_\mathfrak{p} n_0(\mathbf{r})P_\mathfrak{p}(\mathbf{r}, \mathbf{r}')n(\mathbf{r}', t)d\mathbf{r}'d\mathbf{r}$$
$$=\int_\infty\int_\mathfrak{p} n_0(\mathbf{r})P(|\mathbf{r}-\mathbf{r}'|)n(\mathbf{r}', t)d\mathbf{r}'d\mathbf{r}$$
$$=\bar{P}(\kappa_0^2)\int_\mathfrak{p} n(\mathbf{r}', t)n_0(\mathbf{r}')d\mathbf{r}'.$$

The result of the manipulation with Green's theorem is therefore

$$\frac{(k'-k)}{p}\bar{P}_{Av}(\kappa_0^2)=\lim_{T\to\infty}\frac{\int_0^T\int_v \sigma_a(\mathbf{r},t)n(\mathbf{r},t)n_0(\mathbf{r})d\mathbf{r}dt}{\sigma_p\int_0^T\int_v n(\mathbf{r},t)n_0(\mathbf{r})d\mathbf{r}dt}$$

$$+\frac{\int_v n_0(\mathbf{r})\left[\sum_j \bar{P}_j(\kappa_0^2)\{c_j(\mathbf{r},T)-c_j(\mathbf{r},0)\}+\dfrac{n(\mathbf{r},T)-n(\mathbf{r},0)}{v}\right]d\mathbf{r}}{\sigma_p\int_0^T\int_v n(\mathbf{r},t)n_0(\mathbf{r})d\mathbf{r}dt}.$$

Since k' is so adjusted that the pile remains critical on the average after the absorber has been introduced, $n(\mathbf{r},t)$ and $c_j(\mathbf{r},t)$ are bounded as $t\to\infty$; the second term on the right therefore goes to zero at long times T. Thus the required change in k is

$$k'-k=\frac{p}{\bar{P}_{Av}(\kappa_0^2)}\frac{\int_v\langle\sigma_a nn_0\rangle_{Av}d\mathbf{r}}{\sigma_p\int_v\langle nn_0\rangle_{Av}d\mathbf{r}}, \tag{11}$$

where

$$\langle\sigma_a nn_0\rangle_{Av}=\lim_{T\to\infty}\frac{1}{T}\int_0^T\sigma_a nn_0dt. \tag{12}$$

If we introduce the notation

$$S_a=\lim_{T\to\infty}\left[\frac{1}{T}\int_0^T\int_v\sigma_a(\mathbf{r},t)d\mathbf{r}dt\right], \tag{13}$$

$$f(\mathbf{r},t)=\frac{\sigma_a(\mathbf{r},t)}{S_a}, \tag{14}$$

$$\eta=\lim_{T\to\infty}\frac{\int_0^T\int_v f(\mathbf{r},t)n(\mathbf{r},t)n_0(\mathbf{r})d\mathbf{r}dt}{\int_0^T\int_v n(\mathbf{r},t)n(\mathbf{r})d\mathbf{r}dt}, \tag{15}$$

the required k change is

$$\delta k=k'-k=\frac{p}{\bar{P}_{Av}(\kappa_0^2)}\frac{S_a}{\sigma_p}\eta. \tag{16}$$

The quantity S_a is equal to the time average of the absorption cross section per cc of the absorber multiplied by the volume of the absorber; η is the average "statistical weight" of the pile region occupied by the absorber. Thus Eq. (16) is the generalization for a time-varying absorber of the usual statistical weight formula: *the average change in multiplication constant caused by a time-varying absorber is the average cross section multiplied by the average statistical weight of the absorber.* Since the time average is over nn_0, or, approximately, over the square of the neutron density, the average k change is not the same as the k change caused by the absorber if it were stationary in its average position.

The following example illustrates this point. Consider a point absorber which oscillates along the z axis perpendicular to the faces of an infinite slab pile with amplitude ξ and frequency $\omega/2\pi$ around $z=z_0$. Then

$$f(\mathbf{r},t)=\delta(z_0-z+\xi e^{i\omega t})\delta(x)\delta(y),$$

and

$$n(\mathbf{r})\approx\sin\frac{\pi z}{H}\approx n_0(\mathbf{r}),$$

H being the width of the pile, $H\gg\xi$. It is understood throughout that only the real part of the exponential is to be used. If the sink were stationary at its equilibrium point, z_0, the statistical weight, η_0, would be

$$\eta_0=\frac{\sin^2\frac{\pi z_0}{H}}{\int_0^H\sin^2\frac{\pi z}{H}dz}=\frac{2}{H}\sin^2\frac{\pi z_0}{H}.$$

Since the absorber oscillates, its actual average statistical weight is

$$\eta=\frac{\int_0^T\int_0^H\delta(z_0-z+\xi e^{i\omega t})\sin^2\frac{\pi z}{H}dzdt}{\int_0^T\int_0^H\sin^2\frac{\pi z}{H}dzdt}\cong\frac{2}{H}\sin^2\frac{\pi z_0}{H}$$

$$+\frac{\pi^2\xi^2}{H^2}\cos\frac{2\pi z_0}{H}.$$

If the absorber oscillates around $z_0=H/4$, the average k

change is the same as the k change at the average position, since the two statistical weights are the same. If $3H/4>z_0>H/4$ (toward center), the k change is less than the stationary value, while if $z_0<H/4$, the k change is greater.

3. SOLUTION OF THE PILE EQUATION FOR OSCILLATING ABSORBER

We now calculate the pile response to an absorber of small volume V_a and cross section σ_a which is oscillated back and forth about the point $\mathbf{r}_0$ with frequency $\omega/2\pi$ and amplitude $|\boldsymbol{\varrho}|$ in the direction $\boldsymbol{\varrho}$. We assume that $|\boldsymbol{\varrho}|$ is small compared to any pile dimension. Then by definitions (13) and (14),

$$S_a=\sigma_a V_a, \tag{17}$$

$$f(\mathbf{r},t)=\delta(\mathbf{r}_0-\mathbf{r}+\boldsymbol{\varrho}e^{i\omega t}), \tag{18}$$

where $\delta(\mathbf{r})$ is normalized to

$$\int\delta(\mathbf{r})d\mathbf{r}=\int\int\int\delta(x)\delta(y)\delta(z)dxdydz=1.$$

If $|\mathbf{r}_0-\mathbf{r}|$ is large compared to $|\boldsymbol{\varrho}|$, it is appropriate to expand the δ-function formally in Taylor's series and keep only the first two terms:

$$f(\mathbf{r},t)\approx\delta(\mathbf{r}_0-\mathbf{r})+e^{i\omega t}\boldsymbol{\varrho}\cdot\nabla\delta(\mathbf{r}_0-\mathbf{r}), \tag{19}$$

where ∇ is the gradient with respect to $\mathbf{r}_0$. The higher terms in this expansion have frequencies which are multiples of ω; if the detecting equipment is tuned only to ω, these overtones will not be recorded.

The neutron and delayed emitter densities will consist of a stationary part, $(\bar{n},\bar{c}_j)$, and an oscillatory part, $(y(\mathbf{r})e^{i\omega t},\ w_j(\mathbf{r})e^{i\omega t})$:

$$n(\mathbf{r},t)=\bar{n}(\mathbf{r})+y(\mathbf{r})e^{i\omega t}, \tag{20a}$$

$$c_j(\mathbf{r},t)=\bar{c}_j(\mathbf{r})+w_j(\mathbf{r})e^{i\omega t}. \tag{20b}$$

In (20), and in the remaining calculations, only the real part of any complex quantity is significant.

Upon substituting (17), (19), and (20), into the pile equation, (9), and equating time-dependent and time-independent quantities, we obtain for the oscillating part of the flux,

$$D\Delta y-\sigma_p y+\frac{k}{p}(1-\beta)\sigma_p\int_\infty y(\mathbf{r}')P(|\mathbf{r}-\mathbf{r}'|)d\mathbf{r}'$$
$$+\sum_j\int_\infty\frac{w_j(\mathbf{r}')}{\tau_j}P_j(|\mathbf{r}-\mathbf{r}'|)d\mathbf{r}'-\frac{i\omega}{v}y$$
$$=S_a\bar{n}\boldsymbol{\varrho}\cdot\nabla\delta(\mathbf{r}_0-\mathbf{r})+S_a y\delta(\mathbf{r}_0-\mathbf{r})$$
$$-\frac{\delta k}{p}(1-\beta)\sigma_p\int_\infty y(\mathbf{r}')P(|\mathbf{r}-\mathbf{r}'|)d\mathbf{r}', \tag{21a}$$

$$\frac{k}{p}\beta_j\sigma_p y+\frac{\delta k}{p}\beta_j\sigma_p y-\frac{w_j}{\tau_j}-i\omega w_j=0. \tag{21b}$$

Since y vanishes with S_a, the terms $S_a y$, $y\delta k$, and $\delta k\int y(\mathbf{r}')P(|\mathbf{r}-\mathbf{r}'|)d\mathbf{r}'$ are of second order in S_a, and, on the assumption of weak absorber, can be neglected. Similarly, $\bar{n}(\mathbf{r})$ in the term $S_a\bar{n}\boldsymbol{\varrho}\cdot\nabla\delta(\mathbf{r}_0-\mathbf{r})$ can be replaced by $n_0(\mathbf{r})$, the density before the absorber was introduced (this corresponds to using Born's approximation).

Since the amplitude of motion, $|\boldsymbol{\varrho}|$, is small compared to the pile dimension, $n(\mathbf{r})$ [or $n_0(\mathbf{r})$] in (21) can be expanded around $\mathbf{r}_0$. Thus, for points not too near to the absorber,

$$S_a\bar{n}\boldsymbol{\varrho}\cdot\nabla\delta(\mathbf{r}_0-\mathbf{r})\approx S_a[n_0(\mathbf{r}_0)$$
$$+(\mathbf{r}-\mathbf{r}_0)\cdot\nabla n_0(\mathbf{r}_0)][\boldsymbol{\varrho}\cdot\nabla\delta(\mathbf{r}-\mathbf{r}_0)]$$
$$\approx S_a(\boldsymbol{\varrho}\cdot\nabla)[n_0(\mathbf{r}_0)\delta(\mathbf{r}-\mathbf{r}_0)]. \tag{22}$$

In this approximation, therefore, the solution to (21) can be obtained by solving

$$D\Delta\bar{y}-\sigma_p\bar{y}+\frac{k}{p}(1-\beta)\sigma_p\int_\infty\bar{y}(\mathbf{r}')P(|\mathbf{r}-\mathbf{r}'|)d\mathbf{r}'$$
$$+\sum_j\int_\infty\frac{\bar{w}_j(\mathbf{r}')}{\tau_j}P_j(|\mathbf{r}-\mathbf{r}'|)d\mathbf{r}'-\frac{i\omega}{v}\bar{y}$$
$$=S_a n_0(\mathbf{r}_0)\delta(\mathbf{r}-\mathbf{r}_0), \tag{23a}$$

$$\frac{k}{p}\beta_j\sigma_p\bar{y}-\frac{\bar{w}_j}{\tau_j}-i\omega\bar{w}_j=0, \tag{23b}$$

and taking the directional derivative $\boldsymbol{\varrho}\cdot\nabla$ of the results:

$$y(\mathbf{r})=(\boldsymbol{\varrho}\cdot\nabla)\bar{y}(\mathbf{r},\mathbf{r}_0), \tag{24a}$$

$$w(\mathbf{r})=(\boldsymbol{\varrho}\cdot\nabla)\bar{w}(\mathbf{r},\mathbf{r}_0). \tag{24b}$$

The solution $\bar{y}$ of (23a) when multiplied by $e^{i\omega t}$ represents the oscillatory part of the response to

a point absorber at $\mathbf{r}_0$ whose absorption cross section oscillates with amplitude S_a.

To solve (23) we first replace $\bar{w}_j$ in (23a) by its value from (23b):

$$\bar{w}_j=-\frac{k}{p}\frac{\beta_j\sigma_p\bar{y}}{i\omega+1/\tau_j}. \tag{25}$$

We then expand $\bar{y}$ and $\delta(\mathbf{r}-\mathbf{r}_0)$ in the complete orthonormal set

$$Z_\nu(\mathbf{r}),$$

which consists of those solutions of

$$\Delta Z_\nu(\mathbf{r})+\kappa_\nu^2 Z_\nu(\mathbf{r})=0, \tag{26}$$

which vanish on the extrapolated boundary. Thus

$$\bar{y}(\mathbf{r})=\sum_\nu \bar{y}_\nu Z_\nu(\mathbf{r}),$$
$$\delta(\mathbf{r}-\mathbf{r}_0)=\sum_\nu Z_\nu(\mathbf{r})Z_\nu(\mathbf{r}_0), \tag{27}$$

where

$$\bar{y}_\nu=\int_p \bar{y}(\mathbf{r})Z_\nu(\mathbf{r})d\mathbf{r}.$$

The index ν is an abbreviation for the three indices (λ, μ, ν) in case the pile is three dimensional, and the characteristic functions depend on three coordinates.

Since

$$\int_\infty Z_\nu(\mathbf{r}')P(|\mathbf{r}-\mathbf{r}'|)d\mathbf{r}'=\bar{P}(\kappa_\nu^2)Z_\nu(\mathbf{r}), \tag{28}$$

the integral terms in (23a) reduce to

$$\int_\infty \bar{y}(\mathbf{r}')P(|\mathbf{r}-\mathbf{r}'|)d\mathbf{r}'=\sum_\nu \bar{y}_\nu\bar{P}(\kappa_\nu^2)Z_\nu(\mathbf{r}). \tag{29}$$

After substituting the expansion (27) for $\bar{y}(\mathbf{r})$ in (23a) and (23b), and equating coefficients of Z_ν, there results

$$\bar{y}(\mathbf{r})=\frac{S_a}{\sigma_p}\sum_\nu \frac{n_0(\mathbf{r}_0)Z_\nu(\mathbf{r}_0)Z_\nu(\mathbf{r})}{\frac{k}{p}\left\{(1-\beta)\bar{P}(\kappa_\nu^2)+\sum_j\frac{\beta_j}{1+i\omega\tau_j}\bar{P}_j(\kappa_\nu^2)\right\}-L^2\kappa_\nu^2-i\omega\tau}, \tag{30}$$

where $\tau=1/v\sigma_p$ is the lifetime against capture of a thermal neutron in the reactor, and $L=(D/\sigma_p)^{\frac{1}{2}}$ is the diffusion length of the thermal neutrons. With this value for $\bar{y}$, we find, finally,

$$n(\mathbf{r},t)=\bar{n}(\mathbf{r})+y(\mathbf{r})e^{i\omega t}=\bar{n}(\mathbf{r})+\frac{S_a}{\sigma_p}(\boldsymbol{\varrho}\cdot\nabla)n_0(\mathbf{r}_0)$$
$$\times\sum_\nu\frac{Z_\nu(\mathbf{r}_0)Z_\nu(\mathbf{r})e^{i\omega t}}{\frac{k}{p}\left\{(1-\beta)\bar{P}(\kappa_\nu^2)+\sum_j\frac{\beta_j}{1+i\omega\tau_j}\bar{P}_j(\kappa_\nu^2)\right\}-L^2\kappa_\nu^2-1-i\omega\tau}, \tag{31a}$$

$$c_j(\mathbf{r},t)=\bar{c}_j(\mathbf{r})+w_j(\mathbf{r})e^{i\omega t}=\bar{c}_j(\mathbf{r})+\frac{k}{p}\frac{\beta_j\tau_j\sigma_p y(\mathbf{r})}{1+i\omega\tau_j}e^{i\omega t}. \tag{31b}$$

The real parts of Eqs. (31a) and (31b) constitute the formal solution of the problem. We now discuss the physical properties of the solution in various cases.

a. Absorber of Fluctuating Strength Distributed Uniformly throughout Pile

In this case

$$\sigma_a(\mathbf{r},t)=\frac{S_a}{V_p}(1+\alpha e^{i\omega t}), \tag{32}$$

where V_p is the pile volume and α measures the relative amplitude of the oscillation. The oscillatory part of the neutron density can be obtained from $\bar{y}(\mathbf{r})$ (which, except for the factor $e^{i\omega t}$, is the solution for a stationary point absorber whose strength oscillates with amplitude S_a) by integrating with

respect to $\mathbf{r}_0$ over the whole pile and multiplying by $\alpha e^{i\omega t}$. Since $n_0(\mathbf{r}_0)$ is proportional to $Z_0(\mathbf{r}_0)$, all terms except the fundamental disappear in the integration, and the result is

$$n(\mathbf{r},t)=\bar{n}(\mathbf{r})+\frac{\alpha S_a}{V_p\sigma_p}\frac{n_0(\mathbf{r})e^{i\omega t}}{\frac{k}{p}\left\{(1-\beta)\bar{P}(\kappa_0^2)+\sum_j\frac{\beta_j\bar{P}_j(\kappa_0^2)}{1+i\omega\tau_j}\right\}-L^2\kappa_0^2-1-i\omega\tau}. \tag{33}$$

If there are no delayed neutrons, the fluctuating part of the response is

$$n(\mathbf{r},t)-\bar{n}(\mathbf{r})=\frac{\alpha S_a}{V_p\sigma_p}\frac{n_0(\mathbf{r})e^{i\omega t}}{\frac{k}{p}\bar{P}(\kappa_0^2)-L^2\kappa_0^2-1-i\omega\tau}. \tag{34}$$

Since the pile was critical before the absorber was introduced, Eq. (8) holds:

$$\frac{k}{p}\bar{P}(\kappa_0^2)-L^2\kappa_0^2-1=0,$$

hence,

$$\frac{n(\mathbf{r},t)-\bar{n}(\mathbf{r})}{n_0(\mathbf{r})}=-\frac{\alpha S_a e^{i\omega t}}{V_p\sigma_p i\omega\tau}.$$

The amplitude of the neutron response falls off with increasing frequency; it lags behind the absorber oscillation by 90°. This phase lag arises because it is the rate of change of the pile intensity, not the intensity itself, which is determined by the instantaneous value of k. If the delayed neutrons are taken into account, the phase lag is a little less than 90°.

b. Localized Absorber, Slow Oscillation ($\omega\tau_j\ll 1$)

If the absorber moves back and forth slowly, $\omega\tau_j\ll 1$, and (31a) becomes

$$n(\mathbf{r},t)\approx\bar{n}(\mathbf{r})+\frac{S_a}{\sigma_p}(\boldsymbol{\varrho}\cdot\nabla)n_0(\mathbf{r}_0)\sum_\nu\frac{Z_\nu(\mathbf{r}_0)Z_\nu(\mathbf{r})e^{i\omega t}}{\frac{k}{p}\bar{P}_{A\nu}(\kappa_\nu^2)-L^2\kappa_\nu^2-1-i\omega\left[\tau+\sum_j\beta_j\tau_j\bar{P}_j(\kappa_\nu^2)\right]}. \tag{35}$$

Since the pile is critical,

$$\frac{k}{p}\bar{P}_{A\nu}(\kappa_0^2)-L^2\kappa_0^2-1=0,$$

and the ratio of the fundamental to the νth harmonic in the series (35) is

$$\frac{Z_0(\mathbf{r}_0)Z_0(\mathbf{r})}{Z_\nu(\mathbf{r}_0)Z_\nu(\mathbf{r})}\left[\frac{\frac{k}{p}\bar{P}_{A\nu}(\kappa_\nu^2)-L^2\kappa_\nu^2-1-i\omega\left[\tau+\sum_j\beta_j\tau_j\bar{P}_j(\kappa_\nu^2)\right]}{-i\omega\left[\tau+\sum_j\beta_j\tau_j\bar{P}_j(\kappa_0^2)\right]}\right]. \tag{36}$$

This ratio becomes infinite as $\omega\to 0$; i.e., the fundamental predominates as the oscillation becomes slower. In other words, if the oscillation is very slow the pile intensity fluctuates as a whole, the neutron flux at any point having the same phase as at any other point.

The slow oscillation method in which the over-all pile response to a moving absorber is detected has been used in Langsdorf's oscillator for cross-section measurements.

c. Localized Absorber, Fast Oscillation ($\omega\tau_j \gg 1$), or Detector Close to Absorber

If the oscillation is fast, or if the detector is close to the absorber ($\mathbf{r}_0 \approx \mathbf{r}'$), the fundamental no longer predominates, and the series (31a) converges poorly. Since the higher harmonics all have different phases (because the coefficients in the series are complex), the phase of the neutron intensity oscillation will change from point to point. Close to the absorber the intensity will be in phase with the motion of the absorber since the local neutron depression caused by the absorber will be the major part of the intensity fluctuation. Far from the absorber the neutron intensity will tend more and more toward the phase of the fundamental. The disturbance set up by the oscillating absorber is therefore wave-like: the absorber sends out damped waves of neutron intensity which are reflected at the boundary. As will be shown below, the wave-length of the traveling disturbance is short at high frequency and long at low frequency. It is for this reason that the disturbance has the same phase everywhere at low frequencies, and has a varying phase at high frequency.

These qualitative considerations can be made exact by transforming the poorly converging series (31a) into a form which displays the wave character of the disturbance. In order to effect this transformation it will be convenient to specialize the shape of the pile; we therefore suppose the pile to be a rectangular parallelopiped of sides a, b, c. The normalized characteristic functions are

$$Z_{lmn}(\mathbf{r}) = \left(\frac{8}{abc}\right)^{\frac{1}{2}} \sin\frac{l\pi x}{a} \sin\frac{m\pi y}{b} \sin\frac{n\pi z}{c}, \tag{37}$$

and

$$\kappa^2_{lmn} = \frac{l^2\pi^2}{a^2} + \frac{m^2\pi^2}{b^2} + \frac{n^2\pi^2}{c^2}. \tag{38}$$

The intensity, as given by (31a), is therefore

$$n(\mathbf{r}, t) = \bar{n}(\mathbf{r}) + \frac{S_a}{8\sigma_p abc}(\boldsymbol{\varrho}\cdot\nabla)n_0(\mathbf{r}_0)e^{i\omega t} \sum_{l,m,n} \times \frac{\exp\left(i\pi\left\{l\left(\frac{x-x_0}{a}\right)+m\left(\frac{y-y_0}{b}\right)+n\left(\frac{z-z_0}{c}\right)\right\}\right) - \exp\left(i\pi\left\{l\left(\frac{x+x_0}{a}\right)+m\left(\frac{y+y_0}{b}\right)+n\left(\frac{z+z_0}{c}\right)\right\}\right)}{\frac{k}{p}\left\{(1-\beta)\bar{P}(\kappa^2_{lmn}) + \sum_j \frac{\beta_j \bar{P}_j(\kappa^2_{lmn})}{1+i\omega\tau_j}\right\} - L^2\kappa^2_{lmn} - 1 - i\omega\tau}, \tag{39}$$

the sums being taken from $-\infty$ to $+\infty$.

We now apply Poisson's summation formula[6]

$$\sum_{l,m,n} \varphi(l, m, n) = \sum_{\lambda,\mu,\nu} \int\int\int_{-\infty}^{\infty} \varphi(u, v, w) e^{-2\pi i(\lambda u + \mu v + \nu w)} du\,dv\,dw, \tag{40}$$

to the series in (39). The series then becomes, after making the transformation,

$$\sum_{l,m,n} \frac{\exp\left(i\pi\left\{l\left(\frac{x-x_0}{a}\right)+m\left(\frac{y-y_0}{b}\right)+n\left(\frac{z-z_0}{c}\right)\right\}\right) - \exp\left(i\pi\left\{l\left(\frac{x+x_0}{a}\right)+m\left(\frac{y+y_0}{b}\right)+n\left(\frac{z+z_0}{c}\right)\right\}\right)}{k\bar{Q}(\kappa^2_{lmn}) - L^2\kappa^2_{lmn} - 1 - i\omega\tau}$$

$$= \frac{abc}{\pi^3} \sum_{\lambda,\mu,\nu} \int\int\int_{-\infty}^{\infty} \frac{\exp(i\boldsymbol{\xi}\cdot(\mathbf{R}^- - \boldsymbol{\Lambda})) - \exp(i\boldsymbol{\xi}\cdot(\mathbf{R}^+ - \boldsymbol{\Lambda}))}{k\bar{Q}(\xi^2) - L^2\xi^2 - 1 - i\omega\tau} d\xi, \tag{41}$$

[6] Courant-Hilbert, *Methoden der Mathematischen Physik* (Verlag Julius Springer, Berlin, 1931), Vol. I, p. 65.

where

$$\xi=\frac{\pi u}{a}\mathbf{i}+\frac{\pi v}{b}\mathbf{j}+\frac{\pi w}{c}\mathbf{k}, \quad d\xi=\frac{\pi^3}{abc}dudvdw,$$

$$\mathbf{R}^{\pm}=(x\pm x_0)\mathbf{i}+(y\pm y_0)\mathbf{j}+(z\pm z_0)\mathbf{k},$$

$$\mathbf{\Lambda}=2\lambda a\mathbf{i}+2\mu b\mathbf{j}+2\nu c\mathbf{k},$$

$$\bar{Q}(\xi^2)=\frac{1}{p}\left\{(1-\beta)\bar{P}(\xi^2)+\sum_i\frac{\beta_i\bar{P}_i(\xi^2)}{1+i\omega\tau}\right\}.$$

To evaluate the integral in (41) we shift to spherical coordinates and obtain

$$\int\int\int_{-\infty}^{\infty}\frac{\exp[i\xi\cdot(\mathbf{R}-\mathbf{\Lambda})]}{k\bar{Q}(\xi^2)-L^2\xi^2-1-i\omega\tau}d\xi=\frac{4\pi}{|\mathbf{R}-\mathbf{\Lambda}|}\int_0^{\infty}\frac{\sin\xi|\mathbf{R}-\mathbf{\Lambda}|}{k\bar{Q}(\xi^2)-L^2\xi^2-1-i\omega\tau}\xi d\xi$$

$$=\frac{4\pi}{2i|\mathbf{R}-\mathbf{\Lambda}|}\int_{-\infty}^{\infty}\frac{\exp(i|\mathbf{R}-\mathbf{\Lambda}|\xi)}{k\bar{Q}(\xi^2)-L^2\xi^2-1-i\omega\tau}\xi d\xi. \quad (42)$$

To compute this integral we follow a semicircular contour which embraces the entire positive half-plane. If B_s are the zeros (assumed simple) with positive imaginary part of

$$k\bar{Q}(\xi^2)-L^2\xi^2-1-i\omega\tau=0, \quad (43)$$

then the value of the integral is

$$\int_{-\infty}^{\infty}\frac{\exp(i|\mathbf{R}-\mathbf{\Lambda}|\xi)}{k\bar{Q}(\xi^2)-L^2\xi^2-1-i\omega\tau}\xi d\xi=\pi i\sum_s\frac{\exp(iB_s|\mathbf{R}-\mathbf{\Lambda}|)}{k\bar{Q}'(B_s^2)-L^2}, \quad (44)$$

$$\bar{Q}'(B_s^2)\equiv\frac{d}{d(\xi^2)}\bar{Q}(\xi^2)\,|_{\xi=B_s}.$$

Hence

$$\frac{abc}{\pi^3}\int\int\int_{-\infty}^{\infty}\frac{\exp[i\xi\cdot(\mathbf{R}-\mathbf{\Lambda})]}{k\bar{Q}(\xi^2)-L^2\xi^2-1-i\omega\tau}d\xi=\frac{2abc}{\pi|\mathbf{R}-\mathbf{\Lambda}|}\sum_s\frac{\exp(iB_s|\mathbf{R}-\mathbf{\Lambda}|)}{k\bar{Q}'(B_s^2)-L^2}. \quad (45)$$

Substituting this into (41), and then putting the resulting series into (39), we finally obtain the transformed series:

$$n(\mathbf{r},t)-\bar{n}(\mathbf{r})=\frac{S_a}{\sigma_p}(\varrho\cdot\nabla)n_0(\mathbf{r}_0)e^{i\omega t}\sum_{\lambda,\mu,\nu}\sum_s\frac{1}{k\bar{Q}'(B_s^2)-L^2}\left\{\frac{\exp(iB_sR^-_{\lambda\mu\nu})}{4\pi R^-_{\lambda\mu\nu}}-\frac{\exp(iB_sR^+_{\lambda\mu\nu})}{4\pi R^+_{\lambda\mu\nu}}\right\}, \quad (46)$$

where

$$R^{\pm}_{\lambda\mu\nu}=((x\pm x_0-2\lambda a)^2+(y\pm y_0-2\mu b)^2+(z\pm z_0-2\nu c)^2)^{\frac{1}{2}}. \quad (47)$$

Equation (46) can be described as a sequence of positive and negative neutron sources. The positive sources are situated at the points

$$(-x_0+2\lambda a)\mathbf{i}+(-y_0+2\mu b)\mathbf{j}+(-z_0+2\nu c)\mathbf{k},$$

and negative sources at the points

$$(x_0+2\lambda a)\mathbf{i}+(y_0+2\mu b)\mathbf{j}+(z_0+2\nu c)\mathbf{k}.$$

Thus (46) constitutes a sequence of images which are so placed that the boundary conditions are satisfied on the pile surface.

Each term in the series (46) is of the form

$$\frac{S_a}{\sigma_p}\frac{(\varrho\cdot\nabla)n_0(\mathbf{r}_0)}{k\bar{Q}'(B_s^2)-L^2}\frac{\exp[i(\omega t+B_sR)]}{4\pi R}=\frac{S_a}{\sigma_p}\frac{1}{k\bar{Q}'(B_s^2)-L^2}\left\{\frac{\exp[i(\omega t+B_sR)]}{4\pi R}\varrho\cdot\nabla n_0(\mathbf{r}_0)\right.$$
$$\left.+n_0(\mathbf{r}_0)\varrho\cdot\nabla\frac{\exp[i(\omega t+B_sR)]}{4\pi R}\right\}. \quad (48)$$

According to (48), the disturbance represented by each term in (46) is a spherical traveling wave of complex wave-length $1/B_s$. The traveling wave, in the approximation in which $|\varrho|$, the amplitude of oscillation, is small compared to $|\mathbf{r}-\mathbf{r}_0|$, consists of two parts: a spherically symmetric wave emitted by a point sink of strength

$$S_a(\varrho\cdot\nabla)n_0(\mathbf{r}_0),$$

and a non-spherically symmetric wave emitted by a dipole of strength

$$S_an_0(\mathbf{r}_0)|\varrho|.$$

The spherically symmetric wave falls off as $\exp(iB_sR_{\lambda\mu\nu})/R_{\lambda\mu\nu}$ while the dipole wave falls off as $\exp(iB_sR_{\lambda\mu\nu})/R_{\lambda\mu\nu}^2$ hence, far from the absorber only the spherically symmetric wave prevails.

Actually waves corresponding to multipoles of all orders are generated by a periodically moving absorber. The appearance of only the first two multipoles in (48) is a result of the approximation $|\varrho|\ll|\mathbf{r}-\mathbf{r}_0|$, which was the justification for keeping only two terms in the Taylor expansion (22) of the neutron flux. In principle, of course, there is no difficulty in extending the expansion to higher order in $|\varrho|/|\mathbf{r}-\mathbf{r}_0|$; this would lead, in the final answer, to multipole "radiation" of correspondingly higher order.

Corresponding to each different root B_s, the wave sources emit a wave. Each wave has an amplitude and phase which depends on the value of its B_s. The number of roots B_s, and therefore the number of different waves emitted by each source, depends on the slowing-down function—for a general kernel $P(r)$, (43) will be a transcendental equation and there will be an infinite number of roots B_s.

The waves with $s>0$ are significant close to the oscillator; as s increases they fall off more and more rapidly with $|\mathbf{r}-\mathbf{r}_0|$ because the real parts of iB_s increase with s. In order to see more clearly the physical significance of these transient waves, we compute the fluctuating part of the slowing-down density. This is obtained according to (3) and (5) by multiplying each term in (46) by $(k'/p)(1-\beta)\sigma_p\bar{P}(B_s^2)$; i.e.,

$$q(\mathbf{r},t)-\bar{q}(\mathbf{r})=\frac{k'}{p}(1-\beta)\sigma_p\int_\infty[n(\mathbf{r}',t)-\bar{n}(\mathbf{r})]P(|\mathbf{r}-\mathbf{r}'|)d\mathbf{r}'$$
$$=\frac{k'}{p}(1-\beta)S_a(\varrho\cdot\nabla)n_0(\mathbf{r}_0)e^{i\omega t}\sum_{\lambda,\mu,\nu}\sum_s\frac{\bar{P}(B_s^2)}{k\bar{Q}'(B_s^2)-L^2}\left\{\frac{\exp(iB_sR^-_{\lambda\mu\nu})}{4\pi R^-_{\lambda\mu\nu}}-\frac{\exp(iB_sR^+_{\lambda\mu\nu})}{4\pi R^+_{\lambda\mu\nu}}\right\}. \quad (49)$$

Because of the extra factor $\bar{P}(B_s^2)$ in each term of (49) as compared with (46), the slowing-down density is not proportional to the slow neutron flux close to the oscillator. In fact, the spectrum of epithermal neutrons changes continuously from its shape close to the oscillator, where the epithermal neutrons have no singularity while the thermal ones do, to its shape far from the oscillator, where the neutrons of all energies have similar spatial distributions. Thus the transients ($s>0$) are necessary to describe the variation in neutron spectrum which exists in a chain reactor near an absorber which captures only thermal neutrons.

4. PROPERTIES OF THE NEUTRON WAVES

Far from the absorber, and far from the pile surface, only the $s=\lambda=\mu=\nu=0$ spherically symmetric wave persists. From (48) this is

$$n(\mathbf{r},t)-\bar{n}(\mathbf{r})=\frac{S_a}{\sigma_p}\frac{1}{[k\bar{Q}'(B_0^2)-L^2]}\times\frac{e^{i(\omega t+B_0R)}}{4\pi R}(\boldsymbol{\varrho}\cdot\nabla)n(\mathbf{r}_o), \quad (50)$$

R being used to denote $R^-{}_{000}$.

The value of B_0 is calculable explicitly provided the pile is large (i.e., $k\approx 1$) and the oscillation is fast compared to the delayed neutron periods but slow compared to the pile period:

$$\omega\tau\ll 1, \quad \omega\tau_j\gg 1. \quad (51)$$

Since τ_j is of the order of 10 seconds or more, while τ is of the order of 10^{-3} to 10^{-4} sec., an angular frequency ω of 1 to 100 sec.$^{-1}$ will satisfy these conditions. To compute B_0 under these assumptions we return to the definition of $\bar{Q}(\xi^2)$:

$$\bar{Q}(\xi^2)=\frac{1}{p}\left\{(1-\beta)\bar{P}(\xi^2)+\sum_j\frac{\beta_j}{1+i\omega\tau_j}\bar{P}_j(\xi^2)\right\}$$
$$=\frac{4\pi}{p}\left\{(1-\beta)\int_0^\infty P(r)\frac{\sin\xi r}{\xi r}r^2dr+\sum_j\frac{\beta_j}{1+i\omega\tau_j}\int_0^\infty P_j(r)\frac{\sin\xi r}{\xi r}r^2dr\right\}.$$

We expand $(\sin\xi r/\xi r)$ in Taylor's series and integrate term by term; the result, correct to terms of order ξ^2, is:

$$\bar{Q}(\xi^2)=1-\beta+\sum_j\frac{\beta_j}{1+i\omega\tau_j}-\frac{\xi^2}{6}\langle r^2(\omega)\rangle_{Av}+O(\xi^4), \quad (52)$$

or, if the condition (51) is fulfilled,

$$\bar{Q}(\xi^2)\approx(1-\beta)-\frac{\xi^2}{6}\langle r^2(0)\rangle_{Av}+O(\xi^4), \quad (53)$$

where

$$\langle r^2(\omega)\rangle_{Av}=\frac{4\pi}{p}\left[\int_0^\infty P(r)r^4dr+\sum_j\frac{\beta_j}{1+i\omega\tau_j}\int_0^\infty P_j(r)r^4dr\right],$$

and $O(\xi^4)$ is an abbreviation for terms of order ξ^4 and above.

When $\omega=0$,

$$\langle r^2(0)\rangle_{Av}=\frac{4\pi}{p}\left[\int_0^\infty P(r)r^4dr+\sum_j\beta_j\int_0^\infty P_j(r)r^4dr\right];$$

i.e., $\langle r^2(0)\rangle_{Av}$ is the mean square distance which a fission neutron travels while slowing down. In general, for $\omega\neq 0$, $\langle r^2(\omega)\rangle_{Av}$ is a complex number.

We now substitute (53) into the characteristic Eq. (43):

$$M^2\xi^2-k(1-\beta)+1+i\omega\tau-kO(\xi^4)=0, \quad (54)$$

where

$$M^2=\frac{k\langle r^2(0)\rangle_{Av}}{6}+L^2 \quad (55)$$

is called the "migration area." Equation (54) can be solved by successive approximations provided

$$\frac{kO(B_0{}^4)}{M^2B_0{}^2}\ll 1,$$

$B_0{}^2$ being the value of ξ^2 which solves (54). In first approximation,

$$B_0{}^2=\frac{k(1-\beta)-1-i\omega\tau}{M^2}, \quad (56)$$

while the first and most important term in $O(B_0{}^4)$ is

$$O(B_0{}^4)\approx\frac{1}{120}B_0{}^4\langle r^4(0)\rangle_{Av};$$

i.e.,

$$\frac{kO(B_0{}^4)}{M^2B_0{}^2}\approx\frac{1}{120}[k(1-\beta)-1-i\omega\tau]k\frac{\langle r^4(0)\rangle_{Av}}{M^4}$$
$$<\frac{3}{10}\frac{k(1-\beta)-1-i\omega\tau}{k}\frac{\langle r^4(0)\rangle_{Av}}{[\langle r^2(0)\rangle_{Av}]^2}.$$

Now for any physically plausible kernel $\langle r^4(0)\rangle_{Av}/[\langle r^2(0)\rangle_{Av}]^2$ is of order unity; hence since $k-1\ll 1$ and $\omega\tau\ll 1$, the required ratio is small in absolute value, and the successive approximation is justified. The remaining discussion will be based on the value (56) for $B_0{}^2$.

Since

$$k\bar{Q}(\xi^2)\approx k(1-\beta)-k\frac{\xi^2}{6}\langle r^2(0)\rangle_{Av},$$

the quantity in the denominator of (50) is

$$k\bar{Q}'(B_0^2)-L^2\approx -M^2,$$

and therefore

$$n(\mathbf{r},t)-\bar{n}(\mathbf{r})\approx\frac{-S_a}{\sigma_p M^2}\frac{e^{i(\omega t+B_0R)}}{4\pi R}(\varrho\cdot\nabla)n(\mathbf{r}_0). \quad (57)$$

In order to calculate the velocity, wave-length, and attenuation length (distance for wave amplitude to damp by factor e), it is necessary to compute B_0 explicitly. From (56),

$$B_0=\frac{-1}{M}\left(\frac{[X^2+(\omega\tau)^2]^{\frac{1}{2}}+X}{2}\right)^{\frac{1}{2}}+\frac{i}{M}\left(\frac{[X^2+(\omega\tau)^2]^{\frac{1}{2}}-X}{2}\right)^{\frac{1}{2}}, \quad (58)$$

where

$$X\equiv k(1-\beta)-1.$$

Upon substituting (58) into (57), we observe that the resulting damped wave has a velocity

$$\frac{M\omega}{\left(\frac{[X^2+(\omega\tau)^2]^{\frac{1}{2}}+X}{2}\right)^{\frac{1}{2}}}, \quad (59)$$

a wave-length

$$\frac{2\pi M}{\left(\frac{[X^2+(\omega\tau)^2]^{\frac{1}{2}}+X}{2}\right)^{\frac{1}{2}}}, \quad (60)$$

and an attenuation length

$$\frac{M}{\left(\frac{[X^2+(\omega\tau)^2]^{\frac{1}{2}}-X}{2}\right)^{\frac{1}{2}}}. \quad (61)$$

If $X=0$, the medium is neither a net absorber nor producer of prompt neutrons. In this case

$$v=M\left(\frac{2\omega}{\tau}\right)^{\frac{1}{2}}, \quad (62)$$

$$\lambda=2\pi M\left(\frac{2}{\omega\tau}\right)^{\frac{1}{2}}, \quad (63)$$

$$l=M\left(\frac{2}{\omega\tau}\right)^{\frac{1}{2}}. \quad (64)$$

The waves characterized by (62), (63), and (64) are completely analogous to the classical thermal waves set up in a conducting medium in which the ratio of conductivity to specific heat per unit volume is M^2/τ, and the angular frequency of the impressed oscillating heat source is ω.

The authors wish to thank Professor E. P. Wigner for many helpful discussions.

PHYSICAL REVIEW VOLUME 74, NUMBER 8 OCTOBER 15, 1948

Measurement of Neutron Absorption Cross Sections with a Pile Oscillator*

J. I. HOOVER, W. H. JORDAN, C. D. MOAK, L. PARDUE,** H. POMERANCE,
J. D. STRONG,*** AND E. O. WOLLAN
Oak Ridge National Laboratory, Oak Ridge, Tennessee

(Received July 9, 1948)

The following paper deals with the measurement of thermal neutron cross sections by a technique referred to as the pile oscillator. In this method, a neutron absorber is moved back and forth in a field of thermal neutrons such as that existing in a chain reactor. In the vicinity of the absorber there is a depression in the neutron flux and the motion of this depression past a nearby ion chamber produces an oscillating signal whose amplitude is proportional to the total neutron absorption cross section of the sample. In the instrument considered here, the oscillating signal generated in the ion chamber is amplified, rectified, and fed to an integrating circuit. The absorption cross section of an unknown sample is determined by comparing the charge accumulated in the integrating circuit with that produced by a standard gold absorber. The instrument will detect a total absorption cross sestion of about 10^{-3} cm^2 and hence it is suitable for measuring cross sections of separated isotopes which are available only in small quantities. One of the major difficulties in making this instrument useful for absorption measurements has been the elimination of the effects of scattering by the sample. It was found that the signals caused by absorption and scattering are slightly out of phase with each other, and by properly phasing the rectifier, absorption cross sections which are no greater than 1 percent of the corresponding scattering cross sections can be measured. A number of thermal cross section measurements have been made with this instrument, most of which will be published separately; as illustrations, the following thermal cross sections are given: In, 191.2*b*; Ag^{107}, 29.9*b*; Ag^{109}, 83.7*b*.

INTRODUCTION

WHEN a neutron absorber is placed in a chain-reacting pile it produces a change in reactivity which is proportional to the total absorption cross section of the absorbing sample. This fact has been used in the so-called "danger coefficient" method[1] of measuring absorption cross sections in which the change in reactivity produced by a sample is balanced by the change in position of a calibrated control rod. Because of the inherent fluctuations of neutron intensity in a chain reactor, this static danger coefficient method requires rather large amounts of absorber for accurate cross-section measurements. It is therefore not adequate for the measurement of capture cross sections of rare substances such as separated isotopes. In this paper a high sensitivity "pile oscillator" method which has been developed for the measurement of cross sections of small samples will be described. This method is now being used at the Oak Ridge National Laboratory to make a systematic survey of the absorption cross sections of separated isotopes.

The pile oscillator method,[2] as proposed originally by E. P. Wigner, involves oscillating the unknown absorber in and out of the reactor or back and forth within the pile from a region of low neutron flux to a region of high flux. The reactivity of the chain reactor undergoes oscillations about criticality with the same frequency as the oscillations of the absorber, the reactivity being reduced when the absorber is in the pile. This reactivity oscillation produces an oscillation in the over-all neutron flux which then gives rise to a corresponding signal in a neutron-sensitive ion chamber located in the pile. Since the amplitude of the flux oscillation is proportional to the absorption of the sample, the instrument constitutes a means of determining unknown neutron-absorption cross sections by making comparisons with substances for which accurate direct measurements have been made. The gain in sensitivity of the oscillator method over the static danger coefficient method accrues both because it averages effects over so many cycles that random fluctuations tend to cancel, and because it makes a.c. amplification possible.

The original pile oscillator depended for its working on the change in pile reactivity caused by the motion of the absorber. The recording ion

* Declassified February 10, 1948.
** Now at University of Kentucky, Lexington, Kentucky.
*** Now at Hillyer Instrument Co., New York, New York.
[1] H. L. Anderson, E. Fermi, A. Wattenberg, G. Weil, and W. Zinn, Phys. Rev. 72, 16 (1947).
[2] The theory of the pile oscillator is given in A. M. Weinberg and H. C. Schweinler, Phys. Rev. 74, 851 (1948).

chamber in this method is best placed at a large distance from the absorber so that local neutron density changes near the absorber are not picked up. However, it was pointed out in a paper on the theory of the pile oscillator by A. Cahn, A. T. Monk, and A. M. Weinberg,[3] that a significant increase in sensitivity could be achieved by placing the ion chamber very close to the oscillating sample. By this means not only the over-all fluctuation in pile intensity, but also *the local depression in neutron flux which exists in the neighborhood of an absorber is measured.* Thus when the local neutron depression is measured, the pile is used primarily as a neutron flux field; the fact that the reactivity of the chain reactor also depends on the position of an absorber within it is only incidental. It is therefore possible to make measurements wherever there is a strong neutron flux, irrespective of how the reactivity of the pile is affected by the absorber. For example, to measure thermal cross sections it is advantageous to oscillate the sample in the graphite reflector of the pile where there are very few epithermal neutrons, even though the reactivity is little affected by motion of an absorber in the reflector.

While the measurement of the local depression increases the signal to noise ratio and makes it possible to measure thermal neutron cross sections unperturbed by epithermal neutrons, it has a serious disadvantage, namely, that the details of the spatial distribution of the neutron density around an absorber depend on its scattering cross section as well as its absorption cross section. It is therefore necessary to arrange the position of the ion chamber with respect to the absorber so as to reduce the scattering effect as much as possible. The extent to which the scattering signal has been eliminated is discussed below.

The Oak Ridge[4] pile oscillator has undergone a number of changes during its development; it will be described here in its present state in which the absorber is oscillated in close proximity to the ionization chamber and the local depression signal is recorded.

[3] Manhattan Project Report CP-G-2907.

[4] An oscillator depending on the reactivity change effect has been developed by A. Langsdorf at Argonne National Laboratory, a preliminary report of which was presented at the Washington Meeting April 29, 1948.

APPARATUS

The pile oscillator consists essentially of a mechanical device to oscillate the sample, a neutron-sensitive ionization chamber and an electrical system to amplify and convert the voltage pulse generated within the chamber to a quantity which can be readily measured.

The mechanical system for oscillating the sample is shown in Fig. 1. It consists of a washing machine gear box, on the drive shaft of which is mounted an aluminum wheel 30 in. in diameter. A braided steel cable passes over this wheel, over two idler pulleys and over another pulley inside the pile. On the lower cable, which passes into the pile through a $\frac{1}{2}$ in. square channel in a graphite stringer, there is fastened a rectangular beryllium boat with inside dimensions $\frac{3}{8}$-in. $\times\frac{3}{8}$-in. $\times 2\frac{1}{2}$-in. This boat carries the samples to be measured. The to and fro motion of the wheel produces an oscillation of the boat along the graphite channel with a total travel of 32 in. The large drive wheel can be disengaged from the drive shaft so that the boat can be reeled out of the pile for loading and then reeled back into position. The frequency of oscillation which has been used is about 1 cycle per second.

Two types and locations of ionization chambers have been used. One which shall be referred to as *A* was an aluminum chamber, 10 in. long, 1 in. in diameter, coated internally with about

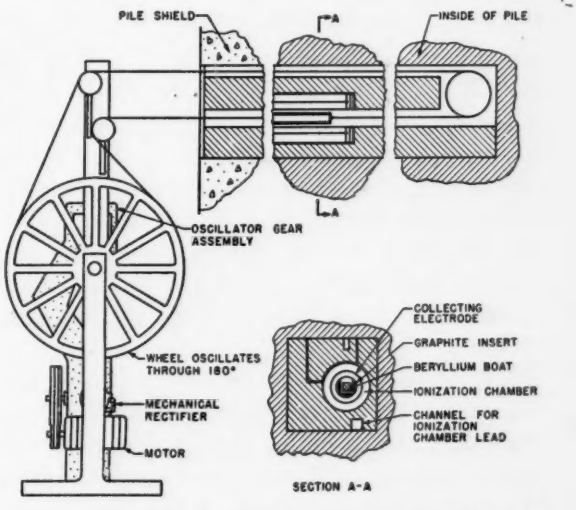

FIG. 1. Pile oscillator mechanical assembly. The portion of the drawing showing the graphite channel and ionization chamber has been enlarged to show details.

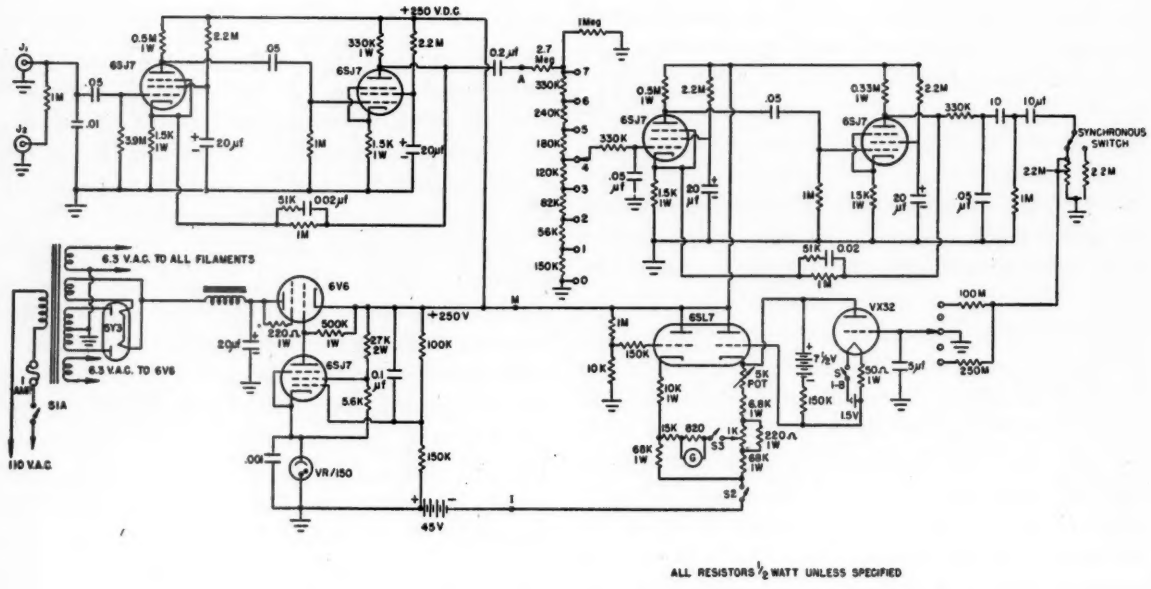

FIG. 2. Amplifier and integrator circuit. The ionization chamber is connected to *J*1 and a 500-volt battery is connected to *J*2.

2 mg/cm² of enriched boron. This chamber was buried in the graphite stringer with its axis parallel to and its center line 1 in. below the axis of the boat channel. A second annular chamber, which will be referred to as *B*, has been found more satisfactory, and this is the chamber that is now being used. This chamber, shown in Fig. 1, is placed coaxially to the path of the oscillating sample, and its center coincides with the midpoint of the absorber's path of oscillation. The active volume is contained between two concentric aluminum tubes 11 in. long, the outer tube being 2 in. o.d. and the inner tube $\frac{7}{8}$ in. o.d. The collecting electrode, which is insulated from the rest of the chamber by polystyrene, is 10 in. long and $1\frac{1}{2}$ in. o.d. It is coated on both sides with 0.5 mg/cm² of boron enriched in B^{10}. A graphite insert machined to the dimensions of the boat channel extends through the inner tube which protrudes 8 in. on either side of the ionization chamber. Graphite was used for the insert to reduce scattering effects which might arise from the streaming of neutrons through the boat channel. The protruding sections of the tube are coated with about 2 mgs/cm² of enriched boron in order to reduce abrupt changes in neutron density at the boundary of the active section of the chamber.

The voltage pulses from the ionization chamber have been measured by both a resonance galvanometer and by an integrating circuit method. The latter method, which is more convenient, is now being used. The signal from the ionization chamber is first amplified by a fairly narrow band feed-back amplifier, then rectified by a synchronous switch and integrated by means of a long time-constant R-C circuit. (See Fig. 2.) The voltage appearing across the integrating condenser is measured by means of a vacuum tube voltmeter. The use of the synchronous rectifier and integrator discriminates strongly against frequencies other than the desired signal so that noise from the chamber, because of statistical fluctuations in the ion current, is greatly reduced.

The rectifying switch is operated by a cam connected to the gear box of the mechanical driver and provision is made for selecting any desired portion of the cycle. This is of importance in connection with reducing the effects of scattering, as discussed in the next paragraph.

THE EFFECT OF SCATTERING BY THE SAMPLE

The voltage pulse from the ionization chamber is primarily caused by the absorption of neutrons in the sample. It is found, however, that by

oscillating a piece of graphite which has negligible absorption, a signal may also be generated by the scattering of the sample. To make the oscillator a satisfactory instrument for absorption cross-section measurements, the effects of scattering must be largely eliminated. Toward this end the voltage pulses produced by absorbers and scatterers have been studied for both the *A* and *B* types of chambers. With the *A*-type chamber, which was located below the oscillating sample, the absorption and scattering signals are so similar that their effects cannot be separated. With the *B*-type chamber, which is coaxial with the oscillating sample, the signal from a nearly pure scatterer is considerably different from that resulting from a sample with a large absorption cross section. This can be seen from the patterns shown in Fig. 3 which were traced from an oscilloscope with an approximately linear sweep on the horizontal plates. The trace started at the left each time the oscillating sample reached its outermost position. Thus two traverses through the chamber appear on each sweep, the first as the sample moves into the pile, the other as it moves out. One of the vertical deflection plates of the oscilloscope was connected to the last stage of the amplifier, ahead of the rectifier and integrator.

Figures 3c and 3d were taken with the amplifier normally used with the equipment, Figs. 3a and 3b with a specially constructed amplifier having extended low and high frequency responses. Traces *b* and *d* are reproductions of the signal shape with graphite in the boat; traces *a* and *c* were obtained by putting cadmium in the boat and reducing the amplifier gain by a factor of 4.

One observes that the scattering signal is opposite in sign, has a steeper rise, and reaches its maximum at an earlier time than the absorbing signal. This can be explained if one assumes that the scattering signal arises chiefly from neutrons which are scattered out of a beam of neutrons streaming down the channel. Neutrons that otherwise would have passed through the central hole of the chamber without being detected are deflected into the chamber by the sample which blocks the channel. This is substantiated by the results obtained when graphite rods are attached to either side of the boat and oscillate with it. In this instance one still obtains a scattering signal caused by the hole in the boat, but, since

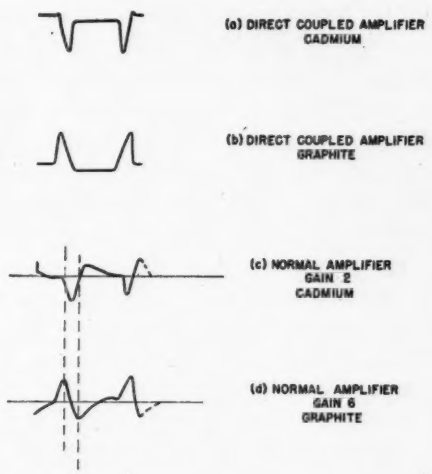

FIG. 3. Wave forms of voltage from amplifier for one complete stroke of sample past the ionization chamber. a and c correspond to pure absorption (cadmium) and b and d to pure scattering (graphite).

the channeling of the neutrons is largely eliminated, the amplitude of the signal is much reduced.

The low frequency response of the amplifier normally used with the pile oscillator has a considerably higher low frequency cut-off than the special amplifier previously referred to, so that transients and low frequency disturbances are very much reduced in the actual measurements. This causes considerable distortion of the signal as shown in (c) and (d). By phasing the rectifying switch so that signal integration occurs only during the interval indicated between the two vertical lines, the galvanometer deflection because of a scatterer can be made very small. With an

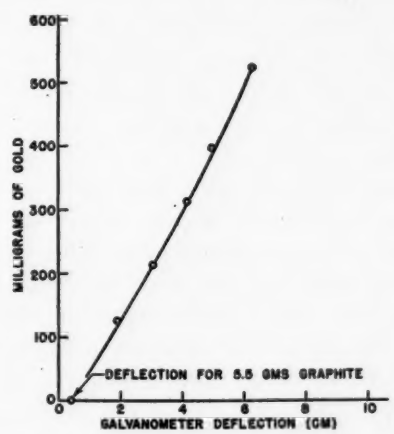

FIG. 4. Galvanometer deflection *versus* amount of gold.

TABLE I. Thermal neutron absorption cross sections of indium and silver.

Sample	σ (barns) Run 1	Run 2	Run 2	Av.	Absorption cross section of sample in mm²
In (153 mg)	189.5	192.7	191.5	191.2	15.3
In (5.0 mg)	186	197	224	202	0.5
Ag^{107} (444 mg. 90%)	29.0	30.8		29.9	9.7
Ag^{109} (373 mg. 92%)	83.9	83.5		83.7	16.6
$0.52\sigma^{107}+0.48\sigma^{109}$	55.6	56.2		55.9	
Natural Ag (357 mg)	59.2	60.5		59.8	11.6

absorbing sample, integration over this same time interval produces a large deflection. It is by this means that we have been able to measure small absorption cross sections without correcting for the scattering by the sample. Evidence for this can be seen from Fig. 4, where the boat was loaded with 5.5 g of carbon corresponding to 132 mm² of scattering cross section and 0.13 mm² of absorption cross section. With the *A* type chamber, 20 mm² of scattering cross section were required to give a signal equal to that produced by 1 mm² of absorption cross section. Although a scattering signal of this size is of minor significance when measurements are being made on materials with large capture cross sections, it would introduce large errors with materials having small capture cross sections. With the *B*-type chamber it was found that by carefully adjusting the rectifier switching points, the scattering effects were reduced to the point where equal scattering and absorption cross section in the sample gave signals in the ratio of 1 to 200. Under these conditions the effects of scattering need only be considered when the samples to be measured have absorption cross sections of a fraction of a barn. When the scattering cross section of a sample is known, corrections can be made for it by subtracting from the over-all response the signal yielded by a graphite sample having the same scattering cross section as the unknown absorber.

Although no extensive theory of the scattering effect has been developed, there are certain qualitative observations concerning scattering which are relevant. The scattering signal should vanish identically if the neutron flux were every where the same, since as many neutrons will be scattered into a given solid angle as are scattered out of it. Under ideal circumstances the oscillator should therefore be placed at some point in the pile where the flux is constant over a distance of a few mean free paths.

Since such a position of uniform flux was not available, it was necessary to place the ion chamber in a region where the flux had gradients both in directions parallel and perpendicular to the direction of oscillation. In a spatially varying neutron flux a pure scatterer will perturb the neutron density in its neighborhood because it blocks neutrons originating in a region of high flux from reaching the region of low flux. A chamber placed on the low neutron intensity ("downstream") side of a scatterer will record a lower signal than when the scatterer is absent, while if the chamber is placed on the high-neutron-intensity side the opposite will be true. Thus, if a chamber is arranged to surround the scatterer, it is plausible to suppose that, to a first approximation, the scatterer will give no signal.

In the actual arrangement in which the chamber is coaxial with the oscillating sample, the effect of the transverse gradient is fairly well eliminated. There is still a large longitudinal gradient and there is a beam of neutrons flowing through the channel. As stated previously, we believe the deflection into the chamber of neutrons streaming down the channel to be the chief cause of the observed scattering signal.

There is one other consequence of using a coaxial chamber and that is a hardening of the neutrons at the center of the chamber as a result of absorption of slow neutrons by the surrounding boron. This can be reduced at some sacrifice in sensitivity by keeping the boron coating thin.

PERFORMANCE

There are certain obvious factors which must be considered in order that accurate measurements of absorption cross sections can be made with the pile oscillator. The scattering effect has been considered separately because it has a fundamental bearing on the design and properties of the instrument. The interpretation of cross-section measurements which involve a comparison of the effects produced by two absorbers placed alternately in a thermal neutron flux must be considered. A standard with which to compare other materials must be chosen for which the cross section is accurately known. We have used gold as a standard since it fulfills the above re-

quirement and in addition its cross section has a $1/v$ dependence in a thermal region. If the unknown absorber sample also has a $1/v$ dependence, a comparison with gold will give an unambiguous value for the cross section of the unknown. If the sample in question has a cross section with an unknown energy dependence, then any comparison method will give some average cross section for the existing neutron energy spectrum. The energy spectrum of the neutrons at the center of the chamber has been investigated by measuring the activity of indium foils with and without cadmium covers. A cadmium ratio of 35 was obtained, showing that the neutrons are well thermalized. Further evidence for this is seen in Table I where the cross section of indium as measured with the pile oscillator agrees very closely with the value of $\sigma_{In}(0.025 \text{ ev}) = 190$ barns obtained by McDaniel[5] and Borst.[6]

As with all cross-section measurements the preparation of the samples with respect to their purity, their physical shape, and their location in the sample carrier must be considered. The samples should be made thin enough so that the corrections for self-absorption are small. Since the measurement involves a comparison, best results can be achieved if the unknown samples and the standard are made as nearly alike as possible with respect to shape, location in the boat, and amount of self-protection.

The amplifier and integrator are subject to the characteristic limitations of electronic equipment. Although the sensitivity changes slightly from day to day, drifts in the instrument are negligible over the period of time necessary to make a measurement. A device has been installed to check the instabilities throughout the electronic circuit and switching mechanism. It consists of an artificial signal which can be introduced to the first stage of the amplifier. The repetition rate of the signal is controlled by the reciprocator wheel, as is the absorber signal, and its amplitude can be adjusted to approximate the absorber signal from the ion chamber. Measurements with these artificial signals from time to time indicate that the major part of the variations between successive sample determinations are not ascribable to the electrical circuits but are due largely to fluctuations in the current in the ionization chamber and in the neutron density. The average neutron density during a series of measurements is held constant to within less than 0.5 percent. The signals which arise from fluctuations in neutron density and in ionization chamber current should be random and should give a small residual signal which causes a variation in successive absorber signal readings. The maximum over-all variation in the integrated signal in terms of the average gold value is about 0.2 mm² and the average deviation from the mean is usually less than 0.1 mm².

RESULTS

The absorption cross sections of a number of elements and isotopes have been measured with this apparatus and these will be reported in a separate paper. The values obtained for indium and silver are reported here in Table I to give some indication of the capabilities of the apparatus. The atomic absorption cross sections are expressed in barns (10^{-24} cm²) on the basis of $\sigma_{Au}(0.025 \text{ ev}) = 95$ barns.

The second row in the table is included to show that the apparatus is capable of measuring small samples of material. The results quoted in the third and fourth rows were derived from measurements on two samples of enriched silver isotopes obtained from the electromagnetic separation plant. One sample was enriched to 90.2 percent of Ag^{107} and the other to 92.2 percent of Ag^{109}. The fifth row gives the values to be expected for natural silver on the basis of the above measurements of the isotopic mixtures, and the last row gives the measured cross section of natural silver. The small discrepancy between the values may be due to contamination of the natural silver sample. Havens and Rainwater[7] have quoted a value of $\sigma_{Ag}(0.025 \text{ ev}) = 57.3$ barns for natural silver.

ACKNOWLEDGMENTS

The authors are indebted to Dr. A. M. Weinberg for the very considerable encouragement and assistance which he has given in the develop-

[5] B. D. McDaniel, Phys. Rev. **70**, 832 (1946).
[6] Borst, Ulrich, Osborne, and Hasbrouck Phys. Rev. **70**, 557 (1946).
[7] W. W. Havens, Jr., and L. J. Rainwater, Phys. Rev. **70**, 154 (1946).

ment of the instrument and the cross-section measurement program. They are also indebted to G. H. Goertzel and H. C. Schweinler for valuable discussions on various problems which have been encountered.

This document is based on work performed under Contract Number W-35-058, Eng. 71 for the Atomic Energy Project, and the information covered therein will appear in the National Nuclear Energy Series (Manhattan Project Technical Section) as part of the contribution of the Oak Ridge National Laboratory.

PHYSICAL REVIEW VOLUME 74, NUMBER 8 OCTOBER 15, 1948

Radioactive Br Isotopes

L. L. WOODWARD,* D. A. McCOWN,** AND M. L. POOL
The Ohio State University, Columbus, Ohio

(Received July 2, 1948)

A radioactive isotope of 2.4-day half-life has been produced in bromine by deuteron bombardment of electromagnetically enriched Se^{76}, and by alpha-particle bombardment of electromagnetically enriched Se^{74}. Assignment of the isotope is made to Br^{77}. A positron end point of 0.4 Mev is determined. In addition to annihilation radiation, gamma-rays and K-capture are observed. The ratio of K-capture to positron emission is determined to be 20. The cross-section ratio of the (d, n) to the $(d, 2n)$ reaction producing the isotope is 0.3. The ratio of the sum of the cross sections for formation of Br^{77} by $Se^{76}(d, n)$ and $Se^{77}(d, 2n)$ to the cross section for Br^{82} by $Se^{82}(d, 2n)$ is 0.4. A radioactive isotope of 1.7-hour half-life has been produced in bromine by deuteron bombardment and by proton bombardment of enriched Se^{74}. Assignment of the isotope is made to Br^{75}. A positron end point of 1.6 Mev is determined. K-capture is observed in the activity. No gamma-ray activity other than that due to annihilation is found. The ratio of K-capture to positron emission from the $Se^{74}(d, n)$ reaction is determined to be 4.4. The ratio of the cross section for formation of Br^{75} by $Se^{74}(d, n)$ to that of Br^{82} by $Se^{82}(d, 2n)$ is 2.1. The 4.4-hour Br^{80} isotope has been produced by a $Se(\alpha, p)$ reaction and found to emit positrons with an end point of 0.8 Mev. In producing Br^{77} by proton bombardment of Se the (p, γ) reaction is observed to be two-thirds as probable as the (p, n) reaction.

CYCLOTRON bombardments have been made with alpha-particles, deuterons, and protons on electromagnetically enriched selenium.*** Samples in which the stable isotope Se^{74} was enriched from 0.9 percent to 14.1 percent and samples in which the stable isotope Se^{76} was enriched from 9.5 percent to 41.5 percent were used. For comparison purposes, bombardments were also made with Hilger selenium.

As a result of these bombardments, two previously unreported radioactive isotopes in bromine have been found. The location and characteristic radiations of these isotopes, and also results of investigations on the 4.4-hour Br^{80} isotope, will be presented in this paper.

* Lt. Col., U.S.A.F. Research under auspices of Air University, Maxwell Air Force Base, Montgomery, Alabama.
** Captain, U.S.A.F. Research under auspices of Air University, Maxwell Air Force Base, Montgomery, Alabama.
*** Supplied by the Y-12 plant, Carbide and Carbon Chemicals Corporation, through the Isotopes Division, U. S. Atomic Energy Commission, Oak Ridge, Tennessee.

THE 2.4-DAY Br^{77} ISOTOPE

Samples of enriched stable Se^{74} and Se^{76} isotopes were prepared for alpha-particle bombardment by pressing equal amounts by weight of the finely ground selenium into the bottom of aluminum target holders under approximately 5000 pounds pressure. The two targets were bombarded simultaneously in the cyclotron by means of a rotating probe.

Figure 1 shows the decay of total activity obtained in each of the samples from this bombardment. A new activity of 2.4-day half-life appeared in the Se^{74} sample but not in the Se^{76} sample, in which only 0.5 percent of stable Se^{74} was present. It was concluded that this 2.4-day period was formed from Se^{74} and must belong either to Kr^{77} or Br^{77}.

To locate the activity, samples of enriched Se^{74} and Se^{76} were bombarded simultaneously with deuterons. The samples were prepared for bombardment in a manner similar to that in the

experiment above. Figure 2 shows the decay curves of Br activity from the two samples. Measurements were taken on a Wulf electrometer attached to a Freon-filled ionization chamber. To obtain the γ-activity curves, a $\frac{1}{4}$-inch aluminum absorber was inserted between the sample and the ionization chamber. This amount of absorber was sufficient to stop all β-radiation and x-ray radiation present. In both samples, the established 34-hour Br^{82} activity and the new 2.4-day activity appeared. The 34-hour Br^{82} activity appeared in nearly equal intensities in both samples since the parent Se^{82} isotope was present in approximately equal percentages in both cases and since equal amounts by weight of the two samples were bombarded. The 2.4-day activity appeared in the Se^{76} sample approximately 28 times as strong as in the Se^{74} sample. Since stable Se^{76} was 28 times as abundant in the Se^{76} sample as in the Se^{74} sample, it was concluded that the 2.4-day activity was that of a Br isotope formed by deuteron bombardment of Se^{76}. Since bombardment of Se with alpha-particles had previously located the activity as either Kr^{77} or Br^{77}, assignment of the activity was made to Br^{77}.

To determine the character of beta-activity in the 2.4-day period, a sample of Br activity from deuteron bombardment of enriched Se^{76} was placed in an electromagnetic field, with a Geiger counter tube located so as to intercept either β^-- or β^+-activity separately, according to the direction of the magnetic field. Figure 3 shows the decay curves obtained from these measurements. In addition to the gamma- and β^--decay curves of the 34-hour Br^{82} period, a 2.4-day positron activity appeared. From the decay curve of this activity it was determined that the Br^{77} isotope emits positrons.

Figure 4 shows the results of aluminum absorption measurements of Br activity from deuteron bombardment of enriched Se^{76}. Measurements of activity were taken with various thicknesses of aluminum absorber placed between the sample and an ionization chamber. The curve of β-activity was obtained by a subtraction of the curve representing electromagnetic activity from the curve representing total activity. A beta-end point of 0.097 g/cm², corresponding to 0.36 Mev by the Sargent range-energy relation, and a beta-end point of 0.172 g/cm², corresponding to 0.50 Mev, were determined. The former was attributed to the 2.4-day Br^{77} activity, and the latter to the 34-hour Br^{82} activity. The end point of the 2.4-day Br^{77} period was confirmed by beta-ray spectrometer measurements.

Figure 5 shows the decay of x-ray activity in the 2.4-day Br^{77} period. The activity was obtained from simultaneous $Se^{76}+d$ and $Se^{74}+d$ bombardments of equal amounts of enriched selenium. Ionization measurements of $(x+\gamma)$-activity were taken with a magnetic field so situated as to prevent all beta-radiation from entering the ionization chamber. The curves of γ-activity were obtained by inserting a $\frac{1}{4}$-inch aluminum absorber between the sample and the ionization chamber. The difference between the curve of $(x+\gamma)$-activity and the curve of γ-activity then represented the activity from the sample due to x-ray radiation. Curves representing this x-ray activity from both bombardments are shown in Fig. 5. In both samples a 2.4-day half-life was determined as the period of the x-ray activity. In the Se^{76} sample this activity appeared with approximately 4.4 times the intensity of the x-ray activity in the Se^{74} sample. Since stable Se^{76} was 4.4 times as abundant in the Se^{76} sample as in the Se^{74} sample, it was concluded

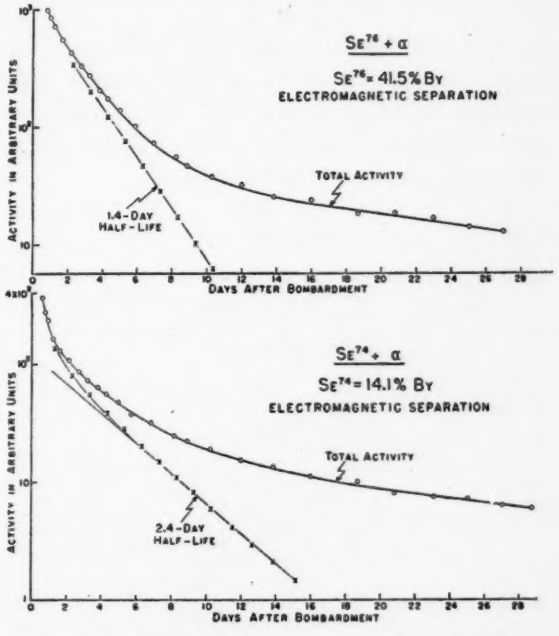

FIG. 1. A comparison of total activity decay from alpha-particle bombardment of enriched Se^{74} and Se^{76}. The new 2.4-day Br^{77} period is shown in the Se^{74} sample.

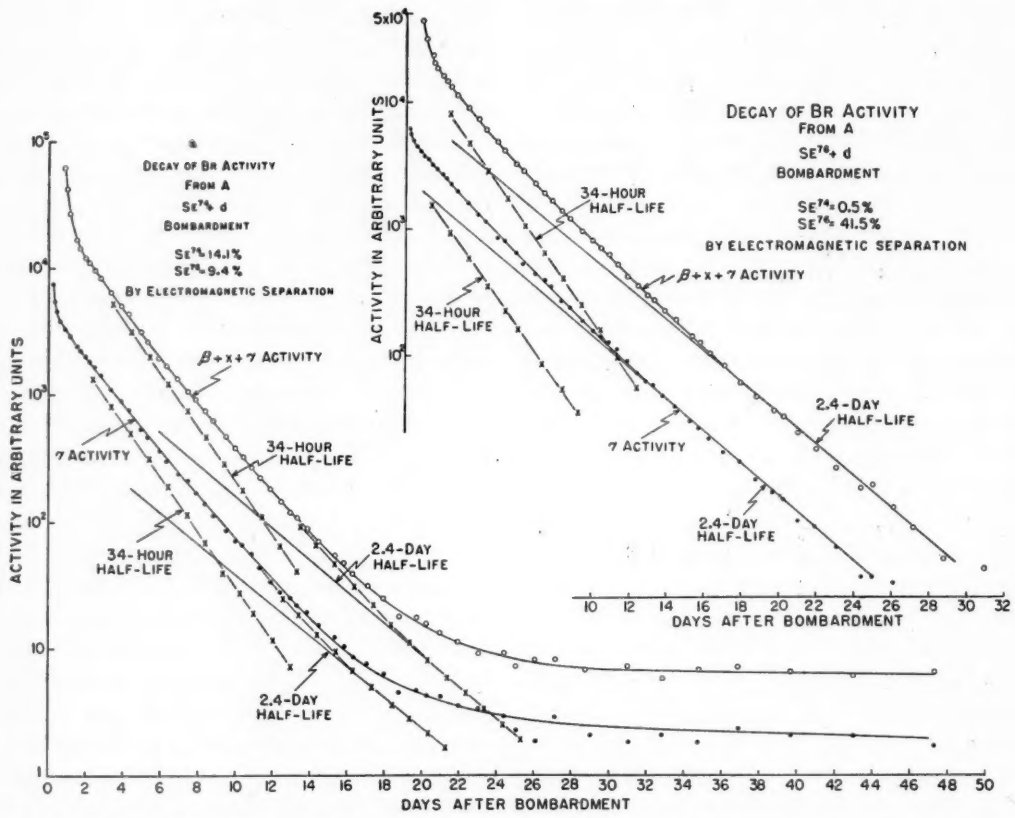

FIG. 2. A comparison of Br activity decay curves from deuteron bombardment of enriched Se^{74} and Se^{76}. The 2.4-day Br^{77} period is found more intense in the Se^{76} sample.

that the Br^{77} isotope emits x-ray radiation. From energy considerations it was determined that this radiation was not due to the "bremsstrahlung" effect. It was thus determined that the K-capture process occurs in the Br^{77} isotope.

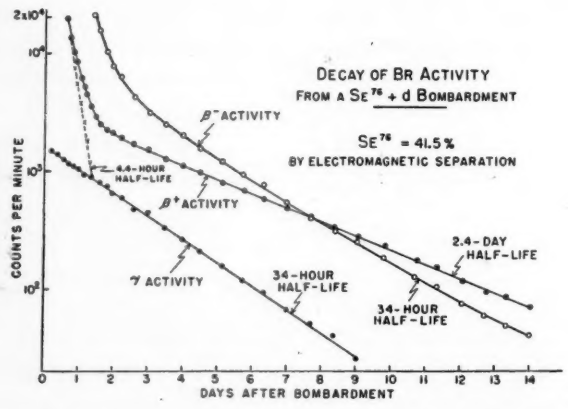

FIG. 3. Decay curves of β^-- and β^+-activity in Br from deuteron bombardment of enriched Se^{76}. β^+-activity of the 2.4-day Br^{77} period and the 4.4-hour Br^{80} period are shown.

The ratio of K-capture processes to positron emissions in Br^{77} is computed to be 20. This ratio was obtained by a determination of saturation intensities and by corrections made for the relative ionization produced by beta radiation and x-ray radiation in the energy ranges involved. The ratio of reaction cross sections for the

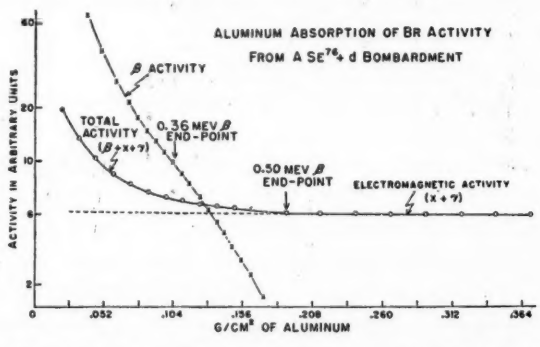
ALUMINUM ABSORPTION OF BR ACTIVITY FROM A Se⁷⁶+ d BOMBARDMENT
β ACTIVITY
TOTAL ACTIVITY (β+x+γ)
0.36 MEV β END-POINT
0.50 MEV β END-POINT
ELECTROMAGNETIC ACTIVITY (x+γ)
ACTIVITY IN ARBITRARY UNITS
G/CM² OF ALUMINUM

FIG. 4. Aluminum absorption measurements showing the 0.36-Mev positron end point of the 2.4-day Br^{77} period. The 0.50-Mev end point of the 34-hour Br^{82} period is also shown.

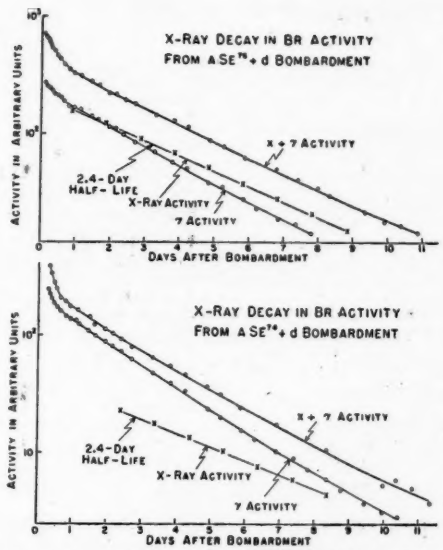

FIG. 5. A comparison of x-ray decay in Br activity from simultaneous deuteron bombardment of enriched Se^{74} and Se^{76}. X-ray activity from the 2.4-day Br^{77} period is seen to be stronger in the Se^{76} sample.

$Se^{76}(d, n)$ and $Se^{77}(d, 2n)$ processes forming the Br^{77} isotope is approximately 0.3. The rate at which the 2.4-day Br^{77} period is produced compared to that of the 34-hour Br^{82} period by deuteron bombardment of selenium is approximately 0.4.

Gamma-ray activity in addition to that due to annihilation is observed in the Br^{77} period.

THE 1.7-HOUR Br^{75} ISOTOPE

A 1.7-hour half-life has been observed in Br activity from simultaneous deuteron bombardment of equal amounts of enriched Se^{74} and Se^{76}. Figure 6 shows a comparison of this 1.7-hour activity in the Se^{74} and Se^{76} samples. A Br^{80} β^--activity of 4.4-hour half-life appeared in both samples. The activity was somewhat stronger in the Se^{74} sample than in the Se^{76} sample due to the fact that the Se^{74} sample contained 40.4 percent of the parent Se^{80}, while the Se^{76} sample contained 30.2 percent of Se^{80}. Gamma-ray activity, due to 34-hour Br^{82}, was also found in both samples. In addition to these periods, a β^+-activity of 1.7-hour half-life appeared in both samples. The intensity of this activity in the Se^{74} sample was greater than that in the Se^{76} sample by a factor equal to the enrichment of stable Se^{74} in the two samples. It was then concluded that the 1.7-hour positron activity was produced by deuteron bombardment of stable Se^{74}.

Simultaneous proton bombardments of equal amounts of enriched Se^{74} and Se^{76} were also made. Figure 7 shows the decay of activity from the $Se^{74}+p$ bombardment, and Fig. 8 the decay of activity from the $Se^{76}+p$ bombardment. Measurements were made with the samples in an electromagnetic field to separate β^-- and β^+-activity. Activities of the 4.4-hour Br^{80} and 34-hour Br^{82} periods appeared in both samples in intensities proportional to the abundance of stable parent isotopes present. The increased

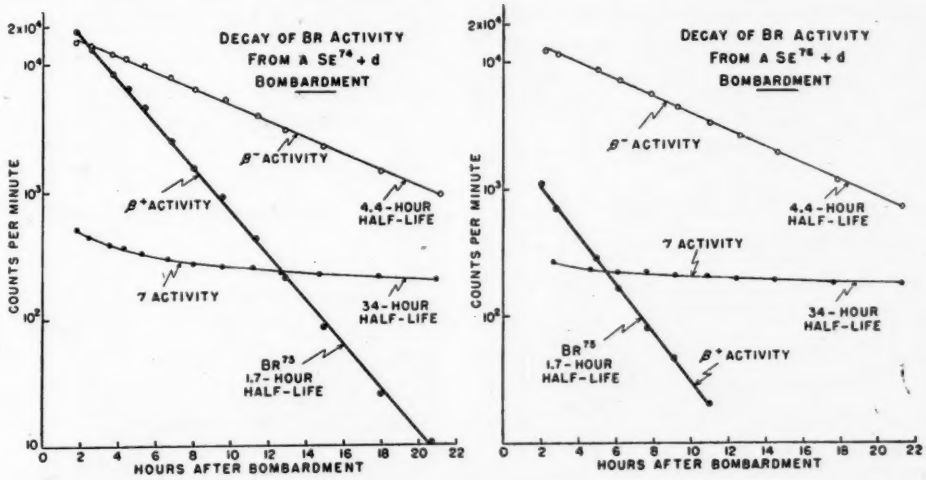

FIG. 6. A comparison of β^-- and β^+-activity in Br from simultaneous deuteron bombardment of enriched Se^{74} and Se^{76}. β^+-activity in the 1.7-hour Br^{75} period is seen to be stronger in the Se^{74} sample than in the Se^{76} sample.

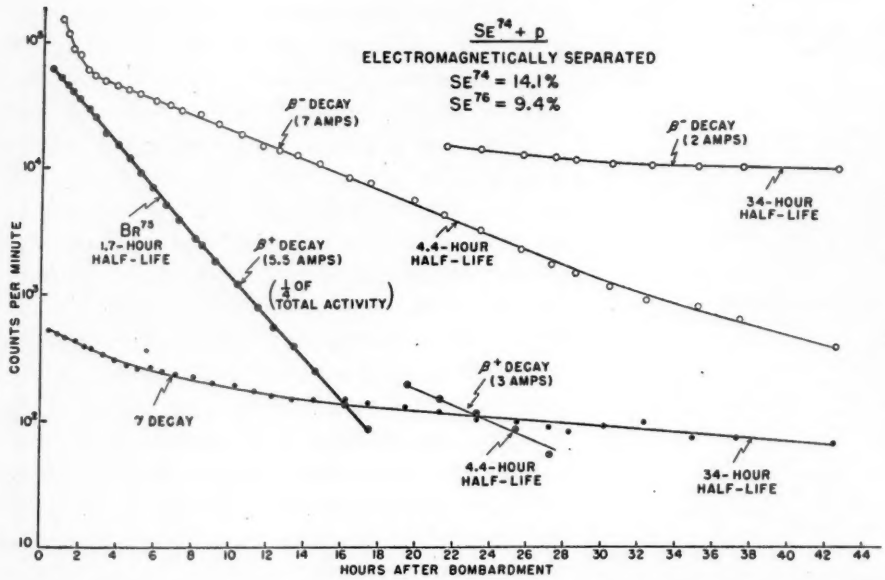

FIG. 7. Decay of activity from proton bombardment of enriched Se^{74}. Strong β^+-activity in the 1.7-hour Br^{75} period is shown. β^+-activity in the 4.4-hour Br^{80} period is also shown. Currents used in producing the electromagnetic field for separating β^-- and β^+-activity are shown for the various decay curves.

intensity of the 1.7-hour half-life in the Se^{74} sample over that in the Se^{76} sample indicated that the activity was produced by proton bombardment of stable Se^{74}.

As a guide to the likelihood of a (p, γ) reaction taking place to produce the 1.7-hour Br activity, the relative probability of the (p, n) to the (p, γ) reactions in forming 2.4-day Br^{77} was estimated. The observed intensities of Br^{77} activity, from simultaneous proton bombardments of enriched Se^{74} and Se^{76}, were compared with known abundances of Se^{76} and Se^{77} present in the two samples. From these comparisons it was determined that in producing Br^{77} by proton bombardment of selenium the ratio of the (p, n) to (p, γ) reactions is 1.5. It is therefore quite possible that the 1.7-hour Br activity is formed by the $Se^{74}(p, \gamma)$ reaction.

In the decay curve of activity from $Se^{74}+p$ bombardment, a 125 ± 5-day half-life appeared

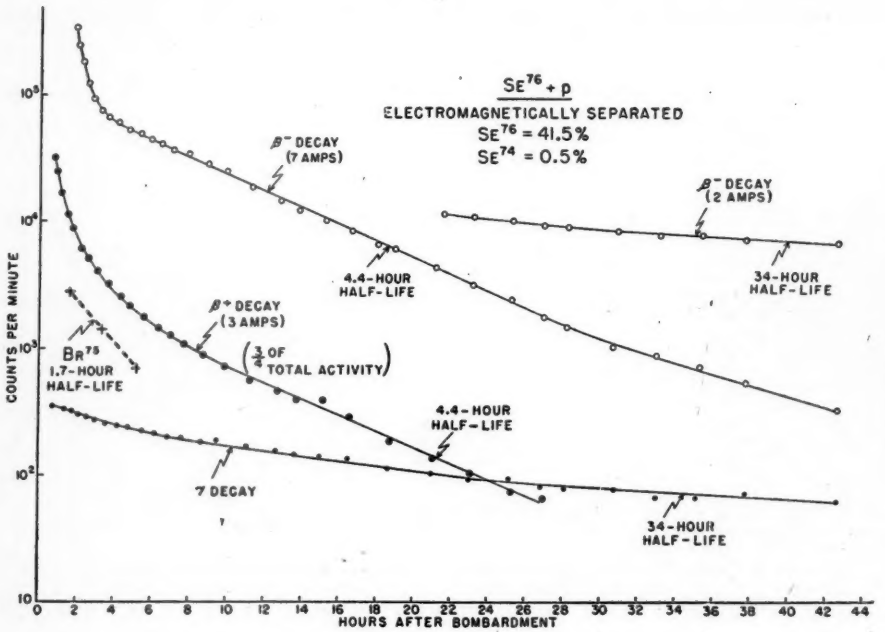

FIG. 8. Decay of activity from proton bombardment of enriched Se^{76}. Weak β^+-activity in the 1.7 hour Br^{75} period is shown. β^+-activity in the 4.4-hour Br^{80} period is also shown. Currents used in producing the electromagnetic field for separating β^-- and β^+-activity are shown for the various decay curves.

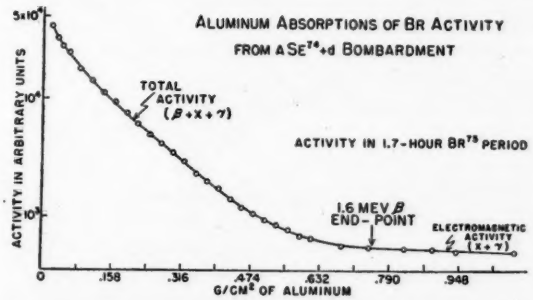

FIG. 9. Aluminum absorption measurements showing the 1.6-Mev positron end point of the 1.7-hour Br^{75} period.

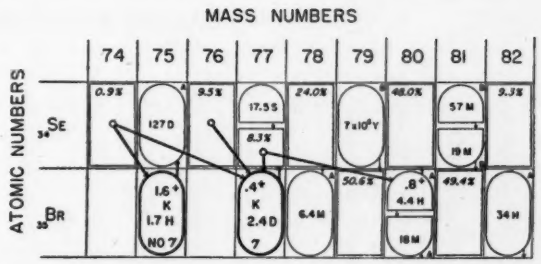

FIG. 10. Se and Br section of the periodic table. The new Br^{77} and Br^{75} isotopes and new reactions reported are indicated by heavy lines.

which was presumed to be that of Se^{75}. The ratio of reaction cross sections for production of the 1.7-hour Br activity compared to the 127-day Se^{75} activity by proton bombardment was determined to be approximately one. This indicated that the 1.7-hour Br activity decays into the 127-day Se^{75} period. From this data, assignment of the 1.7-hour activity was made to Br^{75} as a $Se^{74}(p, \gamma)$ reaction.

Figure 9 shows the results of aluminum absorption measurements of Br^{75} activity from deuteron bombardment of enriched Se^{74}. The end-point energy of Br^{75} positron emission was determined to be 0.75 g/cm², corresponding to 1.6 Mev.

The presence of x-ray emission due to K-capture in the Br^{75} period was determined in the manner described in the preceding section. The ratio of K-capture processes to positron emissions in Br^{75} from deuteron bombardment of selenium is approximately 4.4. The rate at which 1.7-hour Br^{75} is produced by the $Se^{74}(d, n)$ reaction compared to the rate at which Br^{82} is produced by $Se^{82}(d, 2n)$ is approximately 2.1.

No gamma-radiation, other than that due to positron annihilation, was found in the 1.7-hour Br^{75} activity.

THE 4.4-HOUR Br^{80} ISOTOPE

A 4-hour Br^{80} period was first reported[1] as a result of slow neutron bombardment of bromine. Emission of negatively charged beta-particles in the Br^{80} period was reported[2] as a result of neutron and deuteron bombardments of bromine, and also[3] as a result of proton bombardment of selenium. It has also been reported[4] that most of the nuclei in the upper 4.4-hour isomeric state of Br^{80} decay by falling into the lower 18-minute state from which observed disintegration electrons are emitted. Existence of 49 kev and 37 kev internally converted gamma-rays from the 4.4-hour Br^{80} period has been shown.[5]

Figures 7 and 8 show a 4.4-hour bromine β^+-activity resulting from proton bombardment of enriched Se^{74} and Se^{76}. By comparing the activities of this period with the abundance of Se^{80} present in the two samples, it was determined that the 4.4-hour β^+-activity was due to the Br^{80} period. By spectrometer measurements the end point of the 4.4-hour Br^{80} β^+-activity was estimated to be approximately 0.8 Mev.

Figure 3 shows β^+-activity of the 4.4-hour Br^{80} period resulting from deuteron bombardment of selenium.

The 4.4-hour Br^{80} period was also obtained by alpha-particle bombardments of selenium.

Figure 10 shows the Se and Br section of the periodic table. The new Br^{77} and Br^{75} isotopes and new reactions reported are indicated by heavy lines.

ACKNOWLEDGMENTS

The support received from the Ohio State University Development Fund and the Graduate School is gratefully acknowledged. The significant chemical separations which were necessary in this work were very ably performed by Mr. H. L. Finston and Mr. R. M. Dyer.

[1] M. L. Pool, J. M. Cork, and R. L. Thornton, Phys. Rev. **52**, 239 (1937).
[2] A. H. Snell, Phys. Rev. **52**, 1007 (1937).
[3] J. H. Buck, Phys. Rev. **54**, 1025 (1938).
[4] E. Segrè, R. S. Halford, and G. T. Seaborg, Phys. Rev. **55**, 321 (1939).
[5] G. E. Valley and R. L. McCreary, Phys. Rev. **56**, 863 (1939).

Argon 40 in Potassium Minerals

L. T. ALDRICH AND ALFRED O. NIER
Department of Physics, University of Minnesota, Minneapolis, Minnesota
(Received July 8, 1948)

An investigation has been made of the isotopic composition of the argon from four potassium minerals. In each case a high A^{40}/A^{36} ratio compared to that of atmospheric argon is observed showing directly that K^{40} decays to both Ca^{40} and A^{40}. From the absolute amounts of radiogenic A^{40} and K^{40} in the minerals a lower limit on the branching ratio λ_K/λ_β can be made. If the half-life, 7×10^8 yrs., is assumed for $K^{40}\rightarrow Ca^{40}$, λ_K/λ_β must be at least 0.02. The possibility of using this method for measuring geological age is suggested.

IT was suggested by von Weizsäcker[1] in 1937 that the abnormally high abundance of A^{40} in argon might be explained by assuming that K^{40} not only decays to Ca^{40} through β-emission but also to A^{40} through K-capture. Indirect evidence to support this view has been obtained by a number of investigators.[2–6] Bleuler and Gabriel[7] studied the X-radiation emitted during the decay process of potassium and concluded that there are 1.9 times as many K-captures occurring as there are β-rays emitted. Suess[8] was unsuccessful in his search for argon in sylvine and carnallite minerals and concluded from this investigation together with general geological considerations that the branching ratio, λ_K/λ_β, was 0.05 ± 0.02.

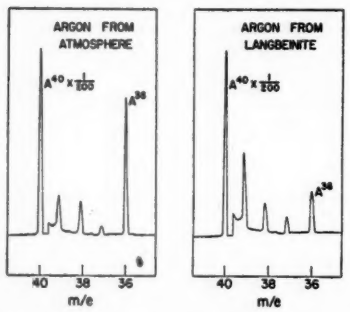

FIG. 1. Mass spectra for atmospheric argon and for argon from mineral Langbeinite. Note that this mineral has an A^{40}/A^{36} ratio greater than three times that for atmospheric argon. Peaks at 37 and 39 and part of 38 are due to residual impurities in spectrometer. There were no detectable residual impurity peaks at either mass 36 or 40.

An investigation of the gas evolved from four potassium minerals has been made with a high sensitivity mass spectrometer. In all cases small amounts of argon were discovered and in each case the A^{40}/A^{36} ratio was appreciably greater than that observed for atmospheric argon. Figure 1 shows a comparison between the spectra observed for atmospheric argon and for the argon found in one of the minerals.

The procedure employed in extracting the argon from the minerals was as follows: A weighed amount of the mineral was introduced into a high temperature vacuum furnace which was heated to a temperature above 1000°C. The condensable vapors were removed by a liquid oxygen trap. If the amount of gas remaining after this treatment was less than 20 std. cc, an investigation of the A^{40}/A^{36} ratio was made directly without further purification. The extremely high sensitivity of the spectrometer permitted one to do this. For samples larger than 20 std. cc the argon concentration was too low to permit accurate isotope analysis and the gas was further purified with hot lithium metal. The principal impurity which diluted the argon was nitrogen. That the lithium treatment had no effect on the A^{40}/A^{36} ratio was shown in a test in which this ratio was determined in a sample of air before and after purification.

Table I contains pertinent data for the minerals investigated. From the data in column 6 together with the ages of the minerals and the decay constant for $K^{40}\rightarrow Ca^{40}$ one may compute the branching ratio. The results of such calcula-

[1] C. v. Weizsäcker, Physik. Zeits. **38**, 623 (1937).
[2] F. C. Thompson and S. Rowlands, Nature **152**, 103 (1943).
[3] L. H. Gray and G. T. P. Tarrant, Proc. Roy. Soc. **A143**, 681 (1934).
[4] O. Hirzel and H. Wäffler, Helv. Phys. Acta **19**, 216 (1946).
[5] E. Gleditsch and T. Graf, Phys. Rev. **72**, 640 (1947).
[6] H. A. Meyer, G. Schwachheim, and M. D. deSousa Santos, Phys. Rev. **71**, 908 (1947).
[7] E. Bleuler and M. Gabriel, Helv. Phys. Acta **20**, 67 (1947).
[8] H. E. Suess, Phys. Rev. **73**, 1209 (1948).

TABLE I. Data for several potassium minerals.

Mineral	Total wt. grams	Potassium* grams	Argon std. cc	Radiogenic A^{40} std. cc†	g radio. A^{40}§ / g K-40	Age of mineral $\times 10^{-9}$ yr.	Branching ratios for three half-lives 4×10^{9} yr.	7×10^{9}	14×10^{9}
Orthoclase	450	62	0.31	0.25	7.0×10^{-2}	14	0.007	0.02	0.07
Microcline	450	72	0.10	0.035	0.8×10^{-2}	3.5	0.010	0.02	0.04
Sylvite	250	135	0.08	0.011	0.13×10^{-2}	2.0	0.003	0.006	0.013
Langbeinite	400	80	0.065	0.045	0.9×10^{-2}	2.0	0.02	0.04	0.09

* This column was estimated from the accepted composition of the mineral. Slight impurities would lower this number.
† This column computed from the measured A^{40}/A^{36} ratio for the mineral and that for air. It was assumed that the non-radiogenic argon had the composition of present-day atmospheric argon.
§ There is good reason to feel that the errors in analysis together with the assumptions made in computation should not affect this ratio by more than 25 percent.

tions are shown for three different assumed decay constants.

Since an exact determination of the potassium content of the mineral was not made, the amount of potassium present is at most that given. Moreover, since it is assumed that the non-radiogenic argon had the composition of present-day atmospheric argon and that no leakage of radiogenic argon occurred during the life of the mineral, the ratio given in column 6, if in error, is too small and would therefore give a minimum value for the branching ratio. Since the branching ratio computed here depends upon the assumed value for the half-life of $K^{40}\rightarrow Ca^{40}$, no definite value can be decided upon until this constant is better established. All three values used here have appeared in the literature.

It is seen from columns 8–10 of the table that there is reasonable agreement among the values of the branching ratio obtained except in the case of sylvite. The low value for the branching ratio for sylvite could be attributed to the leakage of argon from the mineral. The fair agreement obtained for the branching ratio from the other three minerals indicates that with improved techniques in carrying out experimental work of this type, together with a careful redetermination of the half-life of K^{40}, the $K^{40}\rightarrow A^{40}$ decay might become extremely useful in the measurement of geological time.

ACKNOWLEDGMENTS

The mineral samples used in this study were very generously supplied through the courtesy of Professor E. L. Tullis of the South Dakota School of Mines, Professor Adolph Knopf of Yale University, Dr. W. F. Foshag of the U. S. National Museum, and Dr. J. P. Marble, Chairman of the National Research Council Committee on Measurement of Geological Time. The apparatus employed was constructed through a grant from the Graduate School and the Minnesota Technical Research Fund subscribed to by General Mills, Inc., Minneapolis Star-Journal and Tribune, Minnesota Mining & Manufacturing Company, Northern States Power Company, and Minneapolis Honeywell Regulator Company.

The research was made possible by Navy Contract N5ori-147, T. O. III, between the Office of Naval Research and University of Minnesota.

On the Momentum Distribution of the Decay Electrons from Negative Mesons*, **

H. PRIMAKOFF
Washington University, St. Louis, Missouri

(Received June 2, 1948)

The momentum distribution of decay electrons from negative mesons bound in K-orbits is calculated assuming a two-particle disintegration of the meson into an electron and a neutrino or neutretto. The resultant momentum distribution has a spread $\cong Z/137 p_e^{(0)}$, where $p_e^{(0)}$ is the momentum of the decay electron from a free and stationary meson. The effect of the meson's binding on its mean life for decay is also considered and a small decrease in the mean life, $\cong (Z/137)^2 \times 100$ percent, is found.

ABUNDANT evidence now exists that the 2.2 microsecond decay process[1] associated with a (positive or negative) meson of 100 Mev rest energy[2] results in the emission of a (positive or negative) electron.[1] Conservation of momentum and of charge demand, in addition, the simultaneous emission of at least one neutral particle. At the moment, neither the number of neutral particles emitted per disintegration, nor their nature, is definitely known, although it has been shown in the counter experiments of Sard and Althaus and of Hincks and Pontecorvo that the neutral particles cannot be photons.[3] We shall, for the duration of the present discussion, assume that the meson decay is a two-particle disintegration and that, either a zero rest energy neutrino, or a 70 Mev rest energy neutretto, are emitted together with the electron.[4] Thus, the momentum of the decay electron originating from a free and stationary meson, while possessing an unique value, say $p_e^{(0)}$, (two-particle decay assumed), cannot be predicted at present. In addition, negative mesons decay in matter[5]

* The research described in this paper was supported in part by contract N6ori-117, U. S. Navy Department.

** *Note added in proof:* In the April 1948 issue of Physics Abstracts there appeared an abstract of a paper by E. Corinaldesi (Nuovo Cim. **4**, 131 (1947) in which a calculation apparently similar to the present is described. Unfortunately, I have so far been unable to obtain the original paper of Corinaldesi.

[1] F. Rasetti, Phys. Rev. **59**, 613 (1941), **60**, 198 (1941); B. Rossi and N. Nereson, Phys. Rev. **62**, 417 (1942), **64**, 199 (1943); Auger, Maze, and Chaminade, Comptes Rendus **213**, 381 (1941), **214**, 266 (1941); M. Conversi and O. Piccioni, Phys. Rev. **70**, 859 (1946).

[2] W. B. Fretter, Phys. Rev. **70**, 625 (1946); J. G. Retallack and R. B. Brode, Phys. Rev. **73**, 532 (1948).

[3] R. D. Sard and E. J. Althaus, Phys. Rev. **73**, 1251 (1948); E. P. Hincks and B. Pontecorvo, Phys. Rev. **73**, 257 (1948).

[4] The two particle decay scheme of the meson into an electron and neutrino was originally suggested by Yukawa (Proc. Phys. Math. Soc. Japan, **17**, 48 (1935)) on the basis of a theoretical consideration in which the meson decay is pictured as an intermediate step in nuclear beta-decay. This scheme is supported by a cloud chamber picture of Williams and Roberts (Nature, **145**, 102 (1940)) which gives a decay electron of 70 ± 35 Mev, and by decay electron range data of Conversi and Piccioni (Phys. Rev. **70**, 874 (1946)) and of Retallack (Phys. Rev. **73**, 921 (1948)). The two particle decay scheme of the meson into an electron and a 70 Mev rest energy neutretto is supported by two cloud chamber pictures of Anderson, Adams, Lloyd, and Rau (Phys. Rev. **72**, 724 (1947); Rev. Mod. Phys. **20**, 334, (1948)) which give decay electrons of energy 25 ± 5 Mev. A three particle decay scheme: meson$\rightarrow$electron$+$neutrino$+$neutretto, has recently been suggested by Wheeler (Notes by J. A. Wheeler on the March 1948 Nat. Acad. Sci., Physics Conference); this scheme predicts a continuous energy distribution for the decay electrons (from free stationary mesons) peaked at $\cong 25$ Mev and possessing a mean spread $\cong 10$ Mev. If such a three-particle decay actually occurs, the resultant mean spread of the electron momentum distribution, about its peak, arising from a statistical division of the meson's rest energy among the three decay particles, will undoubtedly be considerably greater than the spread, discussed in this paper, which is introduced into the momentum distribution of the negative decay electrons as a result of the K-orbital motion of the (negative) bound parent mesons (see below).

Note added in proof: Recent experimental work on the electron momentum distribution from meson decay has been reported by: E. C. Fowler, R. L. Cool, and J. C. Street, Phys. Rev. **74**, 101 (1948); J. L. Zar, J. Hershkowitz, and E. Berezin, Phys. Rev. **74**, 111 (1948); J. Steinberger, Phys. Rev. **74**, 500 (1948); R. W. Thompson, Phys. Rev. **74**, 490 (1948). The results are all quite preliminary but it is perhaps not unfair to say that the data of the first three of these groups of authors seem to point to a three-particle decay while that of the fourth indicates a two-particle decay into an electron and neutrino.

It may also be mentioned here that Feer (Bull. Am. Phys. Soc. **23**, No. 3, p. 44) has shown that a fraction of the meson's rest energy, equal on the average to $\cong 1/137$, is given up to the radiation field, e.g., to (predominantly low energy) photons, at the instant of decay. Thus, even in the two-particle decay of a free stationary meson, the decay electrons cannot all have exactly the same energy. However the electron momentum spread due to such photon emission should not exceed $1/137 \times$[mean electron momentum] which is small compared to the electron momentum spread to be expected from the decay of (negative) bound mesons ($\cong Z/137 \times$[mean electron momentum]—see below).

[5] The discovery that slowed down negative mesons decay in matter with nuclei of sufficiently small charge number Z, is due to M. Conversi, E. Pancini and O. Piccioni, Phys. Rev. **71**, 209 (1947). See also G. E. Valley, Phys. Rev. **72**, 772 (1947); G. E. Valley and B. Rossi, Phys. Rev. **73**, 177 (1948); H. Ticho and M. Schein, Phys. Rev. **73**, 81

only after first becoming bound in K-orbits about individual nuclei.[6] As a result, the velocities of these mesons at the instant of decay have values appropriate to their K-orbit motion, i.e., values $\cong Z/137c$, so that the momenta, p_e, of the resultant (negative) decay electrons are given by a "Doppler shift" formula,[7]

$$p_e \cong p_e^{(0)}(1+Z/137\cos\theta), \qquad (1)$$

θ being the angle between the electron and meson velocities. Since θ takes on all values between 0 and π with approximately equal probability ($Z/137 \ll 1$) the momenta of the decay electrons will exhibit a "Doppler broadening" and will have a spread about their mean value ($p_e^{(0)}$), which amounts to

$$\cong p_e^{(0)} Z/137 \cong Z/137 \times \begin{bmatrix} 50 \text{ Mev/c; neutral particle} = \text{neutrino} \\ 25 \text{ Mev/c; neutral particle} = \text{neutretto} \end{bmatrix}.$$

A quantitative expression governing the momentum distribution of the decay electrons arising from negative mesons slowed down in matter and bound in K-orbits will be given below in Eq. (4). It is also to be noted that the decay electrons arising from slowed down positive mesons should all have the same momentum (two-particle decay assumed), since positive mesons, not being bound because of nuclear repulsion, will all be effectively free and stationary at the instant of decay. In practice, of course, both positive and negative decay electrons will lose a certain amount of momentum in getting out of the absorber in which the parent mesons are stopped and this momentum loss will have to be taken into account before the true momentum distribution can be determined.

The momentum distribution of the negative decay electrons may be obtained quantitatively by examining the expression given by the time dependent perturbation theory for T, the mean life for decay of the bound negative meson, *viz.*,[7a]

$$T^{-1} = \int\int P(\mathbf{p}_e,\mathbf{p}_n)d\mathbf{p}_e d\mathbf{p}_n = 2\pi/\hbar \int\int \frac{d\mathbf{p}_e d\mathbf{p}_n}{(2\pi\hbar)^6} \sum_{s_e s_n} \left| \left(\frac{g^2}{\hbar c} 4\pi \frac{(\hbar c)^3}{E_m}\right)^{\frac{1}{2}} \times \int \phi^*_{p_n,s_n}(\mathbf{r})\beta\psi_{p_e,s_e}(\mathbf{r})\, U_{E_m}(\mathbf{r})d\mathbf{r} \right|^2 \delta(E_m - E_e - E_n), \qquad (2)$$

where, $P(\mathbf{p}_e,\mathbf{p}_n)d\mathbf{p}_e d\mathbf{p}_n$ = probability per unit time for the decay of the bound meson into an electron with momentum between $\mathbf{p}_e$ and $\mathbf{p}_e + d\mathbf{p}_e$ and a neutrino or neutretto with momentum between $\mathbf{p}_n$ and $\mathbf{p}_n + d\mathbf{p}_n$.

$U_{E_m}(\mathbf{r}) = e^{-r/a}/(\pi a^3)^{\frac{1}{2}}$ = non-relativistic approximation to the wave function associated with the K-orbit of the bound meson (see below); $\mathbf{r}$ is the vector from the nucleus (assumed at rest at the origin of coordinates) to the meson;

(1948); N. Nereson, Phys. Rev. **73**, 765 (1948). At the moment, evidence is available that in matter of large Z, nuclear capture of mesons competes successfully with their decay (see J. G. Retallack, Phys. Rev. **73**, 921 (1948)). For a discussion of the alternative hypothesis of an accelerated decay of the bound meson stimulated by nuclear electric fields see Valley and Rossi, quoted above, and, S. T. Epstein, R. J. Finkelstein and J. R. Oppenheimer, Phys. Rev. **73**, 1140, (1948). See also reference 7a.

[6] E. Fermi, E. Teller and V. Weisskopf, Phys. Rev. **71**, 314 (1947); E. Fermi and E. Teller, Phys. Rev. **72**, 399 (1947).

[7] Equation (1) may be most simply derived by applying the momentum and energy conservation laws to the decay of the bound meson. Here one has: $\mathbf{p}_m = \mathbf{p}_e + \mathbf{p}_n$, and $m_m c^2 + \epsilon_m \cong cp_e + ((cp_n)^2 + (m_n c^2)^2)^{\frac{1}{2}}$ where $m_m c^2$ is the rest energy, ϵ_m the mean kinetic and potential energy, $p_m \cong Z/137\, m_m c \ll m_m c$, the momentum, of the bound meson, and, $m_n c^2$, p_n, the rest energy and the momentum of decay neutrino or neutretto; eliminating p_n and recalling that $m_m c^2 \cong cp_e^{(0)} + ([cp_e^{(0)}]^2 + (m_n c^2))^{\frac{1}{2}}$, one immediately obtains Eq. (1).

[7a] The Lagrangian density of the meson, electron, neutrino and electromagnetic fields, L, on which the present perturbation calculation is based, is,

$$L = -\frac{1}{4\pi}\left\{\sum_{\nu=1}^{4}\left|\left(\frac{\partial}{\partial x_\nu} - \frac{ie}{\hbar c}A_\nu\right)U\right|^2 + \left(\frac{m_m c}{\hbar}\right)^2 |U|^2\right\} + i\hbar c\psi^\dagger\left(\sum_{\nu=1}^{4}\gamma_\nu\left[\frac{\partial}{\partial x_\nu} - \frac{ie}{\hbar c}A_\nu\right] + \frac{m_e c}{\hbar}\right)\psi + i\hbar c\phi^\dagger\left(\sum_{\nu=1}^{4}\gamma_\nu\left[\frac{\partial}{\partial x_\nu} - \frac{ie}{\hbar c}A_\nu\right] + \frac{m_n c}{\hbar}\right)\phi - g(\phi^\dagger\psi U + U^\dagger\psi^\dagger\phi)$$

where U, ψ, ϕ are the (doubly quantized) meson, electron, and neutrino (or neutretto) wave-functions and A_ν are the potentials of the electromagnetic (Coulomb) field arising from the charge on the nucleus about which the meson is bound. U, ψ, ϕ are expanded in the usual way into series of eigenfunctions; the individual terms in these series are creation and destruction operators for the corresponding particles multiplied into the (relativistic) U_{E_m}, ψ_{p_e,s_e}, ϕ_{p_n,s_n} of the text below (the treatment of the expansion of the U into the U_{E_m} follows that given by H. Snyder and J. Weinberg (Phys. Rev. **57**, 307 (1940)) and F. J. Dyson (Phys. Rev. **73**, 617, (1948)). As shown in the last of the references 5, an accelerated decay of the bound meson, stimulated by the electric field of the adjacent nucleus,

$E_m = m_m c^2 - Ze^2/2a = m_m c^2(1 - Z^2/2\cdot 137^2)$ is the energy of the bound meson in its K-orbit; g is a constant, having the dimensions of electric charge, which governs the strength of the interaction between the meson and electron-neutrino or electron-neutretto fields.

$\psi_{p_e,s_e}(\mathbf{r}) = \exp i\mathbf{p}_e\cdot\mathbf{r}_e/\hbar S_e$ = free-particle wave function (normalized per unit volume) associated with the decay electron, p_e being its momentum and $E_e \cong cp_e$, its energy. S_e is a constant spinor wave amplitude involving the spin coordinates of the electron. It is to be noted that the effect of the nucleus' Coulomb field on the electron wave function is neglected; this neglect is justified since the electron is created at a distance from the nucleus ($\sim a$) which is much greater than its $(2\pi)^{-1}\times$[wave-length] $(= (\hbar/p_e) \sim (\hbar/m_m c) \cong Z/137a)$ so that the Coulomb field wave function is well approximated by its asymptotic form—a plane wave (see below).

$\phi_{p_n,s_n}(\mathbf{r}) = \exp -i\mathbf{p}_n\cdot\mathbf{r}_n/\hbar S_n$ = free-particle wave function (normalized per unit volume) associated with the decay neutrino or neutretto (which is assumed to have spin $\frac{1}{2}$ and so obey Dirac's equation) when it is in a state, previous to the meson's decay, with momentum $-p_n$ and energy $-E_n = -((cp_n)^2 + (m_n c^2)^2)^{\frac{1}{2}}$, m_n being the neutrino or neutretto[8] rest mass. The decay of the meson is thus, as usual, pictured as involving its absorption by a neutrino in a negative energy state $-E_n$, the neutrino thereby becoming an electron in a positive energy state E_e, the residual hole being the associated anti-neutrino. S_n is a constant spinor wave amplitude involving the spin coordinates of the neutrino, β is a Dirac matrix, $\phi^*_{p_n,s_n}\beta\psi_{p_e,s_e}$ and U_{Em} being each scalar invariants (spin zero meson); the use of other types of meson fields (e.g., pseudoscalar or even, vector) should lead, in general, to similar results.[9]

δ is the Dirac delta-function whose presence is required by the conservation of energy in the decay, the recoil energy of the atom about whose nucleus the meson is bound ($\cong 10^3$ ev) being neglected at this stage (see below). The integration over $\mathbf{p}_e, \mathbf{p}_n$ runs over all possible values, while the sum over the spin states of the electron and neutrino runs over the two possible states (consistent with a given sign of the energy) for each one of the two particles.

We note that the absolute square of the matrix element:

$$\left|\int \phi^*_{p_n,s_n}(\mathbf{r})\beta\psi_{p_e,s_e}(\mathbf{r})\, U_{Em}(\mathbf{r})d\mathbf{r}\right|^2 = \left|(S_n\beta S_e)\int \exp i(\mathbf{p}_n+\mathbf{p}_e)\cdot\mathbf{r}/\hbar\, U_{Em}(\mathbf{r})d\mathbf{r}\right|^2$$

is, apart from a constant, just the probability that the meson has a momentum $[\mathbf{p}_e+\mathbf{p}_n]$ in the K-orbit so that $P(\mathbf{p}_e,\mathbf{p}_n)$ is proportional to this probability. This last proportionality is in agreement with the picture of the continuous decay electron momentum distribution arising from the fact that the bound meson has not a sharp, but rather a continuous, (probability) distribution of velocity.[10]

The integrals and sums in Eq. (2) can be carried out in a straight-forward manner (e.g., Casimir spur method for sums over spin states) with the result that,

$$T^{-1} = \int_0^{c^{-1}E_m - m_n c} P(p_e)dp_e, \qquad (3)$$

where, $P(p_e)$ the probability per unit time and per unit momentum range that the (negative bound) meson will decay into an electron with momentum p_e and a neutrino with momentum $p_n = ((E_m - cp_e)^2/c^2 - (m_n c)^2)^{\frac{1}{2}}$, is given, if one keeps only the lowest order terms in $Z/137$, by

---

may be obtained by adding coupling terms to the Lagrangian, of the type, e.g.,

$$g'\sum_{\mu,\nu}\left(\frac{\partial A_\nu}{\partial x_\mu} - \frac{\partial A_\mu}{\partial x_\nu}\right)\phi^\dagger\gamma_\mu\gamma_\nu\psi U,$$

with the A_ν, in this case, the potentials of the total electromagnetic field, i.e., of the (Coulomb) field arising from the nucleus and of the Coulomb and quantized transverse fields arising from the charged meson and electron wave fields.

[8] Henceforth we shall refer explicitly to the neutrino only though all the results obtained will, of course, be also applicable to the neutretto providing one sets $m_n c^2 \cong 70$ Mev instead of $m_n c^2 \cong 0$.

[9] It seems fairly clear that Eq. (4) for $P(p_e)$ should be valid (in lowest order in $Z/137$) for mesons and neutrettos of any spin and type of field covariance. This follows since a non-relativistic approximation to the meson wave function has been employed to obtain Eq. (4), and since no neutretto property apart from mass appears explicitly in this equation.

[10] See Eq. (1) and reference 7.

the expression[9]

$$P(p_e)dp_e = T_0^{-1}\left[\frac{8/3\pi}{\left\{1+\left[\frac{p_e-p_e^{(0)}}{p_e^{(0)}\frac{Z}{137}}\right]^2\right\}^3}d\left[\frac{p_e-p_e^{(0)}}{p_e^{(0)}\frac{Z}{137}}\right]\right]. \quad (4)$$

In Eq. (4), $T_0^{-1}\equiv(g^2/\hbar c)(m_m c^2/\hbar)[1-(m_n/m_m)^2]^2$ is the mean life of a free stationary meson,[11] $p_e^{(0)}\equiv(m_m c/2)[1-(m_n/m_m)^2]$ = mean of the decay electron momenta from the bound meson = momentum of the decay electron from a free stationary meson; to within lowest order in $Z/137$, Eqs. (3), (4) yield $T=T_0$. Equation (4) gives the distribution of the decay electron momenta from bound negative mesons. One sees, from Eq. (4), that for $p_e=p_e^{(0)}(1\pm Z/137)$, $P(p_e)=\frac{1}{8}P(p_e^{(0)})$, so that, for example, in aluminum ($Z=13$) there is one decay electron with cp_e between 54.5 and 55.5 Mev for every eight electrons with cp_e between 49.5 and 50.5 Mev (taking $m_m c^2=100$ Mev and $m_n c^2=0$ Mev). Such an effect should be detected if a sufficient number of bound negative mesons is observed to decay (and, of course, if the decay is into two particles).

The evaluation of the integral for T^{-1} in Eq. (2) using the exact expression for $P(\mathbf{p}_e,\mathbf{p}_n)$ or $P(p_e)$ (not the approximation in Eq. (4)) yields,

$$T^{-1}=T_0^{-1}\left[1-\left(\frac{8}{3}\frac{m_m^2}{m_m^2-m_n^2}-\frac{7}{6}\right)\left(\frac{Z}{137}\right)^2 + \text{higher order terms in } (Z/137)\right]. \quad (5)$$

However, relativistic corrections to the bound meson wave function and Coulomb field corrections to the electron wave function, should also give terms in T^{-1} which are $\sim(Z/137)^2$. Consequently, a calculation has been made using the ground state relativistic Klein-Gordon eigenfunction as the U_{Em},[12] and an approximate Coulomb field continuous spectrum Dirac eigenfunction[13] as the ψ_{p_e,s_e}. With these wave functions, the absolute magnitude of the matrix element in Eq. (2) becomes, (apart from a constant normalizing factor),

$$\frac{|(S_n\beta S_e)|8\pi}{\left\{1+\left[\frac{\mathbf{p}_e+\mathbf{p}_n}{\frac{Z}{137}m_m c}\right]^2\right\}^2}\exp\left(\frac{\pi}{2}\frac{Z}{137}\right)\Gamma\left(1+i\frac{Z}{137}\right)\exp\left(-\frac{Z}{137}\tan^{-1}\left[\frac{2\cdot 137 p_e}{Zm_m c}\right]\right)$$

$$\times\left[1-\frac{i}{2}\frac{Z}{137}\left[1-\left[\frac{\mathbf{p}_e+\mathbf{p}_n}{\frac{Z}{137}m_m c}\right]^2\right]+\frac{1}{4}\left(\frac{Z}{137}\right)^2\frac{m_m c}{p_e}\left[1+\left[\frac{\mathbf{p}_e+\mathbf{p}_n}{\frac{Z}{137}m_m c}\right]^2\right]+\text{higher order terms in } Z/137\right],$$

instead of its previous value,

$$\frac{|(S_n\beta S_e)|8\pi}{\left\{1+\left[\frac{\mathbf{p}_e+\mathbf{p}_n}{\frac{Z}{137}m_m c}\right]^2\right\}^2},$$

and one obtains, carrying out the sums over s_e,

[11] H. A. Bethe and L. Nordheim (Phys. Rev. **57**, 998 (1940), Appendix I) derive this formula for T_0 in the case $m_n=0$.

[12] See, for example, A. Sommerfeld, *Wellenmechanic*, (Ungar, New York, 1945), p. 215.

[13] The approximate Coulomb field eigenfunction used is that given by Furry (Phys. Rev. **46**, 391 (1934)) except for a modification (analogous to one introduced by Scherzer (Ann. d. Physik **13**, 137 (1932)) which allows it to reduce asymptotically, in the direction given by $\mathbf{p}_e$, into, essentially, a plane wave only (rather than into a plane wave and into a spherically divergent wave which is the case in Furry's original representation and which is more appropriate to a scattering problem).

s_n, and the integrals over $\mathbf{p}_e, \mathbf{p}_n$, in Eq. (2),

$$T^{-1}=T_0^{-1}\left[1+\left(\frac{1}{6}+\frac{4}{3}\frac{m_m^2}{m_m^2-m_n^2}\right)(Z/137)^2 + \text{higher order terms in } Z/137\right]. \quad (6)$$

To within terms of lowest order in $Z/137$, the decay electron momentum distribution is unchanged by these relativistic and Coulomb field corrections.[9]

Equation (6) shows that the effect of the negative meson's binding in the K-orbit *decreases* its mean life.[14] Numerically however this decrease is very small ($\cong$1.5 percent–3 percent for Al); in heavy elements, on the other hand, (where $(Z/137)^2$ it not so small) the mesons are presumably predominantly captured[15] before any decay can take place. Thus the effect of binding on the mean life for decay is probably unobservable.[16]

Finally one may estimate the average magnitude of the recoil energy of the atom near whose nucleus the negative meson decays. One has,

$$\text{Recoil Energy}=\frac{\langle(\mathbf{p}_e+\mathbf{p}_n)^2\rangle_{Av}}{2M_{\text{atom}}}=\frac{2\pi}{\hbar}\int\int\frac{d\mathbf{p}_e d\mathbf{p}_n}{(2\pi\hbar)^6}\sum_{s_e s_n}$$

$$\frac{\left|\left(\frac{g^2}{\hbar c}\frac{(\hbar c)^3}{4\pi E_m}\right)^{\frac{1}{2}}\int\phi^*_{\mathbf{p}_n,s_n}(\mathbf{r})\beta\psi_{\mathbf{p}_e,s_e}(\mathbf{r})\,U_{E_m}(\mathbf{r})d\mathbf{r}\right|^2\delta(E_m-E_e-E_n)\left[\frac{(\mathbf{p}_e+\mathbf{p}_n)^2}{2M_{\text{atom}}}\right]}{T^{-1}}$$

$$\cong(Z/137)^2[(m_mc)^2/2M_{\text{atom}}]\cong 1000 \text{ ev. (for Neon, } Z=10). \quad (7)$$

Such a recoil energy may conceivably be observed if the negative mesons decay in K-orbits about neon atoms, say, in a cloud chamber and the recoil atoms create sufficient ionization to cause a visible "blob" at the point of origin of the decay electron's track.

I wish to thank Dr. R. D. Sard and Dr. E. Feenberg for several stimulating discussions.

[14] The present small decrease in the mean life for meson decay, arising from the effect of the nucleus' Coulomb field on the wave functions of the (bound) meson and the emitted electron, is to be distinguished from the possibly large decrease which occurs if a direct coupling is postulated (see reference 5, 7a) between the meson, electron, neutrino and total electromagnetic fields.

[15] J. G. Retallack, Phys. Rev. **73**, 921 (1948).

[16] The exact value of the numerical coefficient of $(Z/137)^2$ in Eq. (6) is still somewhat uncertain because the approximate Coulomb field wave functions used to describe the electron may contain errors $\sim(Z/137)^2$. (See Furry, reference 13.) However there is rigorously no binding correction to the meson mean life which is $\sim Z/137$.

PHYSICAL REVIEW VOLUME 74, NUMBER 8 OCTOBER 15, 1948

Motion of an Electron in the Field of a Magnetic Pole

HARISH-CHANDRA
The Institute for Advanced Study, Princeton, New Jersey
(Received June 21, 1948)

The motion of an electron in the field of a magnetic pole is considered. It is shown that in spite of its magnetic moment the electron has no bound states.

RECENTLY Dirac has revived interest in a theory of the electromagnetic field proposed by him some time ago[1] which allows the existence of free magnetic poles. As a consequence of his theory he is able to deduce the fact that the charge of any elementary particle is always an integral multiple of a certain fixed unit. The motion of an electron in the field of a magnetic pole was considered by Dirac[1] and he found that the electron cannot have any bound states. However, Dirac did not take into account the spin of the electron and since the spin gives rise to a magnetic moment, it seemed conceivable that the above conclusion might cease to hold if one used the correct equation of motion. The object of this note is to investigate this point. It turns out that Dirac's result is still valid and so the electron cannot be bound to a magnetic pole.

We put the velocity of light and the Planck's constant equal to 1 and 2π respectively. It is convenient to use tensor notation. Let $(x, y, z) = (x^1, x^2, x^3)$ be the Cartesian coordinates in space and let ϵ^{ijk} be the antisymmetric tensor such that $\epsilon^{123}=1$. Further, let g_{ik} be the metric tensor corresponding to the quadratic form

$$dx^2+dy^2+dz^2=g_{ik}dx^i dx^k.$$

The equations determining the vector potential A_k can then be written as

$$\epsilon^{ijk}(\partial A_j/\partial x^i)=H^k, \tag{1}$$

where H_k are the components of the magnetic field. Now since we wish to consider the field of a magnetic pole it is convenient to introduce polar coordinates (r, θ, φ) given by

$$x=r\sin\theta\cos\varphi, \quad y=r\sin\theta\sin\varphi, \quad z=r\cos\theta,$$

so that

$$dx^2+dy^2+dz^2=dr^2+r^2d\theta^2+r^2\sin^2\theta d\varphi^2.$$

Therefore if $g_{\alpha\beta}(\alpha, \beta$ running over $r, \theta, \varphi)$ denotes the metric tensor in the polar coordinates, we have

$$\begin{aligned} &g_{rr}=1, \quad g_{\theta\theta}=r^2, \quad g_{\varphi\varphi}=r^2\sin^2\theta, \\ &g^{rr}=1, \quad g^{\theta\theta}=1/r^2, \quad g^{\varphi\varphi}=1/r^2\sin^2\theta, \\ &g_{\alpha\beta}=g^{\alpha\beta}=0, \quad \alpha\neq\beta. \end{aligned} \tag{2}$$

On transforming (1) to the new coordinate system (r, θ, φ) according to the usual rules of tensor calculus we get

$$\epsilon^{\alpha\beta\gamma}(\partial A_\beta/\partial\xi^\alpha)=H^\gamma, \tag{3}$$

where α, β, γ run over the three indices r, θ, φ and $(\xi^r, \xi^\theta, \xi^\varphi)=(r, \theta, \varphi)$. It follows from the transformation laws that

$$\epsilon^{r\theta\varphi}=1/(g)^{\frac{1}{2}}=1/r^2\sin\theta,$$

where $g=r^4\sin^2\theta$ is the determinant of the matrix formed by the components $g_{\alpha\beta}$. Let $-e$ be the charge of the electron and n an integer and consider a magnetic pole of strength $\frac{1}{2}n/e$ at the origin. Then $H^\theta=H^\varphi=0$ and $H^r=\frac{1}{2}n/er^2$. A possible solution of (3) is now obtained by putting $A_r=A_\theta=0$ and choosing A_φ such that

$$\frac{1}{r^2\sin\theta}\frac{\partial A_\varphi}{\partial\theta}=\frac{n}{2er^2}. \tag{4}$$

This gives $A_\varphi=(n/2e)(1-\cos\theta)$, the constant of integration having been so chosen as to make $A_\varphi=0$ for $\theta=0$ so that the nodal line[1] runs from the origin along the line $\theta=\pi$. This is seen as follows. Consider the integral

$$\int_c A_k dx^k=\int_c A_\alpha d\xi^\alpha=\int_c A_\varphi d\varphi,$$

taken round a closed curve c surrounding the line $\theta=\theta_0$. Clearly if $\theta_0\neq 0$ or π, $\int_c d\varphi=0$ and therefore the integral tends to zero as c shrinks to a point on $\theta=\theta_0$. On the other hand if $\theta_0=0$ or π, $\int_c d\varphi=2\pi$ and the value of the integral tends

[1] P. A. M. Dirac, Proc. Roy. Soc. 133, 60 (1931).

to $(\pi n/e)(1-\cos\theta_0)$ i.e., 0 or $2\pi n/e$ according as $\theta_0=0$ or π.

Now we come to the equation of motion of the electron. As usual let σ_1, σ_2, σ_3 and ρ_1, ρ_2, ρ_3 be two independent sets of Pauli matrices.[2] Transform σ_1, σ_2, σ_3 as components of a vector to polar coordinates so that

$$\begin{aligned}\sigma_r&=\sigma_k\frac{\partial x^k}{\partial r}=\frac{1}{r}(\boldsymbol{\sigma}\mathbf{x}),\\ \sigma_\theta&=\sigma_k\frac{\partial x^k}{\partial\theta}=\frac{1}{r\sin\theta}(\mathbf{x}(\boldsymbol{\sigma}\mathbf{x})-(\mathbf{x}\mathbf{x})\boldsymbol{\sigma})_3,\\ \sigma_\varphi&=\sigma_k\frac{\partial x^k}{\partial\varphi}=[\mathbf{x}\times\boldsymbol{\sigma}]_3,\end{aligned}\tag{5}$$

where $\mathbf{x}=(x_1, x_2, x_3)$ and $\boldsymbol{\sigma}=(\sigma_1, \sigma_2, \sigma_3)$ and the usual notations for scalar and vector products are used. The Hamiltonian H for the electron can now be written as

$$\begin{aligned}H&=-\rho_1(\boldsymbol{\sigma}\mathbf{p})-\rho_3\mu-\rho_1 e\sigma^\varphi A_\varphi\\ &=-\rho_1(\boldsymbol{\sigma}\mathbf{p})-\rho_3\mu-\rho_1\frac{[\mathbf{x}\times\mathbf{p}]_3\,n}{r^2\sin^2\theta}\frac{}{2}(1-\cos\theta),\end{aligned}\tag{6}$$

where $\mathbf{p}=1/i(\partial/\partial x, \partial/\partial y, \partial/\partial z)$ is the momentum and μ the mass of the electron. Our problem is to find a wave function ψ such that

$$H\psi=E\psi,\tag{7}$$

where E is some eigenvalue of H. Now notice that

$$[\mathbf{x}\times\mathbf{p}]_3=\frac{1}{i}\left(x\frac{\partial}{\partial y}-y\frac{\partial}{\partial x}\right)=\frac{1}{i}\frac{\partial}{\partial\varphi},$$

and $[\mathbf{x}\times\mathbf{p}]+\frac{1}{2}\boldsymbol{\sigma}$ commutes with $H_0=-\rho_1(\boldsymbol{\sigma}\mathbf{p})-\rho_3\mu$ while $[\mathbf{x}\times\mathbf{p}]_3+\frac{1}{2}\sigma_3$ commutes with $[\mathbf{x}\times\boldsymbol{\sigma}]_3$. Therefore

$$[\mathbf{x}\times\mathbf{p}]_3+\tfrac{1}{2}\sigma_3=\frac{1}{i}\frac{\partial}{\partial\varphi}+\tfrac{1}{2}\sigma_3,$$

commutes with H. Hence we can choose ψ in such a way that

$$\left(\frac{1}{i}\frac{\partial}{\partial\varphi}+\tfrac{1}{2}\sigma_3\right)\psi=M\psi,$$

where M is half-an-odd integer. Therefore

$$\psi=e^{i(M-\frac{1}{2}\sigma_3)\varphi}\psi',\tag{8}$$

where ψ' is independent of φ. Now

$$\sigma^k\frac{\partial}{\partial x^k}=\sigma^\alpha\frac{\partial}{\partial\xi^\alpha}=\sigma_r\frac{\partial}{\partial r}+\frac{\sigma_\theta}{r^2}\frac{\partial}{\partial\theta}+\frac{\sigma_\varphi}{r^2\sin^2\theta}\frac{\partial}{\partial\varphi}.\tag{9}$$

From (5) we get

$$\begin{aligned}\sigma_r&=\sin\theta(\sigma_1\cos\varphi+\sigma_2\sin\varphi)+\sigma_3\cos\theta\\ &=\sin\theta\sigma_1 e^{i\sigma_3\varphi}+\sigma_3\cos\theta\\ &=e^{-i\sigma_3\varphi/2}(\sigma_3\cos\theta+\sigma_1\sin\theta)e^{i\sigma_3\varphi/2}\\ &=e^{-i\sigma_3\varphi/2}e^{-i\sigma_2\theta/2}\sigma_3 e^{i\sigma_2\theta/2}e^{i\sigma_3\varphi/2}.\end{aligned}\tag{10a}$$

Similarly

$$\begin{aligned}\sigma_\theta&=r\cos\theta(\sigma_1\cos\varphi+\sigma_2\sin\varphi)-\sigma_3 r\sin\theta\\ &=r\cos\theta\sigma_1 e^{i\sigma_3\varphi}-\sigma_3 r\sin\theta\\ &=re^{-i\sigma_3\varphi/2}(\sigma_1\cos\theta-\sigma_3\sin\theta)e^{i\sigma_3\varphi/2}\\ &=re^{-i\sigma_3\varphi/2}e^{-i\sigma_2\theta/2}\sigma_1 e^{i\sigma_2\theta/2}e^{i\sigma_3\varphi/2},\end{aligned}\tag{10b}$$

$$\begin{aligned}\sigma_\varphi&=r\sin\theta(\sigma_2\cos\varphi-\sigma_1\sin\varphi)\\ &=r\sin\theta e^{-i\sigma_3\varphi/2}e^{-i\sigma_2\theta/2}\sigma_2 e^{i\sigma_2\theta/2}e^{i\sigma_3\varphi/2}.\end{aligned}\tag{10c}$$

Also

$$e^{i\sigma_2\theta/2}\frac{\partial}{\partial\theta}=\left(\frac{\partial}{\partial\theta}-i\frac{\sigma_2}{2}\right)e^{i\sigma_2\theta/2},$$

$$\begin{aligned}e^{i\sigma_2\theta/2}e^{i\sigma_3\varphi/2}\frac{\partial}{\partial\varphi}&=e^{i\sigma_2\theta/2}\left(\frac{\partial}{\partial\varphi}-i\frac{\sigma_3}{2}\right)e^{i\sigma_3\varphi/2}\\ &=\left(\frac{\partial}{\partial\varphi}-\frac{i}{2}e^{i\sigma_2\theta}\sigma_3\right)e^{i\sigma_2\theta/2}e^{i\sigma_3\varphi/2}\\ &=\left\{\frac{\partial}{\partial\varphi}-\frac{i}{2}(\sigma_3\cos\theta-\sigma_1\sin\theta)\right\}e^{i\sigma_2\theta/2}e^{i\sigma_3\varphi/2}.\end{aligned}$$

Hence

$$\begin{aligned}\sigma^k\partial/\partial x^k=e^{-i\sigma_2\theta/2}e^{-i\sigma_3\varphi/2}\Bigg[&\sigma_3\frac{\partial}{\partial r}+\frac{\sigma_1}{r}\left(\frac{\partial}{\partial\theta}-\frac{i\sigma_2}{r}\right)\\ &+\frac{\sigma_2}{r\sin\theta}\left\{\frac{\partial}{\partial\varphi}-\frac{i}{2}(\sigma_3\cos\theta-\sigma_1\sin\theta)\right\}\Bigg]e^{i\sigma_2\theta/2}e^{i\sigma_3\varphi/2}.\end{aligned}$$

Similarly

$$\begin{aligned}ie\sigma^\varphi A_\varphi&=i\frac{\sigma_\varphi}{r^2\sin^2\theta}\frac{n}{2}(1-\cos\theta)\\ &=ie^{-i\sigma_3\varphi/2}e^{-i\sigma_2\theta/2}\frac{\sigma_2}{r\sin\theta}\frac{n}{2}(1-\cos\theta)\\ &\qquad\times e^{i\sigma_2\theta/2}e^{i\sigma_3\varphi/2}.\end{aligned}$$

[2] See P. A. M. Dirac, *Principles of Quantum Mechanics* (Clarendon Press, Oxford, 1947), Chap. XI.

Hence on substituting (8) in (7) and putting $e^{i\sigma_3\theta/2}\psi'=\psi_0$, we get

$$\left[\tfrac{1}{2}\rho_1\left\{\sigma_3\left(\frac{\partial}{\partial r}+\frac{1}{r}\right)+\frac{\sigma_1}{r}\left(\frac{\partial}{\partial\theta}-\frac{\sigma_3}{\sin\theta}\left\{M+\frac{n}{2}(1-\cos\theta)-\frac{\sigma_3}{2}\cos\theta\right\}\right)\right\}+\rho_3\mu+E\right]\psi_0=0. \quad (11)$$

It is clear that

$$-K^2=\left\{\sigma_1\left[\frac{\partial}{\partial\theta}-\frac{\sigma_3}{\sin\theta}\left(M+\frac{n}{2}(1-\cos\theta)-\frac{\sigma_3\cos\theta}{2}\right)\right]\right\}^2,$$

commutes with the operator acting on ψ_0 in (11). Hence we can choose ψ_0 to be an eigenvector of K^2. But

$$\begin{aligned}
-K^2&=\left\{\frac{\partial}{\partial\theta}+\tfrac{1}{2}\cot\theta+\frac{\sigma_3}{\sin\theta}\left(M+\frac{n}{2}(1-\cos\theta)\right)\right\}\left\{\frac{\partial}{\partial\theta}+\tfrac{1}{2}\cot\theta-\frac{\sigma_3}{\sin\theta}\left(M+\frac{n}{2}(1-\cos\theta)\right)\right\}\\
&=\frac{1}{\sin\theta}\left\{\frac{\partial}{\partial\theta}-\tfrac{1}{2}\cot\theta+\frac{\sigma_3}{\sin\theta}\left(M+\frac{n}{2}(1-\cos\theta)\right)\right\}\left\{\sin\theta\frac{\partial}{\partial\theta}+\tfrac{1}{2}\cos\theta-\sigma_3\left(M+\frac{n}{2}(1-\cos\theta)\right)\right\}\\
&=\frac{1}{(1-u^2)}\left\{(1-u^2)\frac{d}{du}-\sigma_3\left(M+\frac{n}{2}\right)+\left(\frac{n}{2}\sigma_3+\tfrac{1}{2}\right)u\right\}\left\{(1-u^2)\frac{d}{du}+\sigma_3\left(M+\frac{n}{2}\right)-\left(\frac{n}{2}\sigma_3+\tfrac{1}{2}\right)u\right\}\\
&=(1-u^2)\frac{d^2}{du^2}-2u\frac{d}{du}-\frac{\left\{\sigma_3\left(M+\frac{n}{2}\right)-\left(\frac{n}{2}\sigma_3+\frac{1}{2}\right)u\right\}^2}{1-u^2}-\left(\frac{n}{2}\sigma_3+\tfrac{1}{2}\right)^2\\
&=(1-u^2)\frac{d^2}{du^2}-2u\frac{d}{du}-\frac{\left\{\left(M+\frac{n}{2}\right)-\left(\frac{n}{2}+\frac{\sigma_3}{2}\right)u\right\}^2}{1-u^2}-\left(\frac{n}{2}+\frac{\sigma_3}{2}\right)^2+\frac{n^2-1}{4},
\end{aligned} \quad (12)$$

where $u=\cos\theta$. Now it is known that if m and j are both integral or both half-integral the only eigenfunctions of the operator

$$(1-u^2)\frac{d^2}{du^2}-2u\frac{d}{du}-\frac{(m-ju)^2}{1-u^2}-j^2, \quad (13)$$

corresponding to the interval $-1\leqslant u\leqslant 1$ are the Jacobi polynomials $P^k_{m,j}(u)$ and the corresponding eigenvalues are $-k(k+1)$, where k is to be so chosen that $k\geqslant|m|$, $|j|$, and $k-j$ is an integer. $P^k_{m,j}(\cos\theta)$ is defined by the identity

$$\frac{\left(t_1\cos\frac{\theta}{2}+t_2\sin\frac{\theta}{2}\right)^{k-j}\left(-t_1\sin\frac{\theta}{2}+t_2\cos\frac{\theta}{2}\right)^{k+j}}{(k-j!k+j!)^{\frac{1}{2}}}=\sum_m\frac{t_1^{k-m}t_2^{k+m}}{(k-m!k+m!)^{\frac{1}{2}}}P^k_{m,j}(\cos\theta), \quad (14)$$

where m runs through the set of values k, $k-1$, $\cdots$, $-k$. Write

$$w_1=t_1\cos\theta/2+t_2\sin\theta/2,$$
$$w_2=t_2\cos\theta/2-t_1\sin\theta/2.$$

If we observe that $\partial w_1/\partial\theta=w_2$, $\partial w_2/\partial\theta=-w_1$, we get immediately on differentiating (14) with respect to θ

$$((k-j)(k+j+1))^{\frac{1}{2}}P^k_{m,j+1}(\cos\theta)-((k+j)(k-j+1))^{\frac{1}{2}}P^k_{m,j-1}(\cos\theta)=2\frac{d}{d\theta}P^k_{m,j}(\cos\theta). \quad (15)$$

Now keep θ fixed and transform from the variables t_1, t_2 to w_1, w_2. Then

$$t_1\frac{\partial}{\partial t_1}-t_2\frac{\partial}{\partial t_2}=\cos\theta\left(w_1\frac{\partial}{\partial w_1}-w_2\frac{\partial}{\partial w_2}\right)-\sin\theta\left(w_1\frac{\partial}{\partial w_2}+w_2\frac{\partial}{\partial w_1}\right).$$

On applying this operator to (14) we get

$$-2j\cos\theta P^k_{m,j}(\cos\theta)$$
$$-\sin\theta(((k-j)(k+j+1))^{\frac{1}{2}}P^k_{m,j+1}(\cos\theta)$$
$$+((k+j)(k-j+1))^{\frac{1}{2}}P^k_{m,j-1}(\cos\theta))$$
$$=-2mP^k_{m,j}(\cos\theta). \quad (16)$$

From (15) and (16) we find at once that

$$\left\{(1-u^2)\frac{d}{du}+m-ju\right\}P^k_{m,j}(u)$$
$$=((k+j)(k-j+1))^{\frac{1}{2}}(1-u^2)^{\frac{1}{2}}P^k_{m,j-1}(u), \quad (17a)$$

$$\left\{(1-u^2)\frac{d}{du}-m+ju\right\}P^k_{m,j}(u)$$
$$=((k-j)(k+j+1))^{\frac{1}{2}}(1-u^2)^{\frac{1}{2}}P^k_{m,j+1}(u). \quad (17b)$$

Now for (12) $m=M+n/2$ and

$$j=(n/2)+(\sigma_3/2)=\begin{pmatrix}\frac{n+1}{2}\\ \frac{n-1}{2}\end{pmatrix}$$

if we choose a representation in which σ_3 is diagonal. Therefore the eigenfunction ψ_0 can be written as

$$\psi_0=\begin{pmatrix}P^k_{M+(n/2),(n+1)/2}(\cos\theta) & \psi^+\\ P^k_{M+(n/2),(n-1)/2}(\cos\theta) & \psi^-\end{pmatrix},$$

where ψ^+, ψ^- depend only on r and

$$k\geq\left|M+\frac{n}{2}\right|,\ \left|\frac{n-1}{2}\right|,\ \left|\frac{n+1}{2}\right| \text{ and } k+\frac{n+1}{2}$$

is an integer. Making use of (17) we find that

$$\sigma_1\left[\frac{\partial}{\partial\theta}-\frac{\sigma_3}{\sin\theta}\left(M+\frac{n}{2}-\frac{n+\sigma_3}{2}\cos\theta\right)\right]$$
$$\times\begin{pmatrix}P^k_{M+(n/2),(n+1)/2} & \psi^+\\ P^k_{M+(n/2),(n-1)/2} & \psi^-\end{pmatrix}$$
$$=-\left(\left(k+\frac{n}{2}+\frac{1}{2}\right)\left(k-\frac{n}{2}+\frac{1}{2}\right)\right)^{\frac{1}{2}}\sigma_1$$
$$\times\begin{pmatrix}P^k_{M+(n/2),(n-1)/2} & \psi^+\\ P^k_{M+(n/2),(n+1)/2} & \psi^-\end{pmatrix}$$
$$=-\left(\left(k+\frac{n}{2}+\frac{1}{2}\right)\left(k-\frac{n}{2}+\frac{1}{2}\right)\right)^{\frac{1}{2}}$$
$$\times\begin{pmatrix}P^k_{M+(n/2),(n+1)/2} & \psi^-\\ P^k_{M+(n/2),(n-1)/2} & \psi^+\end{pmatrix}.$$

Therefore (11) now becomes

$$\left[\frac{1}{i}\rho_1\left\{\sigma_3\left(\frac{\partial}{\partial r}+\frac{1}{r}\right)-\frac{\sigma_1}{r}K\right\}+\rho_3\mu+E\right]\begin{pmatrix}\psi^+\\ \psi^-\end{pmatrix}=0,$$

where

$$K=\left(\left(k+\frac{n+1}{2}\right)\left(k-\frac{n-1}{2}\right)\right)^{\frac{1}{2}}.$$

If we write $\psi=\begin{pmatrix}\psi^+\\ \psi^-\end{pmatrix}$ this equation may be written as

$$\left\{\left(\frac{\partial}{\partial r}+\frac{1}{r}\right)+\frac{i\sigma_2}{r}K\right\}\psi=i\sigma_3(i\rho_2-E\rho_1)\psi. \quad (19)$$

Choose ρ_3 diagonal and split ψ into $\begin{pmatrix}\psi_1\\ \psi_2\end{pmatrix}$ with respect to ρ_3 so that

$$\rho_3\psi=\rho_3\begin{pmatrix}\psi_1\\ \psi_2\end{pmatrix}=\begin{pmatrix}\psi_1\\ -\psi_2\end{pmatrix}.$$

Then

$$(i\rho_2\mu-E\rho_2)\psi=\begin{pmatrix}0 & \mu & -E\\ -\mu & -E & 0\end{pmatrix}\begin{pmatrix}\psi_1\\ \psi_2\end{pmatrix}.$$

Put

$$\mu+E=\frac{1}{a_1},\quad \mu-E=\frac{1}{a_2}.$$

Then (19) can be written as

$$\left\{\left(\frac{\partial}{\partial r}+\frac{1}{r}\right)+\frac{i\sigma_2}{r}K\right\}\psi_1=\frac{i\sigma_3}{a_2}\psi_2, \quad (20a)$$

$$\left\{\left(\frac{\partial}{\partial r}+\frac{1}{r}\right)+\frac{i\sigma_2}{r}K\right\}\psi_2=-\frac{i\sigma_3}{a_1}\psi_1. \quad (20b)$$

Now choose a representation in which σ_2 is diagonal so that

$$\sigma_2=\begin{pmatrix}1 & 0\\ 0 & -1\end{pmatrix},\quad \sigma_3=\begin{pmatrix}0 & 1\\ 1 & 0\end{pmatrix},\quad \sigma_1=\begin{pmatrix}0 & -i\\ i & 0\end{pmatrix}.$$

Write

$$\psi_1=\begin{pmatrix}\psi_1^+\\ \psi_1^-\end{pmatrix},\quad \psi_2=\begin{pmatrix}\psi_2^+\\ \psi_2^-\end{pmatrix}.$$

Then (20) is equivalent to the set of equations

$$\left\{\frac{\partial}{\partial r}+\frac{1}{r}+\frac{iK}{r}\right\}\psi_1^+=\frac{i}{a_2}\psi_2^-, \tag{21a}$$

$$\left\{\frac{\partial}{\partial r}+\frac{1}{r}-\frac{iK}{r}\right\}\psi_2^-=-\frac{i}{a_2}\psi_1^+, \tag{21b}$$

$$\left\{\frac{\partial}{\partial r}+\frac{1}{r}-\frac{iK}{r}\right\}\psi_1^-=\frac{i}{a_2}\psi_2^+, \tag{21c}$$

$$\left\{\frac{\partial}{\partial r}+\frac{1}{r}+\frac{iK}{r}\right\}\psi_2^+=-\frac{i}{a_2}\psi_1^-. \tag{21d}$$

Put $a=(a_1a_2)^{\frac{1}{2}}$ the square root being positive in case $a_1a_2>0$. Then we get

$$\left(\frac{\partial}{\partial r}+\frac{1}{r}-\frac{iK}{r}\right)\left(\frac{\partial}{\partial r}+\frac{1}{r}+\frac{iK}{r}\right)\psi_1^+$$

$$=\left(\frac{i}{a_1}\right)\left(\frac{-i}{a_2}\right)\psi_1^+,$$

i.e.,

$$\left\{\frac{\partial^2}{\partial r^2}+\frac{2}{r}\frac{\partial}{\partial r}+\frac{K^2-iK}{r^2}-\frac{1}{a^2}\right\}\psi_1^+=0. \tag{22a}$$

Similarly

$$\left\{\frac{\partial^2}{\partial r^2}+\frac{2}{r}\frac{\partial}{\partial r}+\frac{K^2+iK}{r^2}-\frac{1}{a^2}\right\}\psi_1^-=0, \tag{22b}$$

(22) is completely equivalent to (21) since (21a) and (21c) can be regarded as the definitions of ψ_2^- and ψ_2^+ respectively. Since the operator

$$\frac{\partial^2}{\partial r^2}+\frac{2}{r}\frac{\partial}{\partial r}+\frac{K^2\pm iK}{r^2}$$

is homogeneous in r it is clear that if $\psi(r)$ is one of its eigenfunctions corresponding to the eigenvalue $1/a^2$ and α is any real constant, the function $\psi(\alpha r)$ is another eigenfunction corresponding to the eigenvalue α^2/a^2. Hence the eigenvalues $E=(\mu^2-1/a^2)^{\frac{1}{2}}$ cannot form a discrete spectrum. We shall now show that for all permissible solutions of (22) $a^2<0$. It is sufficient to consider (22a). Put $\varphi_1^+=fe^{-r/a}$. Then

$$\left\{\frac{\partial^2}{\partial r^2}+\left(\frac{2}{r}-\frac{2}{a}\right)\frac{\partial}{\partial r}+\frac{K^2-iK}{r^2}-\frac{2}{ra}\right\}f=0.$$

The point $r=0$ is a singular point of this equation. According to the usual procedure for solving second-order linear differential equations with analytic coefficients, we make the substitution

$$f=\sum_{\nu\geq 0}c_\nu r^{\nu+\alpha},$$

where $c_0=1$ and ν runs over all non-negative integers. The indical equation is

$$\alpha(\alpha-1)+2\alpha+K^2-iK=0,$$

i.e.,

$$(\alpha+\tfrac{1}{2})^2+\left(K-\frac{i}{2}\right)^2=0.$$

Hence $\alpha=iK$ or $-iK-1$. However the boundary condition at $r=0$ requires[3] that $r\psi_1^+\to 0$ as $r\to 0$. Hence only $\alpha=iK$ is permissible. On substituting

$$f=\sum_{\nu\geq 0}c_\nu r^{\nu+iK},$$

in (23) and equating the coefficients of the various powers of r to zero we get the recurrence relation

$$c_{\nu+1}=-\frac{2}{a}\frac{\nu+iK+1}{(\nu+1)(\nu+2iK+2)}.$$

Since K is real it is clear that the series cannot terminate. It converges like $e^{2r/a}$ and therefore for large r, $\psi_1^+=fe^{-r/a}$ behaves like $e^{r/a}$. Therefore from the boundary condition at infinity it follows that only those solutions are permissible for which a is pure imaginary, i.e., $a^2<0$, or $E^2>\mu^2$. Thus the electron is never bound to the magnetic pole.

[3] See reference 2, p. 269.

A Study of the Radiations from Columbium (95), Rhenium (188), Osmium (191), and Osmium (193)*

C. E. MANDEVILLE, M. V. SCHERB,** AND W. B. KEIGHTON***
Bartol Research Foundation of the Franklin Institute, Swarthmore, Pennsylvania

(Received June 14, 1948)

The characteristic radiations of Cb^{95}, Re^{188}, Os^{191}, and Os^{193} have been investigated by absorption and coincidence methods. Maximum beta-ray energies were determined by aluminum absorption, and maximum quantum energies were measured by coincidence absorption of the secondary electrons in aluminum.

Beta-beta-, beta-gamma-, and gamma-gamma-coincidence rates were measured when possible. Some remarks concerning Sb^{124} and Au^{198} are also included.

INTRODUCTION

THE characteristic radiations of several radio-isotopes produced by slow neutron bombardment in the Oak Ridge pile have been investigated by coincidence and absorption methods. The general method has been previously described.[1] The beta-ray energies were measured by absorption in aluminum; the gamma-ray energies were measured by coincidence absorption, and whenever possible, beta-beta-, beta-gamma-, and gamma-gamma-coincidences were investigated. A coincidence resolving time of 0.10 microsecond was used throughout the course of the experiments.

COLUMBIUM (95)

The 35-day columbium (95) was separated from the fission fragments of the pile at Oak Ridge. The columbium was further purified for the removal of phosphorous, zirconium, copper, and iron as possible impurities. An absorption curve of the beta-rays of Cb^{95}, shown in Fig. 1, gave a maximum beta-ray energy of 0.14 Mev. This value agrees with earlier measurements and is an indication of the purity of the material. A coincidence absorption experiment gave 0.92 Mev as the maximum energy of the gamma-rays. These data are shown in Fig. 2. The beta-gamma-coincidence rate was found to be 1.3×10^{-3} coincidence per beta-ray as shown in Fig. 3. The gamma-ray counter was constructed of "low Z" materials and was calibrated by the beta-gamma-coincidence rate of Sc^{46}. It was thus concluded that the beta-rays of Cb^{95} are followed by 0.92 Mev of gamma-ray energy.

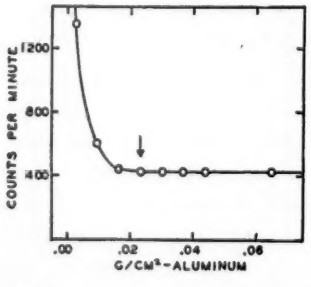

FIG. 1. Absorption in aluminum of the beta-rays of Cb^{95}.

A gamma-gamma-coincidence rate of $(0.28\pm0.02)\times10^{-3}$ coincidence per gamma-ray was also present. This indicates that the Mo^{95} residual nucleus de-excites by emission of the 0.92 Mev gamma-ray or by an alternate mode involving the emission of two or more gamma-rays.

The writers had previously assigned the 0.92 Mev gamma-ray to zirconium (95), the parent element of columbium (95), produced when zirconium is irradiated by slow neutrons.[2] The present data show that the earlier assignment was incorrect, undoubtedly the result of an incomplete chemical separation.

A small number of beta-beta-coincidences were detected in the disintegration of Cb^{95}, confirming that some of the gamma-rays are converted.[3]

* Assisted by the joint program of the Office of Naval Research and the Atomic Energy Commission.

** Now at Princeton University.

*** Also of the Department of Chemistry, Swarthmore College.

[1] C. E. Mandeville and M. V. Scherb, Phys. Rev. **73**, 141 (1948).

[2] C. E. Mandeville and M. V. Scherb, Phys. Rev. **73**, 1434 (1948).

[3] Plutonium Project Report, "Nuclei formed in fission," Rev. Mod. Phys. **18**, 513 (1946).

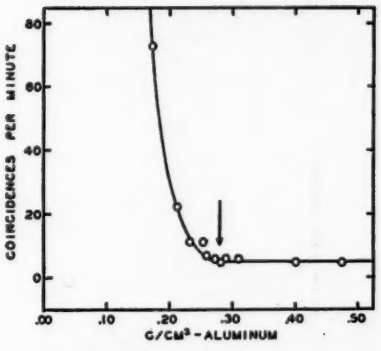

FIG. 2. Coincidence absorption of the secondary electrons of the gamma-rays of Cb^{95}.

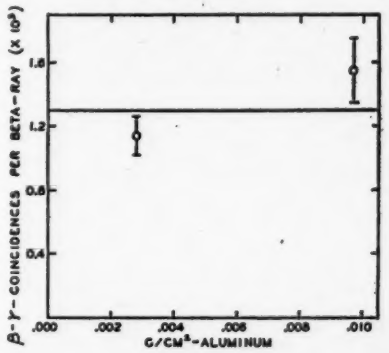

FIG. 3. Beta-gamma-coincidence rate for Cb^{95} as a function of aluminum absorber thickness before the beta-ray counter.

RHENIUM (188)

The eighteen-hour activity was induced in ReO_2, irradiated by slow neutrons for thirty minutes in the pile. Measurements were initiated about twenty hours after removal of the rhenium from the pile. Using the method of coincidence absorption, a calibrated[2] coincidence-counting set gave a maximum quantum energy of 1.39 Mev. This agrees well with 1.43 Mev reported by Miller and Curtiss[4] employing a thin lens spectrometer. The coincidence absorption data are given in Fig. 4.

A very low beta-gamma-coincidence rate, plotted in Fig. 5, was measured in Re^{188}. The beta-gamma-coincidence rate is seen to be constant from 0.5 g/cm² to 0.05 g/cm² where a rise in the curve sets in. The first point of the curve brings the coincidence rate down again. This may have been an unduly large statistical fluctuation or an indication of the presence of conversion electrons of low energy. The break in the curve at 0.05 g/cm² indicates the presence of a beta-ray spectrum having a maximum energy of 0.225 Mev. This spectrum is apparently coupled with the 1.39 Mev gamma-ray and other gamma-rays. From Fig. 5 it is seen that the beta-gamma-coincidence rate of 0.02×10^{-3} coincidence per beta-ray extends beyond a beta-ray energy of 1 Mev. This would indicate that the 2.07 Mev[5] beta-rays of Re^{188} lead to a low-lying excited level of the Os^{188} residual nucleus. Among the gamma-rays reported by Miller and Curtiss[4] is one having an energy of 0.16 Mev which in addition to being to some extent converted, is more intense than the other gamma-rays present. It seems probable that the hard beta-rays of Re^{188} are coupled with this gamma-ray.

Beta-beta-coincidences† were measured in Re^{188}. They drop to zero at 0.018 g/cm² as shown in Fig. 6. This corresponds to a conversion electron energy of 0.12 Mev or a gamma-ray energy of 0.19 Mev. The beta-gamma-coincidence rate in the beta-beta-coincidence counting arrangement was too small to measure with any accuracy so that no estimate of the internal conversion coefficient was obtained.

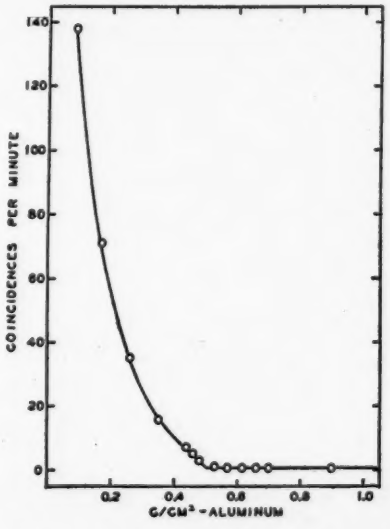

FIG. 4. Coincidence absorption of the secondary electrons of the gamma-rays of Re^{188}.

[4] L. C. Miller and L. F. Curtiss, Phys. Rev. **70**, 983 (1946).
[5] L. J. Goodman and M. L. Pool, Phys. Rev. **71**, 288 (1947).

† All beta-beta coincidence data were obtained by placing aluminum absorbers before both of the beta-ray counters.

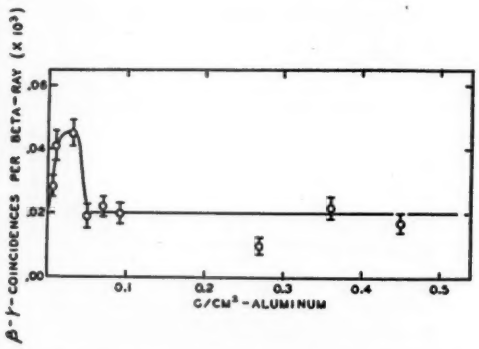

FIG. 5. Beta-gamma-coincidence rate for Re^{188} as a function of the surface density of aluminum placed before the beta-ray counter.

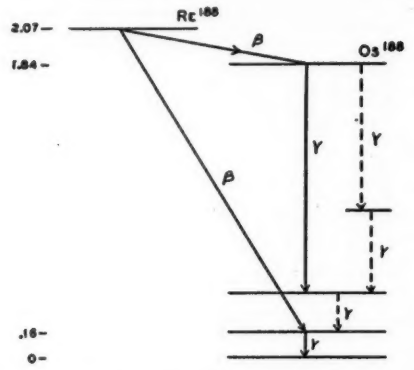

FIG. 7. Tentative disintegration scheme for Re^{188}.

A gamma-gamma-coincidence rate of $(0.096 \pm 0.009) \times 10^{-3}$ coincidence per gamma-ray was observed in the disintegration of Re^{188}, showing that gamma-rays are emitted in cascade.

The absorption and coincidence measurements on Re^{188} are summarized in Fig. 7 where a tentative and incomplete level diagram is given.

It should be remarked that during the time of the measurements, the source appeared to be decaying for the most part with a half-period of 18 hours. It has also been previously shown[6] that the 90-hour Re^{186} emits no gamma-rays so that it would appear that the measurements were hardly affected by its presence.

OSMIUM (191)

The 32-hour activity was induced in osmium irradiated by neutrons for thirty minutes in the pile. The hard beta-rays were absorbed in aluminum as shown in Fig. 8. The end point corresponds to a maximum energy of 1.15 Mev. A small beta-gamma-coincidence rate, 0.03×10^{-3} coincidence per beta-ray, independent of the beta-ray energy, is shown in Fig. 9. As in the case of Re^{188}, this suggests that the hard beta-rays lead to a low-lying excited state of the Ir^{191} residual nucleus.†† This fact is confirmed by the presence of beta-beta-coincidences shown in Fig. 10. This coincidence rate reached zero at 0.024 g/cm², corresponding to a conversion electron energy of 0.14 Mev and a gamma-ray energy of 0.22 Mev. The beta-gamma-coincidence rate in the beta-beta-coincidence counting arrangement was too small to obtain an accurate measure of the conversion coefficient.‡ A coincidence absorp-

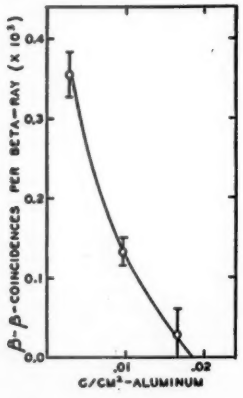

FIG. 6. Beta-beta-coincidence curve for Re^{188}.

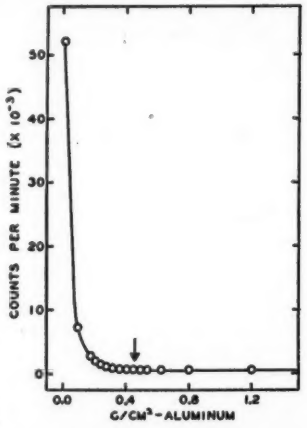

FIG. 8. Absorption in aluminum of the beta-rays of Os^{191}.

[6] E. C. Creutz, Communication to G. T. Seaborg, Rev. Mod. Phys. **16**, 1 (1944).

†† The gamma-rays from such low-lying levels in Os^{188} and Ir^{191} might be delayed. No search for delayed coincidences was made in the course of the present investigations.

‡ Calculation of conversion coefficients for both Re^{188} and Os^{191} would be difficult because the measurements of this paper give evidence of possible complexity of the beta-ray spectra of both elements.

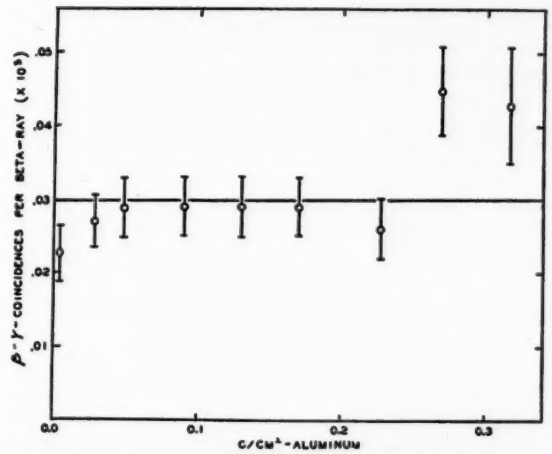

FIG. 9. Beta-gamma-coincidence rate for Os^{191} as a function of the surface density of aluminum placed before the beta-ray counter.

tion curve, shown in Fig. 11, gives a maximum gamma-ray energy of 1.58 Mev. A gamma-gamma-coincidence rate of $(0.13\pm0.03)\times10^{-3}$ coincidence per gamma-ray was also measured.

It appears that the hard gamma-ray must be coupled with a beta-ray spectrum of low energy and low intensity which made no appearance on the beta-gamma-coincidence curve. It is certainly non-coincident with the hard beta-rays.

OSMIUM (193)

After the irradiated osmium had decayed for about forty days, a small residual activity was present, the seventeen-day Os^{193}. Absorption of the beta-rays in aluminum gave a maximum energy of 0.15 Mev. These data are shown in Fig. 12.

Although the source was of low intensity, it was possible to measure beta-gamma-coincidences as shown in Fig. 13. Gamma-gamma-coincidences were also present.‡‡

ANTIMONY (124)

Several authors have recently reported internal conversion in the disintegration of Sb^{124}. Kern, Zaffarano, and Mitchell,[7] and Feister and

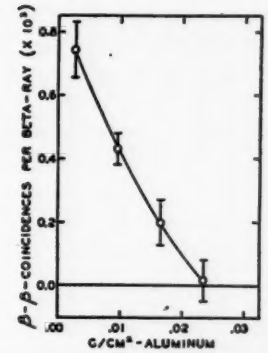

FIG. 10. Beta-beta-coincidence rate for Os^{191}.

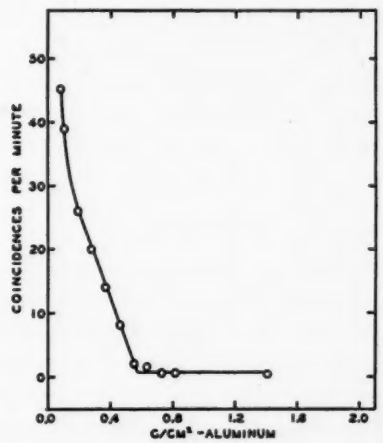

FIG. 11. Coincidence absorption of the secondary electrons of the gamma-rays of Os^{191}.

Curtiss[8] have reported conversion of the 0.6 Mev gamma-ray, and, in addition, Cook and Langer[9] have reported a conversion line corresponding to a quantum energy of 0.12 Mev. Accordingly, beta-beta-coincidences in Sb^{124} were searched for

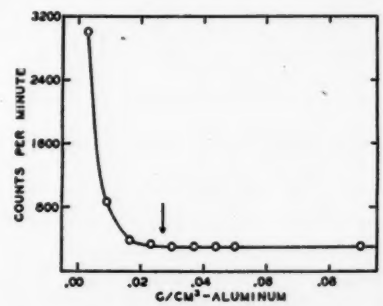

FIG. 12. Absorption in aluminum of the beta-rays of Os^{193}.

‡‡ *Note added in proof:* Saxon, Bull. Am. Phys. Soc. **23**, No. 4, 16 (1948) has reported a spectrometric value of 0.142 Mev for the beta rays of Os^{193}. Katzin and Pobereskin, Phys. Rev. **74**, 264 (1948) give absorption and coincidence data on Os^{193} very similar to those of this paper.

[7] B. D. Kern, D. J. Zaffarano, and A. C. G. Mitchell, Phys. Rev. **73**, 1142 (1948).

[8] I. Feister and L. F. Curtiss, J. Research NBS **40**, No. 4, 315 (1948).

[9] C. S. Cook and L. M. Langer, Phys. Rev. **73**, 1149 (1948).

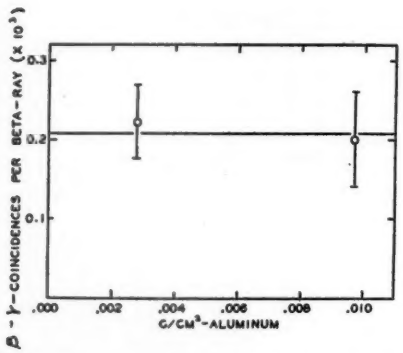

FIG. 13. Beta-gamma-coincidence rate of Os^{193}.

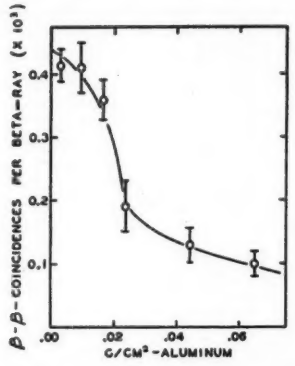

FIG. 14. Beta-beta-coincidence curve for Sb^{124}.

and found by the writers. The coincidence curve is given in Fig. 14. No conclusions have been drawn with regard to a conversion coefficient, because more than one converted gamma-ray is present, and the beta-ray spectrum is very complex.

GOLD (198)

A short time ago, the writers published[10] what they felt constituted conclusive evidence that gamma-gamma-coincidences are present in the disintegration of Au^{198}. Since that time it has been pointed out that the low gamma-gamma-coincidence rate could be explained by the presence of the 23-hour mercury activity. The Au^{198} of the previously performed gamma-gamma-coincidence experiment was chemically purified so that mercury should not have been present. The chemical purification is given in the appendices of this paper.[11]

ACKNOWLEDGMENT

The writers wish to acknowledge the continued interest of Dr. W. F. G. Swann, Director of the Bartol Research Foundation.

APPENDIX I

Chemical Purification of Columbium (95)

One mc of Cb^{95} in solution as the oxalate complex, carrier free, was mixed with a solution of inactive columbium. The solution of inactive columbium was prepared from 0.1 g of Cb_2O_5 fused with $KHSO_4$ and dissolved in ammonium oxalate solution. The combined oxalate solutions were diluted to 60 cc and carefully neutralized with ammonia and hydrochloric acid. Two grams of NH_4Cl were added, and the columbium was precipitated with excess tannin and ignited to Cb_2O_5.

ZrO_2, 0.1 g, was added as a carrier, and the precipitate and carrier were fused with K_2CO_3. The melt, when cold, was leached with cold water to dissolve the columbium, which was then precipitated with SO_2. The precipitate was ignited to Cb_2O_5.

This procedure was intended to separate from the columbium phosphorous, zirconium, copper, and iron.

APPENDIX II

Chemical Purification of Gold (198)

About 15 mg of gold from the pile and an equal quantity of inactive gold were dissolved in boiling aqua regia, and the excess was boiled away. A few milligrams of platinum were added as H_2PtCl_6. 20 ml of water, 1 ml of HCl, and 4 ml of saturated SO_2 solution were then added. After standing on the steam bath for an hour, filter pulp was added; the precipitated gold was washed by decantation with hot dilute HCl (1:99) and collected on a filter. The precipitate was digested for three hours with concentrated ammonia to remove any possible AgCl and was then washed with water.

The gold was again dissolved with dilute aqua regia and washed from the paper pulp with hot, dilute HCl. After adding several milligrams of H_2PtCl_6 the extract was evaporated to dryness, moistened with HCl, and again evaporated. Two

[10] C. E. Mandeville and M. V. Scherb, Phys. Rev. **73**, 634 (1948).

[11] For recent information on the gamma-rays of Au^{198}, see DuMond, Lind, and Watson, Phys. Rev. **73**, 1392 (1948).

repetitions of this process destroyed the HNO_3. The residue, dissolved in 1 ml of HCl, 1 drop of H_2SO_4, and 15 ml of water, was treated with 5 ml of a saturated oxalic acid solution, and boiled for ten to fifteen minutes. After standing for four hours, it was washed with dilute HCl (1:99), filtered with paper pulp, and finally ignited to gold. This procedure was intended to separate the gold from most other metals including platinum, silver, and mercury, calcium, and iron.

PHYSICAL REVIEW VOLUME 74, NUMBER 8 OCTOBER 15, 1948

A Note on the Magnetic Moment of the Electron

J. M. LUTTINGER*
Swiss Federal Institute of Technology, Zurich, Switzerland
(Received May 19, 1948)

Recent experiments seem to require a modification in the g-factor of the electron. It has been suggested that the coupling between the electron and the radiation field is responsible, and Schwinger has calculated the effect on the basis of a general subtraction formalism for the infinities of quantum electrodynamics. It is here shown that the change in magnetic moment may be derived very simply without any reference to an elaborate subtraction formalism.

I.

IT has been suggested recently by Schwinger[1] that the coupling between an electron and the radiation field leads to a change in the g-factor of the electron, as seems to be required by experiment.[2] This result was derived on the basis of his (as yet unpublished) general subtraction formalism for the infinities of quantum electrodynamics. It is the purpose of this note to show that the change in magnetic moment may be derived very simply without any reference to an elaborate subtraction formalism.

We may characterize the problem as follows: Given an electron in a homogeneous magnetic field, what is the energy of this electron as a result of interactions with the zero-point vibrations of the quantized radiation field? It is well known that this energy is infinite, the infinities which arise usually being ascribed to changes in the mass and charge of the electron. What we seek are those parts of the energy which do not correspond to the ordinary mass and charge changes, but those which arise because of the presence of the external magnetic field. The problem of subtracting the original infinities is made very simple in this case by the existence of a state for the electron (in a homogeneous magnetic field) which has as an energy simply $E=m$.[3] This is a direct result of the fact that the (unperturbed) Dirac electron has a g-factor of exactly 2. For this state we have the energy of the orbital magnetic moment exactly canceling the energy of the spin magnetic moment. The change in energy of such a state due to a change in mass ($E_{\text{self}}(0)$) and charge of the electron is simply

$$\Delta E = E_{\text{self}}(0), \tag{1}$$

which is independent of the external field. This means that when we calculate the energy and find terms which depend on the external field strength, these terms must represent the true change in the energy, and they must converge. This expectation is borne out by the calculation of the energy to terms linear in H_0 (the external field strength). The coefficient of this latter term gives immediately the alteration of the g-factor of the electron.

II.

We now proceed to an outline of the calculation. For the electron we must use the quantized formalism of the theory of holes[4] and for the

* Fellow of The Institute for International Education.

[1] J. S. Schwinger, Phys. Rev. **73**, 415 (1948); Bull. Am. Phys. Soc. **23**, 15 (April 1948).

[2] See for example: P. Kusch and H. M. Foley, Phys. Rev. **72**, 256 (1947); **73**, 412 (1948); J. Nafe and E. Nelson, Phys. Rev. **73**, 718 (1948).

[3] We shall use throughout natural units, e.g., $\hbar=c=1$. m is the mass of the electron.

[4] Cf. G. Wentzel, *Ein. in die Quant. Theorie der Wellenfelder* (Franz Deuticke, Wien, 1943), pp. 158–91.

radiation field we must use the formalism of quantum electrodynamics.[5]

The Hamiltonian is then given by

$$H=H_0+H_1+H_{\text{static}}, \tag{2}$$

where

$$H_0=i\int(-\psi^*(\alpha\cdot\nabla-ieA_0)\psi-im\psi^*\beta\psi)d^3x + (1/8\pi)\int(E^2+H^2)d^3x,$$

putting

$$\psi=\sum_n a_n\psi_n,$$

$$H_0=\sum_n a_n^*a_nE_n+\sum_s k_sc_s^*c_s,$$

$$H_1=-e\int(\psi^*\alpha\psi)\cdot Ad^3x = -\sum_{n,s}(eA_s/\sqrt{2})c_s^*a_n^*a_{n'}V_{nn'}^{(s)} + \text{Herm. conj.},$$

$$H_{\text{static}}=\frac{1}{2}\int\int\frac{\rho(x)\rho(x')}{|x-x'|}d^3xd^3x' =\frac{e^2}{2}\sum_{n,n',l,l'}a_n^*a_{n'}a_l^*a_{l'} \times\int\int\frac{(\psi_n(x)\psi_{n'}(x))(\psi_l(x')\psi_{l'}(x'))}{|x-x'|}d^3xd^3x'.$$

The following notations have been used:

α is the Dirac vector matrix $(\alpha_x, \alpha_y, \alpha_z)$;

A_0 is the vector potential of the external field;

E_n, ψ_n are the eigenvalues and eigenfunctions of the Dirac equation

$$(\alpha\cdot((1/i)\nabla-eA_0)+m\beta)\psi_n=E_n\psi_n;$$

a_n^*, a_n are, respectively, the creation and destruction operators of an electron in state n. They satisfy $a_n^*a_{n'}+a_{n'}a_n^*=\delta_{nn'}$, etc.;

c_s^*, c_s are, respectively, the creation and destruction operators of a photon in a state with momentum k_s and polarization vector e_s. $c_sc_{s'}^*-c_s^*c_{s'}=\delta_{ss'}$, etc.;

A is the vector potential of the radiation field—

$$A=\sum_s(A_s/\sqrt{2})(c_se^{ik_s\cdot x}+c_s^*e^{-ik_s\cdot x})e_s;$$

$A_s=(4\pi/k_sG)^{\frac{1}{2}}$, $G=$normalization volume;

$$V_{nn'}^{(s)}\equiv\int d^3x(\psi_n^*\alpha_s\psi_{n'})e^{-ik_s\cdot x}, \quad \alpha_s\equiv e_s\cdot\alpha.$$

We are now interested in calculating the energy to $0(e^2)$. This means that we have to take the mean value of H_{static} for one particle in the state m, and no photons present. This yields:

$$\langle H_{\text{static}}(m)\rangle_{Av}=\frac{e^2}{2}\sum_{\substack{l\\E_l>0}} \times\int\int\frac{(\psi_m^*(x)\psi_l(x))(\psi_l^*(x')\psi_m(x'))}{|x-x'|}d^3xd^3x' +\frac{e^2}{2}\sum_{\substack{n,n\neq m\\E_n>0\\l,E_l<0}}\int\int\frac{(\psi_n^*(x)\psi_l(x))(\psi_l^*(x')\psi_n(x'))}{|x-x'|}d^3xd^3x' +e^2\sum_{\substack{l\\E_l<0}}\int\int\frac{(\psi_m^*(x)\psi_m(x))(\psi_l^*(x)\psi_l(x'))}{|x-x'|}d^3xd^3x'.$$

The third term represents the interaction between the vacuum charge density

$$\rho_0(=\sum_{l,E_l<0}e\psi_l^*(x')\psi_l(x'))$$

and the charge density of the particle

$$\rho_m(=e\psi_m^*(x)\psi_m(x)).$$

This term may be dropped (as well as the corresponding term from H_1 for the interaction between the particle current and vacuum current), since it is well known[6] that a homogeneous magnetic field gives rise to no polarization of the vacuum effects. From this value we must subtract the corresponding value when only the vacuum is present (negative energy states filled). This gives:

$$\langle H_{\text{static}}(\text{vac})\rangle_{Av}=\frac{e^2}{2}\sum_{\substack{n,l\\E_n>0\\E_l<0}} \times\int\int\frac{(\psi_n^*(x)\psi_l(x))(\psi_l^*(x')\psi_n(x')}{|x-x'|}d^3xa^3x'.$$

Defining now the electrostatic energy as

$$\langle H_{\text{static}}(m)\rangle_{Av}-\langle H_{\text{static}}(\text{vac})\rangle_{Av}$$

[5] See reference 4, pp. 107–133.

[6] V. F. Weisskopf, Kgl. Danske Vid. Sels. Math.-Fys. Medd. **14**, 6 (1936).

we get

$$\Delta E_{\text{static}}=\frac{e^2}{2}\sum_l \delta_l \times\int\int \frac{(\psi_m^*(x)\psi_l(x))(\psi_l^*(x')\psi_m(x'))}{|x-x'|}d^3xd^3x', \quad (6)$$

where

$$\delta_l=+1, \quad E_l>0,$$
$$=-1, \quad E_l<0.$$

To calculate the contribution from $H_1(\Delta E_{\text{dynamic}})$, one must use second-order perturbation theory. When this is done, the vacuum value and polarization of the vacuum terms removed, we are left with

$$\Delta E_{\text{dynamic}}=(-2\pi e^2/G)\sum_s \frac{1}{k_s}\sum_l \frac{|V_{ln}^{(s)}|^2}{\delta_l k_s+E_l-E_m}. \quad (7)$$

The total energy will be given by

$$\Delta E=\Delta E_{\text{static}}+\Delta E_{\text{dynamic}}.$$

We now have to sum the series (6) and (7), using the exact eigenfunctions and eigenvalues of the Dirac equation. These are given in the appendix. The state m in question is that with $n=p_2=p_3=0$, $E_m=m$, and

$$\psi_m=(1/G^{\frac{1}{2}})\begin{bmatrix}0\\ v(x)\\ 0\\ 0\end{bmatrix}, \quad (8)$$
$$v(x)=\exp-[(eH_0)x^2/2](eH_0/\pi)^{\frac{1}{4}}.$$

Let us first evaluate the electrostatic energy. Substituting the above value for ψ_m and the values of the eigenfunctions from the appendix, we get:

$$Q\equiv\sum_l \delta_l(\psi_m^*(x)\psi_l(x))(\psi_l^*(x')\psi_m(x'))$$
$$=(m/G^{4/3})\sum_{p_2,p_3}\sum_{n=0}^{\infty}(1/E_n)(v(x)v^{(n)}(x)\cdot\times\exp i(p_2y+p_3z))(v(x')v^{(n)}(x')\times\exp-i(p_2y+p_3z))$$

where

$$E_n=(m^2+p_3^2+2eH_0m)^{\frac{1}{2}}$$
$$v^{(n)}(x)=\exp[-\xi^2/2]H_n(\xi)\times[(eH_0)^{\frac{1}{4}}/\pi^{\frac{1}{4}}2^{n/2}(n!)^{\frac{1}{2}}]$$
$$\xi=(eH_0)^{\frac{1}{2}}[x-(p_2/eH_0)].$$

Therefore,

$$\Delta E_{\text{static}}=\frac{e^2}{2}\int\int\frac{Q}{|x-x'|}d^3xd^3x'$$
$$=\frac{mc^2}{2G^{4/3}}\sum_{p_2,p_3}\sum_n\frac{1}{E_n}\int\int\frac{(v(x)v^{(n)}(x)\exp i(p_2y+p_3z))(v(x')v^{(n)}(x')\exp-i(p_2y'+p_3z'))}{|x-x'|}d^3xd^3x'.$$

It is convenient to go over to momentum space in order to evaluate these integrals. Define

$$\rho_n(x)\equiv v(x)v^{(n)}(x)\exp[i(p_2y+p_3z)],$$

and

$$\rho_n(k)\equiv\int\rho_n(x)\exp[-ik\cdot x]d^3x.$$

Then, as is well known,

$$\int\int[\rho_n(x)\rho_n^*(x')/|x-x'|]d^3xd^3x'=(4\pi/G)\sum_k[\rho_n(k)\rho_n^*(k)/k^2].$$

Therefore

$$\Delta E_{\text{static}}=(2\pi e^2m/G^{7/3})\sum_{p_2,p_3}\sum_{n=0}^{\infty}(1/E_n)\times\sum_k(1/k^2)\rho_n(k)\rho_n^*(k).$$

The integrals giving $\rho_n(k)$ are easily evaluated:

$$\rho_n(k)=G^{2/3}\delta_{k_2p_2}\delta_{k_3p_3}\frac{(-)^n}{2^{n/2}(n!)^{\frac{1}{2}}}\left(\frac{p_2+ik_1}{(eH_0)^{\frac{1}{2}}}\right)^n\times\exp\left[-\frac{p_2^2+k_1^2+2ip_2k_1}{4eH_0}\right],$$

or

$$\Delta E_{\text{static}}=\frac{2\pi e^2 m}{G}\sum_{p_2,p_3}\sum_{n=0}^{\infty}\frac{1}{E_n}\sum_{k_1}\frac{1}{(k_1^2+p_2^2+p_3^2)}\times\frac{\left(\frac{p_2^2+k_1^2}{eH_0}\right)^n}{2^n n!}\exp[-(p_2^2+k_1^2)/2eH_0]$$

$$=\frac{e^2 m}{4\pi^2}\sum_{n=0}^{\infty}\frac{1}{n!}\frac{1}{E_n}\int\int\int_{-\infty}^{\infty}dk_1 dp_2 dp_3\times\frac{1}{(k_1^2+p_2^2+p_3^2)}\left(\frac{p_2^2+k_1^2}{2eH_0}\right)\times\exp[-(p_2^2+k_1^2)/2eH_0].^{**}$$

Going over to polar coordinates for the variable k_1, p_2 we get (writing $r^2=k_1^2+p_2^2$ and $p_3=p$)

$$\Delta E_{\text{static}}=\frac{e^2 m}{2\pi}\sum_{n=0}^{\infty}\frac{1}{n!}\int_{-\infty}^{\infty}dp\int_0^{\infty}rdr\frac{1}{r^2+p^2}\times\left(\frac{r^2}{2eH_0}\right)^n e^{-r^2/2eH_0}\frac{1}{\sqrt{m^2+p^2+2eH_0 n}}$$

$$=\frac{e^2 m}{2\pi}\int_{-\infty}^{\infty}dp\int_0^{\infty}rdr\frac{1}{(r^2+p^2)}f$$

$$f\equiv\sum_{n=0}^{\infty}\frac{\eta^n}{n!(m^2+p^2+2eH_0 n)^{\frac{1}{2}}}e^{-\eta},\quad \eta\equiv\frac{r^2}{2eH_0}.$$

Now we need f for vanishingly small values of H_0, since it is the linear term (in H_0) of ΔE_{static} which gives the change in g-factor of the electron. Therefore, we seek to sum this series for $H_0\to 0$, i.e., for $\eta\to\infty$. The function $\eta^n/n!$ for η very large has a sharp maximum at $n=\eta$. On the other hand the function

$$g(n)=(m^2+p^2+2eH_0 n)^{-\frac{1}{2}}$$

is, under the same conditions, a very slowly varying function of n. We therefore expand it about the point $n=\eta$, and get

$$g(n)=g(\eta)+(n-\eta)g'(\eta)+\frac{(n-\eta)^2}{2!}g''(\eta)+\cdots$$

or

$$f=e^{-\eta}\sum_{n=0}^{\infty}\left(g(\eta)+(n-\eta)g'(\eta)+\frac{(n-\eta)^2}{2!}g''(\eta)+\cdots\right)(\eta^n/n!)$$

$$=g(\eta)+[\eta g''(\eta)/2]+\cdots$$

$$=[1/(m^2+p^2+r^2)^{\frac{1}{2}}]+\tfrac{3}{4}[(eH_0)r^2/(m^2+p^2+r^2)^{5/2}]+\cdots.$$

Therefore,

$$\Delta E_{\text{static}}=\frac{e^2 m}{2\pi}\int_{-\infty}^{\infty}dp\int_0^{\infty}rdr\frac{1}{(r^2+p^2)(m^2+p^2+r^2)^{\frac{1}{2}}}\times\left[1+\frac{3}{4}\frac{(eH_0)r^2}{(m^2+p^2+r^2)^2}+\cdots\right]$$

$$=\Delta E_{\text{static}}(0)+\frac{3e^2 m}{8\pi}\left(\int_{-\infty}^{\infty}dp\int_0^{\infty}rdr\times\frac{r^2}{m(r^2+p^2)(m^2+p^2+r^2)^{5/2}}\right)(eH_0)+\cdots$$

$$=\Delta E_{\text{static}}(0)+(e^2/3\pi)(e/2m)H_0+\cdots. \quad (8)$$

The first term $\Delta E_{\text{static}}(0)$ is simply the electrostatic self-energy of an electron at rest.[7] The remaining term converges, and is to be interpreted as the change of the g-factor of the electron due to its interaction with longitudinal photons.

Proceeding now to the expression for the dynamic self-energy, we find (after carrying out the integration in $V_{mn}^{(s)}$ several obvious summations, and simplifying):

$$\Delta E_{\text{dynamic}}=F(m)-F(-m),$$

where

$$F(m)\equiv\sum_{n=0}^{\infty}(e^2/4\pi)\int_{-\infty}^{\infty}dp\int_0^{\infty}\frac{\eta^n e^{-\eta}}{n!}\times\left\{\frac{1+(p^2/k^2)}{E_{n+1}(k+E_{n+1}-m)}+\frac{1-(p^2/k^2)}{E_n(k+E_n-m)}\right\}rdr,$$

$k^2\equiv p^2+r^2$.

Exactly the same method as before may be used to carry out the summation over n. We

** Here we have replaced the sums by integrals

$$\sum_{k_1}\to(G^{\frac{1}{2}}/2\pi)\int dk_1, \text{ etc.}$$

[7] V. F. Weisskopf, Phys. Rev. 56, 72 (1939).

shall not enter into the details of this straightforward calculation, but shall only quote the result:

$$\Delta E_{\text{dynamic}}=\Delta E_{\text{dynamic}}(0) -(5e^2/6\pi)(e/2m)H_0+\cdots. \quad (9)$$

The first term is simply the dynamic self-energy of an electron at rest (cf. reference 7). What remains converges and is the contribution of the transverse photons to the magnetic moment of the electron. We thus get for the energy of an electron in the state m,

$$\Delta E=\Delta E_{\text{static}}(0)+\Delta E_{\text{dynamic}}(0) -(e^2/2\pi)(e/2m)H_0 \quad (10)$$

(dropping higher powers of H_0). The sum of the first two terms of (10) is simply $E_{\text{self}}(0)$, and according to the ideas of the first section this is to be subtracted. Therefore, we are left with

$$\Delta E_{\text{true}}=-(e^2/2\pi)(e/2m)H_0. \quad (11)^{***}$$

(11) is to be regarded as the true change in energy of an electron in an external magnetic field, due to coupling with the radiation field. To interpret this in terms of a change in g-factor we note that if the electron had a g-factor of $g=2(1+\delta)$, then in the state m its energy would be

$$E=eH_0/2m(1-\tfrac{1}{2}g)=-(eH_0/2m)\delta.$$

Equating E and ΔE_{true} we get

$$\delta=(1/2\pi)e^2,$$

or $\delta=(1/2\pi)(e^2/\hbar c)$ in conventional units. Therefore

$$g=2(1+(1/2\pi)(e^2/\hbar c)). \quad (12)$$

This corresponds exactly to the result of Schwinger.

In conclusion I should like to thank Professor W. Pauli and Doctor Res Jost for many valuable and stimulating discussions.

APPENDIX

The eigenfunctions fall into four classes, corresponding to the two different spins and signs of energy. They are

$$E_1=+[m^2+p_3^2+2eH_0(n+1)]^{\frac{1}{2}},$$

$$\psi_1(n,p_2,p_3)=\exp i(p_2y+p_3z)/[2(E_1^2+mE_1)]^{\frac{1}{2}}\begin{bmatrix}(E_1+m)v^{(n)}\\0\\p_3v^{(n)}\\-(eH_0(2)(n+1))^{\frac{1}{2}}v^{(n+1)}\end{bmatrix}(1/G^{\frac{1}{2}}),$$

$$E_2=+[m^2+p_3^2+2eH_0(n)]^{\frac{1}{2}},$$

$$\psi_2(n,p_2,p_3)=\exp i(p_2y+p_3z)/[2(E_2^2+mE_2)]^{\frac{1}{2}}\begin{bmatrix}0\\(E_2+m)v^{(n)}\\-(2eH_0n)^{\frac{1}{2}}v^{(n-1)}\\-p_3v^{(n)}\end{bmatrix}(1/G^{\frac{1}{2}}),$$

$$E_3=-[m^2+p_3^2+2eH_0(n+1)]^{\frac{1}{2}},$$
$$=-E_1,$$

$$\psi_3(n,p_2,p_3)=\exp i(p_2y+p_3z)/[2(E_1^2-mE_1)]^{\frac{1}{2}}\begin{bmatrix}v^{(n)}(-E_1+m)\\0\\p_3v^{(n)}\\-[eH_0(2)(n+1)]^{\frac{1}{2}}v^{(n+1)}\end{bmatrix}(1/G^{\frac{1}{2}}),$$

*** It should be mentioned that in reality nothing is subtracted from the magnetic moment term. One could have defined $M\equiv-\dfrac{\partial E}{\partial H_0}\Big|_{H_0=0}$, which would have given a finite result automatically. This consideration shows that we can expect our result to be relativistically correct, since we have used a Lorentz invariant formalism throughout.

$$E_4 = -[m^2+p_3^2+2eH_0(n)]^{\frac{1}{2}},$$
$$= -E_2,$$

$$\psi_4(n, p_2, p_3) = \exp i(p_2y+p_3z)/[2(E_2^2-mE_2)]^{\frac{1}{2}} \begin{bmatrix} 0 \\ v^{(n)}(-E_2+m) \\ -v^{(n-1)}(2eH_0n)^{\frac{1}{2}} \\ -p_3v^{(n)} \end{bmatrix} (1/G^{\frac{1}{2}}),$$

where

$$v^{(n)} = e^{-\xi^2/2}H_n(\xi)[(eH_0)^{\frac{1}{2}}/\pi^{\frac{1}{2}}2^{n/2}(n!)^{\frac{1}{2}}], \quad \xi = (eH_0)^{\frac{1}{2}}[x-(p_2/eH_0)].$$

H_n are the ordinary Hermite polynomials.

The usual representations of the Dirac matrices have been used, with the exception that α_y and α_z have been interchanged.

PHYSICAL REVIEW VOLUME 74, NUMBER 8 OCTOBER 15, 1948

On the Life of Self-Quenching Counters*

S. S. FRIEDLAND**
Sloan-Kettering Institute of Memorial Hospital and New York University, New York, New York
(Received June 7, 1948)

A Geiger-Müller counter filled with argon and ethyl acetate was connected to a mass spectrometer, and spectra were obtained after predetermined numbers of counts. Results showed that factors influencing the life of the counter were the disappearance of the quenching vapor and the formation of non-quenching vapors. An argon-methane counter, studied by the same method, showed that contamination of the insides of the counter, by the dissociation products, limited its life. This process occurred before any appreciable fraction of the methane was consumed.

INTRODUCTION

THE purpose of this investigation was to examine the factors influencing the life of self-quenching Geiger-Müller counters. The life of a counter is usually defined to be the number of counts that the counter is capable of detecting before becoming inoperative as a result of internal failure for any reason. Observed lives are known to vary from 10^7 counts for a methane counter to 10^{10} counts for an argon-alcohol counter.

PRESENT THEORIES FOR THE OBSERVED LIFETIME

The finite life of self-quenching counters is explained by theories proposed by S. A. Korff and R. D. Present,[1] by the Montgomerys,[2] and by Stever.[3] The explanation lies in the quenching mechanism of the counter. We first note that there are three essential quenching mechanisms. (a) Absorption of photons from the avalanche, (b) quenching of secondary emission when the positive ions reach the cathode, and (c) electrostatic quenching. The Korff-Present theory deals with mechanism (a) and (b). They showed that the polyatomic gas in a self-quenching counter has two functions: (*i*) To quench the ultraviolet photons that are emitted by the excited states of the inert gas and (*ii*) to quench secondary emission by positive ions reaching the cathode. The authors point out that the characteristic property of a polyatomic molecule which is of importance

* This paper is based partially on work done under Contract N6ori-99 with the Office of Naval Research.
** Now at the University of New Mexico, Albuquerque, New Mexico.

[1] S. A. Korff and R. D. Present, Phys. Rev. 65, 274 (1944).
[2] C. G. Montgomery and D. D. Montgomery, Phys. Rev. 57, 1030 (1940).
[3] H. G. Stever, Phys. Rev. 61, 38 (1942).

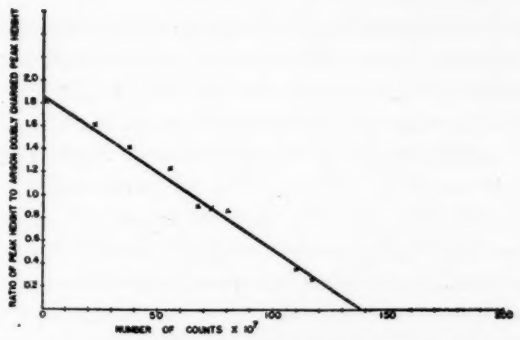

FIG. 1. Decay of mass 87 as a function of the number of counts.

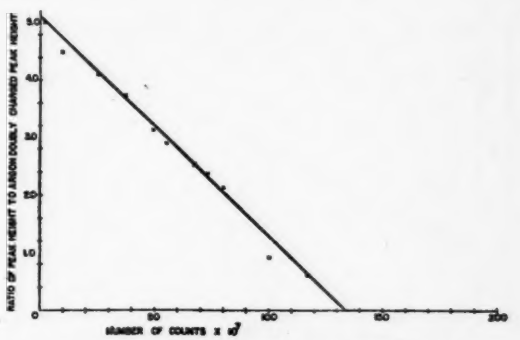

FIG. 3. Decay of mass 61 as a function of the number of counts.

in the counter is its large probability of predissociation from excited electronic states. They found that the quenching of ultraviolet photons in the initial avalanche occurs through the photodecomposition of the polyatomic gas, and that the electron transfer probability ensures that the positive ion sheath, when it reaches the cathode, is composed entirely of polyatomic ions. These are neutralized at distances of about 10^{-7} cm from the wall, and the excited neutral molecules predissociate in 10^{-13} second before they can liberate a secondary electron by an inelastic collision with the wall or by recombination radiation. The authors further show that since no supply of secondary electrons is available the discharge terminates.

As proposed by Montgomery[2] and Stever,[3] the initial electrostatic quenching in the counter takes place because of the positive ions surrounding the central wire. Their presence at the central wire binds electrons to the wire, and as a result the field intensity drops to a value which is insufficient to support a Townsend avalanche.

Since the number of ions per discharge required around the central wire to desensitize the counter is a constant, we can say the sum of organic molecules and inert atoms present in the ion sheath will be a constant, provided the size of the pulse remains the same. However, as the organic vapor is consumed, the ratio of organic ions to argon ions at the central wire will decrease. Korff and Present state that as the sheath drifts outward, there is a transfer of charge from the inert gas to the polyatomic gas. Thus when the sheath reaches the cylinder it is composed entirely of polyatomic molecules, and the counter quenches because of the mechanism described above.

As arguments in favor of the mechanism described above, Korff and Present note the following two considerations. (a) In an average counter there are approximately 10^{20} polyatomic molecules. In each discharge about 10^{10} quenching ions are decomposed at the wall. Therefore, after 10^{10} counts, the quenching mechanism will no longer occur. This is in agreement with results reported by Spatz.[4] (b) If the ionization potential

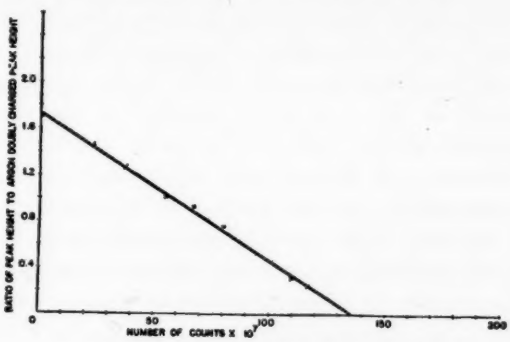

FIG. 2. Decay of mass 70 as a function of the number of counts.

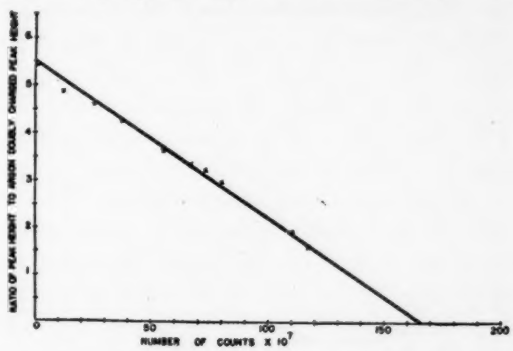

FIG. 4. Decay of mass 45 as a function of the number of counts.

[4] W. D. B. Spatz, Phys. Rev. 64, 236 (1943).

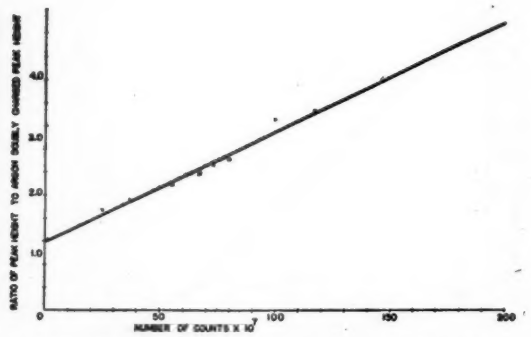

FIG. 5. Growth of mass 44 as a function of the number of counts.

of the polyatomic gas is higher than the ionization potential of the inert gas, the electron transfer of charge will not take place and the counter should therefore not quench. Experiments of Korff and Present verify this point.

There are meager data in the literature showing the dissociation of a gas in a discharge and no direct data for the dissociation in a counter. It was therefore thought advisable to examine the contents of a counter, as it is being used, with a mass spectrometer. If the above theory is correct, the polyatomic molecule should disappear linearly with use as a constant number of ions are dissociated per discharge.

EXPERIMENTAL PROCEDURE

A counter of the thin-walled type[5] of 15-cm length, 2-cm diameter, with a 4-mil tungsten wire was used. The cathode consisted of a silver deposit on the glass surface. The silver portion extended for a length of 8 cm, with the thin-walled section 6 cm long. The glass thickness was of the order of 10^{-2} cm. The counter was connected to a mass spectrometer through a flattened piece of copper tubing[6] bent into a hairpin shape which could be compressed so that no gas flowed into the mass spectrometer between runs.

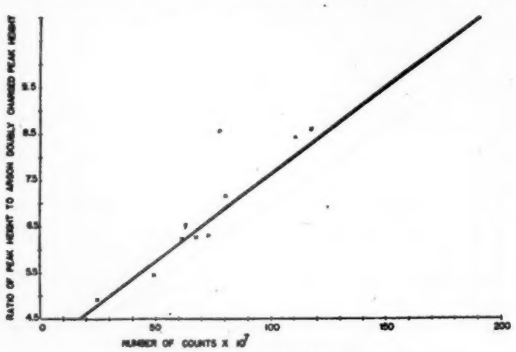

FIG. 6. Growth of mass 28 as a function of the number of counts.

[5] Made by Eck and Krebb, New York City.

A radium source was placed near the counter to maintain a counting rate of 1000 counts per second. The counts were recorded on a mechanical recorder after they were scaled down by a factor of 4096. Frequent checks on the overvoltage were made to insure discharges of uniform size. An overvoltage of 100 volts was used throughout, and a resistor of 2 megohms was placed between the central wire and ground.

The mass spectrometer used was the 90-degree sector type which is located at the Westinghouse Research Laboratories. The instrument is capable of scanning mass numbers 14 through 140 in approximately 15 minutes. The recording system[7] utilizes a speedomax which is connected to an automatic shunt selector.

RESULTS

Results with an Ethyl Acetate-Argon Counter

An ethyl acetate-argon counter was chosen for study as it has been used extensively in this laboratory. The counter was filled to a pressure of 1.5 cm of Hg with ethyl acetate and 10 cm of Hg with argon.

All the peak heights obtained with the mass spectrometer were divided by the peak height of the doubly charged argon which corresponds to mass 20. This was deemed advisable since fragments of an organic molecule formed in the ionization chamber of the mass spectrometer have a low probability of falling on mass 20, and also the number of argon atoms in the counter remains constant.

The ratios thus obtained were plotted as a function of the number of counts. Figures 1–4 show that the fragments of the parent molecule formed in the ionization chamber of the spectrometer all decrease linearly with the number of counts, and Figs. 5 and 6 show that the final non-quenching vapors formed at masses 28 and 44, probably CO and CO_2, increase linearly with the number of counts. The mass spectrometer was not at all times operated in the region of

[6] A. O. Nier, Rev. Sci. Inst. 15, 191 (1947).

[7] D. J. Grove and J. A. Hipple, Rev. Sci. Inst. 18, 191 (1947).

hydrogen masses 1 and 2. The data obtained on the concentration of hydrogen was limited to a new and a completely used counter. A sharp increase in the concentration of hydrogen was detected with a used counter as compared to an unused counter.

The linear decrease of the parent molecule with the number of counts agrees with the Korff-Present theory. Therefore, we can state that one factor influencing the life of a counter is the disappearance of the quenching gas. That this is not the only factor influencing the life of a counter will now be shown.

Results with a Methane-Argon Counter

A counter filled with methane at a pressure of 6 cm of Hg and argon at a pressure of 4 cm of Hg was studied by the same method. However, in this case only two points on the curve were obtained, as the counter no longer quenched after 10^7 counts. A mass spectra showed that a very small percentage of the methane had been consumed. The various peak heights before and after use in a methane-argon counter is shown in Table I.

TABLE I. Peak heights before and after use in a methane-argon counter.

Mass	Unused	Used
2	0.0	15.2
13	10.9	10.5
14	29.7	28.7
15	306.0	290.0
16	406.5	383.5
17	4.3	3.8
18	2.8	1.0
24	0.0	0.5
25	0.0	2.5
26	0.9	17.8
27	1.8	10.6
28	9.0	47.4
29	2.2	11.8
30	1.3	5.0
40	79.0	78.0

The increase of masses 27 and 28 indicates that the fragments of the methane formed in the earlier processes of quenching the counter were polymerizing into organic compounds such as C_2H_4. From these molecules others are probably formed and are eventually deposited upon the cylinder wall. The presence of these hydrocarbons upon the wall interfere with counter action and eventually stop the counter from functioning by contaminating the insides of the counter.

The mass spectra data clearly show that, at least in the case of methane, dissociation does not explain the finite life of a counter. A more detailed study of a methane counter was made by Farmer and Brown, and their result will be discussed in the following paper of this issue.

CONCLUSION

There are two processes which limit the life of a counter. (a) The disappearance of the quenching vapor as a result of dissociation, and (b) the deposition on the cathode cylinder of hydrocarbons from polymerization processes, which contaminates the inside and renders the counter useless.

It should be pointed out that the formation of polymers is known to occur in electrical discharges in the presence of even small quantities of hydrocarbon material.[8]

If we consider the above conclusions, we see that a set of experiments is necessary to conclude which gases are limited in their life for counter use by the two processes mentioned above. Those that are immediately affected by polymerization, such as methane, must be eliminated as quenching vapors. From the data obtained on ethyl-acetate it appears that it is free from the limitation of process two. It may further be pointed out that the ideal counter is one that is free of process two and one that replenishes the polyatomic vapor as it is consumed. Investigations to determine which gases will conform to this requirement are now under way.

ACKNOWLEDGMENTS

This work was conducted under the supervision of Professor Serge A. Korff of New York University. The writer is indebted to him for his helpful suggestions, and for the innumerable discussions which helped to clarify the problem. The writer wishes to thank Dr. Alois Langer of the Westinghouse Research Laboratories for his interest in the problem and for arranging for the above work to be conducted at the Westinghouse Laboratories. He is also indebted to Dr. R. E. Fox and to Mr. Don Groves of the Westinghouse Laboratories for their cooperation and interest while he was using the Westinghouse mass spectrometer.

[8] G. Glockler and S. C. Lind, *The Electrochemistry of Bases and Other Dielectrics* (John Wiley and Sons, Inc., New York, 1939).

A Study of the Deterioration of Methane-Filled Geiger-Müller Counters

EARLE C. FARMER* AND SANBORN C. BROWN
Massachusetts Institute of Technology, Cambridge, Massachusetts

(Received June 7, 1948)

The changes in the characteristics of methane-filled Geiger-Müller counters were studied as a function of counter life. It was found that the counters had a useful life of between 10^7 and 10^8 counts. Mass-spectroscopic analysis of the gas during the life of the counter showed the major decomposition products in the gaseous phase to be hydrogen, ethane, ethylene, and acetylene. These changes in gas composition did not account for the counter deterioration. The heavy hydrocarbon products deposited on the electrodes resulted in counter failure.

ONE of the well-known characteristics of Geiger-Müller counters which are filled with organic vapors for self-quenching action is the finite life for satisfactory counting behavior. Spatz[1] has obtained evidence of the decomposition of the gas in both argon-alcohol and argon-methane counters. The primary decomposition products were thought by Spatz to be free radicals which combine to form a miscellaneous assortment of organic molecules. Some of these decomposition products will be quenching gases. However, with continued use of the counter, all of the larger molecules are broken up and the end products of the decomposition are a non-quenching gas, such as hydrogen or oxygen, and heavy hydrocarbons deposited on the walls.

The observed life of methane counters is 10^7 to 10^8 counts, as against 10^{10} counts for an alcohol counter. Since CH_4 is one of the simplest hydrocarbons, it would be expected to decompose only once or twice before it is reduced to non-quenching diatomic molecules. In general, the number of molecules decomposed in each discharge will depend on the voltage. Thus, operating counters at voltages much above the discharge threshold will decrease the life. As the quenching constituent is decomposed, one might expect the total number of molecules in the counter to increase with a consequent increase in the pressure. Spatz reported such changes in both argon-alcohol and CH_4 counters. Concomitant with such changes in pressure, there would be an increase in starting potential, since this depends both on pressure and on the gas constituents.

This paper reports a study of the life characteristics of methane-filled counters. Methane was chosen for two reasons: first, the gas is one of the simplest of the organic compounds suitable for counter filling, and second, detailed studies have already been carried out on the behavior of methane under ion bombardment and in gas discharges.

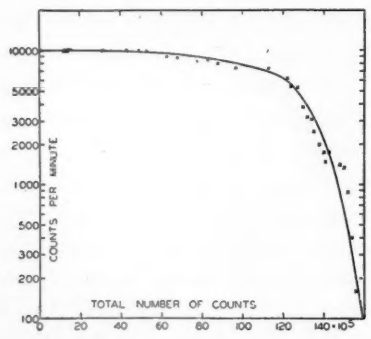

FIG. 1. The counting rate as a function of age for a methane-filled counter for which the applied voltage remains constant.

ELECTROCHEMICAL SUMMARY

Yeddanapalli[2] has made a detailed study of the decomposition of methane in glow discharges at liquid-air temperatures. He reports that the reaction products which are found are hydrogen, a polymer of composition CH_2, ethane, ethylene, and acetylene. The proportions of ethylene and acetylene increase as a result of the dehydrogenating action of atomic hydrogen; i.e., the atomic hydrogen dehydrogenates ethane or the radical fragments to give ethylene and this in turn reacts further to yield acetylene. Bimolecular combinations of the radicals formed by the

* Submitted in partial fulfillment of the requirements of the degree of Master of Science.

[1] W. D. B. Spatz, Phys. Rev. **64**, 236 (1943).

[2] L. M. Yeddanapalli, J. Chem. Phys. **10**, 249 (1942).

variety of collisions occurring in the gas phase and in the walls will lead to the formation of ethane, ethylene, and acetylene.

The hydrogen has two effects: first, it acts as a diluent, taking up a part of the electrical energy proportional to its partial pressure so that the rate of decomposition of CH_4 decreases in direct proportion to the partial pressure of H_2; and second, it acts as a dehydrogenating agent increasing the percentage of the unsaturated hydrocarbons in the reaction products. In a study of CH_4, C_2H_6, and C_3H_8, Bonhoeffer and Harteck[3] showed that atomic hydrogen reacts readily with hydrocarbon gases except methane, with the main reactions being hydrogenation, dehydrogenation and ring rupture.

Other studies of CH_4 in glow discharges at ordinary temperatures have been made. These report the formation of a wax-like, inert substance deposited on the cathode with the chief gaseous products being H_2, acetylene, ethylene, and paraffin hydrocarbons.[4] Numerous experiments on methane have been performed in different types of electrical discharges and under the action of alpha-rays,[5] and more recently under deuteron bombardment.[6] In general there is found H_2, saturated and unsaturated hydrocarbons in the gaseous products, and a solid or liquid residue. The heavier solid or liquid compounds are formed by polymerization of the unsaturated hydrocarbons, which takes place quite readily in the presence of H_2.

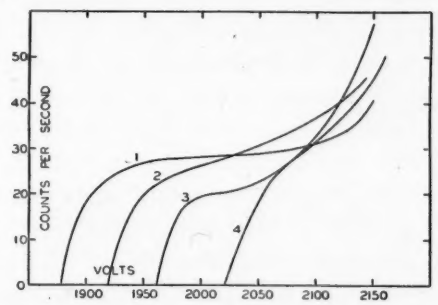

FIG. 2. Operating characteristics for a counter for various ages. Curve (1) was taken after 10^7 counts, (2) after 5×10^7 counts, (3) after 7×10^7 counts, (4) after 10^8 counts.

[3] K. F. Bonhoeffer and P. Harteck, Zeits. f. physik. Chemie, **139**, 75 (1928); Zeits. f. Elektrochemie **34**, 652 (1928).

[4] W. D. Harkins and J. M. Jackson, J. Chem. Phys. **1**, 37 (1933); E. G. Linder, Phys. Rev. **36**, 1375 (1930); E. G. Linder and A. P. Davis, J. Phys. Chem. **35**, 3649 (1931).

[5] S. C. Lind, *The Chemical Effects of Alpha Particles and Electrons* (The Chemical Catalogue Co., New York, 1928) p. 146.

[6] R. E. Honig, C. W. Sheppard, J. Phys. Chem. **50**, 119 (1946).

TABLE I. Summary of mass-spectroscopic results.

Counter	Total counts	H_2	C_2H_6	C_2H_4	C_2H_2	C_3H_8	C_4H_{10}
A	0	0	0.31			0.3	trace
	12.8×10^7	5.97	1.6	trace	0.32	0.6	0.3
B	0	0					
	0.92×10^7	1.5	0.5			trace	
	3.92×10^7	2.8	0.8	trace			
	7.02×10^7	4.5	1.5				
	43.3×10^7	14.0	1.9			trace	
C	14.5×10^7	13.0	1.9	trace		1.7	
D	2.5×10^7	1.54	0.3				
	5.0×10^7	3.1	0.6	trace			
	8.5×10^7	4.5	0.74				trace
	14.5×10^7	6.5	0.85				
	37.0×10^7	13.0	0.89			trace	

EXPERIMENTAL PROCEDURE

The experimental procedure in studying the decomposition products from aging methane gas in Geiger-Müller counters was as follows. The counters were filled with methane to some convenient pressure and operating potential, run at a suitable counting rate on a counting circuit, and samples of the gas were taken off at intervals. These samples were analyzed in a mass spectrometer.

The methane for the counters was purified before use in the following manner. The counters were connected to a vacuum system manifold which was evacuated with a mechanical pump. Tank methane was admitted to the system and frozen into a trap at liquid nitrogen temperature. With boiling nitrogen on the trap, all fractions of the gas except nitrogen, oxygen, and 4 mm pressure of methane (the vapor pressure of CH_4 at liquid nitrogen temperature) were frozen in the

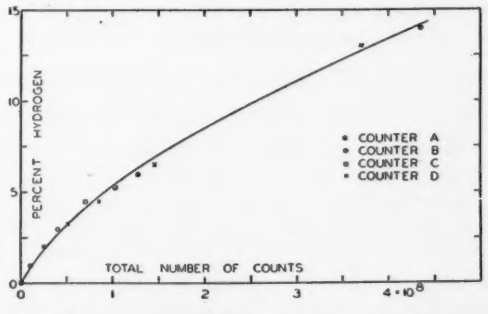

FIG. 3. The build-up of hydrogen gas with age for methane-filled counters is plotted for the counters of Table I.

trap. These impurities were pumped off. The trap bath was then changed to liquid oxygen and the gas system was allowed to build up to the vapor pressure of CH_4, which is 8 cm pressure at liquid oxygen temperature. This purified methane was then used for the counter filling.

Before loading, the counter tubes were outgassed to drive off absorbed gases in the metal and glass walls, and the center wire was flashed for several minutes. The counters were filled to a pressure of 6 cm of mercury.

To the experimental counters were attached a number of glass bulbs with internal break-off seals for collecting samples of the gas. The take-off bulbs had an average volume of 20 cubic centimeters and the volume of the counters was 100 cubic centimeters.

All the analytic work on the gas samples was carried out on a 60° Nier-type mass spectrometer. The gas was allowed to expand into a large reservoir and there flow through a suitable leak into the ionization region of the spectrometer. Here excitation and ionization of the gas molecules were produced by electron impact. After acceleration by variable electric fields, a fraction of the ionized molecules, collimated by several slits to form an ion beam, was analyzed by a magnetic field. The components of the resulting mass spectrum were measured electrically by the collector connected to an FP-54 d.c. amplifier circuit.

The counters were aged by operating them continuously on an ordinary amplifier and scaling circuit. The resistance in series with the counter center wire and the high voltage supply was 10^6 ohms. The counters were run at a rate of about 10^4 counts per minute, giving aging periods of one or two weeks.

RESULTS

The changes in the electrical characteristics of methane counters caused by the decomposition of the filling gas are easily measurable. When such a counter is connected to a constant voltage and data are taken of the observed counting rate as a result of a constant radioactive source as a function of time, it shows a typical behavior, illustrated in Fig. 1. The counting rate is quite constant up to about 10^7 counts, and then the sensitivity drops rapidly. Representative plateau curves are shown in Fig. 2. One can see that the primary reason for the decrease in sensitivity shown in Fig. 1 is the increase in threshold voltage. The aging data for this investigation were taken by keeping the counting rate constant. This was done by increasing the operating voltage to compensate for the rising threshold voltage. From the curves of Fig. 2, it is obvious that the rising threshold is not the only aging effect. The plateau curves become both narrower and steeper and a point is finally reached when the characteristics become so poor that no further operation as a Geiger-Müller counter is possible.

A summary of the mass spectroscopic results is given in Table I. Preliminary runs, of which counter *A* in this table represents an example, showed that the principal decomposition product was hydrogen. The next most abundant product was ethane. Since ethane itself is known to be a good counter-quenching gas and the other products appeared in such small quantities, the principal accuracy of the spectrometer was directed toward the determination of the hydrogen fraction. From the data in Table I, we have plotted in Fig. 3 the percentage of hydrogen formed as a function of the total number of counts. This logarithmic increase in hydrogen concentration with number of counts extends up to the point where the counter could no longer be operated in its Geiger-Müller region. Counter failure occured in all cases for hydrogen concentrations between 13 and 14 percent. In no case do we even approach complete disintegration of the methane molecules. The end products are undecomposed CH_4 molecules, the non-quenching gas hydrogen, slight amounts of saturated hydrocarbons up to C_4H_{10}, ethylene and acetylene.

To determine whether this changing gas concentration could account for the counter failure, a clean counter was filled with 13 percent H_2 and 87 percent CH_4. The plateau characteristics of this filling were identical with the same counter filled with 100 percent CH_4. As a further check to see whether the gas filling was responsible for the counter failure, immediately after a counter had deteriorated it was put on the vacuum system, evacuated and refilled with freshly purified methane. The counter exhibited no better proper-

ties with the fresh methane filling than it did with the methane plus decomposition fragments present.

It was found that after a methane counter had deteriorated it could always be recovered by a thorough cleaning of the electrodes. Usually washing the counter very thoroughly with distilled water, alcohol, benzene, and ether was sufficient. Occasionally a counter did not respond to this treatment, and in these cases, removal of the anode wire showed it was covered with a heavy brown coating which on heating left a carbon black on the wire.

CONCLUSION

The results of these experiments show that methane Geiger-Müller counters deteriorate because of the decomposition of the gas and that the change in the gas composition does not lead to the counter failure. The counter deterioration can be explained by the heavy hydrocarbon decomposition fragments of the methane deposited on both the cathode cylinder and on the anode wire.

It is a pleasure to acknowledge the interest and help of Dr. Richard E. Honig of the Socony-Vacuum Laboratories.

PHYSICAL REVIEW VOLUME 74, NUMBER 8 OCTOBER 15, 1948

The Factorization Method, Hydrogen Intensities, and Related Problems

T. E. HULL AND L. INFELD
University of Toronto, Toronto, Ontario, Canada

(Received June 2, 1948)

The factorization method enables us to calculate in an elementary way the discrete-discrete and discrete-continuous transition probabilities of hydrogen atoms by means of recurrence formulae. From a key intensity all others are found by a repeated application of an l-changing recurrence formula or an n'-changing operator. The results are given:

for l-changing in the formulae: (4.2), (4.3),
for n'-changing in the formulae: (5.1), (5.2) with (3.2).

Some of the formulae apply to more general matrix components.

I. INTRODUCTION

THE value of the Schrödinger hydrogen intensity integral

$$I_{n',n}{}^{l-1\,l}=\int_0^\infty rR_{n'}{}^{l-1}R_n{}^l dr, \qquad (1.1)$$

(where $R_n{}^l=r$ times the Schrödinger normalized hydrogen radial function) has been calculated many times. Originally Schrödinger[1] calculated it for special cases using the generating function for Laguerre polynomials. Wheeler[2] has recently applied this method to the general case of discrete-discrete transitions. Epstein[3] used the theory of hypergeometric functions to solve the same problem, while Eckart[4] evaluated the integral directly. Gordon[5] has treated the discrete-continuous and continuous-continuous as well as the discrete-discrete transitions. We want to show that the factorization method leads to a simple treatment of this problem.

The factorization method gives the *solutions* of a second-order differential equation by means of recurrence formulae[6]; the idea here is to develop recurrence formulae for the integrals involving these solutions—the intensity integral in particular. Besides the recurrence formulae a starting point is needed; in what follows this is found by the method of the Laplace transform. Some of the formulae apply to the calculation of other integrals involved in the Kepler problem.

[1] Schrödinger, *Wave Mechanics* (Blackie & Son, London, 1928), p. 99.
[2] Wheeler, Proc. Roy. Irish Acad. **50**, Sec. A, 3 (1944).
[3] Epstein, Proc. Nat. Acad. Sci. **12**, 629 (1926).
[4] Eckart, Phys. Rev. **28**, 927 (1926).
[5] Gordon, Ann. d. Physik **2**, 1031 (1929).
[6] L. Infeld, Phys. Rev. **59**, 737 (1941).

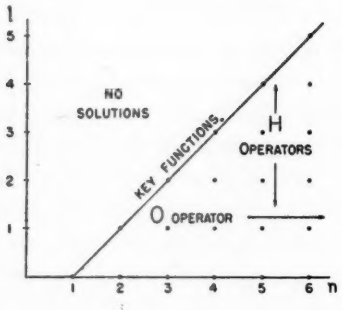

FIG. 1.

II. SOLUTION OF THE RADIAL EQUATION

The factorization method enables us to solve quickly the Schrödinger equation for a Coulomb field. We quote the result for the radial part of that equation.[7]

The equation for the discrete spectrum is:

$$R''+(2/r)R-[l(l+1)/r^2]R-(1/n^2)R=0, \quad (2.1)$$

and the normalized solutions are

$$R_n^{n-1}=(2/n)^n(1/n)[(2n-1)!]^{-\frac{1}{2}}r^n \times\exp(-r/n), \quad (2.2)$$

$$R_n^{l-1}={}^{+}H_n^{l}R_n^{l}, \quad (2.3a)$$

$$R_n^{l}=-H_n^{l}R_n^{l-1}, \quad (2.3b)$$

where

$$\pm H_n^{l}=nl[(n-l)(n+l)]^{-\frac{1}{2}}\left\{\frac{l}{r}-\frac{1}{l}\pm\frac{d}{dr}\right\} =(1/A_n^{l})\left\{\frac{l}{r}-\frac{1}{l}\pm\frac{d}{dr}\right\}. \quad (2.4)$$

There is thus one solution for each pair of integers (n, l) provided $l\leq n-1$ and n is a positive integer. The solutions are represented by dots in Fig. 1. The key functions (2.2) are those on the line $l=n-1$. Using the recurrence formulae (2.3) one can, so to speak, move up or down the ladders if n equals a constant. Replacing n by in in (2.3) and (2.4) gives recurrence formulae for eigenfunctions of the continuous spectrum but, of course, there is no starting point corresponding to (2.2).

III. A NEW RECURRENCE FORMULA

We shall now develop a new recurrence formula which enables us to move to the right along the horizontal lines $l=$constant.[8] To do this we introduce a new function

$$R_n^{l}(s).$$

This function is defined by the same recurrence formula (2.3a) as the corresponding function R_n^{l}. The only difference is that the key functions are now taken to be

$$R_n^{n-1}(s)=(2/n)^n(1/n)[(2n-1)!]^{-\frac{1}{2}}r^n \times[\exp(-sr)]. \quad (3.1)$$

Of course the $R_n^{l}(s)$ are neither orthogonal nor do they satisfy our differential equation, but they have the following important property:

$$[R_n^{l}(s)]_{s=1/n}=R_n^{l}. \quad (3.2)$$

We can now find an operator which enables us to change $R_n^{l}(s)$ into $R_{n+1}^{l}(s)$ from which our solutions can be reached by (3.2). In fact

$$R_{n+1}^{l}(s)=O_{n+1}^{l}R_n^{l}(s),$$

where

$$O_{n+1}^{l}=\frac{n^{l+2}}{(n+1)^{l+2}(2n+1)}\left[\frac{n+l+1}{n-l}\right]^{\frac{1}{2}} \times\left\{2n+1+\left(\frac{1}{n}+s\right)\frac{d}{ds}\right\}. \quad (3.3)$$

We shall prove this theorem by induction: from (2.4) and (3.3) it is easily seen that

$${}^{+}H_{n+1}^{l}=\frac{n+1}{n}\left[\frac{(n-l)(n+l)}{(n+1-l)(n+1+l)}\right]^{\frac{1}{2}}{}^{+}H_n^{l},$$

and

$$O_{n+1}^{l-1}=\frac{n+1}{n}\left[\frac{(n-l)(n+l)}{(n+1-l)(n+1+l)}\right]^{\frac{1}{2}}O_{n+1}^{l}.$$

Using (2.3a), (3.3) and the above equations:

$$R_{n+1}^{l-1}(s)={}^{+}H_{n+1}^{l}R_{n+1}^{l}(s) =\frac{n+1}{n}\left[\frac{(n-l)(n+l)}{(n+1-l)(n+1+l)}\right]^{\frac{1}{2}} \times{}^{+}H_n^{l}O_{n+1}^{l}R_n^{l}(s) =O_{n+1}^{l-1}R_n^{l-1}(s),$$

since the H and O operators commute. Therefore,

[7] L. Infeld, Phys. Rev. 59, 743 (1941); the unit of length is $\hbar^2/me^2Z$ and $1/n=\hbar(-2E)^{\frac{1}{2}}/m^{\frac{1}{2}}e^2Z$.

[8] Schrödinger has developed an n-changing operator of a different kind; see Proc. Roy. Irish Acad. 46, Sec. A, (1940).

if (3.3) is true for the quantum number l, it is true for $l-1$. It is a straightforward matter to check that (3.3) is true for $l=n-1$; the theorem is then established.

Thus with the help of (3.3) we can move to the right along the ladders $l=$constant.

IV. ALGEBRAIC RECURRENCE FORMULAE FOR THE INTENSITIES

Each of the H and O operators leads to a recurrence formula for the intensity integral, the former to an algebraic one as follows: it is not difficult to verify from (2.4) that

$$2lA_{n'}{}^{l}+H_{n'}{}^{l}=(2l+1)A_{n}{}^{l+1}+H_{n}{}^{l+1}+A_{n'}{}^{l+1}-H_{n'}{}^{l+1}+(\text{constant})/r. \quad (4.1)$$

Multiplying (4.1) on the left by $rR_n{}^{l}$, on the right by $R_{n'}{}^{l}$ and integrating gives

$$\begin{aligned}2lA_{n'}{}^{l}&\int_0^\infty rR_n{}^{l+}H_{n'}{}^{l}R_{n'}{}^{l}dr\\ &=(2l+1)A_n{}^{l+1}\int_0^\infty rR_n{}^{l+}H_n{}^{l+1}R_{n'}{}^{l}dr\\ &\qquad+A_{n'}{}^{l+1}\int_0^\infty rR_n{}^{l}-H_{n'}{}^{l+1}R_{n'}{}^{l}dr\\ &=(2l+1)A_n{}^{l+1}\int_0^\infty r(-H_n{}^{l+1}R_n{}^{l})R_{n'}{}^{l}dr\\ &\qquad+A_{n'}{}^{l+1}\int_0^\infty rR_n{}^{l}-H_{n'}{}^{l+1}R_{n'}{}^{l}dr,\end{aligned}$$

because $R_n{}^{l}$, $R_{n'}{}^{l}$ are orthogonal and vanish at $r=0,\ \infty$. We have then:

$$\left.\begin{aligned}&2lA_{n'}{}^{l}I_{n'\ n}{}^{l-1\ l}=(2l+1)A_n{}^{l+1}I_{n'\ n}{}^{l\ l+1}+A_{n'}{}^{l+1}I_{n'\ n}{}^{l+1\ l}.\\ &\text{By interchanging } n, n' \text{ we obtain}\\ &2lA_n{}^{l}I_{n'\ n}{}^{l\ l-1}=A_n{}^{l+1}I_{n'\ n}{}^{l\ l+1}+(2l+1)A_{n'}{}^{l+1}I_{n'\ n}{}^{l+1\ l},\\ &A_n{}^{l}=[(n-l)(n+l)]^{\frac{1}{2}}/nl.\\ &\text{Our derivation (and hence this result) is valid for the discrete-continuous transitions once one replaces } n \text{ by } in.\end{aligned}\right\} \quad (4.2)$$

These are algebraic formulae giving a pair of intensities in terms of the next highest pair in the scheme of Fig. 1.

All intensities can now be calculated once a starting point is found.—An obvious choice is the pair at the top of the n' ladder: $I_{n'\ n}{}^{n'\ n'-1}$ and $I_{n'\ n}{}^{n'-1\ n'}$ where

$$I_{n'\ n}{}^{n'\ n'-1}=0. \quad (4.3a)$$

(We will adopt the convention that n' always refers to the discrete spectrum.) The method of calculation of the other expression is indicated in the appendix. The result is:

$$I_{n'\ n}{}^{n'-1\ n'}=2^{2n'+2}(nn')^{n'+2}\times\left[\frac{(n+n')!}{(n-n'-1)!(2n'-1)!}\right]^{\frac{1}{2}}\frac{(n-n')^{n-n'-2}}{(n+n')^{n+n'+2}}, \quad (4.3b)$$

or, for the discrete-continuous transition,

$$I_{n'\ in}{}^{n'-1\ n'}=2^{2n'+2}(nn')^{n'+2}\times\left[\frac{n^3\prod_{p=1}^{n'}(p^2+n^2)}{\{\exp(2n\pi)-1\}(2n'-1)!}\right]^{\frac{1}{2}}\times\frac{\exp[2n\tan^{-1}(n/n')]}{(n^2+n'^2)^{n'+2}}. \quad (4.3c)$$

From (4.3) we can now calculate pairs of intensities by successive application of (4.2)—the important intensities requiring at most but a few steps.

V. OPERATOR RECURRENCE RELATION FOR INTENSITIES

The results of §3 will now be used to find an n'-changing recurrence relation for the intensities. Indeed, it follows immediately from (3.3) that

$$\left.\begin{aligned}&I_{n'+1\ n}{}^{l-1\ l}(s)=O_{n'+1}{}^{l-1}I_{n'\ n}{}^{l-1\ l}(s),\\ &\text{or}\\ &I_{n'+1\ in}{}^{l-1\ l}(s)=O_{n'+1}{}^{l-1}I_{n'\ in}{}^{l-1\ l}(s),\\ &O_{n'+1}{}^{l-1}=\frac{n'^{l+1}}{(n'+1)^{l+1}(2n'+1)}\times\left[\frac{n'+l}{n'-l+1}\right]^{\frac{1}{2}}\left\{2n'+1+\left(\frac{1}{n'}+s\right)\frac{d}{ds}\right\},\\ &\text{where the intensity } \textit{function} \text{ is defined by}\\ &I_{n'\ n}{}^{l-1\ l}(s)=\int_0^\infty rR_{n'}{}^{l-1}(s)R_n{}^{l}dr.\end{aligned}\right\} \quad (5.1)$$

The starting point needed here is

$$I_{l\,n}{}^{l-1\;l}(s)=\frac{1}{n}\left(\frac{4}{nl}\right)^{l+1}\left[\frac{(n+l)!}{(n-l-1)!(2l-1)!}\right]^{\frac{1}{2}}\times\frac{\left(s-\frac{1}{n}\right)^{n-l-2}}{\left(s+\frac{1}{n}\right)^{n+l+2}}[(l+1)s-1], \quad (5.2a)$$

or[9]

$$I_{l\,in}{}^{l-1\;l}(s)=\left(\frac{4}{nl}\right)^{l+1}\left[\frac{n\prod_{p=1}^{l}(p^2+n^2)}{\{\exp(2n\pi)-1\}(2l-1)!}\right]^{\frac{1}{2}}\times\frac{\exp(2n\tan^{-1}ns)}{\left(s^2+\frac{1}{n^2}\right)^{l+2}}[(l+1)s-1]. \quad (5.2b)$$

The derivation of (5.2) is indicated in the appendix.

Using (5.1) and (5.2a) we can find $I_{l+1\;n}{}^{l-1\;l}(s)$, $I_{l+2\;n}{}^{l-1\;l}(s)\cdots I_{n'\;n}{}^{l-1\;l}(s)$ which, with (3.2), give the intensities. Similarly from (5.2b) we can find . . . $I_{n'\;in}{}^{l-1\;l}$.

VI. REMARKS

(1) The set of values of the quantum numbers for which the intensities are required will determine which of the above two methods should be used. Being algebraic (4.2) is simpler whereas (5.1) has the special characteristic that it is applicable to the problem of calculating more general matrix components

$$\int_0^\infty \phi(r)R_{n'}{}^{l'}R_n{}^l dr.$$

(2) *Example of a calculation:*
To find

$$I_{2n}{}^{01}=\int_0^\infty rR_2{}^0R_n{}^1dr,$$

we can use (4.3) to get immediately

$$I_{2n}{}^{21}=0,$$
$$I_{2n}{}^{12}=3^{-1/2}2^{19/2}n^{9/2}(n^2-1)^{1/2}(n-2)^{n-7/2}(n+2)^{-n-7/2}.$$

From (4.2)

$$I_{2n}{}^{01}=(2A_2{}^1)^{-1}3A_n{}^2I_{2n}{}^{12}+0$$
$$=2^{17/2}n^{7/2}(n^2-1)^{1/2}(n-2)^{n-3}(n+2)^{-n-3}.$$

Alternatively, we can use (5.2a) to get

$$I_{1n}{}^{01}(s)=2^4n^{-5/2}(n^2-1)^{1/2}(s-1/n)^{n-3}\times(s+1/n)^{-n-3}(2s-1).$$

Operating on this expression with

$$O_2{}^0=2^{-\frac{1}{2}}3^{-1}\left\{3+(1+s)\frac{d}{ds}\right\},$$

and then putting $s=\frac{1}{2}$ we get the value above for $I_{2n}{}^{01}$ which is the same as that given by Condon and Shortley[10] for the transition $2s-np$.

(3) *Explicit forms:* The above methods can lead to explicit forms of the intensity integral except in the case of continuous-continuous transitions (though the *algebraic* formulae are valid for these transitions if n', n are replaced by in', in). For example, by means of (4.2), (4.3) and known relations between contiguous hypergeometric functions the results given by Gordon[11] can be proven by induction.

APPENDIX

The Calculation of (4.3) and (5.2)

Define

$$I_n=\int_0^\infty r^l\exp(-sr)R_n{}^l dr. \quad (A.1)$$

We must distinguish between two cases:

Case I: Discrete-discrete

From (2.1):

$$\int_0^\infty r^{l+1}\exp(-sr)\{R''+(2/r)R-[l(l+1)/r^2]R-(1/n^2)R\}dr=0.$$

After two partial integrations of the first term we obtain

$$(s^2-1/n^2)I_n'+[2(l+1)s-2]I_n=0.$$

$$\therefore\quad I_n=C\frac{(s-1/n)^{n-l-1}}{(s+1/n)^{n+l+1}}.$$

[9] Another starting point which may be needed is $I_{l+1\;in}{}^{l\;l-1}(s)$; it is slightly more complicated but can be found easily from the formulas in the appendix.

[10] Condon and Shortley, *Theory of Atomic Spectra* (Cambridge University Press, Teddington, 1935), p. 133.

[11] See Reference 10, p. 1051.

I_n is the Laplace transform of $r^l R_n{}^l$ and therefore[12]

$$R_n{}^l = r^{-l}[\text{residue of } [\exp(sr) I_n] \text{ at } s = -1/n].$$

The coefficient of the lowest power $(l+1)$ of r turns out to be

$$C[\exp(-r/n)]/(2l+1)!. \qquad \text{(A.2)}$$

But from (2.3a), we have:

$$R_n{}^l = +H_n{}^{l+1} + H_n{}^{l+2} \ldots + H_n{}^{n-1} R_n{}^{n-1}.$$

Using (2.2) and (2.4) the coefficient of r^{l+1} can be picked out easily; it is

$$\frac{2^n(n-1)!}{n^{l+2}(2n-1)!!}\left[\frac{(n+l)!}{(n-l-1)!}\right]^{\frac{1}{2}} \times[(2l+3)(2l+5)\ldots(2n-1)] \times[\exp(-r/n)]. \qquad \text{(A.3)}$$

Equating (A.2) and (A.3) we find C so that

$$I_n = \frac{2^{l+1}}{n^{l+2}}\left[\frac{(n+l)!}{(n-l-1)!}\right]^{\frac{1}{2}} \frac{(s-1/n)^{n-l-1}}{(s+1/n)^{n+l+1}}. \qquad \text{(A.4)}$$

Then

$$I_{l\,n}{}^{l-1\,\,l}(s) = \left(\frac{2}{l}\right)^l \frac{1}{l[(2l-1)!]^{\frac{1}{2}}} \times \int_0^\infty r^{l+1} \exp(-sr) R_n{}^l dr$$

$$= \left(\frac{2}{l}\right)^l \frac{1}{l[(2l-1)!]^{\frac{1}{2}}}\left[-\frac{dI_n}{ds}\right].$$

$$I_{l\,n}{}^{l-1\,\,l}(s) = \frac{1}{n}\left(\frac{4}{nl}\right)^{l+1}\left[\frac{(n+l)!}{(n-l-1)!(2l-1)!}\right]^{\frac{1}{2}} \times \frac{(s-1/n)^{n-l-2}}{(s+1/n)^{n+l+2}}[(l+1)s-1]. \qquad \text{(5.2a)}$$

[12] See for example: R. V. Churchill, *Modern Operational Mathematics in Engineering* (McGraw-Hill Book Company, New York, 1944), pp. 170–171.

By putting $l=n'$ and $s=1/n'$, we obtain

$$I_{n'\,n}{}^{n'-1\,\,n'} = 2^{2n'+2}(nn')^{n'+2} \times\left[\frac{(n+n')!}{(n-n'-1)!(2n'-1)!}\right]^{\frac{1}{2}} \times\frac{(n-n')^{n-n'-2}}{(n+n')^{n+n'+2}}. \qquad \text{(4.3b)}$$

Case II: Discrete-continuous

In this case I_{in} turns out to be

$$I_{in} = C(s-i/n)^{-in-l-1}(s+i/n)^{in-l-1} = C\frac{\exp(2n\tan^{-1}ns - n\pi)}{(s^2+1/n^2)^{l+1}}; \quad 0 < \tan^{-1}ns < \frac{\pi}{2},$$

where the constant $n\pi$ was determined by the condition that I_{in} remain finite as $n\to\infty$.

The inverse transform here is[13]

$$R_{in}{}^l = \frac{Cr^{-l}}{2\pi i}\int \exp(sr)(s-i/n)^{-in-l-1} \times(s+i/n)^{in-l-1} ds.$$

From an asymptotic expression for $R_{in}{}^l$ we find[14] the value of C for the usual normalization. The final result in our notation is

$$I_{in} = \left(\frac{2}{n}\right)^{l+\frac{1}{2}}\left[\frac{2\prod_{p=1}^{l}(p^2+n^2)}{\exp(2n\pi)-1}\right]^{\frac{1}{2}} \frac{\exp(2n\tan^{-1}ns)}{(s^2+1/n^2)^{l+1}},$$

and the corresponding starting points are found to be as given in (5.2b) and (4.3c).

[13] Also given by Schrödinger, Ann. der Phys. **79**, 361 (1926).

[14] See for example Bethe, *Handbuch der Physik* (Berlin, Verlag Julius Springer, 1933), 2nd ed., pp. 290–292.

Electrical Breakdown of a Gas between Coaxial Cylinders at Microwave Frequencies*

MELVIN A. HERLIN AND SANBORN C. BROWN
Research Laboratory of Electronics, Massachusetts Institute of Technology, Cambridge, Massachusetts

(Received June 10, 1948)

The criterion for breakdown of a low pressure gas at microwave frequencies is that the ionization rate equal the diffusion rate for electrons. This principle is applied to compute the breakdown of air in coaxial cylinders using previously reported high frequency ionization coefficient data obtained from breakdown experiments between parallel plates. Agreement between computed and measured results at 9.6-cm wave-length supports the validity of the above criterion for breakdown. The method of computation is illustrative of the general problem of computing breakdown fields for tubes of arbitrary shape and field configuration using ionization coefficient data obtained from uniform field breakdown.

ELECTRICAL breakdown of a gas at microwave frequencies has been discussed by the authors in a recent paper.[1] The condition for breakdown has been postulated as a balance between generation of electrons by ionization and loss of electrons by diffusion, and a mathematical procedure for computing breakdown electric field strengths under specified experimental conditions has been given. An ionization coefficient appropriate to the high frequency case is necessary. This coefficient has been measured by experiments on breakdown between parallel plates.[1] The present paper describes a procedure for computing breakdown between coaxial cylinders using the experimental values of the ionization coefficient, and compares the results of the computation with experiment.

Three purposes are fulfilled by the present work on coaxial cylinders. First, this geometry for a discharge tube has long been useful in radioactivity instrumentation. The microwave discharge has been studied for this application[2] and found to have certain advantages over the conventional d.c. discharge. Second, although the procedure for computing breakdown in an arbitrary cavity is straightforward in principle, the detailed computation requires further mathematical study. This paper illustrates a computing technique which is useful generally. Finally, the basic diffusion theory for breakdown is checked experimentally by using the experimental results obtained from parallel plate breakdown to predict the results to be expected for coaxial breakdown. The agreement with experiment indicates that no mechanisms other than ionization, attachment, and diffusion need to be introduced into the breakdown criterion.

The breakdown condition is obtained from the continuity equation for electrons,[1]

$$\partial n/\partial t = \nu n - \nabla \cdot \mathbf{\Gamma},$$

where n is the electron density, ν is the net production rate of electrons per electron, and $\mathbf{\Gamma}$ is the d.c. electron current density in electrons per unit area per second. The production rate per electron is the difference between the ionization rate and the attachment rate,

$$\nu = \nu_i - \nu_a.$$

If there is no electric field present, ν is zero or negative and $\partial n/\partial t$ is negative, indicating a decaying discharge. As the field is raised, ν increases until the time derivative rises and becomes positive. The threshold of breakdown occurs as it goes through zero. Thus, breakdown is computed as the characteristic value of the electric field obtained from the solution of the equation

$$\nu n - \nabla \cdot \mathbf{\Gamma} = 0, \qquad (1)$$

and the boundary condition that the electron density vanish at the cavity surfaces.[1]

The high frequency electric field contributes nothing to the value of $\mathbf{\Gamma}$, so that it is given

* This work has been supported in part by the Signal Corps, the Air Materiel Command, and O.N.R.

[1] M. A. Herlin and S. C. Brown, Phys. Rev. **74**, 291 (1948).

[2] S. C. Brown, Phys. Rev. **73**, 1240 (1948).

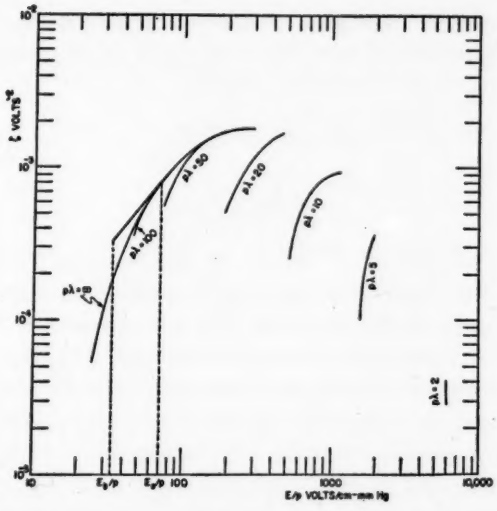

FIG. 1. Ionization coefficient (ionizations/volt²), as a function of E/p (volts/cm-mm Hg) and $p\lambda$ (mm Hg-cm). The straight-line approximation used to compute coaxial breakdown agrees with numerical integration using the correct value to within one percent.

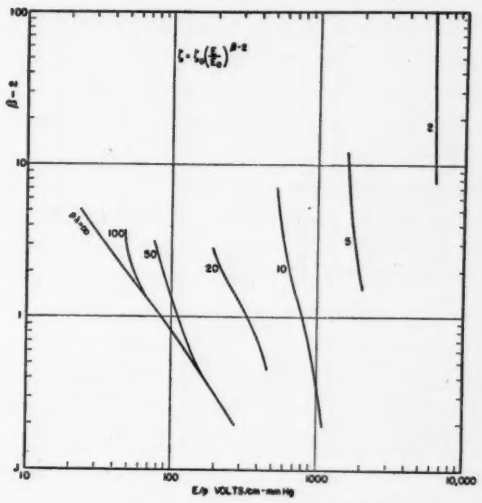

FIG. 2. Slope of ζ *versus* E/p curve on log plot taken from Fig. 1.

entirely by the diffusion equation

$$\Gamma = -\nabla(Dn) = -\nabla\psi, \tag{2}$$

where D is the electron diffusion coefficient. The diffusion coefficient is left under the gradient sign to account for "thermal" diffusion, important here because the electron kinetic energy varies with position in the cavity as a result of the electric field variation. The product of the diffusion coefficient and the electron density, denoted by ψ, is the electron diffusion current density "potential," similar to the hydrodynamic velocity potential.

Equation (1), with Eq. (2) substituted, is written in terms of ψ and the high frequency ionization coefficient, ζ (ionizations/volt²),

$$\zeta = \nu/DE^2, \tag{3}$$

to yield

$$\nabla^2\psi + \zeta E^2\psi = 0, \tag{4}$$

where E is the r.m.s. value of the high frequency electric field strength. The value of ν/D is divided by E^2 in the definition of the ionization coefficient for dimensional reasons[1] and for mathematical convenience.

The ionization coefficient has been measured as a function of E/p and $p\lambda$, where p is the gas pressure and λ is the free-space wave-length of the electric field. The variable E/p enters as determining the energy gained by an electron between collisions at zero frequency, and therefore as determining the energy distribution of the electrons at zero frequency. The energy transfer is modified at high frequencies by the oscillatory nature of the field-induced electron motion. This modification is accounted for by the variable $p\lambda$, which is a measure of the ratio of the collision frequency to the field radian frequency.[1] Figure 1 shows the measured values of the ionization coefficient, reproduced from reference 1.

The value of ζE^2 as a function of position in the discharge cavity is obtained from Fig. 1 and from the electric field as a function of position,

$$E = (V/r \ln b/a)\sin\pi z/L,$$

where V is the "voltage" at the center of the coaxial cavity, a and b are the inner and outer

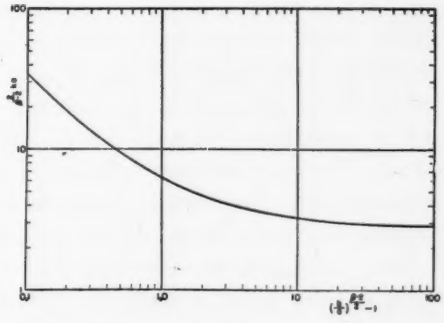

FIG. 3. Solution of the transcendental equation for coaxial breakdown.

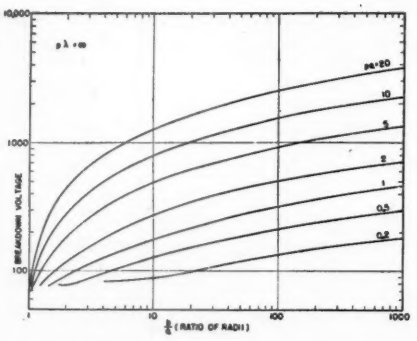

FIG. 4. Breakdown voltage between coaxial cylinders as a function of b/a, ratio of outer conductor radius b to inner conductor radius a, and pa (mm Hg-cm). This family of curves applies for $p\lambda$=infinity. A separate family is required for each value of $p\lambda$, for a complete set of curves.

conductor radii, L is the length of the cavity, and r and z are the radial and axial space coordinates. This expression applies to a half-wave-length-long cavity, which was used experimentally. The value of E at each point in the cavity leads to a value of ζ, through the experimental ζ-curve of Fig. 1. The boundary condition that ψ be zero at the cavity walls leads then to a characteristic value for V which is the breakdown voltage.

The above expression for the electric field is a function of two space coordinates and leads to a non-separable differential equation. This difficulty can be avoided by choosing an inner conductor radius which is small compared to the length L, which is a half-wave-length. The electric field in the region near the center conductor does not vary much with distance along the conductor, so that the conditions of infinite length are approached. We may consider the field to be given by the formula

$$E=V/r\ln(b/a), \tag{5}$$

from which ζE^2 is computed as a function of position. Then to this approximation Eq. (4) is a second-order linear differential equation in r only.

Since ζ is given from numerical data, the differential equation must be integrated numerically in its present form. The work may be simplified by approximating the value of ζE^2 by an algebraic factor. The approximation used has been compared with the results of numerical integration, with agreement to within one percent over the full range of the variables. The plot of ζ against E/p on a logarithmic scale is replaced by a straight line of the slope obtained at the inner conductor of the cavity. Thus,

$$\zeta E^2\simeq k^2(E/E_a)^\beta, \tag{6}$$

where

$$k^2=\zeta_a E_a^2.$$

The subscript "a" refers to the position $r=a$, and the slope on a logarithmic plot of the curve of Fig. 1 at the value of E/p at $r=a$ is $(\beta-2)$. The appropriate $p\lambda$=constant curve is chosen. This approximation expresses the ionization coefficient analytically. It is accurate near the center conductor where the ionization is most pronounced. If the ratio b/a is small it is accurate throughout the cavity, and the resulting breakdown computation is expected to be accurate. If b/a is large the approximation is not accurate at the outer part of the cavity, but since the ionization is low there the inaccuracy has little effect on the solution. The slope $(\beta-2)$ as a function of E/p and $p\lambda$ has been taken from Fig. 1 and plotted in Fig. 2.

Equations (4), (5), and (6) now combine into

$$\frac{d^2\psi}{dr^2}+\frac{1}{r}\frac{d\psi}{dr}+k^2\left(\frac{a}{r}\right)^\beta\psi=0, \tag{7}$$

whose solution is

$$\psi=Z_0\left[\frac{2}{\beta-2}ka\left(\frac{a}{r}\right)^{\frac{1}{2}(\beta-2)}\right],$$

where Z_0 is a Bessel function of zero order. The boundary condition that $\psi=0$ at $r=a$ and $r=b$ leads to the following transcendental equation

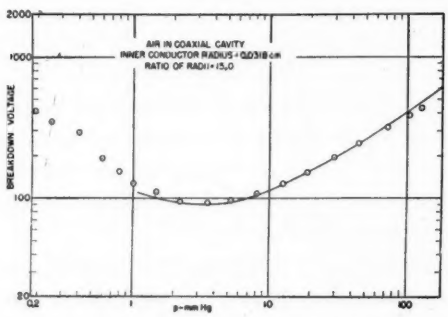

FIG. 5. Comparison of experimental points and theoretical curve for coaxial breakdown.

expressing the breakdown condition

$$J_0(x)N_0[(b/a)^{\frac{1}{2}(\beta-2)}x] - J_0[(b/a)^{\frac{1}{2}(\beta-2)}x]N_0(x)=0, \quad (8)$$

where

$$x=\frac{2}{\beta-2}ka\left(\frac{a}{b}\right)^{\frac{1}{2}(\beta-2)}. \quad (9)$$

Roots of this equation are tabulated,[3] giving x as a function of $(b/a)^{\frac{1}{2}(\beta-2)}$. Multiplying x by $(b/a)^{\frac{1}{2}(\beta-2)}$, the curve of Fig. 3 is obtained, which gives $[2/(\beta-2)]ka$ as a function of $(b/a)^{\frac{1}{2}(\beta-2)}$.

The details of computation are as follows. Values of $p\lambda$ and pa are assumed. Figure 1 with Eq. (5) and Fig. 2 gives k/E_a^2 and $(\beta-2)$, respectively, as functions of E_a/p. Then $2ka/(\beta-2)$ is computed from these, which yields $(b/a)^{\frac{1}{2}(\beta-2)}$ from Fig. 3. From this latter, b/a and V are computed, using Eq. (5).

The results of this calculation for $p\lambda=$infinity are given in Fig. 4. A separate family would be obtained for each value of $p\lambda$, but these are not given in detail here. A few points at other values of $p\lambda$ have been computed for the special case which was measured experimentally.

Figure 5 shows a particular case which has been computed from the foregoing theory and also measured experimentally. A ratio of outer to inner conductor radii of fifteen was chosen as the greatest possible departure from uniform field conditions consistent with mechanical and electrical limitations in the experiment. The experimental technique is similar to that described in reference 1, using a tunable continuous-wave magnetron as a power source, standing-wave technique for impedance measurements, and a bolometer and bridge for power measurements. The coaxial cavity was made of brass and was resonant at 9.6-cm wave-length. The data are shown as points and the curve is derived from theory. The curve is not extended beyond the limit of validity of diffusion theory on the low pressure side.

The electron production and removal processes which have been included in the breakdown condition are linear processes; that is, the electron production and removal rates are proportional to the electron density. Recombination with positive ions and modification of diffusion by space-charge effects are non-linear and would therefore result in a different relationship between uniform-field breakdown between parallel plates and the present coaxial breakdown. Furthermore, the validity of the boundary condition is checked by the present experiment. The condition used is based on the assumption of negligible effect from surface emission of electrons, which in turn results from the absence of a drift motion of the emitted electrons resulting from the field. If the field-induced drift motion of electrons were operating strongly as an electron removal process, the effect of electrons emitted from the cavity walls would be exaggerated by electron multiplication along their path, as happens in d.c. discharges. Also, the differential equation for the electron density would have to be modified. The agreement between theory and experiment indicates that the diffusion theory for breakdown, as developed here and in reference 1, accounts for all of the important processes that affect high frequency breakdown.

[3] E. Jahnke and F. Emde, *Functionentafeln* (B. G. Teubner, Leipzig, 1933), p. 205.

Internal Friction and Precipitation from the Solid Solution of N in Tantalum*

T'ING-SUI KÊ
Institute for the Study of Metals, The University of Chicago, Chicago, Illinois
(Received July 6, 1948)

The internal friction or acoustic absorption peak (*versus* temperature) around 350°C previously observed in tantalum with a frequency of vibration of about one cycle per second was further analyzed. It is shown that this peak has its origin in the stress-induced interstitial diffusion of N in tantalum similar to the cases of C and O in tantalum reported before. The precipitation of N from the solid solution with tantalum was followed by internal friction measurements.

IT has been reported previously that three internal friction or acoustic absorption peaks (*versus* temperature) were observed in tantalum containing small amounts of minor constituents as impurities.[1] With a frequency of vibration of about one cycle per second, these peaks occur at about 150°C, 170°C, and 350°C, respectively. The first two peaks are believed to be caused, respectively, by the stress-induced diffusion of C and of O among the various interstices in tantalum lattice in which the interstices have tetragonal symmetry. This viewpoint was later substantiated by experiments on the temperature-dependence of the relaxation strength associated with these peaks.[2] The physical origin of the third peak at 350°C, however, remained obscure.

It has been found that this 350°C peak does not change by annealing cold-worked metal in vacuum at various temperatures (600°C, 980°C, 1200°C). This indicates that it has nothing to do with cold-working. Furthermore, it does not change with the amount of carbon or oxygen in tantalum. Accordingly, it is not connected with the presence of carbon or oxygen.

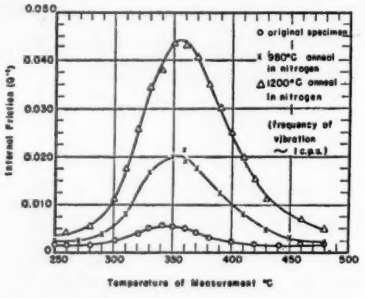
O original specimen
x 980°C anneal in nitrogen
Δ 1200°C anneal in nitrogen
(frequency of vibration ~ 1 c.p.s.)
Internal Friction (Q⁻¹)
Temperature of Measurement °C

FIG. 1. Effect of nitrogen content in tantalum upon the 350°C internal friction peak. The peak is raised when the amount of nitrogen in the specimen was increased by annealing successively at 980°C and 1200°C in nitrogen.

The tantalum specimens used in the following study are similar to those used before. It is 99.9 percent pure and was received in annealed form in wires having a diameter of 0.03 inch. It was fine-grained and had a rather uniform grain size.

Figure 1 shows that the peak concerned was considerably raised when the amount of nitrogen in the specimen was increased by annealing successively at 980°C and 1200°C in an atmosphere of nitrogen. This peak must, therefore, be connected in some way with the presence of nitrogen in tantalum as we have shown that annealing alone did not change this peak. The small peak observed before the "loading" of nitrogen is presumably due to the presence of some trace of nitrogen in the original specimen.

Further experiments have shown that this peak is a manifestation of a relaxation phenomenon. The sudden drop of the shear modulus (in arbitrary units) in the nitrogen-loaded specimen is shown in Fig. 2, and the stress relaxation at very small constant strain is shown in Fig. 3.

It is but natural to think that this peak is caused by the stress-induced diffusion of N in

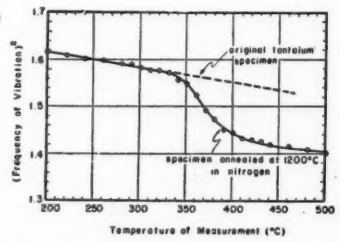
original tantalum specimen
specimen annealed at 1200°C in nitrogen
(Frequency of Vibration)²
Temperature of Measurement (°C)

FIG. 2. Variation of "rigidity" (in arbitrary units) with temperature in tantalum specimen loaded with nitrogen.

* This research has been supported by the Office of Naval Research (Contract No. N-6ori-20-IV).
[1] T. S. Kê, Phys. Rev. 74, 9 (1948).
[2] T. S. Kê, Phys. Rev. 74, 16 (1948).

tantalum similar to the case of C and O in tantalum. But it is puzzling that the nitrogen peak should occur at a temperature 200°C higher than those of carbon and oxygen. We know that the peaks of carbon and oxygen are only about 20°C apart. Another possible interpretation is that this peak may have its origin in the viscous behavior of the interphase boundaries between tantalum nitride and the tantalum matrix, similar to the viscous behavior of the grain boundaries in metals.[3,4] A decisive test on these two possibilities is to ascertain whether the nitrogen responsible for the observed internal friction peak is in solid solution or is in the form of tantalum nitride.

The heat of activation associated with the absorption peak was determined by using the conventional procedure of determining the internal friction curve with two frequencies of vibration (see Fig. 4). This gives a value of about 44,000 calories per mole, which is much larger than the corresponding values for C and O in tantalum which are, respectively, 25,000 and 29,000 calories per mole. It is also much higher than the corresponding value of 20,000 calories per mole for N in alpha-iron.[4] By calculating the theoretical internal friction curve as was done in the case of oxygen,[1] it is shown in Fig. 4 that the observed peak cannot be interpreted in terms of a single relaxation time with a unique heat of activation.

An important clue to this problem was the observation that the internal friction in a tantalum specimen freshly "loaded" with nitrogen decreases with tempering at a given temperature. Figure 5 shows the value of the internal friction (Q^{-1}) at the optimum temperature, 350°C, plotted as a function of tempering time at this temperature. A specimen previously loaded with nitrogen by annealing at 1200°C in an atmosphere of nitrogen was quenched in vacuum from 900°C to room temperature, and internal friction measurements were made at 350°C after quenching (curve *A*). The internal friction reaches a somewhat stable value after about twenty hours. Metallographic examination shows that the specimen after quenching has a clear appearance

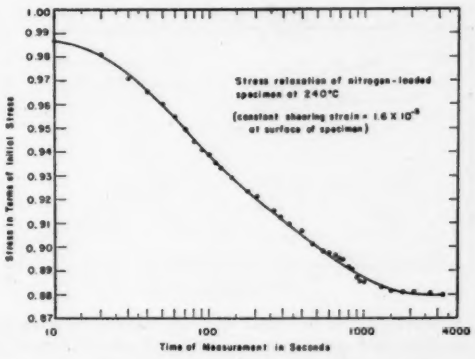

FIG. 3. Stress relaxation under constant strain of nitrogen-loaded specimen at 240°C.

similar to the original specimen before being "loaded" with nitrogen, while the same specimen tempered at 350°C for twenty hours shows needle-like precipitates. When this tempered specimen was again annealed in vacuum at 600°C and then quenched, the initial value of the internal friction is lower than is the case when the quenching was made from 900°C (curve *B*). The initial rate of precipitation for the specimen quenched from 600°C is also slower. The final stable value is, according to Fig. 5, about the same in both cases. Metallographic examination on this specimen shows also needle-like precipitates but these are larger in size.

These observations can be easily understood if we assume that the internal friction observed is caused by the nitrogen in solid solution in tantalum rather than caused by nitrogen precipitated

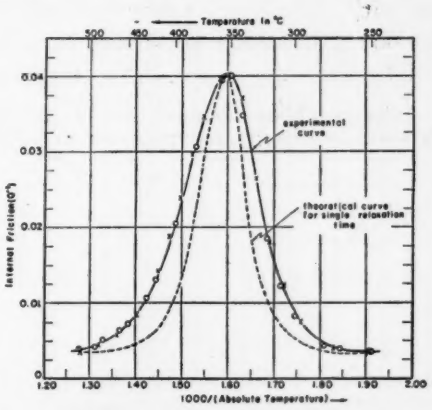

FIG. 4. Determination of heat of activation associated with the nitrogen peak by a relative horizontal shift of two internal friction curves measured with two different frequencies of vibration. (×, lower frequency; ○, higher frequency.) The dotted curve was calculated assuming a single relaxation time and a unique heat of activation.

[3] T. S. Kê, Phys. Rev. **71**, 533 (1947); **72**, 41 (1947); J. App. Phys. **19**, 285 (1948).

[4] T. S. Kê, *Metals Technology* (Tech. Pub. 2370, June, 1948).

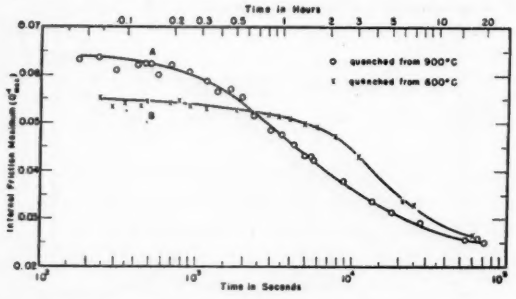

FIG. 5. Variation of internal friction maximum with time in nitrogen-loaded specimens quenched from different temperatures. The curves indicate the precipitation of nitrogen from solid solutions.

as nitride. Evidently a supersaturated solution of N in tantalum is formed by quenching from a higher temperature. The nitrogen then precipitates out from the solution when tempered at a lower temperature. The initial rate of precipitation increases with the degree of supersaturation which, in turn, increases with the temperature from which the quenching was made. The final stable value of internal friction is presumably a measure of the solubility of N in tantalum at the tempering temperature. The internal friction observed cannot be due to nitrogen in precipitated form since then the internal friction should be raised instead of being reduced while precipitation proceeds.

The precipitation of N from the solid solution with tantalum as indicated by internal friction measurements is similar to that observed by Dijkstra[5] in the cases of C and N from the solid solutions with alpha-iron. It may be worth while to point out that such a procedure furnishes a powerful tool for the study of the behavior of nucleation and precipitation from metallic solid solutions. The value of internal friction is a sensitive indicator of the instantaneous concentration of solute atoms in solid solution which is difficult to determine by other methods.

The concept of stress-induced interstitial diffusion of N in tantalum implies that the diffusion distance covered in the relaxation process associated with the diffusion should be of the order of magnitude of, and somewhat smaller than, one atomic diameter of tantalum. An estimation of this diffusion distance from internal friction data by a procedure previously described[4] gives a value which is close to the atomic diameter of tantalum.

The fact that the observed internal friction peak cannot be interpreted by a single relaxation time with a unique heat of activation (see Fig. 4) may mean that the nitrogen atoms are situated at both the octahedral and the tetrahedral interstitial positions in the tantalum lattice similar to the case of oxygen.[1]

It is difficult to see, however, why the heat of activation associated with the nitrogen peak is so much higher than the corresponding cases of C and O resulting in the nitrogen peak occurring at a much higher temperature. A higher heat of activation implies a larger distortion introduced in the lattice by the presence of the solute atoms.

In conclusion, the writer wishes to thank Mr. George S. C. Huang for his help in taking measurements and metallographic examination of the specimens, to Messrs. Harold Hirsch and Gordon Wilkinson for help in "loading" the specimens with nitrogen, and to Dr. C. Zener and Dr. C. S. Barrett for reading the manuscript and making valuable comments.

[5] L. J. Dijkstra, Phillips Research Rep. 2, 357 (1947); also later works by Dijkstra, communicated to A.I.M.E.

The Beta-Ray Spectra of Europium and Tungsten

FRANKLIN B. SHULL*
Randall Laboratory of Physics, University of Michigan, Ann Arbor, Michigan
(Received June 18, 1948)

The primary function of this paper is to report the results of a spectrometric investigation of beta- and gamma-radiations from certain isotopes of europium and tungsten. A secondary function is to publish information concerning the design and operation of the magnetic double-focusing beta-ray spectrometer with which the investigation was carried out. The spectra for europium and tungsten serve also to illustrate the performance of the instrument.

THE magnetic double-focusing beta-ray spectrometer was first proposed by Siegbahn and Svartholm,[1] who subsequently published a number of papers[2] in which were presented the focusing theory and a discussion of the resolving power for this instrument. Somewhat later, Dennison and Shull,[3] working independently, developed the focusing theory by perturbation methods which were complete through the second order of approximation. Some results from this development are repeated below for convenience. A letter by Rosenblum[4] pointed out certain of the characteristics of the focused image as a function of small second-order variations in the shape of the magnetic field.

The essential features of the double-focusing spectrometer can be summarized as follows. The magnetic field is inhomogeneous, but it has both cylindrical symmetry about a vertical axis and mirror symmetry with respect to a horizontal plane (the median plane). In the development of the focusing theory by Dennison and Shull,[3] the field in the median plane was assumed to have the form

$$H=H_0[1-\tfrac{1}{2}(r-a/a)+\beta(r-a/a)^2], \qquad (1)$$

where H_0 = a constant, r = radius from the symmetry axis, a = radial coordinate of the radioactive source, and β = an arbitrary dimensionless constant which determines the second order contribution to the field. To first order, the magnetic field in the median plane falls off radially as $r^{-\frac{1}{2}}$. The presence of the arbitrary constant β allows, in second order, deviations from the $r^{-\frac{1}{2}}$ law.

Expressed in cylindrical coordinates, the trajectory of a beta-particle in the spectrometer is given by the equations

$$r=a+\delta r\cos\frac{\omega t}{\sqrt{2}}+\sqrt{2}a\varphi_r\sin\frac{\omega t}{\sqrt{2}}$$
$$+(\text{second order terms involving }\beta). \qquad (2)$$

$$z=\delta z\cos\frac{\omega t}{\sqrt{2}}+\sqrt{2}a\varphi_z\sin\frac{\omega t}{\sqrt{2}}$$
$$+(\text{second order terms involving }\beta). \qquad (3)$$

In Eqs. (2) and (3), the quantities ω, δr, δz, φ_r, and φ_z are defined as

$$\omega=-eH_0/mc=v/a,$$
$$r_0=a+\delta r,$$
$$z_0=\delta z,$$
$$(\dot{r})_0/v=\varphi_r,$$
$$(\dot{z})_0/v=\varphi_z,$$

where r_0, z_0, $(\dot{r})_0$, and $(\dot{z})_0$ are the coordinates and component velocities of the beta-particle at time $t=0$, when the particle is emitted from the source with total velocity v. With a radioactive source of restricted dimensions, δr and δz are both small compared to a. Thus electrons of the proper energy, emerging from a small source located approximately at $r=a$ and $z=0$, follow trajectories which execute, in general, simultaneous radial and vertical sinusoidal oscillations about the circle $r=a$ in the median plane. Since the two oscillations are in phase with one another, a rather sharp image of the source will be formed after one half-cycle of each, when the angular argument $\omega t/\sqrt{2}=\pi$. The image is displaced from the source through an angle $\theta=\omega t=\pi\sqrt{2}=254°\,33'$.

* Now at Washington University, St. Louis, Missouri.
[1] K. Siegbahn and N. Svartholm, Nature **157**, 872 (1946).
[2] K. Siegbahn and N. Svartholm, Arkiv. f. Mat., Astr. o. Fysik **33A**, No. 21 (1946); N. Svartholm, Arkiv. f. Mat., Astr., o. Fysik **33A**, No. 24 (1946).
[3] F. B. Shull and D. M. Dennison, Phys. Rev. **71**, 681 (1947); **72**, 256 (1947).
[4] E. S. Rosenblum, Phys. Rev. **72**, 731L (1947).

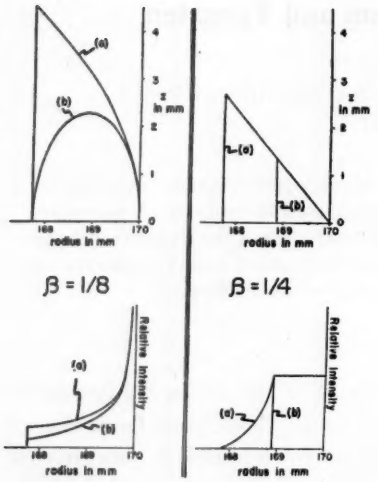

FIG. 1. Image of a point source.

Upper pictures: geometrical areas to which electrons from a monoenergetic point source are focused, with (a) square baffle aperture, and (b) circular aperture.
Lower pictures: intensity distributions across the images pictured above. See text for details.

A very advantageous characteristic of the double-focusing spectrometer has been pointed out by Siegbahn and Svartholm,[2] namely its high linear dispersion. Linear dispersion may be defined as the radial shift Δr in the position of the image of a monoenergetic source when the electron momentum is changed by a small quantity Δp. As shown by Siegbahn and Svartholm,

$$\Delta r \cong 4a(\Delta p/p)$$

for double-focusing, whereas

$$\Delta r = 2a(\Delta p/p)$$

for conventional 180° focusing. This fact leads one immediately to expect a higher resolving power for the double-focusing instrument.

As was shown in the earlier paper,[3] the second-order terms in Eqs. (2) and (3) are essentially "defocusing" terms, which can be minimized (but not completely eliminated) by a careful choice of the arbitrary parameter β. Rosenblum[4] demonstrated that the width of the focused image can be minimized by choosing $\beta=\frac{1}{4}$. However, as a result of an unfortunate error in the early stages of developing the focusing theory, the parameter was chosen to be $\beta=\frac{1}{8}$ for the spectrometer which was built and which is described in this paper. It is of interest, therefore, to investigate the expected performance of a double-focusing spectrometer for both choices for β, and to compare the results with the operational characteristics of the instrument which was constructed.

Let r^* and z^* be the coordinates of an electron at the image position, i.e., when $\omega t/\sqrt{2}=\pi$. Then, for $\beta=\frac{1}{8}$ and $\beta=\frac{1}{4}$, Eqs. (2) and (3) become

$$\begin{aligned} &\beta=\tfrac{1}{8} \\ &r^*=a-\delta r+\delta r^2/2a-5\delta z^2/6a-(4a/3)\varphi_z^2, \quad (4) \\ &z^*=-\delta z+\delta r\delta z/3a-(8a/3)\varphi_r\varphi_z, \end{aligned}$$

and

$$\begin{aligned} &\beta=\tfrac{1}{4} \\ &r^*=a-\delta r+\delta r^2/3a-2\delta z^2/3a-2a(\varphi_r^2+\varphi_z^2)/3, \quad (5) \\ &z^*=-\delta z+(2\delta r\delta z/3a)-(4a/3)\varphi_r\varphi_z. \end{aligned}$$

Using Eqs. (4) and (5), the questions of image formation, line shape, and resolving power can be investigated by graphical methods. In the analysis which follows, the computations assume spectrometer dimensions corresponding to the instrument built for this research. This means that

$$\begin{aligned} a&=170 \text{ mm}, \\ |\varphi_r| &\leqq 0.1 \text{ radian}, \\ |\varphi_z| &\leqq 0.1 \text{ radian}. \end{aligned}$$

The limitations on $|\varphi_r|$ and $|\varphi_z|$ are imposed by a square aperture in a baffle wall located halfway between the electron source and the focus position, i.e., at $\theta=\omega t=\pi/\sqrt{2}$. That this is so (in first approximation) may be seen by substituting $\omega t=\pi/\sqrt{2}$ into Eqs. (2) and (3). This gives

$$\begin{aligned} &r=a+\sqrt{2}a\varphi_r+\text{second order terms}, \\ &z=\sqrt{2}a\varphi_z+\text{second order terms}, \quad (6) \\ &\theta=\pi/\sqrt{2}. \end{aligned}$$

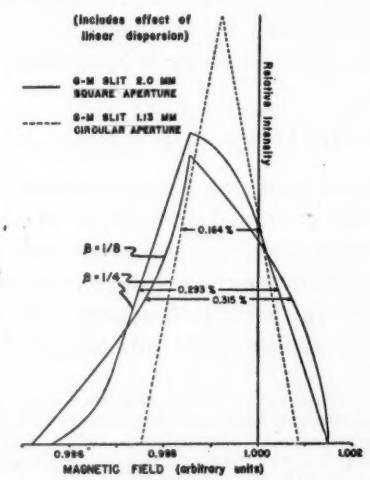

FIG. 2. Apparent line shape from a monoenergetic point source, with various choices for β and for the aperture shape.

If $|r|$ and $|z|$ in Eqs. (6) are limited by a baffle aperture, similar restrictions are imposed on $|\varphi_r|$ and $|\varphi_z|$ as a consequence.

In addition to the conditions outlined above, computations have been made also for the case of a different limitation on φ_r and φ_z, namely

$$(\varphi_r^2+\varphi_z^2)^{\frac{1}{2}}\leqq 0.1 \text{ radian.}$$

This is the case of a circular aperture in the baffle wall at $\omega t=\pi/\sqrt{2}$. The area of this circular aperture is $\pi/4$ times the area of the square aperture described previously.

The results of a graphical analysis of image formation are shown in Figs. 1, 2, and 3. Figure 1 illustrates the geometrical areas into which electrons from a monoenergetic point source (situated at $\delta r=\delta z=0$) are focused, under the condition of unchanging magnetic field ($H_0=$constant). These areas are located in the plane $\theta=\pi\sqrt{2}$. It should be emphasized that intensity is not uniform over these areas; the lower drawings of Fig. 1 illustrate this fact. They represent the counting rate observed from a Geiger counter with a high vertical entrance window of infinitesimal width, as the window is moved radially across the images in equal increments of distance. Of particular interest is the "block" distribution for the case $\beta=\frac{1}{4}$ and circular aperture.

Figure 2 illustrates the apparent line shape to be expected in actual operation of the spectrometer when the electrons originate from a monoenergetic point source (again at $\delta r=\delta z=0$). Here a Geiger counter with a high entrance window of finite width is assumed to be fixed at $r=a$, and the magnetic field H_0 is varied. The observed counting rate is plotted as a function of the magnetic field strength. Into Fig. 2 has gone all of the information contained in Fig. 1, plus the additional effect of linear dispersion. A Geiger tube slit width of two millimeters is used in the prototype spectrometer. Figure 2 indicates that the maximum resolving power to be expected from the prototype instrument under the most ideal conditions is 0.315 percent. With $\beta=\frac{1}{4}$, circular baffle aperture, and slit width of 1.13 millimeters, the maximum resolving power would be 0.164 percent.

If an infinitesimally narrow vertical *line* source is assumed in place of a point source, Fig. 2 would not be altered appreciably. This can be understood by examining Eqs. (6) again. In first approximation, neither δr nor δz appears in Eqs. (6). This means in effect that the limitations on φ_r and φ_z will be the same for all points in a vertical line source, even one of finite width. Thus, except for relatively small second-order contributions depending on δr and δz, the apparent line shapes illustrated in Fig. 2 hold equally well for a vertical line source.

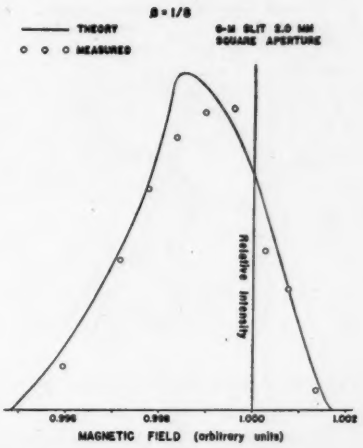

FIG. 3. Apparent line shape from a line source of finite width (0.3 mm) in the prototype spectrometer. Measured points are for the thorium F line. See text for details.

Figure 3 shows the apparent line shape to be expected in the *prototype* spectrometer from a monoenergetic vertical line source of finite width 0.3 millimeter. Into Fig. 3 has gone all the information contained in the corresponding curve of Fig. 2, plus the contribution caused by the term $-5\delta z^2/6a$ in Eq. (4). Superimposed upon the predicted line shape are experimental points from a measurement of the thorium F line. The thorium source used for this experiment was deposited by recoil upon an aluminum wire of 0.3

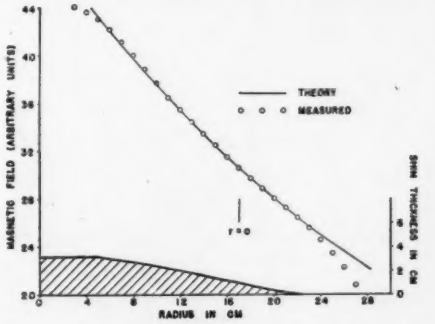

FIG. 4. Comparison of calculated and measured magnetic field shapes, and the contour of one pole shim.

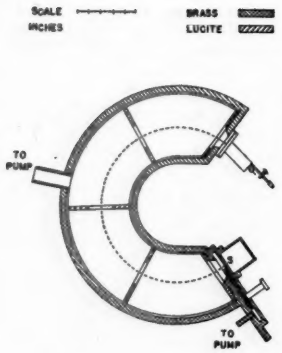

FIG. 5. Simplified drawing of the vacuum chamber.

millimeter diameter. The experimental points have been normalized to an approximate fit with the theoretical line shape. The line shape is not very well confirmed, but the experimental width of the line matches the prediction quite closely. That the predicted line shape is not borne out is not too surprising. As shown in Fig. 3, the experimental points are so closely spaced that variations of only 0.1 percent or less in the magnetic field are necessary to shift from one point to the next. Such small variations demand better accuracy in magnetic field measurements than was feasible.

Frankel[5] has stated that there exists an approximately linear relationship between the resolving power and the transmission factor of a double-focusing spectrometer, where the transmission factor may be defined as the solid angle subtended at the source expressed as a fraction of 4π. That this is so in first approximation for a point source can be seen in Eq. (5) for r^*. The over-all width of the focused image is given by the maximum value of $2a(\varphi_r^2+\varphi_z^2)/3$. Similarly the solid angle subtended at the source is approximately proportional to $(\varphi_r^2+\varphi_z^2)$. Thus both the resolution and the transmission factor are approximately proportional to $(\varphi_r^2+\varphi_z^2)$ and the linear relationship between them is established.

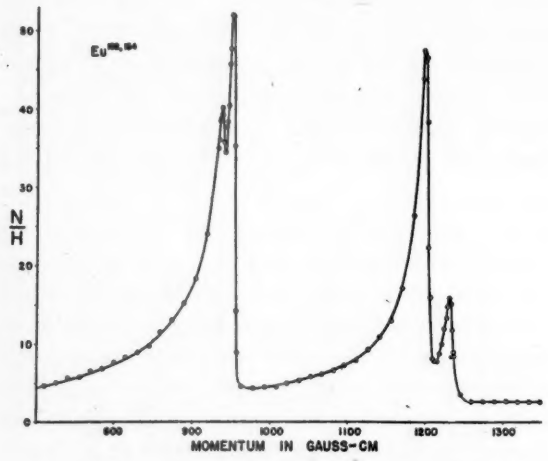

FIG. 6. Internal conversion spectrum of 5–8-year europium, Part 1.

[5] S. Frankel, Phys. Rev. 73, 804 (1948).

DESIGN OF THE SPECTROMETER

The first step in constructing a double-focusing spectrometer is to provide a magnetic field shaped according to Eq. (1). In the present case there was already available an electromagnet of conventional design, with 22-inch circular plane-parallel pole faces, intended originally for a 180° spectrometer. To adapt this magnet for a double-focusing instrument, the pole spacing was increased to six inches, and a one-piece steel shim of variable thickness was added to each face. Figure 4 shows the thickness of one shim as a function of radius and also a comparison between the shape of the field as required by Eq. (1) and as actually measured. The measured shape of the field is correct for values of H_0 between 2 and 1280 gauss, provided the magnet has first been properly cycled to remove remanence effects. The latter precaution is always observed in normal operation of the spectrometer.

A simplified plan view of the vacuum chamber of the spectrometer is shown in Fig. 5. Its design was governed largely by the requirement that the internal height of the chamber should be as great as possible in order to make maximum use

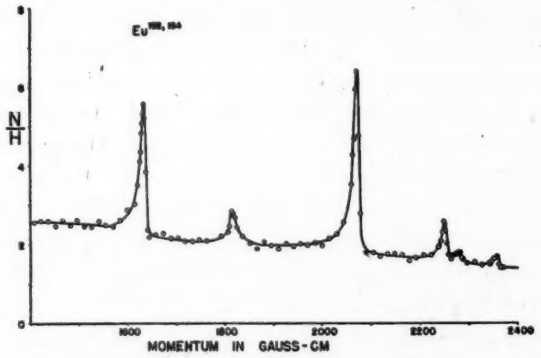

FIG. 7. Internal conversion spectrum of 5–8-year europium, Part 2. Note change of scales.

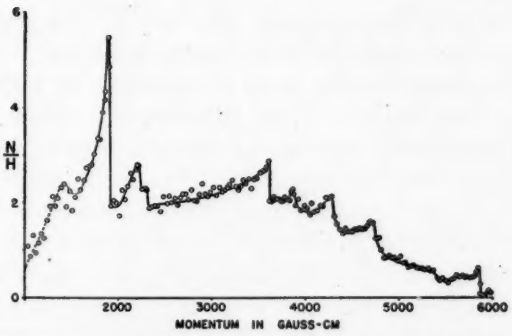

FIG. 8. Photoelectron spectrum of 5–8-year europium, from a Pb radiator.

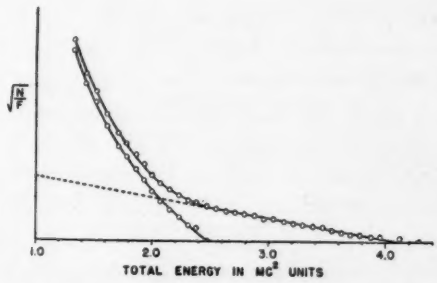

FIG. 9. Fermi plot of the continuous beta-ray spectrum of 5–8-year europium. At least two spectra appear to be present.

of the vertical focusing properties of the shaped magnetic field. Moreover, it was felt that the internal dimensions should be large compared to the cross section of the electron beam so as to minimize wall-scattering troubles within the chamber. The chamber itself is constructed of brass and is lined with thin aluminum sheet. Radial walls, or baffles, of $\frac{1}{4}$-inch Lucite divide the chamber into four compartments of roughly equal volume. Rectangular apertures in the baffles limit the electron beam which can traverse the chamber, and subtend at the source a solid angle of approximately 0.32 percent of 4π steradians. Between the source S and the chamber is interposed a sliding brass shutter, by means of which the source can be isolated from the vacuum whenever it is necessary to remove or change sources. Behind the source, a removable brass cup, lined with cellulose acetate, completes the assembly. The source is so mounted as to keep adjacent metal and plastic surfaces as far removed as possible, thus minimizing trouble caused by secondary electrons engendered by gamma-rays from the source.

Registration of beta-particles is accomplished with an end-fire Geiger tube of conventional cylindrical geometry. The axis of the tube is inclined 8° inward from the normal to the spectrometer wall, so as to give each electron a path length through the effective counting volume of sufficient magnitude to keep the counting efficiency high. Sheet nylon of thickness 0.84 mg/cm² was originally used for the counter window. Such a window is opaque to electrons of energy below 30 kev, and passes 72 percent of 64 kev electrons. At the present time, an alternative window is available which permits the extension of measurements down to about 15 kev. This window consists of a collodion film laid over a phosphor bronze supporting grid. A hexagonal array of holes (0.036 inch diameter) in the grid gives 58 percent open area. The useful range for the thin window is from about 15 to 650 kev.

The methods used for controlling and measuring the magnetic field have been described in an earlier paper.[6] As explained there, the electromagnet is supplied from storage batteries, which in turn are trickle-charged by a d.c. generator. The device used for measuring the magnetic field is essentially the armature of a d.c. generator driven by a synchronous motor. The motor in turn is supplied from a d.c.-a.c. thyratron inverter controlled by a locked-frequency audio oscillator. This gives frequency regulation better than that afforded by the regular 110-volt lines. Repeated determinations of the field of a permanent magnet make reasonable the assumption that the magnetic field can be measured with about 0.1 percent relative accuracy. The absolute accuracy is somewhat less certain. The measuring device and the spectrometer were calibrated as a unit by making an observation of the F line in the internal conversion spectrum of thorium B ($H\rho$ assumed 1383.8 gauss-cm). Thus the absolute accuracy contains an additional factor of uncertainty as a result of an uncertainty in the momentum of the thorium F line.

In the course of several months of operation, the performance of the prototype spectrometer has been most gratifying. The high resolution which it affords makes possible the separation of closely-spaced internal conversion peaks, as illustrated by the europium spectrum in Figs. 6

[6] J. M. Cork, R. G. Shreffler, and F. B. Shull, Rev. Sci. Inst. 18, 315 (1947).

TABLE I.

Ia. Continuous beta-spectra upper energy endpoints

Energy in kev	Relative intensity of spectrum	Identification
751±15	4900	Eu^{152}
1575±150	1200	Could be from either isotope.

Ib. Internal conversion lines

Electron energy in kev	Relative intensity	Possible identifications	Transition energy in kev
73.1	300	*K* conv. in Gd	123.4
74.4	2000	*K* conv. in Gd	124.7
		K photo in Eu	123.0
		K conv. in Sm	121.2
114.0	1740	*L* conv. in Gd	122.4
		L photo in Eu	122.0
		L conv. in Sm	121.7
119.6	330	*M* conv. in Gd	121.5
		M photo in Eu	121.4
		M conv. in Sm	121.3
197.2	70	*K* conv. in Gd	247.5
		K conv. in Sm	244.0
236.1	30	*L* conv. in Gd	244.5
		L conv. in Sm	243.8
		K conv. in Gd	286.4
293.6	90	*K* conv. in Gd	343.9
335.5	17	*L* conv. in Gd	343.9
342.6	8	*M* conv. in Gd	344.5
362.0	4	*K* conv. in Gd	412.3

Ic. Photoelectron lines

Electron energy in kev	Possible identification	Transition energy in kev
155	*K*	243
255	*K*	342
329	*L*, *K*	344, 416
352	*K*	442
684	*K*	772
758	*L*	774
871	*K*	959
995	*K*	1082
1314	*K*	1402

and 7. Moreover, it is possible to establish the existence of low-intensity peaks which would tend to fade into the continuous background in an instrument with lower resolving power. The double-focusing spectrometer also offers advantages in the determination of beta-spectrum shapes as a test of the theory of beta-decay. Recent reports indicate the possibility that the Fermi theory for allowed spectra is not confirmed in the region of very low electron energy. The relatively high transmission factor of a double-focusing spectrometer alleviates somewhat the problem of low counting rates at very low energies. By opening up the baffle apertures, the transmission factor could be increased to facilitate this type of work. This would entail a corresponding decrease in resolving power, but even so, the resolution is still good when compared with a conventional 180° instrument.

The first beta-emitting sources which were examined with the double-focusing spectrometer were selected with a view toward testing the performance of the instrument. One was a long-lived activity in europium which was known to be rich in internal conversion lines. The other was a 75-day activity in tungsten which was known to be a pure beta-emitter. With these it was hoped that the capabilities of the spectrometer in measuring both continuous and line spectra would become evident.

EUROPIUM[152, 154]

When the stable isotopes of europium are irradiated in a neutron pile, active isotopes of atomic weights 152 and 154 are formed by (n, γ) processes. A mass spectrographic analysis by Inghram and Hayden[7] showed that activities can be assigned to these isotopes as follows:

Atomic weight	Half-life
152	9.2 hours
152	5–8 years
154	5–8 years.

The same authors made absorption measurements of the two 5–8 year activities without attempting to distinguish between them, and reported "at least two betas and one gamma." The gamma-energy was given as 1.4 Mev.

The 9.2-hour isomer of Eu^{152} has been studied by Tyler,[8] who used a 180° magnetic spectrometer. He observed a beta-spectrum having an upper energy limit of 1.885 Mev, and internal conversion peaks corresponding to transitions of 123 and 724 kev, all decaying with the 9.2-hour half-life. In addition he noted several indications of other conversion lines, but was unable to resolve them into definite peaks because of the low intensity of his source.

Cork, Shreffler, and Fowler[9] studied the long-

[7] M. G. Inghram and R. J. Hayden, Phys. Rev. **70**, 89; **71**, 130 (1946–47).
[8] A. W. Tyler, Phys. Rev. **56**, 125 (1939).
[9] J. M. Cork, R. G. Shreffler, and C. M. Fowler, Phys. Rev. **72**, 1209 (1947); **73**, 78L (1948).

lived activities of europium in a photographic 180° spectrometer, and reported internal conversion lines corresponding to transitions of 122, 247, 286, 343, and 408 kev. In addition, a 1.23-Mev gamma-ray was indicated by absorption measurements, as well as a continuous beta-spectrum of energy 0.93 Mev.

Wiedenbeck and Chu,[10] using a coincidence-counting technique, reported the continuous beta-spectrum of long-lived europium to be complex, with upper energy limits of 0.62 and 1.0 Mev.

In preparing active europium for the present research, pure Eu_2O_3 was subjected to neutron irradiation in the Oak Ridge pile. Following irradiation, a time lapse of about six months occurred, after which the measurements reported below were undertaken. Thus the 9.2-hour isomer of Eu^{152} was eliminated. Two types of spectra were sought, first an internal conversion line spectrum superimposed on a continuous beta-ray background, and second a photoelectron line spectrum from a lead radiator. The conversion spectrum was determined from a powder source on a substrate of Scotch tape 0.8 millimeter in width. The photoelectron spectrum was determined from a source contained in a lead test tube of one-millimeter bore and one-millimeter wall thickness.

Ten conversion lines and two continuous beta-spectra are observed in the conversion spectrum. Since the conversion lines vary widely in intensity, the over-all spectrum does not lend itself easily to plotting in a single graph. Consequently the spectrum has been broken up into two sections and is plotted to different scales in Figs. 6 and 7. The photoelectron spectrum shows nine peaks and is plotted in Fig. 8. Few of the nine peaks stand out very prominently above the Compton background, and some of them are of dubious reality. The continuous tail of the conversion spectrum can be analyzed by means of a Fermi plot as shown in Fig. 9. Two spectra appear to be superimposed, with energies 0.751 ± 0.015 Mev and 1.575 ± 0.150 Mev. The large uncertainty in the latter is due to extremely low counting rates and very poor statistics. All the data are assembled in tabular form in Table I. Possible identifications, sometimes several of them, are suggested for each conversion or photoelectron peak. In each case, the corresponding nuclear transition energy is given also.

A complete, consistent, and unique interpretation of the internal conversion and the photoelectron line spectra of europium cannot be developed for several reasons. First, the presence of two isotopes, both having approximately the same half-life, makes it almost impossible to show conclusively which radiations are associated with the one and which with the other isotope. Second, the small number of *K-L-M* sets in the conversion spectrum makes it difficult in many cases to decide in which atom the internal conversion process is taking place. Third, purely spectrometric energy measurements cannot give any information about genetic relationships between various nuclear transitions.

Only in one instance is sufficient information known on which to base a strong argument regarding the choice between Eu^{152} and Eu^{154} as the parent of an observed gamma-transition. Tyler[8] found a 1.885-Mev β^--transition and a pair of very strong internal conversion lines at $H\rho=940$ and $H\rho=1186$ in the spectrum of the 9.2-hour isomer of Eu^{152}. In the present investigation of long-lived europium, two β^--spectra were observed, of energy 0.751 and 1.575 Mev; in addition there is a group of very strong conversion lines at $H\rho=938$, 952, 1199, and 1231 gauss-centimeters, of which those underlined are by far the strongest. It seems a reasonable guess that the pair of lines reported by Tyler and the similar lines reported here all result from the same nuclear transition or transitions. The fact that Tyler observed only two lines, as well as the comparatively lower momentum values reported by him, are explainable as being due in part to the rather low resolving power (~1.5 percent) of his 180° spectrometer.

The following argument can be built upon this similarity between the spectra of 9.2-hour and 5–8-year europium. It may be hypothesized that both isomers of Eu^{152} decay by β^--emission. It is therefore assumed that each of the final states in the two cases (immediately following β^--decay) is a member of a single system of excited states of Gd^{152}. The consequences of this argument would be as follows:

[10] M. L. Wiedenbeck and K. Y. Chu, Phys. Rev. **72**, 1164 (1947).

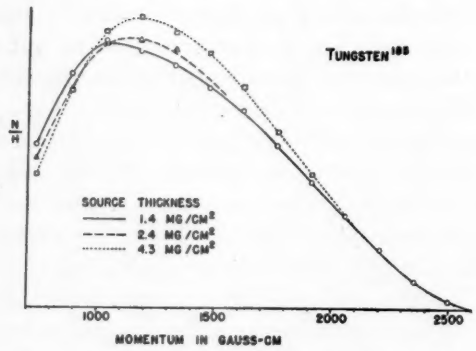

FIG. 10. The continuous beta-ray spectrum of tungsten[185]. Curves are normalized to one another at high energies.

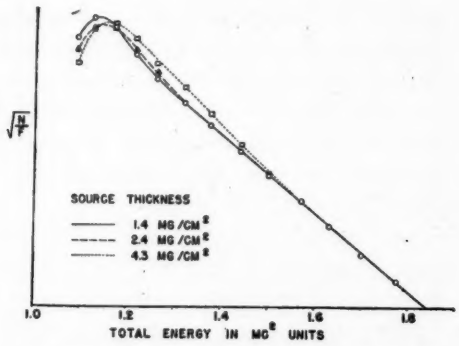

FIG. 11. Fermi plot of the W^{185} beta-spectrum. Curves are normalized to one another at high energies.

(a) The low energy conversion lines observed in 5–8-year europium, which are probably caused by two transitions of approximately equal energy (see further discussion of this point in later paragraphs), must definitely be associated with Eu^{152}, not Eu^{154}.

(b) The 0.751-Mev β^--spectrum of 5–8-year europium must also be associated with Eu^{152}, inasmuch as the much smaller population of the 1.575-Mev spectrum is insufficient by itself to account for the large population of the conversion lines, i.e., the conversion coefficient would then turn out to be greater than unity.

(c) The relative populations of the low-energy conversion lines and of the 0.751-Mev β^--spectrum suggest that the total internal conversion coefficient for at least one of the two alleged transitions is very large, perhaps as large as 80 percent.

(d) By inference, one can draw the much weaker conclusion that some, perhaps all, of the other conversion peaks and gamma rays observed in 5–8-year europium may also be due to transitions in gadolinium following a β^--transition. This argument is included because it is apparent from Table I that assignments of some of the other observed radiations to transitions in gadolinium are either refuted by consideration of the *K-L-M* energy differences or cannot be made at all because of the failure to observe *K-L-M* sets. In particular, it appears in two instances that *K-L-M* or *K-L* differences are found which are most nearly characteristic of samarium. This would require decay of europium either by positron (β^+) emission or *K*-capture. Neither positron emission nor annihilation radiation are found in 5–8-year europium. *K*-capture is still a possibility, but proof of its occurrence could only be obtained through a search for the characteristic samarium x-rays which would accompany it.

Another point of interest in the europium conversion spectrum concerns the interpretation to be placed upon the four peaks of lowest energy. It has been suggested by Cork, Shreffler, and Fowler[9] that all four peaks are the result of a single nuclear transition in gadolinium following a β^--transition from europium. It is assumed that this transition may result either in (a) the direct emission of internal conversion electrons from gadolinium, or in (b) the emission from gadolinium of a gamma-ray which ejects photoelectrons from neighboring europium atoms. Either process could produce a complete group of *K-L-M* peaks. The excitation potentials of gadolinium and europium are such that only the two *K* peaks would differ sufficiently in energy to be resolvable. Thus four distinct peaks would be observed. As indicated in Table I, however, the data reported here do not yield consistent values for the transition energy when interpreted in the above fashion.

Another plausible explanation of these four low-energy conversion peaks is to assume that they are conversion lines resulting from two distinct nuclear transitions of very nearly the same energy. If this be the case, the relative intensities of the two *K* peaks should remain the same when the radioactive sample is made thinner and weaker. In contrast, the mechanism suggested by Cork, Shreffler, and Fowler would require the relative intensities of the two *K* peaks to alter

in favor of the conversion peak when the sample is made thinner and weaker. In order to discover which interpretation is more plausible, this section of the conversion spectrum was remeasured, using a sample whose mass per unit area was about 0.3 times that used originally. No marked alteration was observed in the relative intensities of the two K peaks. It is concluded that the mechanism suggested by Cork, Shreffler, and Fowler is less plausible than the alternative one which requires that two separate nuclear transitions take place.

The presence of two indistinguishable isotopes and the absence of information concerning the genetic relationships of the beta- and gamma-rays from europium make it impossible to reason out a plausible energy level scheme which will account for the observed radiations. Some attempts in this direction have been made, but the results are unquestionably dubious. For instance, if one were to assume that eleven gamma-transitions take place all in one type of nucleus, with gamma-energies of 123, 124, 247, 286, 344, 412, 442, 772, 959, 1082, and 1402 kev, a system of seven energy levels (including the ground level) can be found which might account for them within one or two kev accuracy. This system would have levels at 123, 247, 533, 877, 1206, and 1649 kev above the ground level. However, a series of experiments involving coincidence spectrometry will be necessary before any acceptable conclusions can be drawn with respect to an energy-level diagram.

TUNGSTEN[185]

Tungsten has five stable isotopes of atomic weights 180, 182, 183, 184, and 186. Minakawa[11] and Fajans and Sullivan[12] investigated the activities induced in tungsten by slow neutron bombardment, and discovered two activities of 24-hour and about 75-day half-life, which they attributed to W^{187} and W^{185} respectively. Minakawa reported W^{185} to be a beta-emitter, with an upper energy limit of 0.4–0.5 Mev based on aluminum absorption measurements. Fajans and Sullivan found the upper energy limit of W^{185} to be 0.55–0.65 Mev on the basis of absorption data, and 0.64–0.72 Mev as a result of preliminary cloud-chamber work. A later paper by Sullivan[13] placed the limit at 0.55 Mev on the basis of more complete absorption data, and reported also that no gamma-rays could be detected. Jnanananda[14] measured the beta-spectrum of W^{185} in a lens type spectrometer, and observed the upper limit at 0.675 Mev. There is considerable suspicion that this high value was due to the presence of a small contaminant of iridium in his sample. Saxon[15] also investigated tungsten with a lens spectrometer and reported the energy limit as 0.43 Mev.

The samples from which the W^{185} beta-spectrum was measured were obtained by neutron irradiation of tungsten oxide. Samples were prepared by allowing the finely powdered oxide to fall out of a water suspension onto a substrate of nylon of thickness 0.84 mg/cm^2. The spectrum was measured three times, from samples of thickness 1.4, 2.4, and 4.3 mg/cm^2, respectively. The measured spectra, normalized to coincide with one another at high energies, are plotted as functions of momentum in Fig. 10, and the corresponding Fermi plots appear in Fig. 11. It is immediately obvious that the low energy portions of the spectrum are markedly subject to self-scattering effects within the sample. An extrapolation of the Fermi plot to its intersection with the energy axis yields a value for the transition energy of 1.84 mc^2 or 0.428 Mev, which agrees very well with the determination made by Saxon.

According to the lifetime-energy criterion developed by Konopinski[16] the W^{185} beta-transition falls into a category of twice-forbidden transitions. From the data obtained with the thinnest sample, it appears that the spectrum has the allowed shape down to energies somewhat less than 150 kev. Below this energy it is quite possible that experimental difficulties contribute to the observed deviations.

ACKNOWLEDGMENTS

The author is deeply grateful to the Eastman Kodak Company for fellowship support during the 1947–8 academic year. The spectrometer project was sponsored and supported by the Office of Naval Research.

[11] O. Minakawa, Phys. Rev. **57**, 1189L (1940).
[12] K. Fajans and W. H. Sullivan, Phys. Rev. **58**, 276 (1940).
[13] W. H. Sullivan, Phys. Rev. **68**, 277 (1945).
[14] S. Jnanananda, Phys. Rev. **72**, 1124 (1947).
[15] D. S. Saxon, private communication to S. Jnanananda.
[16] E. J. Konopinski, Rev. Mod. Phys. **15**, 209 (1943).

Large-Angle Scattering of Na^{24} Gamma-Radiation

ERNEST POLLARD AND DAVID E. ALBURGER*
*Sloane Physics Laboratory, Yale University,** New Haven, Connecticut*
(Received June 23, 1948)

Scattering of the 1.38-Mev and 2.76-Mev gamma-radiation of Na^{24} has been observed at a mean angle of 135°. Mg, Al, Pb, and Hg scatterers were used, and three definite components of scattered radiation were observed. The softest, of energy about 200 kev, is Compton-scattered radiation; the next hardest, of energy 500 kev, is the positron annihilation radiation. The third has an energy between 1.1 and 2.8 Mev. It is due, in part, to bremsstrahlung, but seems to be somewhat too hard to be wholly explained by this process. It is not sharply resonant nuclear scattering since it appears nearly equally in Mg and Al, while only Mg should be sharply resonant. From the lack of sharp resonance with the Mg^{24} level at either 1.38 Mev or 2.76 Mev, it is concluded that these levels must be less than 1/100 ev wide and that the corresponding transitions are of quadrupole or higher order.

I. INTRODUCTION

THE large-angle scattering of gamma-radiation is of interest because the predominant Compton scattering is both low in intensity and long in wave-length. The study therefore reveals the presence of any other processes of interest. It was employed by Chao[1] and Gray and Tarrant[2] and revealed the presence of the 0.5-Mev component resulting from annihilation radiation developed in the scatterer by the positron part of pairs.

The present work was begun with the object of detecting nuclear resonant scattering from Mg^{24} nuclei which are excited by resonant radiation from the radioactive Na^{24} nuclei. These decay by beta-ray emission to Mg^{24} following which two gamma-rays are emitted in cascade.[3] The excitation of Mg^{24} by one of these gamma-rays would therefore be expected.

The experimental observation is not easy because the act of gamma-ray emission lowers the gamma-ray energy resulting from the recoil of the nucleus so that the energy is about 90 ev off resonance. While other factors exist, these in general do not compensate for the recoil effect, and it can be estimated that the expected cross section should be less than 10^{-27} cm². If it is detectable at all, a very carefully conducted experiment is required.

Early study[4] of the large-angle scattering process showed that for lead a hard component exists. There was some evidence for a preferential scattering by Mg as compared with Al. It was therefore decided to construct an automatic scattering apparatus which would permit long periods of counting in order to search for very small effects. The results of these experiments are given here.

While this work was in progress a note by Schiff[5] appeared, calling attention to the potency of the large-angle scattering method. An attempt to observe resonance absorption in lead has been made by Zuber.[6]

II. THEORETICAL CONSIDERATIONS

If the difference of energy of two eigenvalues corresponding to the emission of a quantum is E, then the frequency ν_E of an emitted quantum will be slightly less than the relation $h\nu_E=E$ would assert because momentum has to be given to the recoiling atom. If M is the mass of the atom the conservation of energy and momentum leads to

$$E-h\nu_E=\frac{h^2\nu_E^2}{2Mc^2}. \quad (1)$$

Similarly, if radiation is to excite the nucleus by

* Now at Brookhaven National Laboratory.
** Assisted by the Office of Naval Research under Contract N6ori-44.
[1] C. Y. Chao, Phys. Rev. **36**, 1519 (1930).
[2] L. H. Gray and G. T. P. Tarrant, Proc. Roy. Soc. **136**, 662 (1932).
[3] L. G. Elliott, M. Deutsch, and A. Roberts, Phys. Rev. **63**, 386 (1943).
[4] E. C. Pollard and B. B. Benson, Phys. Rev. **71**, 134(A) (1947).
[5] L. I. Schiff, Phys. Rev. **70**, 761 (1946).
[6] K. Zuber, Helv. Phys. Acta **16**, 429 (1943).

the amount E, there also has to be supplied the kinetic energy of the atom receiving the momentum of the incident quantum. If ν_A is the frequency of a quantum which precisely fits this condition for absorption, then

$$h\nu_A - E = \frac{h^2\nu_A^2}{2Mc^2}. \tag{2}$$

Combining (1) and (2), we have

$$h\nu_A - h\nu_E = \frac{E^2}{Mc^2}. \tag{3}$$

The inelastic scattering of protons by Mg, as observed by Dicke and Marshall,[7] indicates that the first excited state of Mg^{24} is at 1.32 Mev. For Mg^{24} Eq. (3) gives a difference of 90 ev. Hence, if radiation from a source of Na^{24}, which decays to Mg^{24} and then emits gamma-radiation, is used to excite Mg^{24}, the radiation will be off resonance by 90 ev.

Although there exist factors which can reduce this deviation from resonance, we may first consider the cross section expected for scattering of such radiation. The expression for resonant absorption (which would be followed by emission to give scattered radiation) from Heitler's book[8] (p. 115) is

$$\sigma = \frac{\pi^2 c^2 \gamma^2}{2\pi\nu_0^2\left[(\nu-\nu_0)^2+\frac{\gamma^2}{4}\right]},$$

where γ is the chance of a transition per atom per second, and ν and ν_0 are the actual and resonant frequencies. Rewriting this in terms of Γ, the line width, E and E_0 the actual and resonant energies, all in electron volts, this becomes

$$\sigma = \frac{2.4\times10^{-8}\Gamma^2}{E_0^2\left[(E-E_0)^2+\frac{\Gamma^2}{4}\right]}. \tag{4}$$

For Mg^{24} we have, to a close approximation,

$$\sigma = \frac{1.2\times10^{-20}\Gamma^2}{90^2}.$$

Thus an actual measurement of σ gives information regarding Γ, the line width.

The value expected for Γ depends on the selection rules for the transition. Thus, if the radiation is dipole the value of Γ, according to a formula given by Helmholz,[9] is roughly 1.3 ev, while if it is quadrupole the value is one thousand times less.

The cross sections expected in the two cases are 10^{-23} cm^2 and 10^{-29} cm^2. The former could be detected, but the latter only with great difficulty. The study of large-angle scattering by Mg and Al can therefore, as a minimum, decide whether the radiation from the first excited state of Mg^{24} is dipole or of higher order.

III. BETA-RAY AND CASCADE GAMMA-RAY MOMENTUM CONSIDERATIONS

There exists a possibility that the gamma-radiation is emitted while the nucleus still has the recoil momentum from the beta-ray. A second possibility is that the first of a cascade gamma-ray emission process gives recoil momentum to the nucleus which is still present when the second gamma-ray emerges. Either of these processes can change the distribution of gamma-ray energies considerably.

The analysis of either case is simple and the following results are obtained:

Case I, gamma-ray emitted at an angle θ to the beta-ray,

$$E - h\nu_E = \frac{E^2}{2Mc^2} + \frac{E}{Mc}p_\beta\cos\theta, \tag{5}$$

where $p_\beta = m_0 c\beta/(1-\beta^2)^{\frac{1}{2}}$ is the momentum of the beta-ray.

Case II, first gamma-ray emitted at an angle φ to the second,

$$E - h\nu_E = \frac{E^2}{2Mc^2} + \frac{EE'}{Mc^2}\cos\varphi, \tag{6}$$

where E' is the energy of the first gamma-quantum and E that of the second.

Both of these equations offer very interesting possibilities if the resonant process is ever detected, since the use of coincidence methods permits a complete knowledge of the process to be

[7] Robert H. Dicke and John Marshall, Jr., Phys. Rev. 63, 86 (1943).

[8] W. Heitler, *The Quantum Theory of Radiation* (Oxford University Press, London, 1936).

[9] A. C. Helmholz, Phys. Rev. 60, 415 (1941).

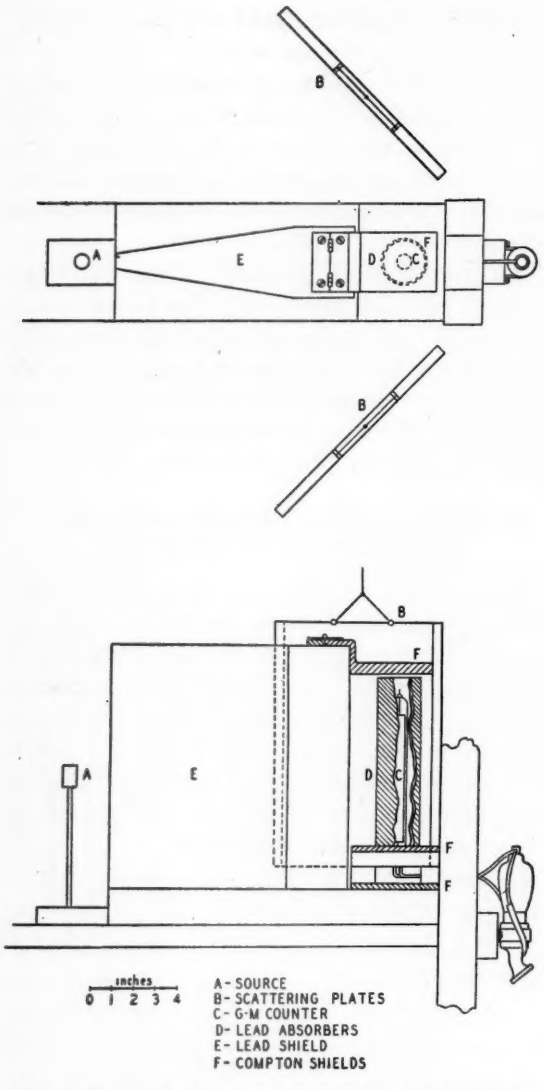

FIG. 1. Top and side views of experimental arrangement for measuring the absorption of large-angle scattered gamma-radiation.

established. The only missing item is the momentum of the neutrino. Experimentally, this can be neglected by selecting only those beta-rays having close to the maximum energy. For resonance to occur in a scattering nucleus the emitted frequency ν_B of Eq. (5) must be equal to the ν_A of Eq. (2). Combining these two we have

$$\frac{E^2}{2Mc^2}+\frac{E}{Mc}p_\beta\cos\theta=-\frac{E^2}{2Mc^2},$$

or

$$\cos\theta=-\frac{E}{p_\beta c}. \qquad (7)$$

In the case of Na^{24} the momentum of the 1.4-Mev beta-ray is 3.8 m_0c. If $E=1.38$ Mev then

$$\cos\theta=-\frac{1.38\times 2m_0c^2}{3.8m_0c^2}=-0.71.$$

Resonance therefore occurs in the scattering Mg^{24} nucleus if the angle between the beta-ray and gamma-quantum emitted by the source nucleus is approximately 135°. The assumption is made that no interactions of the source nucleus with surrounding matter occur in the time between beta-ray and gamma-ray emission events.

This process cannot actually take place in the element studied, since two gamma-rays are emitted in cascade. This destroys the above momentum relationship. It might occur for Fe^{56}, the daughter element of Mn^{56}. In a clear-cut case, Eq. (7) presents the possibility of varying the angle θ and obtaining the contour of the energy level E.

IV. EXPERIMENTAL RESULTS

An attempt was first made to exploit Eq. (7). A "spectrometer" was constructed consisting of

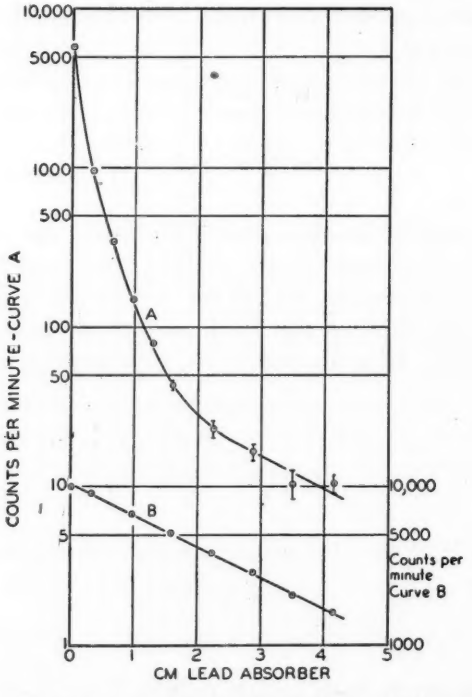

FIG. 2. Curve A, absorption of sodium (24) gamma-radiation scattered by magnesium. Curve B, absorption of direct sodium (24) gamma-radiation.

a source, a beta-ray counter, a scattering block, and a gamma-ray counter shielded from direct radiation but arranged to detect radiation scattered from the block. Double coincidences were counted between beta-rays and scattered gamma-rays. The source used in one case was Na^{24}, the scatterer Mg, in a second case Mn^{56} and Fe^{56} were used as source and scatterer. It was not found possible to overcome the exceedingly high rate of random coincidences. The experiment requires a counter resolution time of the order of 10^{-8} second, whereas the counters used had a resolution time at least one hundred times as great.

Following this unsuccessful attempt it was decided to look for resonant large-angle scattering. Figure 1 shows top and side views of the experimental arrangement. The direct radiation from the source (*A*) was shielded out by 11 inches of lead (*E*). A Herbach-Rademan GLC-11 counter (*C*) was used to detect the scattered radiation. Two scattering plates (*B*) of up to 1-inch thickness were arranged to give a maximum yield consistent with a range of scattering angles between 120° and 150°. A set of cylindrical lead absorbers (*D*) could be placed over the counter, out to about 4-cm radial thickness. Lead "Compton" shields (*F*) were placed above and below the counter to reduce radiation scattered from the floor and ceiling of the room and entering the counter end-on. These effected a substantial reduction in background.

TABLE I. Sample scattering data from one run.

Counter absorption (cm Pb)	Net Mg	Net Al	Ratio
0.00	124	117	1.06
	88*	95*	0.93
0.18	37.7	33.5	1.12
	19.1*	19.1*	1.00
0.35	35.9	31.5	1.14
	6.6*	6.6*	1.00
0.67	5.8	3.6	1.60
	2.8*	3.1*	0.90
1.34	0.32	0.0	—
	0.72*	1.65*	0.44
2.19	0.31*	0.34*	0.91
3.36	0.92	0.00	—
4.03	0.54	0.37	1.46

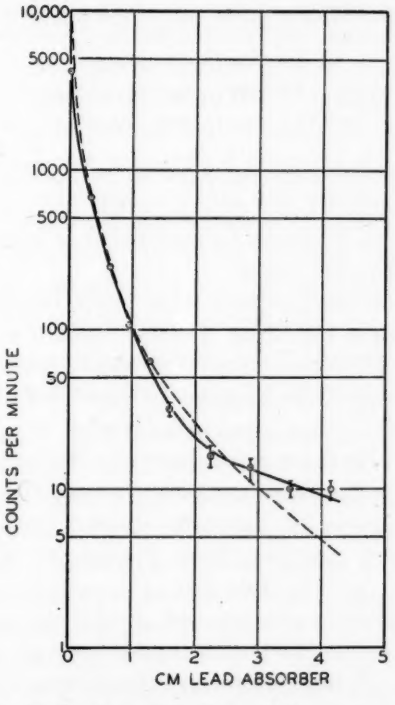

FIG. 3. Absorption of sodium (24) gamma-radiation scattered by aluminum. The dashed curve is a rough theoretical estimate, including Compton-scattered, positron annihilation, and bremsstrahlung components.

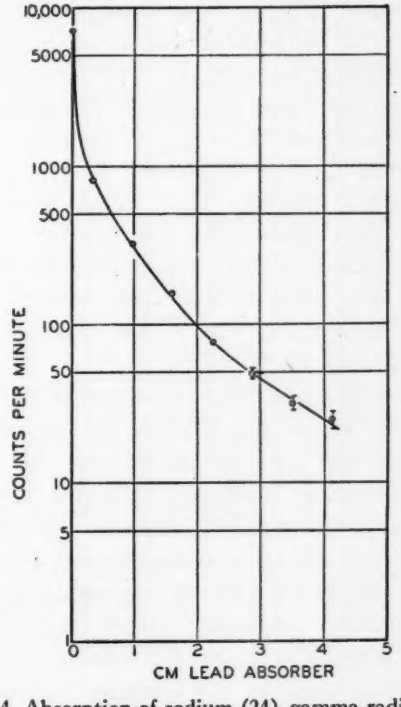

FIG. 4. Absorption of sodium (24) gamma-radiation scattered by lead.

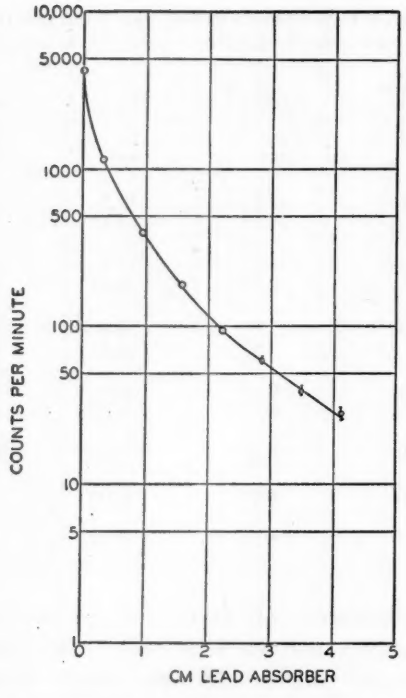

FIG. 5. Absorption of sodium (24) gamma-radiation scattered by mercury.

Four sets of experiments were tried. The first was an attempt to detect resonant scattering in Fe^{56}, using Mn^{56} as the resonant gamma-ray source. The experiment was not very thorough, but it showed that no large (10^{-24} cm^2) scattering cross section exists peculiar to this experiment. An attempt was also made to observe resonant scattering in C^{13}, using N^{13} as the resonant gamma-ray source. This failed because no gamma-rays other than annihilation radiation were detected. A third experiment was carefully carried out aimed at observing resonant scattering by Mg^{24}, using Na^{24} as the resonant source. This can now be described.

The object was the observation of an increase in scattering by Mg over Al at various thicknesses of lead absorber placed over the counter. The resonantly scattered radiation should be more penetrating than Compton scattered radiation and annihilation radiation and accordingly an increase in the ratio of magnesium scattering to aluminum scattering should take place at higher absorption. In order to obtain statistically significant numbers of particles counted, and avoid systematic errors due to source decay and counter variation, an automatic scatterer-changing device was constructed.[10] This changed the scatterers every five minutes in the order MgNoAlAlNoMg, etc., where "No" indicates the absence of a scatterer. Separate recorders and clocks measured the total counts and total time for each scatterer in position and for background over a half-hour or one-hour period at a given absorption. By subtracting out the background counting rate the net scattering yield was obtained for each element. This was done at a number of values of absorption, and for comparison all results were referred to a standard source strength by correcting for decay. The results of one run are given in Table I. The star indicates data taken with a second counter. The number of counts at each point was well over ten thousand, but at the high absorptions the yield of scattered radiation of any kind was so small that the effects of random fluctuations became very large. From Table I it can be seen that the results up to 0.67-cm absorption yield a ratio which has reasonable consistency, but that thereafter the ratio is widely varying, indicating that statistical fluctuations are not removed. The count at 4.03 cm gave the following figures:

Al 13,610 in 211.6 minutes
Mg 13,880 in 211.9 minutes
No 13,250 in 210.6 minutes.

Thus while there appears to be no doubt that both elements do give a penetrating scattered radiation, it cannot be asserted that one scatters more than the other.

Similar comparisons were made between lead and copper radiators. These showed a very definite yield from lead at high absorptions but not very much from copper. In view of this it was decided to plot absorption curves for Mg, Al, Pb, and Hg scatterers separately. Mg and Al were used for the reasons already given. Pb and Hg were chosen in case Pb showed any specific resonance resulting from the known 2.62-Mev gamma-ray; Hg then served as comparison. The Hg scatterers consisted of sheet-iron containers $\frac{1}{4}$ inch thick filled with liquid mercury. Sources were made by deuteron bombardment of metallic sodium and varied from 20 to 60 millicuries in

[10] D. E. Alburger and E. C. Pollard, Phys. Rev. 72, 169(A) (1947).

strength. The results are given in Figs. 2–5. These show the absorption of scattered radiation from magnesium, aluminum, lead, and mercury, respectively. It can be seen that for each element there are present several components of scattered radiation and that one of these is definitely too hard to be explained as annihilation radiation or Compton-scattered radiation. Curve *B* of Fig. 2 shows the absorption of direct radiation for comparing with the hard scattered component and also for furnishing a check on the absorbers and geometry. To obtain this a well-decayed sodium source was dissolved in water and spread uniformly on a piece of cardboard cut to the same length and width as the scattering plates. This large-area source, approximating the geometry of a uniformly illuminated scattering plate, was then placed in the position normally occupied by one of the scatterers and the absorption curve plotted. The absorption coefficient is approximately what one would expect at 2.8 Mev from theoretical curves given by Heitler.

V. DISCUSSION

Three processes which can give scattered quanta are known to occur when gamma-radiation strikes a radiator. These are Compton scattering, pair production and positron annihilation, and bremsstrahlung. The first two can be numerically estimated quite readily. If it is assumed that the number of effective scattering atoms is N, of atomic number Z, that the product of two the solid angle factors is Ω, and that the counter efficiency is ϵ for 250-kv radiation (Compton-scattered) and is proportional to the energy of the gamma-rays,[11] we find

$$\text{Compton-scattered yield} = 2.27\times10^{-25}ZN\Omega\epsilon,$$
$$\text{Pair-annihilation yield} = 1.87\times10^{-27}Z^2N\Omega\epsilon.$$

These are based on the expressions given in Heitler's book[8] (pp. 156 and 200).

For bremsstrahlung the theoretical calculation is difficult. An approximate estimate was made as follows. The bremsstrahlung is due to Compton recoil electrons which can suffer energy loss by radiation. The distribution in energy of these electrons can be inferred from the angular dependence of Compton scattering, since the electron possesses the residual energy lost by the quantum. A rough distribution curve was plotted, and the yield of bremsstrahlung in the four intervals of energy 2.0–2.5, 1.5–2.0, 1.0–1.5, and 0.5–1.0 Mev estimated. The electrons are assumed to obey the Feather range relation,[12] and the cross sections for bremsstrahlung given by Heitler[8] (p. 173) were used. An additional factor is the angular dependence of the radiation with respect to the electron which loses energy. This has been measured by Petrauskas, Van Atta, and Meyers[13] for energies up to 2.35 Mev. At the 135° average angle of scattering used in this work the radiation is about $\frac{1}{10}$ of the maximum. Therefore, we have included a factor of 0.1 to allow for this angular dependence. At lower energies the value is higher, so that this procedure emphasizes relatively the high energy components of the bremsstrahlung. The net result of this rough analysis is to predict a yield $1.87\times10^{-29}Z^3N\Omega\epsilon$ with an effective absorption coefficient in lead in the range 0.5 cm to 4.5 cm of 0.63 cm^{-1}.

The shape of the absorption curve predicted for Al is shown as a dashed line in Fig. 3. The curve for Mg is very nearly the same. It can be seen that agreement at the low energy end is quite good. However, there appears to be an added component for both Al and Mg of very nearly the full energy of the gamma-radiation from Na^{24}, as seen from Fig. 2. The existence of a high energy component was found by Gray and Tarrant,[2] but it had a lower energy and probably can be identified with bremsstrahlung. Our results indicate a still harder component of weak intensity and as yet unexplained origin. The expected yield for nuclear Compton scattering is much less than this. It is possible that some general type of scattering process exists, involving mesons in the nucleus. We do not feel that our experimental data are good enough to assert definitely that an added hard component is present. To settle the matter, sources of one hundred times the intensity should be used. Facilities are not available here for this kind of work.

One result is certain. No *specific nuclear* resonance occurs with a cross section greater than 1/500 of the Compton cross section or greater

[11] Bradt, Gugelot, Huber, Medicus, Preiswerk, and Scherrer, Helv. Phys. Acta 19, 77 (1946).

[12] N. Feather, Proc. Camb. Phil. Soc. 34, 599 (1938).

[13] A. A. Petrauskas, L. C. Van Atta, and F. E. Meyers, Phys. Rev. 63, 389 (1943).

than 10^{-27} cm^2. This cross section corresponds to an upper limit to the line width for this 1.4-Mev transition of 1/100 electron volt. The line is thus exceedingly sharp and certainly quadrupole or higher.

We wish to acknowledge considerable help from discussions with Professor E. R. Beringer. A great deal of the early work was performed by Dr. B. B. Benson to whom we are greatly indebted.

PHYSICAL REVIEW VOLUME 74, NUMBER 8 OCTOBER 15, 1948

Structure of the ^2D Terms of the Arc Spectrum of Lithium

K. W. MEISSNER, L. G. MUNDIE,* AND P. H. STELSON
Purdue University, Lafayette, Indiana

(Received June 23, 1948)

Interferometric wave-length measurements of high precision carried out by employing an atomic beam light source have been used for the study of several features of the arc spectrum of Li^7. Due to the great sharpness of the spectral lines produced by this source it was possible to determine the splitting of several ^2D terms. The hyperfine structure of the line 6708A was found in approximate agreement with earlier investigations. Precise wave-length measurements have been carried out relative to krypton standards. Discrepancies between the wave-lengths of this investigation and those of earlier investigators must be ascribed to lack of resolution or inadequate comparison methods employed in earlier investigations. This consideration is substantiated by our measurements carried out with a vacuum lithium arc, the results of which are consistent with the atomic beam values. Isotopic shift (Li^6 and Li^7) of the resonance line 6708A was measured.

I. INTRODUCTION

ALTHOUGH the arc spectrum of lithium has been extensively investigated, the wave-length material available contains many discrepancies and is not sufficiently accurate for reliable conclusions regarding the structure of the ^2D terms.

At first glance the measurements of Datta and Bose[1] seem to be the most reliable ones as far as average wave-lengths are concerned. These authors employed a vacuum arc and concave grating and claim an accuracy of a few thousandths A. However, the fact that with one exception they did not resolve the $^2P_{1/2,3/2}$ structure makes one doubt this accuracy.

The first observation of the fine structure of lithium lines was made by Zeeman[2] who resolved the resonance line 6708A as a doublet.

Without undertaking absolute wave-length measurements, Kent[3] carried out a detailed investigation of the doublet structure of lithium lines and their Zeeman effect. Using a quartz discharge tube as light source and a Michelson transmission echelon as resolving instrument, he succeeded in resolving the resonance line 6708A, the first two members of the sharp series (8126A and 4972A), and the first two members of the diffuse series (6103A and 4603A) as close doublets. The error involved in the measurements of the separations was one to two percent but the results are sufficiently accurate to show a definite difference between the doublet intervals obtained from the principal and sharp series and those obtained from the diffuse series. The average value of the three ^2S-^2P combinations is 0.338 cm^{-1} and represents the $^2P_{1/2,3/2}$ splitting. The intervals observed with two pairs of the diffuse series are 0.309 cm^{-1} for 6103A and 0.328 cm^{-1} for 4603A. These separations are distinctly smaller than the $^2P_{1/2,3/2}$ splitting. Kent himself did not discuss these results since he was mainly interested in the Zeeman and Paschen-Back effect of these lines, but it is easy to see that these results are to be expected from

* Now at Naval Ordnance Laboratory, White Oak, Maryland.

[1] S. Datta and P. C. Bose, Zeits. f. Physik **97**, 321 (1935).
[2] P. Zeeman, Physik. Zeits. **14**, 405 (1913).
[3] N. A. Kent, Astrophys. J. **40**, 337 (1914).

the structure of the terms involved and that it is possible to draw conclusions about the structure of the D terms. This will be discussed in detail in Section IIIC.

The present investigation was undertaken in order to establish more precise wave-length material for confirming Kent's results and extending our knowledge to higher D terms. The small intervals involved make it necessary to employ a Perot-Fabry interferometer and a light source producing very sharp lines. As the latter we chose the atomic beam *emission* light source which in earlier investigations proved to be far superior to other existing light sources in this respect.[4a–e]

II. EXPERIMENTAL DETAILS

A. Atomic Beam Source

The atomic beam source was essentially the same as described by Mundie and Meissner.[4e] The furnace consisted of a beryllium oxide cylinder which was wound with tungsten wire in bifilar manner in order to avoid magnetic effects. A hollow steel cylinder with removable top cover was used as container for the lithium. The cover was provided with a circular opening of about 4 mm in diameter. The collimation angle of the beam could be changed between $\frac{1}{8}$ and $\frac{1}{16}$ by selecting image apertures of different sizes.

The excitation of the beam by electron bombardment was accomplished by two electron guns, the construction of which was the same as that described in the earlier investigation.

B. Spectral Apparatus

The spectrograph was a Steinheil instrument. Both the collimator and camera lenses had focal lengths of about 65 cm. Since the dispersion needed was relatively small, one flint prism was sufficient.

A *Perot-Fabry interferometer* was combined with the spectrograph in the usual way. It was inserted immediately behind the collimator lens and was mounted in an airtight chamber which was provided with a jacket through which water of constant temperature circulated. Thermostatic control secured a constancy of temperature within 0.02°C over a period of several hours.

The spectra were photographed on Eastman Kodak plates, types 103F and 103E for the visible region, type IN, hypersensitized with ammonia, for the infra-red line 8127A.

The *measurements* of the spectrograms were carried out with an Abbe comparator (Zeiss Model A, 1937).

As *standard line* for the final determination of the lithium lines the green krypton line 5570 ·2890A was used. The procedure of measurement was the usual one.[5] The correction for dispersion of phase change was negligible, as was seen from the agreement between wave-length values obtained with spacers of different length. The correction for air conditions was also neglected, being less than the experimental error.

TABLE I. Wave-lengths obtained with atomic beam source.

Int.*	λ I.A.		ν cm^{-1}	Combination
st	8126.452	12	302.116	$2^2P_{3/2}$—$3^2S_{1/2}$
w	8126.231	12	302.450	$2^2P_{1/2}$—$3^2S_{1/2}$
w	6707.912	14	903.662	$2^2S_{1/2}$—$2^2P_{1/2}$
st	6707.761	14	903.998	$2^2S_{1/2}$—$2^2P_{3/2}$
Sat	6103.664	16	379.077	$2^2P_{3/2}$—$3^2D_{3/2}$
st	6103.649	16	379.118	$2^2P_{3/2}$—$3^2D_{5/2}$
w	6103.538	16	379.415	$2^2P_{1/2}$—$3^2D_{3/2}$
st	4971.745	20	108.069	$2^2P_{3/2}$—$4^2S_{1/2}$
w	4971.661	20	108.408	$2^2P_{1/2}$—$4^2S_{1/2}$
st	4602.894	21	719.399	$2^2P_{3/2}$—$4^2D_{5/2}$
w	4602.826	21	719.720	$2^2P_{1/2}$—$4^2D_{3/2}$
st	4273.127	23	395.507	$2^2P_{3/2}$—$5^2S_{1/2}$
w	4273.066	23	395.841	$2^2P_{1/2}$—$5^2S_{1/2}$
st	4132.191	24	193.439	$2^2P_{3/2}$—$5^2D_{5/2}$
w	4132.135	24	193.767	$2^2P_{1/2}$—$5^2D_{3/2}$
st	3985.538	25	083.648	$2^2P_{3/2}$—$6^2S_{1/2}$
w	3985.485	25	083.981	$2^2P_{1/2}$—$6^2S_{1/2}$
st	3915.346	25	533.321	$2^2P_{3/2}$—$6^2D_{5/2}$
w	3915.295	25	533.653	$2^2P_{1/2}$—$6^2D_{3/2}$
10	6707.9174	14	903.6498	$2^2S_{1/2}{}^2$—$2^2P_{1/2}{}^{1,2}$
6	6707.9043	14	903.6789	$2^2S_{1/2}{}^1$—$2^2P_{1/2}{}^{1,2}$
20	6707.7661	14	903.9861	$2^2S_{1/2}{}^2$—$2^2P_{3/2}{}^{0,1,2,3}$
12	6707.7542	14	904.0125	$2^2S_{1/2}{}^1$—$2^2P_{3/2}{}^{0,1,2,3}$

* st = strong, w = weak component of doublet.

[4a] R. Minkowski and H. Bruck, Zeits. f. Physik. **95**, 274 (1935); [b] K. W. Meissner and K. F. Luft, Ann. d. Physik **28**, 667 (1937); Zeits. f. Physik **106**, 362 (1937); Ann. d. Physik **29**, 698 (1937); Berl. Ber. **118**, (1937); [c] R. A. Fisher, Phys. Rev. **51**, 381 (1937); [d] K. W. Meissner, Ann. d. Physik **31**, 505, 518 (1938); [e] L. G. Mundie and K. W. Meissner, Phys. Rev. **65**, 265 (1944).

[5] Details have been described by K. W. Meissner, J. Opt. Soc. Am. **31**, 405 (1941).

TABLE II. Wave-length values obtained with vacuum arc compared with those of other sources.

Int.	Vacuum arc	Atomic beam Table I	Atomic beam c.g.*	Datta and Bose	Values listed in M.I.T. tables
st	8126.452	0.452	0.378		0.52[1]
w	8126.230	0.231			
w	6707.915	0.912	0.811	0.950	0.844[2]
st	6707.768	0.761		0.728	
sat.		0.664			
st	6103.654	0.649	0.612	0.521	0.642[2]
w	6103.540	0.538			
st	4971.748	0.745	0.717	0.743	0.990
w	4971.662	0.661			
st	4602.896	0.894	0.871	0.863	0.863[3]
w	4602.829	0.826			
st	4273.128	0.127	0.107	0.070	0.28[4]
w	4273.067	0.066			
st	4132.192	0.191	0.173	0.244	0.29[4]
w	4132.140	0.135			
st	3985**	0.538	0.520	0.553	0.79[4]
w	3985**	0.485			
st	3915**	0.346	0.329	0.343	0.0[4]
w	3915**	0.295			

* Center of gravity wave-length.
** Strong bands prevented measurement.
[1] W. F. Meggers, Bull. Bur. Stand. 14, 371 (1918).
[2] C. W. Hetzler, R. W. Boreman, and Keivin Burns, Phys. Rev. 48, 656 (1935).
[3] S. Datta and P. C. Bose, Zeits. f. Physik 97, 321 (1935).
[4] A. Fowler, Report on "Series in line spectra."

The *spacers* employed ranged in length from 6 mm to 66 mm. The proper size was selected in such a way as to resolve clearly the fringe patterns belonging to the different components of the doublet structure. Fortunately, a convenient property of the Perot-Fabry patterns is that with a properly selected spacer all doublets of equal interval $\Delta\nu$ can be resolved at once, regardless of their wave-length.[6] Optimum resolution of a doublet is obtained if the fringes of one component fall just midway between the fringes of the other component. In our case, all of the doublets of the sharp and diffuse series were clearly resolved with available spacers of 8, 10, and 20 mm. For higher accuracy, however, it is necessary to employ higher order numbers, i.e., spacers of greater length. To this end, a spacer of 36 mm (producing overlapping of two orders) was used for most of the lines. In the case of the line at 6103A, a spacer of 60 mm (overlapping of three orders) proved to be satisfactory.

In general, it was not possible to obtain the rather weak satellites of the *PD* combinations. It was only in the case of 6103A that we were able to separate clearly the satellite and the strong component. This required the selection of a spacer which produced a pattern in which the $2^2P_{1/2}$—$3^2P_{3/2}$ and $2^2P_{3/2}$—$3^2D_{5/2}$ lines were coincident and, the $2^2P_{3/2}$—$3^2D_{3/2}$ line fell just midway between the former lines in the pattern. Utilizing the results of preliminary measurements with 20-mm and 36-mm spacers it was easy to calculate a suitable spacer size fulfilling these conditions. A spacer of 66 mm, formed by combining a 60-mm and a 6-mm spacer, gave the desired result. The weak satellite appeared clearly between the orders of the superimposed patterns of the strong components. A spacer of this size was necessary in order to resolve the interval of only 0.015A.

The application of the same method for obtaining the satellites of the higher members of the *D* series is difficult since they are much weaker and since the ^2D splitting decreases rapidly. Therefore, no great effort was made to obtain the satellites and to measure the splitting of the higher ^2D terms directly.

III. RESULTS

A. Wave-Lengths with Atomic Beam

Table I contains the final wave-lengths and wave numbers obtained with the atomic beam source. Numerical values of estimated intensities have been omitted since they would be without any value. Only in the case of the hyperfine structure of 6708A have the theoretical intensity values of the observed components been added.

[6] Let $P=p+\epsilon$ be the order at the center of the P.F. fringes, where p is the integer order of the first bright fringe and ϵ the fraction. Then, for two lines with wave numbers ν_1, and ν_2 we have $P_1=2t\nu_1$ and $P_2=2t\nu_2$. Therefore, $\nu_2-\nu_1=(P_2-P_1)/2t=(p_2+\epsilon_2-p_1-\epsilon_1)/2t=[(p_2-p_1)+(\epsilon_2-\epsilon_1)]/2t$. Introducing the range of dispersion $\langle\Delta\nu\rangle=1/2t$ we get $\nu_2-\nu_1=\langle\Delta\nu\rangle(k+\epsilon_2-\epsilon_1)$. The integer k determines the number of overlapping orders. For constant $\nu_2-\nu_1$ the differences $\epsilon_2-\epsilon_1$ are constant, independent of wave-length.

The estimated relative intensities correspond closely to these values. The principal quantum numbers used in the last column are the theoretical ones indicating the shell of the "running" electron. The numbers on the upper right of the term symbols of 6708A are the fine quantum numbers corresponding to a nuclear moment of $\frac{3}{2}$. The wave-length values are given to the nearest thousandth of an angstrom. The experimental error is, however, generally smaller than this.

B. Measurements with Vacuum Arc

As was mentioned in the introduction, the wave-length data available in the literature concerning lithium contain serious discrepancies. In some cases the values are so uncertain that they could not be used for the determination of the correct order number of spectrograms taken with such large plate separations (36 to 60 mm) as were used with the atomic beam source. It was, therefore, necessary, to carry out an additional series of measurements using smaller spacers. Thus all ambiguity in the assignment of order numbers could be eliminated.

Since most of the wave-length values obtained with the atomic beam disagreed with those of the literature, it was decided to carry out further interferometric measurements with a vacuum arc.

The electrodes of the arc consisted of graphite cylinders of 10 mm in diameter. The anode was provided with a bore of about 5 mm in diameter and 10 mm in depth. The cavity was filled with LiCl or metallic lithium. When used on a 220-volt d.c. line with the current limited to 1.5 to 2 amperes a rather stable arc was obtained. The vacuum was maintained below 1 mm Hg. Numerous spectrograms were taken and of these the fifteen best ones selected for the final wave-length determinations. Spacers of 6 mm and 8 mm were used. The results of the different runs agreed with each other within a few thousandths of an A. Greater accuracy could not be expected since the interference fringes were rather broad due to the high temperature of this source. However, the fringes were sufficiently narrow for a clear separation of the 2^2P splitting.

The resonance line 6708A exhibited a peculiar behavior caused by strong self-reversal which made the interpretation of the interference patterns rather difficult. This difficulty was overcome by feeding the arc with sodium to which a small amount of lithium was added.

The results obtained using the vacuum arc are presented in Table II. For purposes of comparison, the wave-lengths obtained with the atomic beam and those published by other investigators have been included. The agreement between the atomic beam and the vacuum arc values is very satisfactory, the differences being within the limit of error of the vacuum arc measurements which may be estimated as ± 0.005A.

The close agreement between our vacuum arc and atomic beam values shows clearly that the discrepancies between our values and those of the other investigators must be due either to lack of resolution or to inadequate methods of comparison employed in the earlier investigations. We believe that the latter is true with the measurements given by Datta and Bose who employed a grating. Lack of resolution may be the reason for the disagreement with the interferometric measurements of Hetzler, Boreman, and Burns. Their value for 6707.844A comes very close to the average of the atomic beam values 6707.837A, a result one would expect if the patterns were overexposed. Their value 6103.642A, on the other hand, is rather close to the value of the strong component.

Since these authors used an interferometer, it is surprising that they were unable to resolve the doublet structures; they may, perhaps, have used plate separations which were not favorable for this resolution.

C. Structure of ^2D Terms

Table I, listing the results of our measurements, contains the resonance line 6708A, four members of the sharp series, and four members of the diffuse series. Only one doublet of the latter, 6103A, could be resolved completely, whereas the three others appeared only as double lines with indication of the satellite.

The splitting of the 3^2D terms can be obtained directly from the patterns of 6103A as difference of the wave numbers of satellite and strong component. The splitting of the three other members of the series can be obtained only in an indirect

TABLE III. $2^2P_{1/2}-2^2P_{3/2}$ values in cm^{-1}.

Wave-length	Atomic beam	Kent	Jackson and Kuhn
8126	0.336 ±0.001	0.340	
6708	0.3366±0.0005*	0.336	
6708	0.3360±0.0005**		0.3372 ±0.0005
4971	0.337 ±0.002	0.339	
4273	0.334 ±0.004		
3985	0.337 ±0.005		

* From patterns with unresolved hyperfine structure.
** From measurement of hyperfine structure patterns.

way. The lines of these members are the two strongest components of the 2^2P-m^2D combination ($m=4,5,6$) namely $2^2P_{1/2}-m^2D_{3/2}$ and $2^2P_{3/2}-m^2D_{5/2}$. The observed intervals ($\Delta\nu$) of these lines involve the $2^2P_{1/2,3/2}$ splitting (ΔP) as well as that of the ^2D terms (ΔD). Employing the relation $\Delta\nu=\Delta P-\Delta D$ one can find the splitting of the D terms ΔD as difference between the ΔP splitting and the measured interval $\Delta\nu$. The ΔP splitting can be found from measurements of the resonance line and members of the sharp series, where ΔP appears directly as interval of the measured doublet lines. The fact that all observed $\Delta\nu$ values of the diffuse series are smaller than the ΔP splitting reveals that all m^2D terms ($m=3,4,5,6$) of Li^7 exhibit regular term order since the 2^2P term is known to be a regular term.

Unfortunately, the lines of the sharp series are rather weak in the atomic beam source, and the strongest member ($n=3$) lies in the infra-red (8126A). Therefore, precision measurements of ΔP by employing these lines are difficult. The resonance line, on the other hand, is very strong and good interference patterns can be obtained with rather short exposure times. However, in this case the line structure is more complex since the splitting of the 2^2S term, due to the nuclear moment, is of appreciable size and gives rise to hyperfine structure. With small spacers (8 and 10 mm), the hyperfine structure was not resolved and, therefore, the $\Delta\nu$ values derived under these conditions must give values very close to the true ΔP. On the other hand, employing suitable greater separation of the interferometer plates gives complete resolution of the hyperfine structure (due to 2^2S splitting), and by employing theoretical relative intensity values of the observed component one is able to obtain the ΔP splitting with sufficient accuracy.

Both methods have been employed. The ΔP value obtained from patterns with unresolved h.f. structure agrees within the limit of error with that found by Jackson and Kuhn[7] who investigated the resonance line by means of an atomic beam in absorption. The ΔP value derived from the resolved h.f. pattern is decidedly smaller than their value. A possible explanation is given below in Section IIID.

Table III is a compilation of the $\Delta\nu$-values of the sharp series and the resonance line. For the measurement of these separations more plates were employed than for the wave-length values in Table I. Therefore, slight differences with the $\Delta\nu$ values derived from Table I may occur. The values of Table III are more reliable than those obtained from Table I. As most probable value of the ΔP splitting we accept 0.3366 ± 0.0005 cm^{-1}, a value which is in good agreement with that of Jackson and Kuhn, 0.3372 ± 0.0005 cm^{-1}.

Table IV is a compilation of the results obtained for the members of the diffuse series. The $\Delta\nu$ values presented in the third column represent the separation of the strong and weak components. The difference between $\Delta P=0.3366$ cm^{-1} and these $\Delta\nu$ values gives the splitting of the D terms and is presented in the fifth column. In the case of 6103A a direct measurement of the D splitting was possible and the value obtained directly is in agreement with that obtained by this calculation.

In principle, the presence of the weak satellite which is unresolved from the strong component, may increase the apparent $\Delta\nu$ values of this series. With the low exposure employed in the work with the atomic beam, however, it is felt that the satellite would be so greatly underexposed that the effect would not be noticeable. On the other hand, we believe that the greater values measured by Kent and by us with the relatively intense vacuum arc may be due to the action of the satellite, which with higher exposures shifts the apparent position of the strong component towards longer wave-lengths, increasing in this way the measured $\Delta\nu$. A rough

[7] D. A. Jackson and H. Kuhn, Proc. Roy, Soc. **A173**, 278 (1939).

calculation by means of the theoretical intensities of a PD combination confirms this assumption. In the case of 6103A, we obtain for the wave-length difference between the center of gravity of (strong line+satellite) and the weak component the value $\Delta\lambda=0.113$A, which is in agreement with $\Delta\lambda=0.114$A obtained with the vacuum arc and with $\Delta\lambda=0.115$A obtained by Kent.

It is seen from Table IV that the observed $\Delta\nu$ values of all observed D doublets increase regularly with m, approaching the value of the ΔP splitting. From this behavior one concludes that the ^2D terms of Li^7 are regular. The steady decrease of ΔD with m is also quite normal.

D. Hyperfine Structure of 6708A

Originally it was not intended to study the hyperfine structure of the resonance line 6708A. However, several plates taken with a spacer of 36 mm exhibited the hyperfine structure so well defined that we decided to evaluate them, inasmuch as one can also obtain the ΔP fine splitting from these patterns.

The procedure for evaluating the patterns has been described by Jackson and Kuhn[7] who made a thorough investigation of the hyperfine structure of Li 6708A. They employed the absorption method using highly collimated beams. The resolving instrument was a compound interferometer consisting of two Perot-Fabry interferometers of 5-mm and 50-mm plate separation. They derived from their measurements the following intervals:

Multiplet splitting $\Delta P_{1/2,3/2}$
$\Delta P=0.3372\pm0.0005$ cm^{-1},
Hyperfine splitting of $2^2S_{1/2}$
$\Delta\nu_1=0.0275\pm0.0003$ cm^{-1},
Hyperfine splitting of $2^2P_{1/2}$
$\Delta\nu_2=0.0015\pm0.0009$ cm^{-1}.

The respective values derived from our own measurements are $\Delta P=0.3360\pm0.0005$ cm^{-1}, $\Delta\nu_1=0.0278-0.0008$ cm^{-1} and $\Delta\nu_2=0.007-0.002$ cm^{-1}.

The values of $\Delta\nu_1$ agree rather well with each other but are not in accord with the most reliable value 0.026805 cm^{-1} found with the radiofrequency method.[8] Our value for ΔP, however, is decidedly smaller than that of Jackson and Kuhn and is also smaller than our value found from patterns obtained with smaller spacers in which the hyperfine structure was not resolved (see Section IIIC). The values of $\Delta\nu_2$ disagree completely.

TABLE IV. Observed $\Delta\nu$ values of diffuse doublets and calculated term separations $\Delta m^2D_{3/2,5/2}$ in cm^{-1}.

m	λ	Atomic beam	Kent	$\Delta m^2D_{3/2,5/2}$	Kent
3	6103	0.2996±0.0005	0.309	0.0370±0.0008 0.0374±0.0005*	0.027
4	4603	0.332 ±0.001	0.328	0.015 ±0.002	0.008
5	4132	0.327 ±0.002		0.010 ±0.003	
6	3915	0.332 ±0.003		0.005 ±0.003	

* From direct measurement of satellite and strong component.

It is difficult to find a satisfactory explanation of those discrepancies. Since the compound interferometer used by these workers eliminates overlapping orders we are inclined to assume that the deviations are due to insufficient separation of the hyperfine components on our plates. In this case the Oldenberg effect[9] can influence the values appreciably and produce a "shrinking" of the measured intervals. Employment of larger spacers or of a compound interferometer could decide this question, but we did not extend our efforts in this respect since the ΔP value is already known more accurately than the other factors ($\Delta\nu$ values of lines of the diffuse series) which are involved in the calculated values of the D-term fine structure.

E. Isotopic Shift

Several strongly exposed plates taken with a 10-mm etalon showed very clearly a weak companion line in the patterns of 6708A. The presence of this line was first mentioned in the paper of Kent[3] and has been investigated several times since.[10] According to the explanation of Schueler and Wurm, this line is the weak doublet component of the resonance line of Li^6. The values of the isotopic shift of the weak component, given in different papers, lie between 0.15 and 0.16A, which is about the value of the ΔP splitting of 6708A. This particular circumstance

[8] P. Kusch, S. Millman, and I. I. Rabi, Phys. Rev. 57, 765 (1940).

[9] O. Oldenberg, Ann. d. Physik 67, 253 (1922).

[10] H. Schueler and K. Wurm, Naturwiss. 15, 971 (1927); D. S. Hughes and Carl Eckart, Phys. Rev. 36, 694 (1930); D. A. Jackson and H. Kuhn, see reference 7.

causes a blend of the weak component of Li^7 with the strong component of Li^6. Therefore, the line complex consists of only three lines instead of the expected four ones.

A thorough investigation of the isotopic shift of lithium was carried out by Jackson and Kuhn[7] who employed a liquid air-cooled Schueler tube. They found for the shift of the weak component of Li^6 the value $\Delta\nu=-0.345$ cm^{-1} ($\Delta\lambda=+0.156$A). Furthermore, they derived in an indirect way the isotopic shift of the strong component as $\Delta\nu=-0.365$ cm^{-1} ($\Delta\lambda=+0.164$A) and arrived at the result that the multiplet separation of the isotope Li^6 equals 0.317 cm^{-1} while that of Li^7 is 0.3372 cm^{-1}.

We were able to determine the wave-length of the Li^6 line as $\lambda=6708.072\pm0.001$A, whereas the wave-length of the corresponding Li^7 line, as given in Table I, is 6707.912A. From this follows the isotopic shift of the weak component $\Delta\lambda=+0.160$A($\Delta\nu=-0.356\pm0.002$ cm^{-1}). In principle, it is possible to find the value of the isotopic shift from the Perot-Fabry patterns of the line complex directly, as Jackson and Kuhn did, but considering the strong overexposure of the Li^7 fringes we preferred the evaluation from wave-length measurements carried out with patterns of normal exposure. Our value derived from the complex patterns is +0.159A and agrees with the first one within the limit of error.

Our value of the isotopic shift is decidedly larger than that of Jackson and Kuhn and we are not able to account for this discrepancy. On the other hand, we can confirm their result that the effective wave-length of the blend is shifted towards longer wave-lengths by +0.002A (-0.004 cm^{-1}), but we consider the accuracy of our values not sufficient for drawing conclusions regarding the doublet splitting of the two isotopes.

We plan to continue the investigation of isotopic shift in lithium by employing samples enriched in Li^6.

PHYSICAL REVIEW VOLUME 74, NUMBER 8 OCTOBER 15, 1948

A Relativistic Cut-Off for Classical Electrodynamics

R. P. FEYNMAN
Cornell University, Ithaca, New York

(Received June 8, 1948)

Ordinarily it is assumed that interaction between charges occurs along light cones, that is, only where the four-dimensional interval $s^2=t^2-r^2$ is exactly zero. We discuss the modifications produced if, as in the theory of F. Bopp, substantial interaction is assumed to occur over a narrow range of s^2 around zero. This has no practical effect on the interaction of charges which are distant from one another by several electron radii. The action of a charge on itself is finite and behaves as electromagnetic mass for accelerations which are not excessive. There also results a classical representation of the phenomena of pair production in sufficiently strong fields.

QUANTUM electrodynamics is built from a classical counterpart that already contains many difficulties which remain upon quantization. It has been hoped that if a classical electrodynamics could be devised which would not contain the difficulty of infinite self-energy, and this theory could be quantized, then the problem of a self-consistent quantum electrodynamics would be solved. For this reason many successful attempts have been made to produce such a classical theory. The field equations can be made non-linear,[1] the fields produced by or acting on an electron can be redefined,[2,3] or one may resort to some averaging of the fields over space or time.[4] These theories have, however, met with considerable difficulties when an attempt has been made to quantize them. In this paper a consistent classical theory is described which the author believes can be quantized. Some preliminary results of the quantization of this theory will be discussed in a future paper. Some of the physical ideas of the classical form of the theory are sufficiently interesting in themselves to warrant their discussion first in a separate paper.

The potential at a point in space at a given time depends on the charge at a distance r from the point at a time previous by $t=r$ (taking the speed of light as unity). Speaking relativistically, interaction occurs between events whose four-dimensional interval, s, defined by $s^2=t^2-r^2$, vanishes. There results, however, an infinite action of a point electron on itself. The present theory modifies this idea by assuming that substantial interaction exists as long as the interval s is time-like and less than some small length, a, of order of the electron radius. When t is large since $\Delta(s^2)=2t\cdot\Delta t$ this means a spread in the time of arrival of a signal of amount of order $a^2/2t$. For charges separated by many electron radii there is, therefore, essentially no effect of the modification. For the action of an electron on itself, however, there is a considerable modification. The result is to reduce the infinite self-energy to a finite value. For accelerations which are not extreme, the action of an electron on itself appears simply as an electromagnetic mass. If desired in the classical theory, all the mass of an electron may be represented as electromagnetic. (In the quantum theory this cannot be done in a reasonable way as the electromagnetic mass comes out quite small under reasonable assumptions for a.) We have, therefore, a consistent classical theory which does not disagree with classical experience.

In the remainder of the paper we formulate this idea mathematically, and draw one or two simple consequences. We then discuss a curious

[1] M. Born and L. Infeld, Proc. Roy. Soc. London **A144**, 425 (1935).
[2] P. A. M. Dirac, Proc. Roy. Soc. London **A167**, 148 (1938). An excellent discussion of these matters is given by C. J. Eliezer, Rev. Mod. Phys. **19**, 147 (1947).
[3] J. A. Wheeler and R. P. Feynman, Rev. Mod. Phys. **17**, 157 (1945).
[4] There are many theories of this nature. The author's theory is essentially that of F. Bopp, Ann d. Physik **42**, 573 (1942). R. Peierls and H. McManus have developed a theory in which the electron is pictured as a rigid distribution of charge in both space and time. The theory can be shown to be exactly equivalent to the present one, at least for a class of f functions. Their physical ideas may offer advantages over the present one in which the function f is not so directly interpretable. I thank Dr. McManus for a copy of his thesis. For a summary of another theory of this type see B. Podolsky and P. Schwed, Rev. Mod. Phys. **20**, 40 (1948). A somewhat different type is that of N. Rosen, Phys. Rev. **72**, 298 (1947).

feature of this theory. It can give a classical representation of the phenomena of pair production in sufficiently strong fields. This is of interest because the physical ideas may possibly be carried over to give a clearer understanding of the hole theory of positrons.

The main result which is to be carried over to quantum problems is this: In any process in which there is no permanent emission of quanta one must assume the field quanta to have a "density" $g(k_4,\mathbf{K})$ in frequency, and wave number space. This replaces the usual assumption that the frequency k_4 equals the magnitude of the wave number, K, and that the density in wave numbers $\mathbf{K}$, is uniform (corresponding to $g(k_4,\mathbf{K})=\delta(k_4^2-K^2)$). The properties $g(k_4,\mathbf{K})$ ought to have are discussed more fully below.

MATHEMATICAL FORMULATION

It is most convenient (but not necessary) to formulate these ideas in the language of action at a distance.[3] Hence a brief summary of that point of view is given here. We start with Fokker's action principle that the action

$$S=\sum_a m_a\int(da_\mu da_\mu)^{\frac{1}{2}} +\sum_{a,b}{}'e_ae_b\int\int\delta(s_{ab}^2)da_\mu db_\mu \quad (1)$$

is an extremum. Here a_μ represents, for $\mu=1$ to 4, the three space coordinates and the time coordinate of a particle a of mass m_a, charge e_a. We shall later consider them as functions of a parameter α, say. The b_μ are corresponding quantities for a particle b, etc. The symbol $x_\mu y_\mu$ means $x_4y_4-x_1y_1-x_2y_2-x_3y_3$ and $s_{ab}^2=(a_\mu-b_\mu)(a_\mu-b_\mu)$. The δ is Dirac's delta function.

The integrals are taken over the trajectories of the particles. The $\sum'$ means the sum over all pairs a, b with $a\neq b$. We consider varying the path $a_\mu(\alpha)$ of particle a. Defining

$$A_\mu^{(b)}(x)=e_b\int\delta(s_{xb}^2)db_\mu, \quad (2)$$

where x stands for x_μ, a point in space time, we can write (1) as

$$S=\sum_a m_a\int(da_\mu da_\mu)^{\frac{1}{2}}+\sum_a\sum_{b\neq a}e_a\int A_\mu^{(b)}(a)da_\mu.$$

The result of seeking an extremum of this is to lead in the well-known way to the equations of motion,

$$m_a\frac{d}{d\tau_a}\left(\frac{da_\nu}{d\tau_a}\right)=e_a\frac{da_\mu}{d\tau_a}\sum_{b\neq a}F_{\mu\nu}^{(b)}(a), \quad (3)$$

where we can call $F_{\mu\nu}^{(b)}(x)$ the field at x caused by particle b. It is given by

$$F_{\mu\nu}^{(b)}(x)=\partial A_\mu^{(b)}(x)/\partial x_\nu-\partial A_\nu^{(b)}(x)/\partial x_\mu.$$

We have written $d\tau_a=(da_\mu da_\mu)^{\frac{1}{2}}$ for the proper time along the path of a.

Since $\Box^2\delta(s_{xb}^2)=4\pi\delta(x_1-b_1)\delta(x_2-b_2)\delta(x_3-b_3)\times\delta(x_4-b_4)$, where $\Box^2=(\partial/\partial x_\mu)(\partial/\partial x_\mu)$, Eq. (2) gives

$$\Box^2A_\mu^{(b)}(x)=4\pi e_b\int\delta(x_1-b_1)\delta(x_2-b_2)\times\delta(x_3-b_3)\delta(x_4-b_4)db_\mu, \quad (4)$$

which is 4π times the current four-vector of a point charge e_b. Thus $F_{\mu\nu}^{(b)}(x)$ satisfies Maxwell's equations. But the special solution (2) is not the usual retarded solution but is rather half the retarded plus half the advanced solution of Lienard and Wiechert[5] (since $\delta(t^2-r^2)=(1/2r)\times(\delta(t+r)+\delta(t-r)$.) Thus we may write (dots representing derivatives with respect to τ_a, and the fields being calculated at the point $x_\mu=a_\mu$),

$$m_a\ddot{a}_\nu=e_a\dot{a}_\mu\sum_{b\neq a}(\tfrac{1}{2}F^{(b)}{}_{\mu\nu\text{ ret}}+\tfrac{1}{2}F^{(b)}{}_{\mu\nu\text{ adv}}). \quad (5)$$

This can be compared to the usual theory which just uses retarded effects by writing it in the form

$$m_a\ddot{a}_\nu=e_a\dot{a}_\mu\Big\{\sum_{b\neq a}F^{(b)}{}_{\mu\nu\text{ ret}}+\tfrac{1}{2}\sum_{\text{all }b}[F^{(b)}{}_{\mu\nu\text{ adv}}-F^{(b)}{}_{\mu\nu\text{ ret}}]-\tfrac{1}{2}[F^{(a)}{}_{\mu\nu\text{ adv}}-F^{(a)}{}_{\mu\nu\text{ ret}}]\Big\}, \quad (6)$$

as in the paper[3] by Wheeler and Feynman. As in that paper the first term is the retarded field of other charges, the second term vanishes in a world where all emitted light is eventually ab-

[5] This use of advanced and retarded potentials is really unnecessary for an understanding of the modifications of electrodynamics which is the main point of the paper. It results from the aurhor's desire to start with a principle of least action, for it is in this form that the transition to quantum theory can be made.

sorbed,[6] and the third term, depending only on the motion of a, is the force of radiative damping. Thus (1) is equivalent to (6) and thus satisfactorily describes the known laws of classical electrodynamics. There is no self-energy.

According to the above, a particle does not act upon itself, as the term with $a=b$ in the sum $\sum'_{a,b} e_a e_b \int \cdots$ in the action has been omitted. (Radiation resistance is pictured as in indirect effect of source on absorber and absorber on source.) The field of each particle must be kept separate in order to exclude, when asking for the force on a particle, the field of the particle itself.

There is no *need* to do so, but it is an interesting question to try to reinstate the idea of a universal field. This requires that a particle be allowed to act on itself and the term $a=b$ included in the action sum. This leads immediately to an infinite self force. This difficulty can be eliminated if the $\delta(s_{ab}^2)$ is replaced, as Bopp[4] has suggested, by some other function $f(s_{ab}^2)$ of the invariant s_{ab}^2, which behaves like $\delta(s_{ab}^2)$ for large dimensions but differs for small. (We shall discuss the properties of this function later, but as an example to keep in mind, consider $f(s^2)=(1/2a^2)\exp(-|s|/a)$ for $s^2>0$, and $f(s^2)=0$ for $s^2<0$ with a of order of the electron radius e^2/mc^2.)

We study the consequences of replacing (1) by the law that S is extremum if

$$S=\sum_a m_a \int (da_\mu da_\mu)^{\frac{1}{2}} + \tfrac{1}{2}\sum_a \sum_b e_a e_b \int\int f(s_{ab}^2) da_\mu db_\mu. \quad (7)$$

The term with $a=b$ may be written

$$\tfrac{1}{2} e_a^2 \int\int f(s^2{}_{aa'}) da_\mu da_\mu', \quad (8)$$

where a and a' are two points on the world-line of a. The variation problem clearly leads to

$$m_a \ddot{a}_\nu = e_a \dot{a}_\mu \Big[\sum_{b\neq a} \bar{F}_{\mu\nu}{}^{(b)}(a) + \bar{F}_{\mu\nu}{}^{(a)}(a) \Big], \quad (9)$$

where

$$\bar{F}_{\mu\nu}{}^{(b)}(x) = \partial \bar{A}_\mu{}^{(b)}(x)/\partial x_\nu - \partial \bar{A}_\nu{}^{(b)}(x)/\partial x_\mu \quad (10)$$

and the bar over the field quantities indicate that they are calculated from the f function rather than the δ function. That is,

$$\bar{A}_\mu{}^{(b)}(x) = e_b \int f(s_{zb}^2) db_\mu. \quad (11)$$

This theory differs from the usual in two respects: A. There is an extra force $h_\nu = e_a \dot{a}_\mu \bar{F}_{\mu\nu}{}^{(a)}(a)$ on particle a depending only on the motion of a. This we shall study in a moment and show that it represents inertia. B. The fields of other particles are given by the curl of a potential but the potential (11) no longer solves the Maxwell equations (4). However, since $f(s^2)$ is close to $\delta(s^2)$ this means that except for particles very close together nothing is changed very much. Thus $f(t^2-r^2)$ is large only when $t=r$ is nearly satisfied, but for large t near $+r$, say, $f(t^2-r^2) \cong f(2t(t-r))$ so that the function which has width a^2 in its argument s^2 has width $a^2/2t$ in $t-r$. Thus for increasing distances from the source the potentials satisfy Maxwell's equations ever more accurately.

The analog of Eq. (6) becomes

$$m_a \ddot{a}_\nu = e_a \dot{a}_\mu \Big\{ \sum_{b\neq a} \langle F\rangle^{(b)}{}_{\mu\nu\ \mathrm{ret}} + \tfrac{1}{2} \sum_{\text{all } b} [F^{(b)}{}_{\mu\nu\ \mathrm{adv}} - F^{(b)}{}_{\mu\nu\ \mathrm{ret}}] - \tfrac{1}{2}[F^{(a)}{}_{\mu\nu\ \mathrm{adv}} - F^{(a)}{}_{\mu\nu\ \mathrm{ret}}] + \bar{F}^{(a)}{}_{\mu\nu} \Big\}, \quad (12)$$

where we define $\langle F\rangle_{\mathrm{ret}} = \bar{F} + \tfrac{1}{2}F_{\mathrm{ret}} - \tfrac{1}{2}F_{\mathrm{adv}}$. Thus only the δ part, so to speak, of the fields becomes retarded. It would not do to replace F by $\bar{F}$ throughout in (6) for then we could not deduce that the second term is zero at the source because it was zero at infinity for it would not then be a solution of Maxwell's equation in empty space. The damping term is unaltered. It plus the self-force can be written $\langle F\rangle^{(a)}{}_{\mu\nu\ \mathrm{ret}}$ (see

[6] That the second term vanishes in these circumstances may be seen as follows. If a source radiates for a time, at a very long time afterwards the total retarded field vanishes, for all the light is absorbed. But also the total advanced field vanishes at this time (for charges are no longer accelerating and the advanced field exists only at times previous to their motion). Hence, the difference vanishes everywhere at this time and, since it is a solution of Maxwell's homogeneous equations, at all times.

footnote 5), so in practice one can write simply

$$m_a\ddot{a}_\nu = e_a\dot{a}_\mu \sum_{\text{all } b} \langle F\rangle^{(b)}_{\mu\nu \text{ ret.}}$$

The effect of the modification in the theory using retarded fields is therefore to change, slightly, the field of one particle on another when they are very close, and to add a self-force h_μ.

We now turn to a study of the self-force h_μ. This can be calculated directly from the formulae (10), (11) but a simpler way is from the action term (8). This term in the action can be re-expressed approximately if we assume that the accelerations are not too great. Only values of a' near a are important. Let us define a parameter along the path and say a corresponds to the value α of this parameter, a' to the value $\alpha'=\alpha+\epsilon$. Assuming a' not to vary too rapidly with ϵ we can approximate $s_{aa'}{}^2=(a_\mu-a_\mu')\times(a_\mu-a_\mu')$ by $\epsilon^2(da_\mu/d\alpha)(da_\mu/d\alpha)=\epsilon^2(d\tau_a/d\alpha)^2$. Likewise $da_\mu da_\mu'$ is to sufficient accuracy $(da_\mu/d\alpha)(da_\mu/d\alpha)d\alpha d\epsilon$. Thus the self-action term is approximately $\frac{1}{2}e_a{}^2\int\int f(\epsilon^2(d\tau_a/d\alpha)^2)\cdot(d\tau_a/d\alpha)^2 \times d\epsilon d\alpha$. Then calling $\eta=\epsilon(d\tau_a/d\alpha)$ we can write this as

$$\mu_a\int(d\tau_a/d\alpha)d\alpha=\mu_a\int(da_\mu da_\mu)^{\frac{1}{2}}, \qquad (13)$$

where we have set

$$\mu_a=\tfrac{1}{2}e_a{}^2\int_{-\infty}^{\infty}f(\eta^2)d\eta. \qquad (14)$$

That is, the self-action term to this approximation represents pure electrodynamic mass. The term readily combines with $m_a\int d\tau_a$ for the mass is correctly invariant. We can go further and assume that originally m_a is zero and all mass of electrons is electrodynamic, but for protons this would then not be so.

The function $f(s^2)$ is to be normalized such that

$$\int_{-\infty}^{\infty}f(s^2)d(s^2)=1. \qquad (15)$$

The condition (14) says the range in η of $f(\eta^2)$ is of order e^2/μ, or if μ is the electron mass, of order of the electron radius. The function $f(s^2)$ is chosen so that it is symmetrical near past and future light cones since any asymmetry drops out in the form (7) of the action. Other than these conditions, there are strictly no further conditions on $f(s^2)$. It is convenient to assume $f(s^2)$ to be zero if s^2 is negative (space-like). It is also very desirable to have $f(s^2)$ fall rapidly away from the light cone, rather than oscillate indefinitely, and to have $f(s^2)$ finite everywhere.

By taking the Fourier transform of (11), one can represent the field as a superposition of the effects of harmonic oscillators in the usual way. However, the oscillators corresponding to waves of wave number k_1, k_2, k_3 need not have a frequency k_4 equal to the magnitude of the wave number. Instead we can take the density of the oscillators to be k_4 times, $g(k_\mu k_\mu)dk_1dk_2dk_3dk_4$ where g is defined for positive k_4 only, and is

$$g(k_\mu k_\mu)=(1/4\pi^2)\int f(s^2{}_{xy})\cos(k_\mu(x_\mu-y_\mu)) \times dx_1dx_2dx_3dx_4.$$

It is a function of the invariant $k_\mu k_\mu$ only. The ordinary case, $f(s^2)=\delta(s^2)$ corresponds to $g(k_\mu k_\mu)=\delta(k_\mu k_\mu)$. The condition that $f(s^2)$ be finite on the light cone implies that $g(k_\mu k_\mu)$ can be written in the form

$$g(k_\mu k_\mu)=\int_0^\infty[\delta(k_\mu k_\mu)-\delta(k_\mu k_\mu-\lambda^2)]G(\lambda)d\lambda. \qquad (16)$$

Here $G(\lambda)$ is normalized such that $\int_0^\infty G(\lambda)d\lambda=1$, in view of (15). It is otherwise arbitrary, as $f(s^2)$ is. The λ values for which g must exist must be large, going up to order μ/e^2.

If G is chosen as $\delta(\lambda-\lambda_0)$ the resulting $f(s^2)$ is (for $s^2\geqslant 0$) the Bessel function, $\lambda_0J_1(\lambda_0 s)/s$. For large t, if $s=(t^2-r^2)^{\frac{1}{2}}$, this does not die off fast with $t-r$, but oscillates with phase varying as $\lambda_0(t^2-r^2)^{\frac{1}{2}}$. That is, it oscillates with frequency $\lambda_0(1-r^2/t^2)^{-\frac{1}{2}}$ at a time corresponding to arrival of signals with velocity r/t and thus in quantum mechanics would represent arrival of radiated "particles" of mass $\hbar\lambda_0$. The free emission of such "particles" is removed in classical theory by interference among the various values of λ if a smooth distribution, $G(\lambda)$, of λ is used. This is required if f is to represent say a function decaying rather than oscillating (see appendix).

It appears that the quantum mechanical result is simply this: For processes without permanent radiation the oscillator density g is to replace $\delta(k_\mu k_\mu)$. The negative sign in (16) proves embarrassing (see appendix) if quanta of mass λ_0 can be freely radiated so a wide distribution

in λ corresponding to a monatonic $f(s^2)$ is preferable. As an example, for $f(s^2)=(1/2a^2)\times\exp(-|s|/a)$ find $G(\lambda)=(3a^2\lambda)(1+a^2\lambda^2)^{-5/2}$.

The electrostatic potential at a distance r from a stationary charge, is according to (11),

$$\bar{A}_4(r)=e\int_{-\infty}^{\infty}f(t^2-r^2)dt. \tag{17}$$

For large r, in view of (15) this is readily seen to be e/r. At the origin $r=0$ however, it is finite being $e\int_{-\infty}^{\infty}f(t^2)dt$ or $2\mu/e$. This has a simple interpretation if all mass is electromagnetic. The energy released in bringing a positron and electron charge together and so canceling out all external fields is just 2μ, the rest mass these particles have in virtue of their fields. Or put otherwise, the rest mass particles have is simply the work done in separating them against their mutual attraction after they are created. No energy is needed to create a pair of particles at the same place. (These ideas do not have direct quantum counterparts since in quantum theory all mass does not appear to be electromagnetic self energy, at least in the same simple way.) There may be a maximum field of attraction between two like charges at some separation since, for some functions f the force arising from (17) vanishes at the origin, and of course again at infinity.

There remains to discuss a curious point about the solutions of the least action principle (7) with the mechanical mass term m_a absent. First let us study the simple problem of an ordinary single particle of mass μ in a potential A_4 (caused by other charges) which depends only on one coordinate x. Call the time t, and use this for the parameter α. The action is

$$S=\mu\int(1-\dot{x}^2)^{\frac{1}{2}}dt+e\int A_4dt. \tag{18}$$

Now suppose the potential A_4 is zero outside a small band in x say $|x|<b/2$ (potential barrier) and that it is large positive, and constant within the region. Consider, in Fig. 1, the paths from a point 1 to a point 2 which make S a local maximum. A typical solution is the solid line which is kinked out of the straight line so as to increase the time integral of A_4. This represents a particle moving from 1 rapidly toward the barrier,

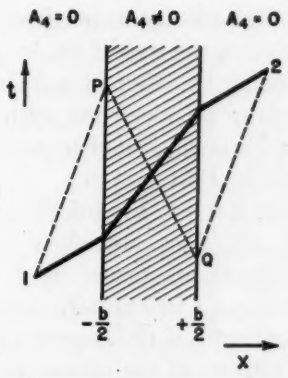

FIG. 1. If two points 1, 2 are separated by a high potential barrier, there are two paths which make action an extremum. One (solid line) represents passage of a fast electron. The other (dotted line) has a section reversed in time and is interpreted as the effective penetration of the barrier by a slow electron by means of a pair production at Q and annihilation at P, section PQ representing the motion of the positron.

entering the region of high potential, losing energy and thus going slower in this region. The high velocity is regained on passing out of the region to 2. Slow particles cannot penetrate the barrier.

But there may be another local maximum. Consider the path $1PQ2$. In the interval PQ the proper time integral must be taken positively as can be verified from a study of the derivation of (13). Now moving the point P upward by Δt might be expected to increase the action by over $2\mu\Delta t$ because the length of $P1$ and PQ are both increased. On the other hand, the integral $\int A_4dt$ is now negative and if A_4 exceeds 2μ such a curve may be a local maximum. Thus for A_4 greater than 2μ there is a new way that slow particles can penetrate the barrier. This is a classical analog of the Klein Paradox.

How would such a path appear to someone whose future gradually becomes past through a moving present? He would first see a single particle at 1, then at Q two new particles would suddenly appear, one moving into the potential to the left, the other out to the right. Later at P the one moving to the left combines with the original particle at 1 and they both disappear, leaving the right moving member of the original pair to arrive at 2. We therefore have a classical description of pair production and annihilation. The particle whose trajectory has its proper time opposed in sign to the true time t (section

PQ) would behave as a particle of opposite sign, for changing the sign of db_μ in (7) is equivalent to changing the sign of e_b. This idea that positrons might be electrons with the proper time reversed was suggested to me by Professor J. A. Wheeler in 1941.

The field at $x=\pm b/2$ is infinite. If it is finite the action (18) does not show such a local maximum, the sharp corner at P becoming a cusp which can go indefinitely into the future. On the other hand, if the correct self-force from (7) is used instead of the approximation (13), a path reversal again becomes a possibility. It is only necessary that the field exceed a critical value, namely, that maximum value of attraction of two unlike particles mentioned above. This field represents a potential of 2μ in a distance of the order of an electron radius and must be as great as this to get the pair of newly created particles apart over the potential barrier of their mutual attraction. (The actual field required to produce pairs in quantum mechanics is 137 times weaker. One might ascribe this to a quantum mechanical penetration of the potential barrier over a Compton wave-length.)

There are many interesting problems presented by these ideas. For example, will pairs be produced *ad infinitum* by the field, or only to that extent that we can guarantee that the positrons will be annihilated by electrons in the future? Again, in a weak field can a large number of pairs be created which separate slightly in the field (which is insufficient to tear the two apart) and thus produce a large polarization of that field? It is hoped that an application of these ideas to a study of positron hole theory will appear in a future paper.

I should like to thank Professor J. A. Wheeler for inoculating me with many ideas without which this work would not have been done.

APPENDIX

The difficulties in a theory such as the one presented here have been discussed by many authors. A very brief discussion of them will be given in this appendix.

The first point is that the action S defined in (1) or (7) is infinite and meaningless because of the infinite extent of the integrals along the path of the particles. The principle of extreme action which we mean to apply can be more rigorously defined as follows. Consider any given variation in paths δa_μ such that $\delta a_\mu \to 0$ as $\alpha \to \pm\infty$. Then define δS as the limit of the quantity δS calculated from (7) with this path variation, the limit being taken as the range of integration passes to infinity. Then the law of motion shall be $\delta S=0$ for all variations which satisfy $\delta a_\mu \to 0$ as $\alpha \to \pm\infty$. The equations of motion (9) are then consequences of the action principle, of course, but not all solutions of these equations satisfy the principle of least action as defined here. There are certain runaway solutions of the equations of motion, such as those discussed by Dirac[2] in the case of Eq. (6), in which the kinetic energy and momentum of a particle increase exponentially with time. These are excluded for they do not satisfy the principle of least action.

Bopp[4] has studied in great detail the consequences of equations of motion. However, he assumes that the function f acts only at retarded times. He finds that the radiation resistance of an oscillator decreases below the normal value with increasing frequency of the oscillator. However, if an oscillator is enclosed in a large, light tight box the fields at the walls of the box are effectively unchanged by the use of f rather than δ. (We are assuming that f decays and does not oscillate. Below, we discuss the situation if f oscillates.) Hence the energy absorbed by the walls will not, apparently, decrease with the increase in oscillator frequency and the radiation resistance will not keep up with it. In the modification described in this paper, in such a box, only the δ-part of f is to be retarded. The radiation resistance has its normal value at all frequencies, and the energy lost will all be found eventually in the walls of the box.

The conservation of quantities like energy (and momentum) can be demonstrated directly if a theory starts from a principle of least action, the form of which action is invariant under a change of origin of the time (and space). For the action (7) consider the quantity

$$g_\nu=\sum_a \left\{ m_a \dot{a}_\nu + e_a \sum_b \bar{A}_\nu^{(b)}(a) \right\}_{\text{at } a_\mu(\alpha_0)}$$

$$-\sum_a \sum_b e_a e_b \int_{-\infty}^{\alpha_0}\int_{\beta_0}^{\infty} 2(a_\nu - b_\nu) f'(s_{ab}^2) da_\mu db_\mu \quad (19)$$

where $f'(x)=df(x)/dx$. The points $\alpha_0, \beta_0, \ldots$ are an arbitrary set of points, one chosen on the world-line of each particle. In virtue of the equations of motion (9) the derivative of g_r with respect to any of the α_0's is zero. This is a generalization of the usual conservation of energy. Ordinarily, we would choose all the α_0 such that all $a_4(\alpha_0)$ are equal, and find g_r is independent of this common value of a_4. The energy is seen to consist of a self-energy, an energy caused by the presence of the potential on each particle, and (since this last would count each interaction twice) a further correction to interaction energy. This is described as a line integral over the paths of the particles, but since one point is in the future and the other in the past, the actual range of integration does not extend beyond the time during which b could interact with a at α_0 and that a could interact with b at β_0. This is the way in which energy which is usually spoken of as being in the field is represented in a theory of action at a distance between particles. Since it is an integral only over a limited range, the energy of motion of the particles is conserved in the long run. (It is easy to generalize (19) to the case that paths may reverse themselves in time.)

We now consider the situation in which the function f oscillates rather than decays. If, as was discussed by Bopp[4] and others (e.g., B. Podolsky and P. Schwed[4]), f is replaced by a Bessel function $\lambda_0 J_1(\lambda_0 s)/s$, the theory corresponds as we have seen to that of interaction through ordinary "quanta" *minus* those corresponding to a mass $\hbar\lambda_0$. The f function does not appear as a pure δ-function at large distances, but another component appears if the frequency of the source exceeds λ_0. Thus, a source at high frequency ω emits waves of two wave-lengths, light of wave number $K=\omega$ and "λ_0-quanta" of wave number $K=(\omega^2-\lambda_0^2)^{\frac{1}{2}}$. Again Bopp's equations (using retarded potentials only) show that the radiative resistance force on a dipole oscillator of amplitude x, frequency ω, is constant at $2e^2\omega^3x^2/3c^3$ for $\omega<\lambda_0$ and falls off as ω exceeds λ_0, as $(2e^2x^2/3c^3)[\omega^3-(\omega^2+\frac{1}{2}\lambda_0^2)(\omega^2-\lambda_0^2)^{\frac{1}{2}}]$, remaining positive, however, for all frequencies. The decrease at higher frequencies must correspond to a negative contribution to radiation resistance accompanying the emission of "λ_0-quanta." That is, the λ_0-quanta behave as though they had negative energy. That this is so and that it results in fundamental difficulties may be seen from a few examples. If through interference the rate of emission of "λ_0-quanta" can be enhanced relative to the rate for the ordinary light quanta, a net negative radiation resistance will result. For example, a set of two vertical dipoles oscillating in phase (at frequency $\omega=2\lambda_0/3^{\frac{1}{2}}$), separated horizontally by one-half the wave-length of light, and one-fourth the wave-length of the λ_0-quanta of the same frequency, shows a negative net radiation resistance. It would oscillate with ever-increasing amplitude, the large emission of negative energy λ_0-quanta supplying the increase in energy of the oscillators and the energy of the light quanta emitted. Again a beam of λ_0-quanta passing through a medium containing damped (energy-absorbing) oscillators increases in amplitude. The wave of λ_0-quanta scattered by the oscillators in the forward direction which ordinarily interferes destructively with the incident wave, in this case has a reversed sign and enhances the incident wave. (The light scattered forward has the incorrect wave-length to make an appreciable effect by interference.) A beam of λ_0-quanta can be separated from light of the same frequency by having the radiation from a source of a given frequency impinge on a diffraction grating of scattering centers. The λ_0-quanta and light quanta will then be scattered in different directions as they have different wave-lengths.

What results if instead of using only retarded waves for λ_0-quanta, we start from the least action principle and analyze the situation of a source enclosed in a box? Then the derivation of Eq. (12) is still incomplete as $\langle F\rangle_{\text{ret}}$ still contains both advanced and retarded components (of λ_0-quanta) at large distances. We could now split off the advanced parts for λ_0-quanta just as we did for light. The resulting equation is just that used by Bopp, namely all retarded interactions but negative contribution of λ_0-quanta to radiation resistance, and therefore leads this time to conservation of energy but to diverging solutions. Such diverging solutions are, as indicated above, excluded by the least action principle so this form of the equation is not convenient. Non-divergent motions do exist. To see this it is better to split off the retarded part of

the λ_0-quanta. What results is that light goes by retarded waves, λ_0-quanta by advanced waves,[7] and the radiation resistance of both contribute positively. Thus an accelerating charge will emit light, but it is predestined that negative energy λ_0-quanta were coming toward it to be absorbed, still further increasing the radiation resistance. This avoids the divergent solutions only to predict observable advanced effects.

For these reasons it is better to restrict oneself to the case of a decaying f-function (distribution of λ) for which a consistent theory can be made. Then the modifications of classical electrodynamics will only appear at very small distances from a charge. On the other hand, these distances are well within the Compton wave-length so that modifications caused by quantum mechanics would in any case appear before the ones here discussed. There is, therefore, little reason to believe that the ideas used here to solve the divergences of classical electrodynamics will prove fruitful for quantum electrodynamics. Nevertheless, the corresponding modifications were attempted with quantum electrodynamics and appear to solve some of the divergence difficulties of that theory. This will be discussed in a future paper.

[7] This may be understood in that, as indicated above, the energy-absorbing walls of the box absorb retarded light waves, but cannot be presumed to absorb retarded λ_0-quanta. Instead, in fact, they spontaneously emit such waves (warming up in the process) and non-divergent solutions result only if they emit just exactly the λ_0-quanta which can later be absorbed by the accelerating charge at the center.

PHYSICAL REVIEW VOLUME 74, NUMBER 8 OCTOBER 15, 1948

Concentration of He^3 by Thermal Diffusion

B. B. McINTEER, L. T. ALDRICH, AND ALFRED O. NIER
Department of Physics, University of Minnesota, Minneapolis 14, Minnesota

(Received July 9, 1948)

A thermal diffusion plant for the enrichment of He^3 has been constructed consisting of cylindrical columns followed by a hot wire column. In the case of the cylindrical columns excellent agreement with the theory of Jones and Furry has been obtained. In the case of the hot wire column, discrepancies exist between the observed performance and that predicted by theory. Under continuous operating conditions it was possible to produce with the expenditure of 16.6 kw, 14 std. cc of helium per day having a He^3/He^4 ratio of 0.0021 when well helium was used as a source of gas.

IN view of the great interest in He^3, both as a tool in superflow studies of liquid helium and as one of the simplest nuclei whose properties need to be determined, an investigation has been started to determine the effectiveness of thermal diffusion as a means of concentrating this isotope. A thermal diffusion plant was constructed consisting of two cylindrical columns followed by a hot wire column. While the general design was similar to that proposed by Jones and Furry,[1] the dimensions were somewhat different.

Figure 1 shows a schematic drawing of the arrangement of the columns. The concentric cylindrical tube sections, 1 and 2, consisted of electrically heated steel tubes surrounded by brass water jackets. The hot wire section (3) consisted of a fine platinum wire surrounded by a brass water jacket. Table I gives dimensions and miscellaneous operating details for the plant.

Well helium, $He^3/He^4 = 1.5 \times 10^{-7}$, is caused to circulate past the bottom of section 1. Since sections 1 and 2 are joined by a tube approximately 11 cm long and 6 cm in diameter, no special circulating system is needed at this point. The circulating system between sections 2 and 3 consists of 900 cm of 0.4-cm i. d. copper tubing in series with a small centrifugal blower. A continuously heated palladium thimble 10 cm long and

[1] R. C. Jones and W. H. Furry, Rev. Mod. Phys. 18, 151 (1946).

0.3 cm in diam. connected to the circulating line removes most of the hydrogen which is concentrated at the top of section 2. A second palladium thimble at the top of section 3 removes any hydrogen missed by the first thimble. The effectiveness of the columns in separating hydrogen from helium is such that without the palladium thimbles even a trace of hydrogen impurity concentrates so strongly at the top of the plant as to make the helium isotope separation process ineffective.

PERFORMANCE OF CYLINDRICAL AND HOT WIRE SECTIONS INDIVIDUALLY

Steady State Operation

If helium is removed at a constant rate σ from the top of a uniform column of length L while the isotopic composition is held constant at the bottom, the ratio of He^3 concentration at the top, c_f, to that at the bottom, c_i, is given by formula (231) of reference 1 as

$$c_f/c_i=(1+n)/(e^{-2AL(1+n)}+n), \qquad \text{(A)}$$

where $n=\sigma/H$ and A and H may be computed in terms of constants of the gas and dimensions of the column. For the columns and operations discussed here $n\ll 1$ and $2AL\gg 0$. Thus (A) reduces to (B)

$$c_f/c_i=1/n=H/\sigma, \qquad \text{(B)}$$

from which H may be computed for comparison with theory inasmuch as c_f/c_i and σ may be determined experimentally. Table II shows pertinent data as well as a comparison between the experimentally and theoretically determined values for H for the two columns. The gas constants used were those cited by Jones and Furry,[1] except that α, the thermal diffusion factor, was taken as 0.059[2] rather than 0.0758. H (theoretical) was computed by the methods employed by Jones and Furry. Although the cylindrical column employed here consisted of two sections of different cross sections, it is assumed that the entire column has the cross section of the larger section inasmuch as the change in cross section has negligible effect on Eq. (A).

It is to be noted that there is good agreement between the experimentally and theoretically determined values of H for the cylindrical column. On the other hand, although the ratio of the experimentally determined values of H for the hot wire column at two pressures varies as the square of the pressure as predicted by theory, the absolute values are in serious disagreement. This disagreement will be discussed later.

TABLE I. Dimensions and operating details for thermal diffusion plant.

Type	Section 1 concentric cylinder	Section 2 concentric cylinder	Section 3 hot wire
Length (cm)	350	350	254
Hot wall			
Material	steel	steel	platinum
Radius (cm)	3.02	1.75	0.018
Temperature °K	600	600	1100
Power (kw)	10	5	1.6
Voltage	220 a.c.	220 a.c.	130 d.c.
Cold wall			
Material	brass	brass	brass
Radius (cm)	3.65	2.38	0.466*
Temperature °K	300	300	300

* This dimension was incorrectly reported in reference 2.

TABLE II. Experimental determination of H.

	Pressure atmospheres	σ Std. liters/day	c_f/c_i	H (std. liters/day) Experimental $H=\sigma c_f/c_i$	Theoretical
Hot wire column	7.8	0.050	330	16.5	9.5
	9.7	0.080	310	24.8	14.8
Cylindrical column	7.8	0.667	386	257	266*

* This value has been corrected for cylindricity by Jones and Furry's Eq. (100) assuming a Maxwellian gas. Without the correction the value would have been 247.

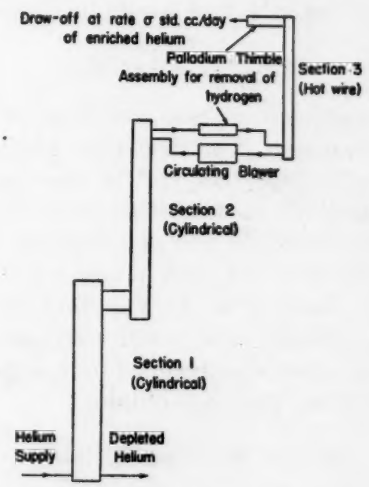
Draw-off at rate σ std. cc/day of enriched helium
Palladium Thimble Assembly for removal of hydrogen
Section 3 (Hot wire)
Circulating Blower
Section 2 (Cylindrical)
Section 1 (Cylindrical)
Helium Supply
Depleted Helium

FIG. 1. Schematic diagram showing flow system for three-section thermal diffusion plant.

[2] B. B. McInteer, L. T. Aldrich, and A. O. Nier, Phys. Rev. 72, 510 (1947).

TABLE III. Experimental determination of $2A$.

	Cylindrical column Sections 1 and 2		Hot wire column Section 3	
Pressure (atmos.)	7.8	9.7	7.8	9.7
$(c_f/c_i)/c_i t$ (day^{-1})	60	69	80	112
μ (std. liters/cm)	0.039*	0.048	0.0033	0.0041
M (std. liters)	2.0	2.5	0.060	0.000
H (std. liters/day)	257	400**	16.5	24.8
$2A$ experimental (cm^{-1})	0.017	0.012	0.023	0.019
$2A$ theoretical (cm^{-1})	0.020***	0.014***	0.052	0.062

* These values for μ and the results for ($2A$) refer to section 2 while (H) is that for section 1.
** Calculated from the experimental result for H obtained for 7.8 atmos.
*** These values have been corrected for cylindricity by Jones' and Furry's Eqs. (100)–(108).

Time Rate of Increase of c_f with No Draw-Off ($\sigma=0$)

Another test of the performance of the columns which can be made conveniently is to observe the manner in which the concentration increases with time at the top ends with no draw-off, while the concentration at the lower ends is maintained constant. Such a test was made and for both the cylindrical columns (sections 1 and 2) and the hot wire column (section 3) a linear increase in concentration is observed as may be seen in Fig. 2.

Jones' and Furry's Eq. (384) may be modified slightly to give an approximate value of the slope which may then be compared with that observed here. Jones and Furry showed that for a column with no reservoir at the top, operated as were the columns in the present test, the initial concentration rise with time would be given by

$$c_f - c_i = Hc_i t/(\mu/2A), \qquad \text{(C)}$$

where μ=amount of gas contained in a unit length of column. This equation assumes that the entire transport of He^3 at the lower end, Hc_i, accumulates in a short length at the upper end which effectively acts as a reservoir containing an amount of gas $\mu/2A$ having a He^3 concentration c_f. Because of the fact that the actual columns employed had small reservoirs at the top, the equation was modified to include the gas stored in them. Thus one obtains

$$c_f - c_i = Hc_i t/((\mu/2A)+M), \qquad \text{(D)}$$

where M is the mass of gas stored in the small reservoir at the top of the column. This equation may be used to calculate $2A$ inasmuch as all of the other quantities in the equation may be determined experimentally. The value obtained may then be compared with that calculated directly from the constants of the gas and the dimensions of the column. Table III shows the results obtained. As was true in our determination of H, the agreement between experimental and theoretical values is good for the cylindrical column but poor for the hot wire column.

The reason for the disagreement in the latter case is by no means obvious. The low theoretical value for H could be due to the fact that α, at the higher temperature of the hot wire column, is more than was assumed in the computations. This would not, however, explain the low value of A actually observed unless imperfections in the column or other spurious effects reduced A more than enough to make up for the fact that the value of α is undoubtedly more than was assumed. Such a hypothesis is not completely unreasonable inasmuch as spurious effects are generally believed to reduce A more than H. In any event, really close agreement is hardly to be expected since the theory of the hot wire columns assumes that helium atoms behave as Maxwellian molecules, a very rough assumption.

Performance of Cylindrical and Hot Wire Sections in Series

From the data obtained in the previous sections a calculation may be made as to how the plant would operate under continuous draw-off conditions if all three sections are connected in series. Since the rate of draw-off is small and $2AL$ for each of the three sections is large, Eqs.

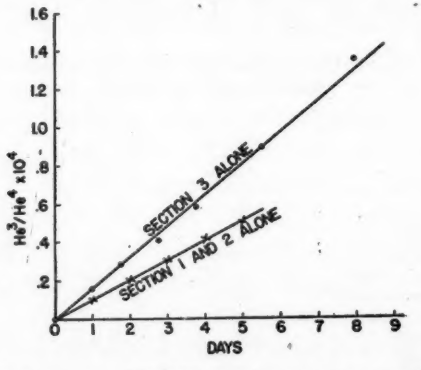

FIG. 2. Increase of He^3/He^4 ratio at tops of cylindrical column (sections 1 and 2) and hot wire column (section 3), when operated individually with no draw-off at top. He^3/He^4 concentration at bottoms maintained constant at 1.5×10^{-7} (well helium). Pressure = 9.7 atmospheres.

(A) and (B) may be assumed to hold for the plant as a whole or the hot wire section alone. Table IV gives the results of such a calculation for the plant operating at a pressure of 7.8 atmospheres and the supply concentration having an average He^3/He^4 ratio of 1.15×10^{-7}. This concentration corresponds to a removal of about 25 percent of the He^3 from the well helium supply.

A test was made with the columns operating at a pressure of 7.8 atmospheres and with a constant draw-off of 14 std. cc/day. After a steady state was reached, data were taken for a week of continuous operation. The concentrations observed at the top of the plant and at the top of section 2 were 2.11×10^{-3} and 1.9×10^{-6}. It is seen that these results are in excellent agreement with the corresponding figures in Table IV. In the course of the experiments a number of other results were obtained. For example, in one test it was found that the hot wire column alone could have a separation factor between its ends of at least 10^4. Since the production capacity of the plant is strictly limited by the H of section 1 (or, in words, the size of section 1), another manner of operation which was employed was to isolate section 3 from 1 and 2 and allow enriched He^3 to accumulate at the top of section 2 for several weeks. If the isolating valves were then opened, the concentration at the top of section 3 would rapidly rise to a high value. By this means it has been possible to produce several hundred standard cc of gas having a He^3/He^4 ratio of as much as 0.0086.

TABLE IV. Calculated performance of entire plant based on measurements on individual sections.

Rate of draw-off, σ std. cc/day	Concentration at top of plant	Concentration at top of section 2	Over-all enrichment	Time required before draw-off begins, days
28	1.05×10^{-3}	1.8×10^{-6}	9,100	7
14	2.10×10^{-3}	1.8×10^{-6}	18,300	14
7	4.20×10^{-3}	1.8×10^{-6}	36,600	29
3.5	8.40×10^{-3}	1.8×10^{-6}	73,000	58

ACKNOWLEDGMENTS

This research was assisted by Navy Contract N5ori 147, T. O. III, between the Office of Naval Research and the University of Minnesota. The construction of the apparatus was made possible by a grant from the Graduate School and the Minnesota Technical Research Fund subscribed to by General Mills, Inc., the Minneapolis Star Journal and Tribune, the Minnesota Mining and Manufacturing Company, the Northern States Power Company, and the Minneapolis Honeywell Regulator Company.

PHYSICAL REVIEW VOLUME 74, NUMBER 8 OCTOBER 15, 1948

Phenomenological Quantum-Electrodynamics

J. M. JAUCH AND K. M. WATSON*
Department of Physics, State University of Iowa, Iowa City, Iowa
(Received May 24, 1948)

The quantization of the pure radiation field in a uniformly moving refractive medium is carried through both in the Hamiltonian and in the symmetrical four-dimensional form. The total energy and momentum are diagonalized. For a medium velocity larger than c/n there occur photons with negative energy.

PART I. THE PURE RADIATION FIELD AND ITS QUANTIZATION

1. Introduction

IN the classical description of electromagnetic phenomena in matter two points of view have been found useful. The first, which also is the historically older one, is the so-called phenomenological approach. In this the actual properties of matter are considered only in so far as they can be directly expressed in terms of the electromagnetic field quantities. For isotropic insulators these properties are embodied in the two characteristic constants: the dielectric constant ϵ and the magnetic permeability μ. This theory gives no information about the actual values of ϵ and μ nor of their dependence on the frequency of the radiation or dispersion.

In the second approach matter is described in terms of the fundamental properties of the constituent elementary particles. The field equations of the phenomenological theory appear as equations between certain average values of the field quantities in this theory taken over volumes containing a large number of particles. The actual values of the phenomenological constants ϵ and μ as well as their frequency dependence can be expressed in terms of the fundamental properties of the elementary particles. It is at once evident that the latter approach is more fundamental and far-reaching.

The quantum mechanical formulation of the electromagnetic field equations has so far been applied principally to the second case. That is, the quantization is applied to the field equations for a vacuum only and the interaction of the field with matter is usually introduced as a direct interaction of the field with elementary particles. As far as we are aware, no systematic development of the quantum theory of phenomenological electrodynamics exists. It is clear from the foregoing remark that from such a theory there cannot be expected any new results. That is, if the quantum electrodynamics for a vacuum were completely satisfactory it would contain all the results that could be derived from a phenomenological theory and in addition it would reduce the phenomenological constants to the fundamental parameters in the theory such as the mass m and charge e of the interacting particles, Planck's constant h and the velocity of light c. However there are primarily three reasons why it seemed to us desirable to have this theory developed. First, the theory presents certain interesting aspects from a purely formal point of view. Formally it appears as an extension or generalization of the quantum electrodynamics of a vacuum in which it goes over in the limiting case $\epsilon \to 1$, $\mu \to 1$. Second, it seems that certain types of problems can be handled much more easily in the phenomenological than in the atomistic theory. This is the case, for instance, for the discussion of the Čerenkov radiation and the radiation of charged particles passing a discontinuity in ϵ or μ. In the third place, we were interested in such a theory with a view to a possible application of the theory for a vacuum. It is well known that the hole theory predicts a polarizability of the vacuum. So far, this prediction could not be taken seriously because the field-proportional part of the polarization is divergent. A phenomenological approach might give new information as to the possible form which such a vacuum polarization can have.

The relativistic invariance of this theory is guaranteed if we use the four-dimensional tensor

* Now at Institute for Advanced Study, Princeton, New Jersey.

notation. However, it must be kept in mind that such a theory always introduces a preferred coordinate system, usually the system for which the medium is at rest. When applied to a polarizable vacuum the relativity principle in such a theory is thus violated in the sense that it is possible in principle to detect an absolute motion by referring it to the motion of the medium.[1]

2. The Classical Radiation Field

The fundamental equations for an electromagnetic field in a medium were given in the relativistically invariant form by Minkowski.[2] In the absence of charges and currents they are, for the medium at rest,

$$\nabla\times\mathbf{E}=-\dot{\mathbf{B}}, \qquad \nabla\cdot\mathbf{B}=0, \tag{1}$$

$$\nabla\times\mathbf{H}=\dot{\mathbf{D}}, \qquad \nabla\cdot\mathbf{D}=0, \tag{2}$$

$$\mathbf{D}=\epsilon\mathbf{E}, \tag{3}$$

and

$$\mathbf{B}=\mu\mathbf{H}.$$

For the relativistically invariant formulation we use the notation $x^0=-x_0=ct$, $x^k=x_k$, $(k=1,2,3)$. Furthermore we shall put $n^2=\epsilon\mu$ for the index of refraction. Equations (1) and (2) may then be written in tensor form by introducing the following two antisymmetrical tensors

$$F_{\lambda\mu}=\begin{Vmatrix} 0 & B_3 & -B_2 & +E_1 \\ -B_3 & 0 & B_1 & +E_2 \\ +B_2 & -B_1 & 0 & +E_3 \\ -E_1 & -E_2 & -E_3 & 0 \end{Vmatrix} \tag{4}$$

and

$$G_{\lambda\mu}=\begin{Vmatrix} 0 & B_3 & -B_2 & +n^2E_1 \\ -B_3 & 0 & +B_1 & +n^2E_2 \\ +B_2 & -B_1 & 0 & +n^2E_3 \\ -n^2E_1 & -n^2E_2 & -n^2E_3 & 0 \end{Vmatrix}. \tag{5}$$

It is easily seen that the field equations (1) and (2) are then identical with the tensor equations:

$$\partial_\lambda F_{\mu\nu}+\partial_\mu F_{\nu\lambda}+\partial_\nu F_{\lambda\mu}=0, \tag{6}$$

and

$$\partial_\mu G^{\lambda\mu}=0. \tag{7}$$

Here $\partial_\lambda\equiv\partial/\partial x^\lambda$.

It follows from Eq. (6), that $F_{\lambda\mu}$ can be derived from a four-vector potential

$$F_{\lambda\mu}=\partial_\lambda\phi_\mu-\partial_\mu\phi_\lambda. \tag{8}$$

[1] An interesting special case where the results are independent of the medium velocity is to be discussed in Part III.

[2] H. Minkowski, Göttinger Nachrichten, p. 53 (1908), Math. Ann. 68, 472 (1910).

With this choice of $F_{\lambda\mu}$, Eq. (6) is identically satisfied. The connections (3) between **E** and **D** on the one hand and **H** and **B** on the other can be written in relativistically covariant form by introducing the four-vector v^μ of the medium velocity. Here $v^\mu=dx^\mu/d\tau$, where τ is the proper time of the medium $(v^\mu v_\mu=-1)$. Introducing further the abbreviation $\kappa=n^2-1$ we have,

$$G_{\lambda\mu}=F_{\lambda\mu}+\kappa(F_{\mu\sigma}v^\sigma v_\lambda-F_{\lambda\sigma}v^\sigma v_\mu). \tag{9}$$

Since in the system for which the medium is at rest, $v^k=0$, $v^0=1$, it is easy to verify that (9) reduces in this case to (3).

Equation (9) can be solved for $F_{\lambda\mu}$. We need simply remark that the transformation from G to F is the same as that from F to G with ϵ and μ replaced by $1/\epsilon$ and $1/\mu$ respectively or κ replaced by $-\kappa/(1+\kappa)$. We obtain in this way without further calculation:

$$F_{\lambda\mu}=G_{\lambda\mu}+\frac{\kappa}{1+\kappa}(G_{\lambda\sigma}v^\sigma v_\mu-G_{\mu\sigma}v^\sigma v_\lambda). \tag{9'}$$

Equation (9′) can also be verified directly by substituting it back into the right-hand side of (9).

The field equations for the four-vector potential are obtained by introducing (9), together with (8), into (7). Here one can make use of the freedom of choice of the ϕ_λ by imposing on the ϕ_λ the subsidiary condition

$$\chi\equiv\partial^\rho\phi_\rho-\kappa v^\sigma\partial_\sigma v^\rho\phi_\rho=0. \tag{10}$$

We find then from (7)

$$(\partial^\mu\partial_\mu-\kappa\partial_\mu v^\mu\partial_\sigma v^\sigma)\Psi^\lambda=0, \tag{11}$$

where

$$\Psi^\lambda=\phi^\lambda-\kappa\phi^\sigma v_\sigma v^\lambda. \tag{12}$$

Since (12) can be solved for ϕ^λ by the linear transformation

$$\phi^\lambda=\Psi^\lambda+\frac{\kappa}{1+\kappa}\Psi^\sigma v_\sigma v^\lambda, \tag{13}$$

we see that the vector potential ϕ^λ also satisfies

$$(\partial^\mu\partial_\mu-\kappa\partial_\mu v^\mu\partial_\sigma v^\sigma)\phi^\lambda=0. \tag{14}$$

Equations (8) and (14), together with the subsidiary condition (10), may be considered as the fundamental equations of the theory.

3. The Lagrangian for the Radiation Field

In order to prepare the theory for the quantum formalism we shall first show that the field equations can be derived from a variational principle. For that purpose we consider the Lagrange function

$$L=\int \mathfrak{L}d^3x, \tag{15}$$

with the Lagrange density function defined by

$$\mathfrak{L}=-\tfrac{1}{4}(\partial_\rho\phi_\sigma-\partial_\sigma\phi_\rho)(\partial^\rho\phi^\sigma-\partial^\sigma\phi^\rho)-\tfrac{1}{2}\chi^2 -\tfrac{1}{2}\kappa(\partial^\nu\phi^\rho-\partial^\rho\phi^\nu)(\partial_\rho\phi_\sigma-\partial_\sigma\phi_\rho)v^\sigma v_\nu. \tag{16}$$

The variational principle,

$$\delta\int Ldx^0=0, \tag{17}$$

leads then at once to the differential equations

$$\partial^\lambda(\partial/\partial(\partial^\lambda\phi^\mu))=0. \tag{18}$$

Since

$$\frac{\partial\mathfrak{L}}{\partial(\partial^\lambda\phi^\mu)}=-(\partial_\lambda\phi_\mu-\partial_\mu\phi_\lambda)-\kappa[(\partial_\mu\phi_\sigma-\partial_\sigma\phi_\mu)v^\sigma v_\lambda -(\partial_\lambda\phi_\sigma-\partial_\sigma\phi_\lambda)v^\sigma v_\mu] -(g_{\lambda\mu}-\kappa v_\lambda v_\mu)\chi, \tag{19}$$

the Eqs. (18) are equivalent with

$$\partial^\lambda G_{\lambda\mu}+\partial^\lambda(g_{\lambda\mu}-\kappa v_\lambda v_\mu)\chi=0, \tag{20}$$

with $G_{\lambda\mu}$ given by (9).

From this follows, since $G_{\lambda\mu}=-G_{\mu\lambda}$,

$$(\partial^\lambda\partial_\lambda-\kappa\partial^\lambda v_\lambda\partial^\mu v_\mu)\chi=0. \tag{21}$$

Equation (20) is only equivalent to (7) or (14) if we impose the subsidiary condition $\chi=0$. This can be done by requiring that $\chi=0$ and $\dot\chi=0$ for all positions at a given time. It follows from (21), which is a partial differential equation of second order in the space and time variables, that $\chi=0$ holds then for all times. From this it is evident that (17) or (18) together with the condition (10) is equivalent to (14).

4. Hamiltonian Formalism

The canonically conjugate variables π_μ are defined by

$$\pi_\mu=\frac{\partial\mathfrak{L}}{\partial(\partial_0\phi^\mu)}$$

From (19) it follows that

$$\pi_\mu=G_\mu{}^0-(g_\mu{}^0-\kappa v^0v_\mu)\chi, \tag{22}$$

where $g_\mu{}^\lambda$ is the metric tensor and χ is given by (10). In particular for $\mu=0$, we have

$$\pi_0=-(1+\kappa v_0{}^2)\chi, \tag{23}$$

and for $\mu=k$, $(k=1, 2, 3)$,

$$\pi_k=G_\mu{}^0+\kappa v^0v_k\chi. \tag{24}$$

The Hamiltonian may then be written as

$$H=\int \mathfrak{H}d^3x$$

with

$$\mathfrak{H}=\pi_\mu\dot\phi^\mu-\mathfrak{L}. \tag{25}$$

In this expression we must consider the $\dot\phi^\mu$ as functions of π^μ, ϕ_λ and their space derivatives. The canonical equations

$$\dot\pi_\mu=-\delta H/\delta\phi^\mu,$$

and

$$\dot\phi^\mu=\delta H/\delta\pi_\mu, \tag{26}$$

are then equivalent to Eqs. (8), (9), and (20). The explicit expression of H is very complicated. In the following, however, it will not be used since we restrict ourselves to the special case in which the subsidiary condition (10) holds, which corresponds to the Maxwell field. In this case the Hamiltonian can be calculated explicitly. In order to do this we use a three-dimensional vector notation: $\mathbf{v}$, $\boldsymbol{\phi}$, $\boldsymbol{\pi}$, $\mathbf{V}$ and $\mathbf{W}$ are the vectors with components v_k, ϕ_k, π_k, $V_k=F_{0k}$ and $W_k=F_{ij}$ $(i, j, k$ cyclic). On account of (10) we have then $\pi_0=0$ and

$$\pi_k=G_k{}^0.$$

For $\dot{\boldsymbol{\phi}}$ we have in this notation

$$\dot{\boldsymbol{\phi}}=\mathbf{V}+\nabla\phi_0. \tag{27}$$

By separating space and time parts in (9) we obtain

$$\mathbf{V}(1+\kappa v_0{}^2)-\kappa\mathbf{v}(\mathbf{v}\cdot\mathbf{V})=\boldsymbol{\pi}+\kappa v^0(\mathbf{v}\times\mathbf{W}). \tag{28}$$

This equation can be solved for $\mathbf{V}$ in the following form

$$\mathbf{V}=\frac{1}{1+\kappa v_0{}^2}\left\{\boldsymbol{\pi}+\kappa v^0(\mathbf{v}\times\mathbf{W})+\frac{\kappa}{1+\kappa}(\boldsymbol{\pi}\cdot\mathbf{v})\mathbf{v}\right\}. \tag{29}$$

By substituting $\mathbf{V}$ into the right-hand side of

(27) we obtain $\dot{\phi}$ as a function of the space derivatives of ϕ and of π alone. On account of $\pi_0=0$ we shall not need the expression for ϕ_0. The expressions for $\dot{\phi}^\mu$ may be substituted into (25) and we obtain in this way for the Hamiltonian the following result:

$$\mathfrak{H}=\frac{1}{2(1+\kappa v_0^2)}\Big\{\pi\cdot\pi+2\kappa v^0(\mathbf{v}\times\mathbf{W})\cdot\pi+\frac{\kappa}{1+\kappa}(\pi\cdot\mathbf{v})^2+\kappa(\mathbf{v}\times(\mathbf{v}\times\mathbf{W}))\cdot\mathbf{W}\Big\}+\tfrac{1}{2}\mathbf{W}\cdot\mathbf{W}+\pi\cdot\nabla\phi_0. \quad (30)$$

The last term can be removed because it is equal to

$$\pi\cdot\nabla\phi_0=\nabla\cdot(\pi\cdot\phi_0)-(\nabla\cdot\pi)\phi_0.$$

The first term is a space divergence and will not contribute anything to the total Hamiltonian. The last term is zero, because from (20) and (22) it follows

$$\partial^\mu\pi_\mu=-2(1+\kappa v_0^2)\partial^0\chi+2\kappa v^0(\nabla\cdot\mathbf{v})\chi,$$

or with the help of (23)

$$\nabla\cdot\pi=-(1+\kappa v_0^2)\partial^0\chi+2\kappa v^0(\nabla\cdot\mathbf{v})\chi=0,$$

on account of (10). We denote this new Hamiltonian density with $\mathfrak{H}_0$:

$$\mathfrak{H}_0=\frac{1}{2(1+\kappa v_0^2)}\Big\{\pi\cdot\pi+2\kappa v^0(\mathbf{v}\times\mathbf{W})\cdot\pi+\frac{\kappa}{1+\kappa}(\pi\cdot\mathbf{v})^2+\kappa(\mathbf{v}\times(\mathbf{v}\times\mathbf{W}))\cdot\mathbf{W}\Big\}+\tfrac{1}{2}\mathbf{W}\cdot\mathbf{W}. \quad (31)$$

5. Quantization of the Radiation Field

The quantum theory of the radiation field is obtained by interpreting the field variables as operators which satisfy certain commutation rules. In doing this we can choose either the Schrödinger or the Heisenberg representation. In the former the canonical variables are constant operators depending only on the space variables $\mathbf{x}$ but not explicitly on the time $t=x^0$. The Schrödinger functional $\Omega(q,t)$ is then time dependent and satisfies the Schrödinger equation

$$H\Omega(q,t)=i\dot{\Omega}(q,t). \quad (32)$$

In the Heisenberg representation the Schrödinger functional describing the state of a system is constant and the operators depend explicitly on time. The connection between the time-dependent and the time-independent operators is given by[3]

$$\phi_\lambda(x)=e^{iHt}\phi_\lambda(\mathbf{x})e^{-iHt},$$

and

$$\pi_\mu(x)=e^{iHt}\pi_\mu(\mathbf{x})e^{-iHt}. \quad (33)$$

In the canonical formalism we postulate between the time-independent field variables the commutation rules

$$[\phi_\lambda(\mathbf{x}),\ \pi_\mu(\mathbf{x}')]=ig_{\lambda\mu}\delta(\mathbf{x}-\mathbf{x}'), \quad (34)$$

where $\delta(\mathbf{x}-\mathbf{x}')$ represents the three-dimensional δ-function. All other variables commute.

Since there is complete analogy between commutators and Poisson brackets in classical mechanics and since the canonical equations (26) can always be written in terms of Poisson brackets, it follows that the canonical commutation rules lead back to the Eqs. (8), (9), and (20), which now hold as operator equations. Here the time derivative of any operator 0 not depending explicitly on the time (such as $\phi_\lambda(\mathbf{x})$ or $\pi_\mu(\mathbf{x})$) is defined by

$$\dot{0}=i[H,0]. \quad (35)$$

In particular, it follows again from (20) that the operator χ defined by (10) satisfies the equation (21). This enables us to specialize our field to the Maxwell field by imposing on the Schrödinger functional the subsidiary condition

$$\chi\Omega(q,t)=0. \quad (36)$$

Since Eq. (21) is of second order in t it is obviously sufficient to require only the initial conditions[4]

$$\chi(\mathbf{x})\Omega(q,0)=0, \quad \text{and} \quad \dot{\chi}(\mathbf{x})\Omega(q,0)=0. \quad (37)$$

[3] Here and in the following we shall always use the notation $x=(x^0, x^1, x^2, x^3)$ and $\mathbf{x}=(x^1, x^2, x^3)$ to describe four vectors and space vectors.

[4] For a more detailed discussion of the analogous situation in the vacuum case, cf. G. Wentzel, *Einführung in die Quantentheorie der Wellenfelder* (Wien, F. Deuticke 1943), p. 111ff. The notation here used is the obvious generalization of Wentzel's notation.

The relativistic invariance of the canonical quantization procedure is most easily shown by transforming the commutation rules to the symmetrical four-dimensional form. This can be done by introducing the field variables (33) which depend explicitly on the time. We shall show that the commutation rules (34) are a consequence of the commutation rules

$$i[\phi_\lambda(x),\ \phi_\mu(x')]=\Gamma_{\lambda\mu}D(x-x'), \tag{38}$$

with

$$\Gamma_{\lambda\mu}=g_{\lambda\mu}+\frac{\kappa}{1+\kappa}v_\lambda v_\mu. \tag{39}$$

The D-function which occurs here may be defined by the integral

$$D(y)=\pm\frac{1}{(2\pi)^4}\int_{C_\mp}d^4k\frac{\exp(ik_\rho y^\rho)}{k_\rho k^\rho-\kappa v^\rho v^\sigma k_\rho k_\sigma}, \tag{40}$$

Here the symbol $C_\mp$ below the integral sign indicates the path of integration for the k^0 variable, which is defined in the following way. Let k', k'' denote the two roots for k^0 of the quadratic equation

$$k_\sigma k^\sigma-\kappa v^\sigma v^\rho k_\sigma k_\rho=0. \tag{41}$$

The explicit expressions for these roots are

$$\begin{aligned}k'&=\frac{\kappa(\mathbf{v}\cdot\mathbf{k})v^0+((1+\kappa v_0^2)k^2-\kappa(\mathbf{v}\cdot\mathbf{k})^2)^{\frac{1}{2}}}{1+\kappa v_0^2},\\ \text{and}\qquad k''&=\frac{\kappa(\mathbf{v}\cdot\mathbf{k})v^0-((1+\kappa v_0^2)k^2-\kappa(\mathbf{v}\cdot\mathbf{k})^2)^{\frac{1}{2}}}{1+\kappa v_0^2}.\end{aligned} \tag{42}$$

The sign of the radicand is always greater than zero, and the roots k', k'' therefore always real, since by Schwartz' inequality

$$\begin{aligned}(1+\kappa v_0^2)k^2-\kappa(\mathbf{v}\cdot\mathbf{k})^2&\\ =k^2(1+\kappa)+\kappa(v^2k^2-(\mathbf{v}\cdot\mathbf{k})^2)>0.&\end{aligned}$$

The integrand in (40), therefore, has two poles on the real axis. The paths indicated by $C_\mp$ are such that they go along the real axis in the k^0-plane from $-\infty$ to $+\infty$ deformed into the negative (C_-) or positive (C_+) imaginary half plane so as to avoid the poles at the points $k^0=k'$ and $k^0=k''$. Which of the two paths is to be chosen is determined by the sign of y^0 as follows: C_+ for $y^0>0$, C_- for $y^0<0$. The sign in front of the integral must be chosen so that either the upper or lower sign applies throughout.

If we carry out the integration over k^0 according to this prescription we find for $y^0>0$

$$D(y)=\frac{1}{(2\pi)^4(1+\kappa v_0^2)}\int d^3k e^{i\mathbf{k}\cdot\mathbf{y}}\times\int_{C_+}dk^0\frac{e^{-ik^0y^0}}{(k^0-k')(k^0-k'')}. \tag{43}$$

The integral over k^0 can be evaluated with the residue theorem.

$$\int_{C_+}\frac{e^{-ik^0y^0}}{(k^0-k')(k^0-k'')}=+\frac{2\pi i}{k''-k'}\times\{e^{-ik''y^0}-e^{-ik'y^0}\}. \tag{44}$$

This gives for (43)

$$D(y)=\frac{i}{(2\pi)^3(1+\kappa v_0^2)}\times\int\frac{d^3k}{k''-k'}e^{i\mathbf{k}\mathbf{y}}\{e^{-ik''y^0}-e^{-ik'y^0}\}.$$

Since from (42) we have $k'(-\mathbf{k})=-k''(\mathbf{k})$ we can transform this last integral into

$$D(y)=\frac{1}{(2\pi)^3(1+\kappa v_0^2)}\times\int\frac{d^3k}{k'-k''}\{\sin(\mathbf{k}\cdot\mathbf{y}-k''y^0)-\sin(\mathbf{k}\cdot\mathbf{y}-k'y^0)\}. \tag{45}$$

Exactly the same result is obtained for $y^0<0$. From (40) it is obvious that D is an invariant function of its arguments. The form (45) however is more convenient to verify the following relations:

$$D(y)_{y^0=0}\equiv D(\mathbf{y})=0, \tag{46}$$

$$\dot{D}(y)_{y^0=0}=\delta(y)/(1+\kappa v_0^2), \tag{47}$$

$$\partial_i D(y)_{y^0=0}=0,\quad (i=1,\ 2,\ 3) \tag{48}$$

$$(\partial_\rho\partial^\rho-\kappa\partial^\rho v_\rho\partial^\sigma v_\sigma)D=0. \tag{49}$$

It remains to be shown that the commutation rules (34) follow from (38). We notice first that on account of (12) and (13), (38) may also be written

$$i[\Psi_\lambda(x),\ \phi_\mu(x')]=g_{\lambda\mu}D(x-x'). \tag{50}$$

Since $\chi=\partial^\lambda\Psi_\lambda$ it follows immediately that

$$i[\chi(x),\ \phi_\mu(x')]=\partial_\mu D(x-x'), \tag{51}$$

and

$$i[\chi(x),\ F_{\lambda\mu}(x')]=i[\chi(x),\ G_{\lambda\mu}(x')]=0. \tag{52}$$

Moreover,

$$i[\chi(x),\ \chi(x')]=(\partial^\mu\partial_\mu-\kappa\partial_\rho v^\rho\partial_\sigma v^\sigma)D(x-x')=0, \tag{53}$$

on account of (49).

From (38) we obtain:

$$i[F_{\lambda\mu}(x),\ \phi_\nu(x')]=(\partial_\lambda\Gamma_{\mu\nu}-\partial_\mu\Gamma_{\lambda\nu})D(x-x'), \tag{54}$$

and with the help of (9)

$$i[G_{\lambda\mu}(x),\ \phi_\nu(x')]=\{\partial_\lambda g_{\mu\nu}-\partial_\mu g_{\lambda\nu}+\kappa\partial_\sigma v^\sigma(\Gamma_{\lambda\nu}v_\mu-\Gamma_{\mu\nu}v_\lambda)\}D(x-x'). \tag{55}$$

With the help of (22) and (51) we obtain finally

$$i[\pi_\lambda(x),\ \phi_\nu(x')]=\{\partial_\lambda g_\nu{}^0-\partial^0 g_{\lambda\nu}+\kappa\partial_\sigma v^\sigma(\Gamma_{\lambda\nu}v^0-\Gamma_\nu{}^0 v_\lambda)-\partial_\nu g_\lambda{}^0+\kappa v_\lambda v^0 v_\nu\}D(x-x'). \tag{56}$$

By specializing this expression for $x_0=x_0'$ and by using the relations (46), (47), (48), this reduces to

$$i[\pi_\lambda(\mathbf{x}),\ \phi_\nu(\mathbf{x}')]=g_{\lambda\nu}\delta(\mathbf{x}-\mathbf{x}'),$$

which is Eq. (34). In order to complete the proof that (38) reduces to the canonical commutation rules it remains to be shown that all the other variables commute. For the components ϕ_λ this is an immediate consequence of (38) and (46). Furthermore from (23), (52) and (53) it follows also that $[\pi_0,\ \pi_i]=0$. A rather lengthy, although straightforward, calculation shows then that the space components π_i commute also among themselves. This completes the proof that (38) are the four-dimensional invariant commutation rules of the radiation field.

6. Transition to Momentum Space

We carry out the transition to momentum space by introducing the new variables $Q_\nu(\mathbf{k})$ and $P_\nu(\mathbf{k})$,

$$\phi_\nu=(2\pi)^{-\frac{3}{2}}\int d^3k Q_\nu(\mathbf{k})e^{i\mathbf{k}\cdot\mathbf{x}},$$

and

$$\pi_\nu=(2\pi)^{-\frac{3}{2}}\int d^3k P_\nu(\mathbf{k})e^{-i\mathbf{k}\cdot\mathbf{x}}. \tag{57}$$

The reality conditions for ϕ_ν and π_ν require that

$$\begin{aligned}Q_\nu{}^+(\mathbf{k})&=Q_\nu(-\mathbf{k})\\ P_\nu{}^+(\mathbf{k})&=P_\nu(-\mathbf{k}).\end{aligned} \tag{58}$$

The operators Q_ν and P_ν satisfy the canonical commutation rules

$$i[P_\nu(\mathbf{k}),\ Q_\mu(\mathbf{k}')]=g_{\nu\mu}\delta(\mathbf{k}-\mathbf{k}') \tag{59}$$

while all the other variables commute. Substituting (57) into the Hamiltonian (31) and using the vector notation for the spatial components of Q and P we have

$$H_0=\tfrac{1}{2}\int d^3k\left[\frac{1}{1+\kappa v_0{}^2}\left\{\mathbf{P}^+\cdot\mathbf{P}+2\kappa i v^0(\mathbf{v}\cdot\mathbf{Q})(\mathbf{k}\cdot\mathbf{P})-2\kappa i v^0(\mathbf{v}\cdot\mathbf{k})(\mathbf{Q}\cdot\mathbf{P})+\frac{\kappa}{1+\kappa}(\mathbf{P}^+\cdot\mathbf{v})(\mathbf{P}\cdot\mathbf{v})-\kappa(\mathbf{v}\times(\mathbf{k}\times\mathbf{Q}^+))\cdot(\mathbf{v}\times(\mathbf{k}\times\mathbf{Q}))\right\}+\tfrac{1}{2}(\mathbf{k}\times\mathbf{Q}^+)\cdot(\mathbf{k}\times\mathbf{Q})\right]. \tag{60}$$

This expression can be simplified by using the subsidiary condition (36) and its consequences. It follows then that the second term in (60) vanishes. A further simplification is introduced if we choose for each $\mathbf{k}$ a special coordinate system by putting

$$\mathbf{e}_1=\frac{\mathbf{k}\times\mathbf{v}}{|\mathbf{k}\times\mathbf{v}|};\quad \mathbf{e}_2=\frac{\mathbf{k}\times(\mathbf{k}\times\mathbf{v})}{|\mathbf{k}\times(\mathbf{k}\times\mathbf{v})|};\quad \mathbf{e}_3=\frac{\mathbf{k}}{k}, \tag{61}$$

and

$$\begin{aligned}\mathbf{P}&=P^{(1)}\mathbf{e}_1+P^{(2)}\mathbf{e}_2+P^{(3)}\mathbf{e}_3,\\ \mathbf{Q}&=Q^{(1)}\mathbf{e}_1+Q^{(2)}\mathbf{e}_2+Q^{(3)}\mathbf{e}_3.\end{aligned} \tag{62}$$

This coordinate system is orthogonal and normalized

$$(\mathbf{e}_i\cdot\mathbf{e}_j)=\delta_{ij}. \tag{63}$$

We obtain thus for

$$\left.\begin{aligned}P^{(i)}&=(\mathbf{P}\cdot\mathbf{e}_i),\\ Q^{(i)}&=(\mathbf{Q}\cdot\mathbf{e}_i),\end{aligned}\right\} \tag{64}$$

and

$$\mathbf{P}\cdot\mathbf{v}=-vP^{(2)}|\sin\alpha|+vP^{(3)}\cos\alpha \tag{65}$$

$$(\mathbf{k}\times\mathbf{Q})=k(-Q^{(2)}\mathbf{e}_1+Q^{(1)}\mathbf{e}_2) \tag{66}$$

$$(\mathbf{v}\times(\mathbf{k}\times\mathbf{Q}))=v\cdot k(-Q^{(1)}\cos\alpha\,\mathbf{e}_1-Q^{(2)}\cos\alpha\,\mathbf{e}_2-Q^{(2)}|\sin\alpha|\mathbf{e}_3), \tag{67}$$

where α is the angle between $\mathbf{v}$ and $\mathbf{k}$. Since $\mathbf{e}_1$ and $\mathbf{e}_3$ change sign with $\mathbf{k}$, the reality conditions (58) are now

$$\begin{aligned} Q^{+(1)}(\mathbf{k}) &= -Q^{(1)}(-\mathbf{k}), \\ Q^{+(2)}(\mathbf{k}) &= Q^{(2)}(-\mathbf{k}), \\ Q^{+(3)}(\mathbf{k}) &= -Q^{(3)}(-\mathbf{k}), \\ P^{+(1)}(\mathbf{k}) &= -P^{(1)}(-\mathbf{k}), \\ P^{+(2)}(\mathbf{k}) &= P^{(2)}(-\mathbf{k}), \\ P^{+(3)}(\mathbf{k}) &= -P^{(3)}(-\mathbf{k}). \end{aligned} \tag{58'}$$

In these variables we obtain for (60):

$$\begin{aligned} H_0 = \frac{1}{2}\int d^3k \Bigg[& \frac{1}{1+\kappa v_0^2}\Bigg\{ P^{(1)}+P^{(1)} \\ & + P^{(2)}+P^{(2)}\left(1+\frac{\kappa v^2 \sin^2\alpha}{1+\kappa}\right)\Bigg\} \\ & + k^2\left(1-\frac{\kappa v^2\cos^2\alpha}{1+\kappa v_0^2}\right)Q^{(1)}+Q^{(1)} \\ & + k^2\left(1-\frac{\kappa v^2}{1+\kappa v_0^2}\right)Q^{(2)}+Q^{(2)} \\ & - 2\kappa i v^0 v\cdot k\cos\alpha(Q^{(1)}P^{(1)}+Q^{(2)}P^{(2)})\Bigg]. \end{aligned} \tag{68}$$

The operators $Q^{(i)}$, $P^{(i)}$ satisfy the commutation rules

$$i[Q^{(j)}(\mathbf{k})\, P^{(i)}(\mathbf{k})] = \delta_{ij}\delta(\mathbf{k}-\mathbf{k}'), \tag{69}$$

since the transformation (62) is orthogonal.

It is possible to diagonalize this Hamiltonian by introducing the absorption and emission operators $a(k)$, $a^+(k)$ by setting

$$\begin{aligned} Q^{(1)}(\mathbf{k}) &= \frac{1}{\sqrt{2}}\alpha(a_1(\mathbf{k})-a_1{}^+(-\mathbf{k})), \\ P^{(1)}(\mathbf{k}) &= \frac{i}{\sqrt{2}}\frac{1}{\alpha}(a_1{}^+(\mathbf{k})+a_1(-\mathbf{k})), \\ Q^{(2)}(\mathbf{k}) &= \frac{1}{\sqrt{2}}\beta(a_2(\mathbf{k})+a_2{}^+(-\mathbf{k})), \end{aligned} \tag{70}$$

and

$$P^{(2)}(\mathbf{k}) = \frac{i}{\sqrt{2}}\frac{1}{\beta}(a_2{}^+(\mathbf{k})-a_2(-\mathbf{k})).$$

The factors α and β will be determined later.

The inverse formulas are

$$\begin{aligned} a_1(\mathbf{k}) &= \frac{1}{\sqrt{2}}\left\{\frac{1}{\alpha}Q^{(1)}(\mathbf{k})+i\alpha P^{+(1)}(\mathbf{k})\right\}, \\ \text{and} \\ a_2(\mathbf{k}) &= \frac{1}{\sqrt{2}}\left\{\frac{1}{\beta}Q^{(2)}(\mathbf{k})+i\beta P^{+(2)}(\mathbf{k})\right\}. \end{aligned} \tag{71}$$

From these follow the commutation rules for the a's in the form:

$$[a_i(\mathbf{k}),\, a_j{}^+(\mathbf{k}')] = \delta_{ij}\delta(\mathbf{k}-\mathbf{k}'). \tag{72}$$

Introducing the $a_i(\mathbf{k})$ of (71) into (68) we can make the cross products of the form $a_1(\mathbf{k})a_1(-\mathbf{k})$ and $a_2(\mathbf{k})a_2(-\mathbf{k})$ vanish by choosing α, β according to the following expressions:

$$\left.\begin{aligned} \alpha &= [k^2(1+\kappa v_0^2-\kappa v^2\cos^2\alpha)]^{-\frac{1}{4}} \\ \beta &= \left[\frac{1+\kappa v_0^2-\kappa v^2\cos^2\alpha}{k^2(1+\kappa)^2}\right]^{\frac{1}{4}}. \end{aligned}\right\} \tag{73}$$

The Hamiltonian (68) reduces then to

$$H_0 = \tfrac{1}{2}\sum_r \int d^3k\,\epsilon_k\{a_r(\mathbf{k})a_r{}^+(\mathbf{k})+a_r{}^+(\mathbf{k})a_r(\mathbf{k})\}, \tag{74}$$

with

$$\epsilon_k = k' = \frac{\kappa v^0(\mathbf{v}\cdot\mathbf{k})+\sqrt{k^2(1+\kappa v_0^2)-\kappa(\mathbf{v}\cdot\mathbf{k})^2}}{1+\kappa v_0^2}. \tag{75}$$

The operator $N_r(\mathbf{k})$ defined by

$$N_r(\mathbf{k})+\tfrac{1}{2} = \tfrac{1}{2}\{a_r(\mathbf{k})a_r{}^+(\mathbf{k})+a_r{}^+(\mathbf{k})a_r(\mathbf{k})\}, \tag{76}$$

is the operator for the photon number associated with the state $(\mathbf{k}, r)$. It has the eigenvalues 0, 1, 2, $\cdots$. The total energy operator is thus diagonal in a representation which makes the $N_r(\mathbf{k})$ diagonal since we have

$$H_0 = \sum_r \int (N_r(\mathbf{k})+\tfrac{1}{2})\epsilon_k d^3k. \tag{77}$$

This last result shows that the quantum theory of this field behaves in every respect like the quantum theory of the radiation field in vacuum. There is one important difference, however. In the expression (75) for ϵ_k there occurs only the positive square root. For the vacuum case this corresponds to the fact that only the quanta with positive energy $k^0 = k'$ contribute to the total

energy. Indeed the expression (75) reduces for $\kappa \to 0$ to k. However, unlike the vacuum case the expression for ϵ_k is no longer positive under all circumstances, on account of the first term. If the velocity of the medium is sufficiently high it may become negative. The critical velocity for which this may occur is obtained from the equation

$$\kappa v^0 vk = (k^2(1+\kappa v_0^2) - \kappa v^2 k^2)^{\frac{1}{2}},$$

or

$$v^2(1+v^2) = (1+\kappa)/\kappa^2. \tag{78}$$

In terms of the ordinary velocity $u = c \cdot (v/(1+v^2)^{\frac{1}{2}})$ this means

$$u = c(1/(1+\kappa)^{\frac{1}{2}}) = c/n. \tag{79}$$

This singularity of the radiation field for a medium velocity larger than the critical one is intimately connected with the occurrence of the Čerenkov radiation. The appearance of negative quanta is necessary in this case because when a particle with velocity greater than c/n is transformed to rest by introducing the coördinate system which moves with the particle, such a particle may spontaneously radiate under emission of quanta corresponding to the Čerenkov radiation. It is well known, however, that for such a process energy and momentum cannot be conserved with positive energy for the quanta. The detailed theory of the Čerenkov radiation will be dealt with in the second part of this paper.

We complete the discussion of the radiation field by calculating also the total momentum of the quanta. An expression for the total momentum may be obtained from a discussion of the canonical energy-momentum tensor

$$T_{\mu\nu} = [\partial \mathfrak{L}/\partial(\partial^\mu \phi^\rho)]\partial_\nu \phi^\rho - g_{\mu\nu}\mathfrak{L}. \tag{80}$$

This expression is not symmetrical in the indices μ and ν. Furthermore, it involves the potentials explicitly. We shall not enter here into the well-known difficulties which arise from the ambiguity of the energy-momentum densities.[5] Here we shall need only the expression for the total energy and the total momentum. We shall assume, moreover, that we are dealing with a Maxwell field where the subsidiary condition $\chi = 0$ holds. For the total momentum we obtain then

$$P_i = \int T_{0i} d^3x = \int \frac{\partial \mathfrak{L}}{\partial(\partial^0 \phi^\rho)} \partial_i \phi^\rho d^3x. \tag{81}$$

We may transform this integral into one which involves only the field quantities $F_i{}^\rho$, $G_{0\rho}$ by adding the term

$$-\frac{\partial \mathfrak{L}}{\partial(\partial^0 \phi^\rho)} \partial^\rho \phi_i = +\partial^\rho \left(\frac{\partial \mathfrak{L}}{\partial(\partial^\rho \phi^0)} \phi_i \right) + 2\partial^\rho \phi_i (g_{\rho 0} - \kappa v_\rho v_0)\chi. \tag{82}$$

The first term on the right may also be written as

$$\partial^\rho \left(\frac{\partial \mathfrak{L}}{\partial(\partial^\rho \phi^0)} \phi_i \right) = \partial^i \left(\frac{\partial \mathfrak{L}}{\partial(\partial^i \phi^0)} \phi_i \right) - (1+\kappa v_0^2)\dot{\chi}.$$

Thus apart from terms proportional to χ and $\dot{\chi}$ the total momentum is given by

$$P_i = \int \frac{\partial \mathfrak{L}}{\partial(\partial^0 \phi^\rho)} F_i{}^\rho d^3x = -\int G_{0\rho} F_i{}^\rho d^3x = -\int \pi_j F_i{}^j d^3x. \tag{83}$$

We note here in passing that the tensor

$$T_{\mu\nu}' = G_{\mu\rho} F_\nu{}^\rho - g_{\mu\nu}\mathfrak{L},$$

is essentially the energy-momentum tensor used by Minkowski[2] in his phenomenological theory of classical electrodynamics.

In momentum space the expression (83) for the total momentum is

$$P_i = \int d^3k k_i (N(\mathbf{k}) + \tfrac{1}{2}). \tag{84}$$

We note in particular that in the rest system the energy of a photon with momentum k is given by $\epsilon_k = k/n$.

[5] For a discussion of these questions see W. Pauli, Relativitätstheorie, Encyklopädie der Math. Wiss. V, 665ff.

PHYSICAL REVIEW VOLUME 74, NUMBER 8 OCTOBER 15, 1948

On the Theory of Diffraction by an Aperture in an Infinite Plane Screen. I

HAROLD LEVINE AND JULIAN SCHWINGER
Lyman Laboratory of Physics, Harvard University, Cambridge, Massachusetts

(Received June 9, 1948)

The diffraction of a scalar plane wave by an aperture in an infinite plane screen is examined theoretically. The wave function at an arbitrary point in space is expressed in terms of its values in the aperture, and constructed so as to vanish on the screen, in accordance with the assumed boundary condition. An integral equation to determine the aperture field is obtained from the continuity requirement for the normal derivative of the wave function on traversing the plane of the aperture. Utilizing the integral equation (whose solution is generally unobtainable), the amplitude of the diffracted spherical wave at large distances from the aperture is exhibited in a form which is stationary with respect to small variations (relative to the correct values) of the aperture fields arising from a pair of incident waves. This expression is independent of the scale of the aperture fields. The transmission cross section of the aperture for a plane wave is found to be simply related to the diffracted amplitude observed in the direction of incidence. The variational formulation is applied in detail for a wave incident normally on a circular aperture. By comparison with the exact results available for this problem, it appears that the use of suitable trial aperture fields in the variational formulation yields approximate, yet accurate, expressions for the diffracted amplitude and transmission cross section over a wide range of frequencies.

1. INTRODUCTION

THE steady-state problem of diffraction by an aperture in an infinite plane screen has attracted attention for many years. Exact solutions are restricted to a few cases where the aperture is of simple geometric shape and may be conveniently described in a coordinate system in which the wave equation is separable; the available theoretical methods for approximating these solutions, and those of other cases, are valid for only a limited range of frequencies or wave-lengths.

The diffraction of waves in a scalar field is considered in treatises on physical optics, after requiring that the wave function vanish on the (perfectly conducting) screen, as befits a rectangular, tangential component of the electric field intensity.[1] A brief description of the approximate and exact theoretical methods follows; these have all been applied in detailed calculations for a circular aperture.

A well-known approximate solution is due to Kirchoff, in which the aperture field is identified with the incident field, and the normal derivative of the wave function is assumed to vanish on the back side of the screen. This procedure is not self-consistent, for the transmitted field so determined from the incident field in the aperture does not vanish on the screen. The results possess a measure of validity only when the aperture dimension is large compared to the wave-length of the vibrations, since then the back side of the screen lies in the shadow and the diffracted field is relatively small; such a condition is amply realized for light diffraction by apertures of macroscopic dimensions.

Another approximate solution is due to Lord Rayleigh,[2] whose results in the case of plane waves incident normally on the screen are applicable when the aperture dimension is small in comparison with the wave-length. The procedure stems from the observation that in the neighborhood of the aperture (at distances from it large in comparison with its dimension, yet small in comparison with the wave-length), the conditions are essentially static, or the same as if the wave-length were infinite. These conditions are described by reference to known solutions for the steady flow of incompressible fluids. The nature of the field at large distances from the aperture is readily determined from the aperture field.

An integral equation formulation of the related mathematical problem of normal acoustic diffraction is described by King.[3] An indication is

[1] According to a form of the Babinet principle (see reference 5), this wave function, appearing in the role of a velocity potential, also describes the diffraction of sound by a rigid disk in the form of the aperture, as well as the radiation of sound by the freely vibrating disk.

[2] Lord Rayleigh, Phil. Mag. **43**, 259 (1897); Sci. Pap. IV, p. 283.

[3] L. V. King, Proc. Roy. Soc. **A153**, 1 (1935).

given of its solution by a method of successive approximations, based on the known solution of the corresponding equations in potential theory. Due to the increasing difficulty of computation in higher approximations, King furnishes only the numerical coefficients of the first few terms in a development of the diffracted amplitude in ascending powers of the characteristic parameter, radius of disk/wave length. Sommerfeld[4] gives a more elegant and detailed mathematical discussion of the integral equation, involving an expansion in characteristic functions and the approximate determination of some of the coefficients; the results also apply for small values of the parameter.

Bouwkamp[5] presents an exact theoretical analysis of the problem of diffraction of a scalar plane wave by a circular aperture, based on the construction of normal solutions of the wave equation, which is separable in oblate spheroidal coordinates. The wave function on the far side of the screen, with the character of a diverging spherical wave at large distances from the aperture, is expanded in an infinite series of these normal solutions (which have the proper symmetry with respect to the plane of the screen, so that the individual terms fulfill the boundary condition on it). The expansion coefficients are determined in the course of satisfying a boundary condition in the aperture. From the amplitude of the asymptotic spherical wave, the energy passing through the aperture is obtained, and then the transmission coefficient, t (transmission cross section/area of aperture), on division by the incident energy flux through the same area. To simplify the numerical calculations, Bouwkamp considers only the case of normal incidence, in which the entire field possesses rotational symmetry. The transmission coefficient is evaluated for a number of wave-lengths in the range $\infty > \lambda/a > 0.6$, where a is the radius of the aperture; at shorter wave-lengths the computations are progressively more difficult, owing to the slow convergence of the series involved.

It is clear from this survey that a general formulation which permits accurate numerical evaluation of the diffracted amplitude and transmission cross section for a wide range of frequencies, is of considerable interest. The purpose of this and a companion paper is to illustrate the utility of variational principles for such calculations. The present paper describes a reformulation of the scalar diffraction problem for an arbitrary aperture in terms of a first variational principle. An important role is assumed by the amplitude of the diffracted spherical wave at large distances from the aperture, expressed in terms of the aperture field. For plane-wave excitation, this quantity is a function of the directions of propagation of the incident wave and of observation for the diffracted wave.

When a plane wave is incident on the aperture from direction (1) and the diffracted wave observed from direction (2), the amplitude obtained is equal to that of a reverse situation, in which the wave is incident in direction (2) and observation made from direction (1). Using this reciprocity relation, the amplitudes are exhibited in a form which is stationary with respect to small variations (relative to the correct values) of the aperture fields arising from the two incident waves. In addition, this expression is independent of the scale of the aperture fields, and is therefore suitable for a first approximation with simple forms of the aperture fields.

From a consideration based on the fact that the energy transmitted through the aperture is the same as that appearing at any remote surface which intersects the plane of the screen, the transmission cross section is recast in appropriate limiting forms at low and high frequencies. From the first of these, the (wave-length)$^{-4}$ proportionality is obtained (as in Rayleigh's theory of diffraction by obstacles small compared to the wave-length), independently of the assumed aperture field, provided the boundary condition at the rim of the screen is satisfied. The second form, on identification of aperture and incident fields, leads to the geometrical optics result, where the cross section is simply the area of the aperture projected on a plane normal to the direction of the incident wave.

Owing to the restricted class of trial aperture fields, in virtue of the imposed boundary condition, the first variational principle is most useful in the low frequency range. Here the

[4] A. Sommerfeld, Ann. d. Physik **42**, 389 (1942).

[5] C. J. Bouwkamp, *Theoretische En Numerieke Behandeling van de Buiging Door Een Ronde Opening* (Dissertation, University of Groningen, 1941); R. D. Spence, J. Acous. Soc. Am. **20**, 380 (1948).

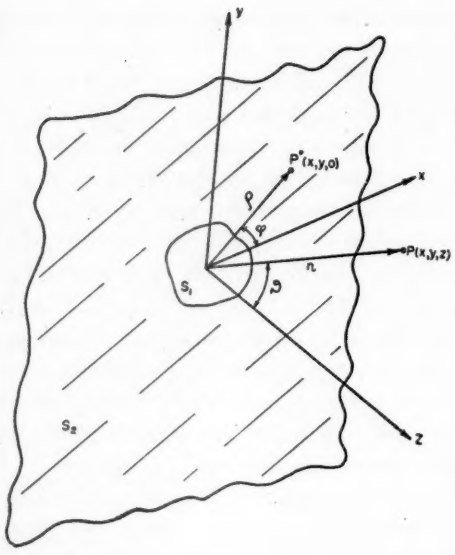

FIG. 1. Diffracting aperture in a plane screen.

qualitative information concerning static aperture fields allows accurate calculations of amplitude and cross section at higher frequencies than are feasible with the existing approximation procedures. Corrections to the geometrical optics result are more difficult to achieve with this formulation. To improve the accuracy of high frequency calculations, a second variational principle for the diffracted amplitude is devised, with details relegated to a separate paper. In this, the discontinuity in normal derivative of the field at the screen (akin to the surface current in the optical problem) replaces the aperture field, although there are additional modifications arising from the infinite extent of the screen. The trial functions adopted for the discontinuity in normal derivative are unrestricted with regard to a boundary condition at the rim of the screen. In particular, the approach to the geometrical optics result with increasing frequency can be well approximated if this function is calculated from the incident field on the illuminated face of the screen.

The distinction between these variational principles in the choice of trial functions is not uniquely related to the boundary condition assumed for the wave function. For a boundary condition which requires that the wave function have vanishing normal derivative at the screen, a pair of analogous variational principles exist, based on (i) the normal derivative of the field in the aperture and (ii) the discontinuity of the field at the screen. Only in the second of these is it necessary to impose a boundary condition on the trial field. Thus it appears that derivatives of the field variable are not restricted by conditions at the boundary of their domain, whereas this is so for the field variables themselves. The reason is that Green's functions and their derivatives, respectively, are factors which naturally accompany these quantities in the formulation, and non-integrable singularities arise in the latter case unless the boundary conditions are satisfied.

To obtain a practical test of the degree of approximation afforded by the variational principles, detailed application is made in this and a companion paper to the evaluation of the transmission coefficient for normal incidence on a circular aperture. Numerical results of the variational and other calculations are compared with the exact values obtained for this problem by Bouwkamp. In addition, the extent to which the two variational principles complement (and agree with) each other for the entire range of frequencies provides a general estimate of their accuracy.

2. INTEGRAL EQUATION FORMULATION FOR AN APERTURE OF ARBITRARY OPENING

We consider an infinitesimally thin plane screen S_2, of infinite extent, which is perforated by an aperture S_1. A rectangular coordinate system is chosen with origin at some point of the aperture, and oriented so that the screen lies in the x,y plane (Fig. 1).

A plane wave is incident upon the aperture in the half-space $z<0$, and it is desired to investigate the diffracted field. The incident wave, propagating in the direction ϑ', φ' (ϑ' measured from the positive direction of the z axis, and φ' from the positive direction of the x axis in the x,y plane) is described by the scalar wave function

$$\phi^{\text{inc}}(\mathbf{r})=\exp(ik\mathbf{n}'\cdot\mathbf{r})=\exp[ik(x\sin\vartheta'\cos\varphi'+y\sin\vartheta'\sin\varphi'+z\cos\vartheta')], \quad (2.1)$$

where $\mathbf{n}'$ is a unit vector in the direction of propagation, $k=2\pi/\lambda$ is the free space propagation constant, and λ the corresponding wave-length. The harmonic time dependence, $\exp(-ikct)$, with

c the velocity of wave propagation, is omitted throughout.

The wave function describing the complete (incident+diffracted) field satisfies the wave equation

$$(\nabla^2+k^2)\phi(\mathbf{r})=0 \tag{2.2}$$

at all points of space, and is subject to the prescribed boundary condition

$$\phi(\mathbf{r})=0, \quad \mathbf{r} \text{ on } S_2; \tag{2.3}$$

in addition, the wave function and its normal (i.e., z) derivative vary continuously on passing through the aperture.

In one method of formulating this boundary value problem, it is convenient to classify the wave functions (2), (3) according to their symmetry in the z coordinate. A symmetric function has vanishing normal derivative in the aperture, whereas an antisymmetric function has the same form as though the aperture were absent. The wave functions of opposite symmetry, appropriate to the incident wave (1), are obtained from the solution of individual boundary value problems in the half-space $z\leqslant 0$; with these we construct, by suitable combination, the wave function in the problem of physical interest.

A solution of the wave equation (2) at any point in the half-space $z\leqslant 0$, which assumes (as yet) arbitrary values in the aperture and satisfies the boundary condition (3) on the remainder of the plane, is given in terms of a Fourier integral,

$$\phi(\mathbf{r})=2i\sin(kz\cos\vartheta')\exp(ik\mathbf{n}'\cdot\boldsymbol{\varrho})$$
$$+\int_{S_1}\int_{\substack{k_x,\,k_y\\=-\infty}}^{\infty}\phi(\mathbf{r}')_{z'=0}\frac{\partial}{\partial z'}\left\{\frac{\exp[i\{k_x(x-x')+k_y(y-y')+(k^2-k_x^2-k_y^2)^{\frac{1}{2}}(z'-z)\}]}{4\pi^2 i(k^2-k_x^2-k_y^2)^{\frac{1}{2}}}\right\}_{z'=0}dk_x dk_y dS', \tag{2.4}$$

where $\boldsymbol{\varrho}$ denotes a position vector in the x,y plane, and dS' an element of area in the x',y' plane. It is readily verified that (4) is a solution of the wave equation; furthermore, on performing the indicated differentiation, we find

$$\phi(\mathbf{r})=2i\sin(kz\cos\vartheta')\exp(ik\mathbf{n}'\cdot\boldsymbol{\varrho})$$
$$+\frac{1}{4\pi^2}\int_{S_1}\int_{\substack{k_x,\,k_y\\=-\infty}}^{\infty}\phi(\mathbf{r}')_{z'=0}\exp[i\{k_x(x-x')+k_y(y-y')-(k^2-k_x^2-k_y^2)^{\frac{1}{2}}z\}]dk_x dk_y dS',$$

and thus, using the integral property of the Dirac delta function,

$$\begin{aligned}\phi(\mathbf{r})_{z=0}&=\frac{1}{4\pi^2}\int_{S_1}\int_{-\infty}^{\infty}\phi(\mathbf{r}')_{z'=0}\exp[i\{k_x(x-x')+k_y(y-y')\}]dk_x dk_y dS'\\&=\int_{S_1}\phi(\mathbf{r}')_{z'=0}\delta(x-x')\delta(y-y')dS'\\&=\phi(\mathbf{r})_{z=0}=\phi(\boldsymbol{\varrho}), \quad \boldsymbol{\varrho} \text{ on } S_1,\\&=0, \quad \boldsymbol{\varrho} \text{ on } S_2,\end{aligned}$$

in accord with the boundary values.

Introducing the free-space scalar Green's function,

$$\begin{aligned}G(\mathbf{r},\mathbf{r}')&=\frac{\exp(ik|\mathbf{r}-\mathbf{r}'|)}{4\pi|\mathbf{r}-\mathbf{r}'|}=\frac{1}{8\pi^3}\int_{-\infty}^{\infty}\frac{\exp[i\{k_x(x-x')+k_y(y-y')+k_z(z-z')\}]}{k_x^2+k_y^2+k_z^2-k^2}dk_x dk_y dk_z\\&=\frac{i}{8\pi^2}\int_{-\infty}^{\infty}\frac{\exp[i\{k_x(x-x')+k_y(y-y')+(k^2-k_x^2-k_y^2)^{\frac{1}{2}}|z-z'|\}]}{(k^2-k_x^2-k_y^2)^{\frac{1}{2}}}dk_x dk_y\end{aligned} \tag{2.5}$$

$$|\mathbf{r}-\mathbf{r}'|=((x-x')^2+(y-y')^2+(z-z')^2)^{\frac{1}{2}},$$

which satisfies the inhomogeneous wave equation,

$$(\nabla^2+k^2)G(\mathbf{r},\mathbf{r}')=-\delta(\mathbf{r}-\mathbf{r}'), \tag{2.6}$$

and the radiation condition,[6] the wave function (4) becomes

$$\phi(\mathbf{r})=2i\sin(kz\cos\vartheta')\exp(ik\mathbf{n}'\cdot\boldsymbol{\varrho})$$
$$-2\int_{S_1}\phi(\boldsymbol{\varrho}')\frac{\partial}{\partial z'}G(\mathbf{r};x',y',0)dS', \quad z\lesseqgtr 0. \tag{2.7}$$

The first term of (7) describes the field in the absence of an aperture, being a superposition of incident and specularly reflected waves, whose phases are adjusted so that the combined wave function vanishes at all points of the screen. We denote this antisymmetric function of z by

$$\phi_{\text{odd}}(\mathbf{r})=2i\sin(kz\cos\vartheta')\exp(ik\mathbf{n}'\cdot\boldsymbol{\varrho}). \tag{2.8}$$

On requiring that the z derivative of the wave function (7) vanish in the aperture, we obtain the integral equation

$$k\cos\vartheta'\exp(ik\mathbf{n}'\cdot\boldsymbol{\varrho})=\int_{S_1}\phi(\boldsymbol{\varrho}')K(\boldsymbol{\varrho},\boldsymbol{\varrho}')dS',$$
$$\boldsymbol{\varrho}\text{ on }S_1, \tag{2.9}$$
$$K(\boldsymbol{\varrho},\boldsymbol{\varrho}')=(\partial/\partial z)(\partial/\partial z')G(x,y,0;x',y',0)$$
$$=K(\boldsymbol{\varrho}',\boldsymbol{\varrho}),$$

for the determination of the aperture field, and the resultant symmetrical function of z,

$$\phi_{\text{even}}(\mathbf{r})=-2i\sin(k|z|\cos\vartheta')\exp(ik\mathbf{n}'\cdot\boldsymbol{\varrho})$$
$$\mp 2\int_{S_1}\phi(\boldsymbol{\varrho}')(\partial/\partial z')G(\mathbf{r};x',y',0)dS'. \tag{2.10}$$

The upper or lower sign in (10) is to be used for $z<0$, $z>0$, respectively, since G is an even function of $z-z'$.

To describe the physical situation arising from the incidence of the plane wave (1) upon the aperture, we combine the antisymmetric and symmetric functions (8), (10). The resulting wave function has different forms on opposite sides of the screen, owing to the asymmetry of excitation; these are

$$\phi^{(+)}(\mathbf{r})=\tfrac{1}{2}[\phi_{\text{odd}}(\mathbf{r})+\phi_{\text{even}}(\mathbf{r})]$$
$$=\int_{S_1}\phi(\boldsymbol{\varrho}')(\partial/\partial z')G(\mathbf{r};x',y',0)dS',$$
$$z\gtrsim 0 \tag{2.11}$$

and

$$\phi^{(-)}(\mathbf{r})=\tfrac{1}{2}[\phi_{\text{odd}}(\mathbf{r})+\phi_{\text{even}}(\mathbf{r})]$$
$$=2i\sin(kz\cos\vartheta')\exp(ik\mathbf{n}'\cdot\boldsymbol{\varrho})$$
$$-\int_{S_1}\phi(\boldsymbol{\varrho}')\frac{\partial}{\partial z'}G(\mathbf{r};x',y',0)dS',$$
$$z\lesssim 0. \tag{2.12}$$

The wave functions (11), (12) vanish on the respective faces of the screen, and are equal at any point of the aperture

$$\phi^{(-)}(\boldsymbol{\varrho})=\tfrac{1}{2}\phi(\boldsymbol{\varrho})=\phi^{(+)}(\boldsymbol{\varrho}),\quad \boldsymbol{\varrho}\text{ on }S_1; \tag{2.13}$$

furthermore, their z derivatives are continuous across the aperture, in consequence of the integral equation (9). In particular, it may be noted that

$$\frac{\partial}{\partial z}\phi^{(+)}(x,y,0)=\frac{1}{2}\frac{\partial}{\partial z}\phi_{\text{odd}}(x,y,0)$$
$$=\frac{\partial}{\partial z}\phi^{\text{inc}}(x,y,0). \tag{2.14}$$

Thus (9), (11), (12) constitute the formal solution of the diffraction problem.

The preceding formulation involves the identity of the two regions $z<0$, $z>0$. An alternative treatment, which is also applicable when such symmetry does not exist, is based on the representation of the field in each region by an appropriate Green's function. The Green's function for our problem, that for a half-space, can be obtained by the method of images, and is

$$\Gamma(\mathbf{r},\mathbf{r}')=G(\mathbf{r},\mathbf{r}')-G(\mathbf{r},\mathbf{r}'-2\mathbf{n}_z\mathbf{n}_z\cdot\mathbf{r}')$$
$$=\Gamma(\mathbf{r}',\mathbf{r}), \tag{2.15}$$
$$\Gamma(x,y,z;x',y',0)=0,$$

where $\mathbf{n}_z$ is a unit vector in the z direction.

We write

$$\phi(\mathbf{r})=\phi^{(+)}(\mathbf{r}),\quad z\gtrsim 0,$$
$$=\phi^{(-)}(\mathbf{r}),\quad z\lesssim 0, \tag{2.16}$$

[6] The radiation condition requires that the Green's function describe outgoing spherical waves; this imposes the restriction $\arg(k^2-k_x^2-k_z^2)^{\frac{1}{2}}\gtrsim 0$.

and consider the application of Green's second scalar identity in the form

$$\int [\Gamma(\mathbf{r}', \mathbf{r})(\nabla'^2+k^2)\phi(\mathbf{r}') - \phi(\mathbf{r}')(\nabla'^2+k^2)\Gamma(\mathbf{r}', \mathbf{r})]d\tau' = \int\left[\Gamma(\mathbf{r}', \mathbf{r})\frac{\partial}{\partial n'}\phi(\mathbf{r}') - \phi(\mathbf{r}')\frac{\partial}{\partial n'}\Gamma(\mathbf{r}', \mathbf{r})\right]dS', \quad (2.17)$$

where the derivative in the surface integral is taken in the direction of the outward normal at each point.

In the half-space $z \gtrless 0$, we find with the use of (2), (3), (6), and (15) in (17), that the wave function at any point assumes the form

$$\phi^{(+)}(\mathbf{r}) = \int_{S_1} \phi^{(+)}(\boldsymbol{\rho}')\frac{\partial}{\partial z'}\Gamma(\mathbf{r}; x', y', 0)dS' = \int_{S_1} \phi(\boldsymbol{\rho}')\frac{\partial}{\partial z'}G(\mathbf{r}; x', y', 0)dS', \quad (2.18)$$

where $\phi^{(+)}(\boldsymbol{\rho}) = \frac{1}{2}\phi(\boldsymbol{\rho})$. On the remote surface which intersects the plane of the screen, $\phi^{(+)}(\mathbf{r})$ and $\Gamma(\mathbf{r}, \mathbf{r}')$ have the character of diverging spherical waves, and the two terms of the integrand cancel. In the half-space $z \lessgtr 0$ of the incident wave, the contribution from the corresponding surface integral supplies just the field in the absence of an aperture; thus

$$\phi^{(-)}(\mathbf{r}) = 2i\sin(kz\cos\vartheta')\exp(ik\mathbf{n}'\cdot\boldsymbol{\rho}) - \int_{S_1} \phi(\boldsymbol{\rho}')\frac{\partial}{\partial z'}G(\mathbf{r}; x', y', 0)dS'. \quad (2.19)$$

The reversal in sign of the integral in (19) as compared to (18) is a consequence of the oppositely directed normal derivatives at the plane of the aperture. Equality of the z derivatives of the functions (18), (19) in the aperture provides an integral equation identical with (9), and completes the formal solution.

We shall confine our attention to the properties of the diffracted field at distances from the aperture large compared to its dimensions and the wave-length, since a rigorous and explicit solution of the integral equation (9) is not in general feasible. For effective use of approximate solutions to the integral equation, we cast the far field amplitude in a form which is stationary with respect to small variations of the aperture fields about their correct values.

On introducing the asymptotic form of the free space Green's function

$$G(\mathbf{r}, \mathbf{r}') \simeq \exp[ik(r-\mathbf{n}\cdot\mathbf{r}')]/4\pi r, \quad \mathbf{n} = \mathbf{r}/r, \quad r\to\infty \quad (2.20)$$

in (11), we obtain the transmitted field in the form of a diverging spherical wave,

$$\phi^{(+)}(\mathbf{r}) \simeq -(ik/4\pi)\cos\vartheta(e^{ikr}/r) \times \int_{S_1} \phi_{\mathbf{n}'}(\boldsymbol{\rho}')\exp(-ik\mathbf{n}\cdot\boldsymbol{\rho}')dS', \quad (2.21)$$

with explicit indication that the aperture field is generated by a wave incident in a definite direction $\mathbf{n}'$. It is clear from (11), (12) that a similar spherical wave appears on the other side of the screen. In terms of the amplitude

$$A(\mathbf{n}, \mathbf{n}') = -(ik/4\pi)\cos\vartheta \times \int_{S_1} \phi_{\mathbf{n}'}(\boldsymbol{\rho})\exp(-ik\mathbf{n}\cdot\boldsymbol{\rho})dS, \quad (2.22)$$

of the spherical wave (21), we have

$$\lim_{r\to\infty} r^2|\phi^{(+)}(\mathbf{r})|^2 = |A(\mathbf{n}, \mathbf{n}')|^2. \quad (2.23)$$

We assume as the expression for the time average energy flux per unit area,

$$\mathbf{S} = Re(1/ik)\phi^*(\mathbf{r})\nabla\phi(\mathbf{r}), \quad (2.24)$$

and verify that this corresponds to dissipationless transport of energy by the waves, for

$$\nabla\cdot\mathbf{S} = Re\nabla\cdot((1/ik)\phi^*(\mathbf{r})\nabla\phi(\mathbf{r})) = Re(1/ik)(|\nabla\phi(\mathbf{r})|^2 - k^2|\phi(\mathbf{r})|^2) = 0. \quad (2.25)$$

Since $(\partial/\partial r)\phi^{(+)}(\mathbf{r}) \sim ik\phi^{(+)}(\mathbf{r})$, $r\to\infty$, we find with the use of (23), (24) that the average power transmitted into the solid angle $d\Omega$, about the direction $\mathbf{n}$ is

$$P(\mathbf{n}, \mathbf{n}')d\Omega = |A(\mathbf{n}, \mathbf{n}')|^2 d\Omega; \quad (2.26)$$

thus, the ratio of the total transmitted power to that falling on the aperture per unit area normal to the direction of the incident wave (transmis-

sion cross section) becomes

$$\sigma(\mathbf{n}')=\int_0^{2\pi}\int_0^{\pi/2}|A(\mathbf{n},\mathbf{n}')|^2\sin\vartheta d\vartheta d\varphi. \quad (2.27)$$

A simpler expression for the transmission cross section can be derived as follows. We note that the power transmitted normally through the aperture is the same as that appearing at any remote surface which intersects the plane of the screen; thus, from (24),

$$\sigma(\mathbf{n}')=Re(1/ik)\int_{S_1}\phi^{(+)*}(\boldsymbol{\rho})(\partial/\partial z)\times\phi^{(+)}(x,y,0)dS. \quad (2.28)$$

(The same result is obtained on integrating (25) in the volume bounded by this surface and the plane $z=0$, and observing that the wave function and its complex conjugate vanish on the screen.) Using (13), (14) the expression (28) becomes

$$\begin{aligned}\sigma(\mathbf{n}')&=\tfrac{1}{2}Re\cos\vartheta'\int_{S_1}\phi_{\mathbf{n}'}{}^*(\boldsymbol{\rho})\exp(ik\mathbf{n}'\cdot\boldsymbol{\rho})dS\\&=-(2\pi/k)Re\,iA(\mathbf{n}',\mathbf{n}')^*\\&=-(2\pi/k)Im\,A(\mathbf{n}',\mathbf{n}'). \quad (2.29)\end{aligned}$$

The transmission cross section is thus proportional to the imaginary part of the amplitude of the transmitted spherical wave observed in the direction of the incident plane wave. A relation of the form (29) holds generally in scattering problems, its physical interpretation being that a decrease in amplitude of the incident wave is consequent to the generation of scattered waves.

3. VARIATIONAL PRINCIPLE FOR DIFFRACTED WAVE AMPLITUDE

If we multiply through in the integral equation (2.9) by $\phi_{\mathbf{n}''}(\boldsymbol{\rho})$ and integrate over the area of the aperture, there results

$$\begin{aligned}&\cos\vartheta'\int_{S_1}\phi_{\mathbf{n}''}(\boldsymbol{\rho})\exp(ik\mathbf{n}'\cdot\boldsymbol{\rho})dS\\&=(1/ik)\int_{S_1}\phi_{\mathbf{n}''}(\boldsymbol{\rho})K(\boldsymbol{\rho},\boldsymbol{\rho}')\phi_{\mathbf{n}'}(\boldsymbol{\rho}')dSdS'. \quad (3.1)\end{aligned}$$

Since the right-hand member of this equation is symmetrical in $\mathbf{n}'$, $\mathbf{n}''$ (or the angular coordinates ϑ', φ', and ϑ'', φ''), division by the left-hand member and a similar term in which $\mathbf{n}'$ and $\mathbf{n}''$ are interchanged, and use of (2.22), yields

$$\frac{1}{A(\mathbf{n}'',\mathbf{n}')}=\frac{1}{A(-\mathbf{n}',-\mathbf{n}'')}=\frac{(4\pi/k^2)\int_{S_1}\phi_{\mathbf{n}'}(\boldsymbol{\rho})K(\boldsymbol{\rho},\boldsymbol{\rho}')\phi_{-\mathbf{n}''}(\boldsymbol{\rho}')dSdS'}{\cos\vartheta'\cos\vartheta''\int_{S_1}\phi_{\mathbf{n}'}(\boldsymbol{\rho})\exp(-ik\mathbf{n}''\cdot\boldsymbol{\rho})dS\int_{S_1}\phi_{-\mathbf{n}''}(\boldsymbol{\rho})\exp(ik\mathbf{n}'\cdot\boldsymbol{\rho})dS}. \quad (3.2)$$

Here $\phi_{-\mathbf{n}}(\boldsymbol{\rho})$ denotes the aperture field generated by a plane wave incident in the direction opposite to $\mathbf{n}$. Equality of the wave amplitudes $A(\mathbf{n}'',\mathbf{n}')$ and $A(-\mathbf{n}',-\mathbf{n}'')$ describes a reciprocity condition for incidence and observation along a pair of directions in space.

The expression (2) is homogeneous in the fields $\phi_{\mathbf{n}'}(\boldsymbol{\rho})$, $\phi_{-\mathbf{n}''}(\boldsymbol{\rho})$ and stationary with respect to independent first-order variations about their correct values (determined by integral equations of the form (2.9)). Thus, on performing such a variation, we obtain

$$\begin{aligned}&\delta A(\mathbf{n}'',\mathbf{n}')\int_{S_1}\phi_{\mathbf{n}'}(\boldsymbol{\rho})K(\boldsymbol{\rho},\boldsymbol{\rho}')\phi_{-\mathbf{n}''}(\boldsymbol{\rho}')dSdS'\\&=\int_{S_1}\delta\phi_{\mathbf{n}'}(\boldsymbol{\rho})dS\Big[(k^2/4\pi)\cos\vartheta'\cos\vartheta''\\&\times\exp(-ik\mathbf{n}''\cdot\boldsymbol{\rho})\int_{S_1}\phi_{-\mathbf{n}''}(\boldsymbol{\rho})\exp(ik\mathbf{n}'\cdot\boldsymbol{\rho})dS\\&-A(\mathbf{n}'',\mathbf{n}')\int_{S_1}K(\boldsymbol{\rho},\boldsymbol{\rho}')\phi_{-\mathbf{n}''}(\boldsymbol{\rho}')dS'\Big]\\&+\int_{S_1}\delta\phi_{-\mathbf{n}''}(\boldsymbol{\rho})dS\Big[(k^2/4\pi)\cos\vartheta'\cos\vartheta''\\&\times\exp(ik\mathbf{n}'\cdot\boldsymbol{\rho})\int_{S_1}\phi_{\mathbf{n}'}(\boldsymbol{\rho})\exp(-ik\mathbf{n}''\cdot\boldsymbol{\rho})dS\\&-A(\mathbf{n}'',\mathbf{n}')\int_{S_1}K(\boldsymbol{\rho},\boldsymbol{\rho}')\phi_{\mathbf{n}'}(\boldsymbol{\rho}')dS'\Big]. \quad (3.3)\end{aligned}$$

If A is stationary for arbitrary variations, the quantities within brackets on the right side of (3) must vanish. From the latter of these we find

$$ik\cos\vartheta' \exp(ik\mathbf{n}'\cdot\varrho)\left[-(ik/4\pi)(\cos\vartheta''/A(\mathbf{n}'',\mathbf{n}'))\int_{S_1}\phi_{\mathbf{n}'}(\varrho)\exp(-ik\mathbf{n}''\cdot\varrho)dS\right]=\int_{S_1}K(\varrho,\varrho')\phi_{\mathbf{n}'}(\varrho')dS'$$

which, with the exception of the (constant) factor in brackets, is just the integral equation (2.9) for $\phi_{\mathbf{n}'}(\varrho)$.[7] Similarly, $\phi_{-\mathbf{n}'}(\varrho)$ obeys a corresponding integral equation.

We next examine the forms assumed by the transmission cross section (Cf. (2.29), (2)),

$$\sigma(\mathbf{n})=-\tfrac{1}{2}k\cos^2\vartheta\, Im\frac{\int_{S_1}\phi_{\mathbf{n}}(\varrho)\exp(-ik\mathbf{n}\cdot\varrho)dS\int_{S_1}\phi_{-\mathbf{n}}(\varrho)\exp(ik\mathbf{n}\cdot\varrho)dS}{\int_{S_1}\phi_{\mathbf{n}}(\varrho)K(\varrho,\varrho')\phi_{-\mathbf{n}}(\varrho')dSdS'},\tag{3.4}$$

in the limits of low and high frequencies, respectively. The frequency expansion of the Green's function,

$$\begin{aligned}G(\mathbf{r},\mathbf{r}')&=\exp(ik|\mathbf{r}-\mathbf{r}'|)/4\pi|\mathbf{r}-\mathbf{r}'|\\&=G_s(\mathbf{r},\mathbf{r}')+(ik/4\pi)-(k^2/8\pi)|\mathbf{r}-\mathbf{r}'|\\&\quad-(ik^3/24\pi)|\mathbf{r}-\mathbf{r}'|^2+O(k^4),\end{aligned}$$

where

$$G_s(\mathbf{r},\mathbf{r}')=1/4\pi|\mathbf{r}-\mathbf{r}'|$$

is the static value, yields

$$\begin{aligned}&K(\varrho,\varrho')\doteq K_s(\varrho,\varrho')+(ik^3/12\pi),\\&K_s(\varrho,\varrho')=(1/4\pi)(\partial/\partial z)(\partial/\partial z')(1/|\mathbf{r}-\mathbf{r}'|)_{z,z'=0}\end{aligned}\tag{3.5}$$

in the lowest order of real and imaginary terms. Thus, in the static limit the integral equation (2.9) becomes

$$ik\cos\vartheta\doteq\int_{S_1}\phi_{\mathbf{n}}(\varrho')K_s(\varrho,\varrho')dS',\tag{3.6}$$

which shows that the corresponding aperture field $\phi_{\mathbf{n}}(\varrho)$ is wholly imaginary and independent of the incident direction, save for the constant factor $\cos\vartheta$. Introducing (5) in (4) and omitting indices as well as scale factors for the aperture fields, we find as the leading term in the frequency expansion of the transmission cross section,

$$\sigma(\mathbf{n})=\frac{k^4}{24\pi}\cos^2\vartheta\frac{\left(\int_{S_1}\phi(\varrho)dS\right)^4}{\left(\int_{S_1}\phi(\varrho)K_s(\varrho,\varrho')\phi(\varrho')dSdS'\right)^2},\qquad k\to 0.\tag{3.7}$$

The frequency (or wave-length) dependence contained in (7) agrees with that of Rayleigh's general theory of diffraction by obstacles small compared to the wave-length. In addition, the correct angular variation of the cross section is secured independently of the form of the aperture field. As remarked in the introduction, the class of admissible trial aperture fields in (7) is restricted to those satisfying the boundary condition (2.3) on the rim of the screen. Additional terms in the frequency expansion of the cross section can be obtained; these, in common with (7), are independent of the scale of the aperture fields.

At high frequencies, we assume as the aperture field

$$\phi_{\mathbf{n}}(\varrho)=\Phi_{\mathbf{n}}(\varrho)\phi_{\mathbf{n}}{}^{\mathrm{inc}}(\varrho)=\Phi_{\mathbf{n}}(\varrho)\exp(ik\mathbf{n}\cdot\varrho),\qquad\phi_{-\mathbf{n}}(\varrho)=\phi_{\mathbf{n}}{}^*(\varrho),\tag{3.8}$$

where $\Phi_{\mathbf{n}}(\varrho)$ is a real function which is slowly varying over distances comparable to the wave-length. Inserting this field and its complex con-

[7] The bracketed term is actually equal to unity, by (2.22), so that the integral equations are identical; however, this is not essential to the argument.

jugate in (4), we obtain

$$\sigma(\mathbf{n})=-\tfrac{1}{2}k\cos^2\vartheta\, Im\frac{\left(\int_{S_1}\Phi_{\mathbf{n}}(\boldsymbol{\varrho})dS\right)^2}{\int_{S_1}\Phi_{\mathbf{n}}(\boldsymbol{\varrho})\exp(ik\mathbf{n}\cdot\boldsymbol{\varrho})K(\boldsymbol{\varrho},\boldsymbol{\varrho}')\Phi_{\mathbf{n}}(\boldsymbol{\varrho}')\exp(-ik\mathbf{n}\cdot\boldsymbol{\varrho}')dSdS'}. \tag{3.9}$$

Employing the Fourier integral representation (2.5), the integral in the denominator of (9) becomes

$$I=\frac{i}{8\pi^2}\int_{S_1}\int_{-\infty}^{\infty}(k^2-k_x^2-k_y^2)^{\frac{1}{2}}\Phi_{\mathbf{n}}(\boldsymbol{\varrho})\Phi_{\mathbf{n}}(\boldsymbol{\varrho}')$$
$$\times\exp[i\{\alpha(x-x')+\beta(y-y')\}]dk_xdk_ydSdS',$$

where

$$\alpha=k\sin\vartheta\cos\varphi+k_x,\quad \beta=k\sin\vartheta\sin\varphi+k_y.$$

As $k\to\infty$, the phase variations of the exponential factors in the integrand occur with increasing rapidity, so that the range of the variables x,y may be extended over the entire plane $z=0$. Introducing

$$x-x'=\xi,\quad y-y'=\eta$$

and ignoring the variations of ξ, η in the argument of $\Phi_{\mathbf{n}}(\boldsymbol{\varrho})$, we find that integration with respect to the new variables leads to

$$I\simeq\frac{i}{2}\int_{S_1}\int_{-\infty}^{\infty}(k^2-k_x^2-k_y^2)^{\frac{1}{2}}\Phi_{\mathbf{n}}^2(\boldsymbol{\varrho}')$$
$$\times\delta(k\sin\vartheta\cos\varphi+k_x)$$
$$\times\delta(k\sin\vartheta\sin\varphi+k_y)dk_xdk_ydS'$$
$$=\frac{i}{2}k\cos\vartheta\int_{S_1}\Phi_{\mathbf{n}}^2(\boldsymbol{\varrho})dS,$$

and finally,

$$\sigma(\mathbf{n})=\cos\vartheta\frac{\left(\int_{S_1}\Phi_{\mathbf{n}}(\boldsymbol{\varrho})dS\right)^2}{\int_{S_1}\Phi_{\mathbf{n}}^2(\boldsymbol{\varrho})dS},\quad k\to\infty. \tag{3.10}$$

The expression (10) is stationary for first-order variations of the function $\Phi_{\mathbf{n}}(\boldsymbol{\varrho})$ about a constant value, the cross section being equal to the projected area of the aperture on a plane normal to the direction of the incident wave. This corresponds to the limit of geometrical optics, in which the aperture field is identified with the incident field, and the energy falling on the aperture is transmitted without diffraction effects. By appealing to the Schwarz inequality, it follows that the cross section obtained from (10) with any other form of the function $\Phi_{\mathbf{n}}(\boldsymbol{\varrho})$ is necessarily smaller than the geometrical optics result. The representation of the cross section by an asymptotic series in reciprocal powers of k requires a more elaborate analysis.

4. DIFFRACTION BY A CIRCULAR APERTURE

In this section we illustrate the utility of the variational formulation by applying it to the case of normal incidence of a plane wave on a circular aperture. We calculate, in particular, the transmission coefficient t of the aperture as a function of the characteristic parameter,

$$ka=2\pi(\text{radius of aperture})/(\text{wave-length}).$$

The expression (3.2) for the diffracted amplitude A observed in the direction of incidence ($\vartheta=0$) involves a single aperture field; on introducing polar coordinates ρ, φ in the plane of the aperture (with origin at its center), and noting that the common aperture field is independent of φ, we obtain

$$A=\frac{(k^2/4\pi)\left(\int_{S_1}\phi(\rho)\rho d\rho d\varphi\right)^2}{\int_{S_1}\phi(\rho)K(\boldsymbol{\varrho},\boldsymbol{\varrho}')\phi(\rho')\rho d\rho d\varphi\rho' d\rho' d\varphi'}. \tag{4.1}$$

To evaluate A we expand the aperture field in the complete set of functions (see Appendix 1 and reference 4),

$$\phi(\rho)=\sum_{n=1}^{\infty}A_n(1-(\rho^2/a^2))^{n-\frac{1}{2}} \tag{4.2}$$

where the A_n are arbitrary coefficients; the individual terms of this expansion satisfy the boundary condition (2.3) on the rim of the screen. We define

$$B_n=\int_{S_1}(1-(\rho^2/a^2))^{n-\frac{1}{2}}\rho d\rho d\varphi$$
$$=2\pi a^2/(2n+1), \quad (4.3)$$

and

$$C_{mn}=\int_{S_1}(1-(\rho^2/a^2))^{m-\frac{1}{2}}K(\varrho,\varrho')(1-(\rho'^2/a^2))^{n-\frac{1}{2}}$$
$$\times\rho d\rho d\varphi\rho' d\rho' d\varphi'=C_{nm}; \quad (4.4)$$

thus (1) becomes

$$A\sum_{m,n=1}^{\infty}A_mA_nC_{mn}=(k^2/4\pi)(\sum_{n=1}^{\infty}A_nB_n)^2. \quad (4.5)$$

On differentiating (5) with respect to A_m, it follows, in view of the stationary character of A, that[8]

$$A\sum_{n=1}^{\infty}A_nC_{mn}=(k^2/4\pi)B_m\sum_{n=1}^{\infty}A_nB_n,$$
$$m=1,\cdots. \quad (4.6)$$

We next define a set of coefficients D_n by the relation

$$A_n=(k^2/4\pi A)D_n\sum_{n=1}^{\infty}A_nB_n \quad (4.7)$$

and find, on multiplying through by B_n, and summing over n,

$$A=(k^2/4\pi)\sum_{n=1}^{\infty}B_nD_n. \quad (4.8)$$

Finally, by inserting (7) in (6), we obtain the infinite set of inhomogeneous linear equations to determine the coefficients D_n,

$$\sum_{n=1}^{\infty}C_{mn}D_n=B_m, \quad m=1,\cdots \quad (4.9)$$

with which to calculate A from (8).

A rigorous solution of (9) is not attempted; rather, we reduce these to a finite set of linear equations by placing B_n, $D_n=0$, $n>N$. The corresponding approximation to A is given by

$$A^{(N)}=(k^2/4\pi)\sum_{n=1}^{N}B_nD_n, \quad (4.10)$$

where

$$\sum_{n=1}^{N}C_{mn}D_n=B_m, \quad m=1,\cdots,N. \quad (4.11)$$

It will now be demonstrated that a few terms of (10) suffice to give a very accurate approximation to A. For this purpose we require explicit knowledge of the quantities B_n, C_{mn}. B_n is obtained directly from (3); to determine C_{mn} we make use of the integral representation for the free-space Green's function,[9]

$$\frac{\exp(ik|\mathbf{r}-\mathbf{r}'|)}{4\pi|\mathbf{r}-\mathbf{r}'|}=\frac{1}{4\pi}\int_0^{\infty}J_0(\zeta R)$$
$$\times\frac{\zeta\exp[-(\zeta^2-k^2)^{\frac{1}{2}}(z-z')]}{(\zeta^2-k^2)^{\frac{1}{2}}}d\zeta, \quad z-z'\geqslant 0, \quad (4.12)$$
$$R=(\rho^2+\rho'^2-2\rho\rho'\cos(\varphi-\varphi'))^{\frac{1}{2}},$$

where J_0 denotes the Bessel function of order zero, and the path of integration avoids the singularity $\zeta=k$ by an indentation below the singular point, and

$$\arg(\zeta^2-k^2)^{\frac{1}{2}}=0, \ \zeta>k; \ =-\pi/2, \ \zeta<k.$$

Inserting (12) in (4), and employing the addition theorem for Bessel functions,

$$J_0(\zeta R)=\sum_{n=0}^{\infty}(2-\delta_{0n})J_n(\zeta\rho)J_n(\zeta\rho')\cos n(\varphi-\varphi'),$$
$$\delta_{pq}=\begin{cases}0, & p\neq q\\ 1, & p=q\end{cases} \quad (4.13)$$

we find, on performing the angular integrations,

$$C_{mn}=-\pi\int_0^{\infty}\zeta(\zeta^2-k^2)^{\frac{1}{2}}d\zeta\int_0^a\rho\left(1-\frac{\rho^2}{a^2}\right)^{m-\frac{1}{2}}$$
$$\times J_0(\zeta\rho)d\rho\int_0^a\rho'\left(1-\frac{\rho'^2}{a^2}\right)^{n-\frac{1}{2}}J_0(\zeta\rho')d\rho'.$$

[8] We use a symmetrical formulation, although it is only the relative amplitudes A_n/A_1 that are important for the variational calculation.

[9] G. N. Watson, *A Treatise on the Theory of Bessel Functions* (Cambridge University Press, Teddington, 1945), p. 416.

With the change of variables

$$\rho = a\sin\vartheta, \quad \rho' = a\sin\vartheta',$$

and use of Sonine's first finite integral,[10]

$$\int_0^{\pi/2} J_\mu(z\sin\vartheta)\sin^{\mu+1}\vartheta\cos^{2\nu+1}\vartheta d\vartheta = 2^\nu\Gamma(\nu+1)z^{-(\nu+1)}J_{\mu+\nu+1}(z),\ Re\mu,\ \nu > -1, \quad (4.14)$$

we obtain

$$C_{mn} = -2\pi a(2/ka)^{m+n-2}\Gamma(m+\tfrac{1}{2})\Gamma(n+\tfrac{1}{2}) \times\int_0^\infty v^{-(m+n)}(v^2-1)^{\frac{1}{2}}J_{m+\frac{1}{2}}(kav) \times J_{n+\frac{1}{2}}(kav)dv. \quad (4.15)$$

The integral

$$F_{mn}(\alpha) = \int_0^\infty v^{-(m+n)}(v^2-1)^{\frac{1}{2}} \times J_{m+\frac{1}{2}}(\alpha v)J_{n+\frac{1}{2}}(\alpha v)dv \quad (4.16)$$

can be reduced to a suitable form for numerical evaluation. An indication of this procedure, which is the more laborious for large values of m,n, is given in Appendix 2.

Resolving $F_{mn}(\alpha)$ into real and imaginary parts,

$$F_{mn}(\alpha) = R_{mn}(\alpha) - iI_{mn}(\alpha), \quad (4.17)$$

where

$$I_{mn}(\alpha) = \int_0^1 v^{-(m+n)}(1-v^2)^{\frac{1}{2}} \times J_{m+\frac{1}{2}}(\alpha v)J_{n+\frac{1}{2}}(\alpha v)dv \quad (4.18)$$

and

$$R_{mn}(\alpha) = \int_1^\infty v^{-(m+n)}(v^2-1)^{\frac{1}{2}} \times J_{m+\frac{1}{2}}(\alpha v)J_{n+\frac{1}{2}}(\alpha v)dv, \quad (4.19)$$

we find, for the first few values of m, n,

$$I_{11}(\alpha) = \frac{\alpha}{2\pi} - \frac{1}{4\pi\alpha} + \frac{1}{8\alpha^2}S_0(2\alpha) - \frac{1}{16\alpha^3}\int_0^{2\alpha} S_0(t)dt - \frac{1}{4\alpha}\int_0^{2\alpha} t^{-1}S_1(t)dt,$$

$$I_{12}(\alpha) = \frac{\alpha^2}{9\pi} - \frac{1}{4\pi} - \frac{3}{8\pi\alpha^2} + \frac{3}{16\alpha^3}S_0(2\alpha) + \frac{1}{8\alpha^2}S_1(2\alpha) + \frac{1}{8\alpha^2}\left(1-\frac{3}{4\alpha^2}\right)\int_0^{2\alpha} S_0(t)dt - \frac{1}{4\alpha^2}\int_0^{2\alpha} t^{-1}S_1(t)dt,$$

$$I_{22}(\alpha) = \frac{\alpha^3}{36\pi} - \frac{\alpha}{12\pi} + \frac{3}{32\pi\alpha} - \frac{45}{64\pi\alpha^3} - \frac{9}{32\alpha^2}\left(1-\frac{5}{4\alpha^2}\right)S_0(2\alpha) + \frac{1}{16\alpha}\left(1+\frac{9}{2\alpha^2}\right)S_1(2\alpha) - \frac{1}{16\alpha}\left(1-\frac{21}{4\alpha^2}+\frac{45}{16\alpha^4}\right)\int_0^{2\alpha} S_0(t)dt - \frac{27}{64\alpha^3}\int_0^{2\alpha} t^{-1}S_1(t)dt,$$

$$R_{11}(\alpha) = \frac{1}{4\alpha}\left(1+\frac{1}{4\alpha^2}\right)\int_0^{2\alpha} J_0(t)dt - \frac{1}{8\alpha^2}J_0(2\alpha) - \frac{1}{4\alpha}J_1(2\alpha),$$

$$R_{12}(\alpha) = \frac{1}{8\alpha^2}\left(1+\frac{3}{4\alpha^2}\right)\int_0^{2\alpha} J_0(t)dt - \frac{3}{16\alpha^3}J_0(2\alpha) - \frac{3}{8\alpha^2}J_1(2\alpha),$$

$$R_{22}(\alpha) = \frac{1}{16\alpha}\left(1+\frac{3}{2\alpha^2}+\frac{45}{16\alpha^4}\right)\int_0^{2\alpha} J_0(t)dt + \frac{9}{32\alpha^2}\left(1-\frac{5}{4\alpha^2}\right)J_0(2\alpha) - \frac{1}{16\alpha}\left(1+\frac{45}{4\alpha^2}\right)J_1(2\alpha).$$

In these expressions S_0, S_1 and J_0, J_1 denote the zero- and first-order Struve and Bessel functions, respectively.

With this information relating to B_n, C_{mn}, we return to (10), (11) and prepare for the detailed evaluation of the first two approximations to the

[10] See reference 9, p. 373.

transmission coefficient. With $N=2$, we find

$$A^{(2)}=\frac{k^2}{4\pi}\left[\frac{B_1^2}{C_{11}}+\frac{(B_2C_{11}-B_1C_{12})^2}{C_{11}(C_{11}C_{22}-C_{12}^2)}\right] \\ =A^{(1)}+\frac{k^2}{4\pi}\frac{(B_2C_{11}-B_1C_{12})^2}{C_{11}(C_{11}C_{22}-C_{12}^2)}; \tag{4.20}$$

thus, using (2.29),

$$t^{(2)}=-\frac{2}{ka^2}ImA^{(2)} \\ =-\frac{k}{2\pi a^2}Im\left[\frac{B_1^2}{C_{11}}+\frac{(B_2C_{11}-B_1C_{12})^2}{C_{11}(C_{11}C_{22}-C_{12}^2)}\right] \\ =t^{(1)}-\frac{k}{2\pi a^2}Im\left[\frac{(B_2C_{11}-B_1C_{12})^2}{C_{11}(C_{11}C_{22}-C_{12}^2)}\right]. \tag{4.21}$$

Inserting the expressions for B_1, B_2, C_{11}, C_{12} and C_{22} in (21), it follows that

$$t^{(1)}=\frac{4}{9\pi}kaIm\frac{1}{F_{11}(ka)} \\ =\frac{4}{9\pi}ka\frac{I_{11}(ka)}{(I_{11}(ka))^2+(R_{11}(ka))^2}, \tag{4.22}$$

and

$$t^{(2)}=\frac{4}{9\pi}kaIm\frac{F_{22}(ka)-\frac{2}{5}kaF_{12}(ka)+(1/25)(ka)^2F_{11}(ka)}{F_{11}(ka)F_{22}(ka)-F_{12}^2(ka)}. \tag{4.23}$$

Numerical values of the transmission coefficients $t^{(1)}$, $t^{(2)}$ are given in Fig. 2, for the interval $0<ka<10$, together with exact values calculated by Bouwkamp. The approximation $t^{(1)}$, based on the aperture field $\phi^{(1)}(\rho)=[1-(\rho^2/a^2)]^{\frac{1}{2}}$ (a constant factor is of no importance here), exhibits considerable accuracy if $0<ka<2.5$. Using the expansions

$$I_{11}(\alpha)=\frac{2\alpha^3}{27\pi}-\frac{4\alpha^5}{675\pi}+\frac{16\alpha^7}{55125\pi}-\cdots, \\ R_{11}(\alpha)=\frac{1}{3}-\frac{\alpha^2}{15}+\frac{\alpha^4}{140}-\cdots$$

(see Appendix 2) in (22), we obtain the transmission coefficient in a form appropriate to small values of ka:

$$t^{(1)}=(8/27\pi^2)(ka)^4[1+0.32(ka)^2 \\ +0.049061(ka)^4+\cdots]. \tag{4.24}$$

The Rayleigh approximation, comprising the first term of (24), is obtained by determining the magnitude of $\phi^{(1)}(\rho)$ in the low frequency limit (see Appendix 1); its restricted range of validity is evident from Fig. 2.

On comparing (24) with Bouwkamp's result,

$$t=(8/27\pi^2)(ka)^4[1+0.32(ka)^2 \\ +0.027427(ka)^4 \\ -0.004393(ka)^6+\cdots], \tag{4.25}$$

we note that the numerical coefficients of the first two terms in the expansion of $t^{(1)}$ coincide with the exact values.[11]

The approximation $t^{(2)}$, derived from an aperture field of the form

$$\phi^{(2)}(\rho)=A_1(1-\rho^2/a^2)^{\frac{1}{2}}+A_2(1-\rho^2/a^2)^{\frac{3}{2}},$$

holds exactly for values of ka ranging up to 4.5. The expansion of $t^{(2)}$ in powers of ka,

$$t^{(2)}=(8/27\pi^2)(ka)^4[1+0.32(ka)^2 \\ +0.047823(ka)^4+\cdots], \tag{4.26}$$

differs almost negligibly from $t^{(1)}$ in the numerical coefficient of the $(ka)^4$ term (within brackets), as can be anticipated from Fig. 2. This behavior indicates that successive variational approximations yield improved values for the entire set of coefficients in similar expansions.

It is of interest to examine the behavior of the approximations $t^{(1)}$, $t^{(2)}$ at high frequencies, where the correct transmission coefficient tends to the value unity. Using the asymptotic forms

$$I_{11}(\alpha)\simeq\alpha/2\pi,\quad I_{12}(\alpha)\simeq\alpha^2/9\pi,\quad I_{22}(\alpha)\simeq\alpha^3/2\pi, \\ R_{11}(\alpha),\quad R_{12}(\alpha),\quad R_{22}(\alpha)\simeq 0,\quad \alpha\to\infty$$

(see Appendix 2), in (22), (23) it follows that

$$t^{(1)}\simeq(4/9\pi)(ka/I_{11}(ka))\simeq(8/9),\quad ka\to\infty \tag{4.27}$$

[11] Equation (36) of King's paper (reference 3) is given incorrectly, and should be replaced by

$$\chi\simeq\frac{2}{3\pi}ika^3\left[1+\left(\frac{1}{5}-\frac{\sin^2\vartheta}{10}\right)(ka)^2-\frac{2i}{9\pi}(ka)^3\right]\cos\vartheta\frac{e^{ikr}}{r};$$

the corresponding asymptotic form of the diffracted wave on the far side of the screen is, to terms of relative order $(ka)^2$, (in our notation)

$$\phi^{(+)}(\mathbf{r})\simeq-(2/3\pi)k^2a^3\left[1+\left(\frac{1}{5}-\frac{\sin^2\vartheta}{10}\right)(ka)^2\right]\cos\vartheta\frac{e^{ikr}}{r}.$$

From this we find

$$t=\frac{2}{a^2}\int_0^{\pi/2}r^2|\phi^{(+)}(\mathbf{r})|^2\sin\vartheta d\vartheta=(8/27\pi^2)(ka)^4 \\ \times[1+(8/25)(ka)^2],$$

in agreement with (24), (25).

and

$$t^{(2)}\simeq\frac{4}{9\pi}ka\frac{I_{22}(ka)-(2/5)kaI_{12}(ka)+(1/25)(ka)^2I_{11}(ka)}{I_{11}(ka)I_{22}(ka)-I_{12}^2(ka)}\simeq\frac{24}{25}. \tag{4.28}$$

In general, the asymptotic values of the high frequency approximations to the transmission coefficient are more conveniently obtained by use of (3.10). Recalling the expansion (2), and defining

$$B_n=\int_{S_1}(1-\rho^2/a^2)^{n-\frac{1}{2}}\rho d\rho d\varphi=2\pi a^2/(2n+1),$$

$$C_{mn}=\int_{S_1}(1-\rho^2/a^2)^{m+n-1}\rho d\rho d\varphi=\pi a^2/(m+n),$$

we find, as in the derivation of (10),

$$t^{(N)}=2\sum_{n=1}^{N}D_n/(2n+1),\quad ka\to\infty \tag{4.29}$$

where

$$\sum_{n=1}^{N}D_n/(m+n)=2/(2m+1),\qquad m=1,\cdots,N. \tag{4.30}$$

With the latter relations we readily obtain the values of $t^{(1)}$, $t^{(2)}$ given in (27), (28); moreover, it appears that for the Nth approximation,

$$t^{(N)}\simeq 1-[1/(2N+1)^2],\quad ka\to\infty. \tag{4.31}$$

For purposes of comparison, the transmission coefficient on the basis of the Kirchoff approximation is also included in Fig. 2. The wave function here is obtained by identifying the aperture field with the (constant) incident field,

$$\phi_K^{(+)}(\mathbf{r})=2\int_{S_1}\frac{\partial}{\partial z'}G(\mathbf{r};x',y',0)dS', \tag{4.32}$$

and the transmission coefficient turns out to be

$$t_K=1+J_1(2ka)/ka-(1/ka)\int_0^{2ka}J_0(t)dt \tag{4.33}$$
$$\simeq 1,\quad ka\gg 1,$$
$$\simeq(ka)^2/6,\quad ka\ll 1.$$

An improvement of the Kirchoff result (33) at low frequencies cannot be obtained from the variational formulation by using a constant aperture field. The reason is that this field violates the boundary condition (2.3) on the rim of the screen, and the multiple integral in (1) involving a product of such functions together with $K(\varrho,\varrho')$ diverges. The correct field at high frequencies is constant over most of the area of the aperture, with variations confined to a distance of the order of a wave-length from the rim; it is only in the limit of vanishing wave-length that the boundary condition for the aperture field is relaxed.

The assistance of Miss J. Klimas and Mrs. D. Abkowitz with numerical calculations is gratefully acknowledged. This work was supported in part by the Office of Naval Research Contract N5ori-76, T.O.I.

APPENDIX I.

Solution of the Integral Equation (2.9) for Normal Incidence on a Circular Aperture

On employing the differential equation (2.6) satisfied by the space Green's function, the integral equation for normal incidence,

$$ik=-\int_{S_1}\phi(\rho')(\partial^2/\partial z^2)G(\rho,\varphi,0;\rho',\varphi',0)\rho'd\rho'd\varphi' \tag{A.1}$$

may be written

$$\left(\frac{1}{\rho}\frac{d}{d\rho}\rho\frac{d}{d\rho}+k^2\right)\int_0^a\phi(\rho')\bar{G}(\rho,\rho')\rho'd\rho'=ik, \tag{A.2}$$

where

$$\bar{G}(\rho,\rho')=\int_0^{2\pi}G(\rho,\varphi,0;\rho',\varphi',0)d\varphi,$$

$$G(\rho,\varphi,0;\rho',\varphi',0)=\frac{\exp[ik(\rho^2+\rho'^2-2\rho\rho'\cos(\varphi-\varphi'))^{\frac{1}{2}}]}{4\pi(\rho^2+\rho'^2-2\rho\rho'\cos(\varphi-\varphi'))^{\frac{1}{2}}}.$$

Integrating (2) as an inhomogeneous Bessel differential equation, we find

$$\int_0^a\phi(\rho')\bar{G}(\rho,\rho')\rho'd\rho'=(i/k)+AJ_0(k\rho), \tag{A.3}$$

with the linearly independent function $N_0(k\rho)$ absent, by virtue of its singularity for $\rho=0$. The integration constant A is conveniently obtained from (3) on taking $\rho=0$; thus

$$A=-(i/k)+\tfrac{1}{2}\int_0^a\phi(\rho)\exp(ik\rho)d\rho. \tag{A.4}$$

In order to solve the integral equation (3), we construct an expansion of $\bar{G}(\rho,\rho')$ in terms of a product of orthogonal functions which form a complete set in the region of the

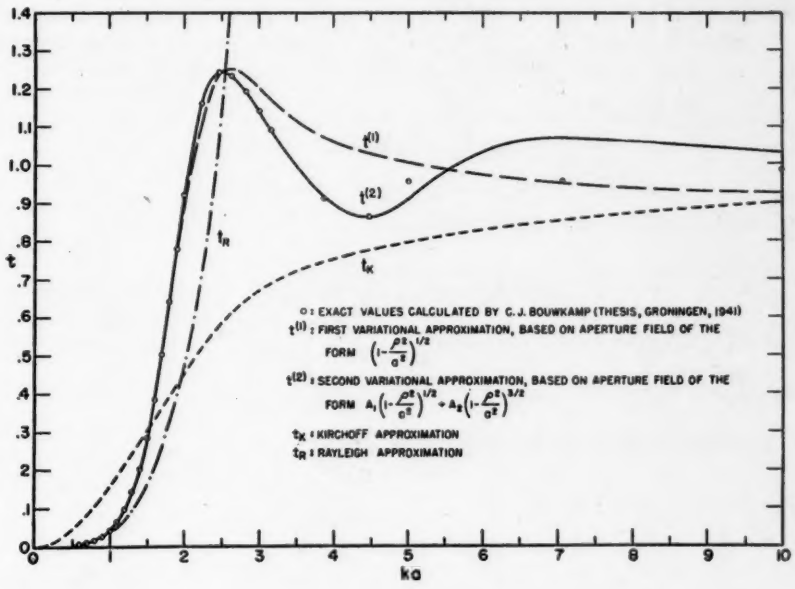
t
ka
$t^{(1)}$
$t^{(2)}$
t_R
t_K
○ : EXACT VALUES CALCULATED BY C. J. BOUWKAMP (THESIS, GRONINGEN, 1941)
$t^{(1)}$: FIRST VARIATIONAL APPROXIMATION, BASED ON APERTURE FIELD OF THE FORM $\left(1-\frac{\rho^2}{a^2}\right)^{1/2}$
$t^{(2)}$: SECOND VARIATIONAL APPROXIMATION, BASED ON APERTURE FIELD OF THE FORM $A_1\left(1-\frac{\rho^2}{a^2}\right)^{1/2}+A_2\left(1-\frac{\rho^2}{a^2}\right)^{3/2}$
t_K : KIRCHOFF APPROXIMATION
t_R : RAYLEIGH APPROXIMATION

FIG. 2. Transmission coefficient of circular aperture for normally incident plane waves, as a function of the parameter $ka=2\pi$(radius of aperture/wavelength). Scalar wave function assumed to vanish on the screen.

aperture, $0\leqslant\rho\leqslant a$. This representation is facilitated by the change of variable $\rho=a\sin\xi$, whence (3) takes the form

$$\int_0^{\pi/2}\phi(a\sin\xi')\bar{G}(\xi,\xi')\cos\xi'\sin\xi'd\xi' = (i/ka^2)+(A/a^2)J_0(ka\sin\xi). \quad (A.5)$$

Referring to (2.5) we find, on introducing $k_x=\kappa\cos\psi$, $k_y=\kappa\sin\psi$, along with $x=a\sin\xi\cos\varphi$, $y=a\sin\xi\sin\varphi$ (and similarly for x', y'),

$$\frac{\exp[ika(\sin^2\xi+\sin^2\xi'-2\sin\xi\sin\xi'\cos(\varphi-\varphi'))^{\frac{1}{2}}]}{4\pi(\sin^2\xi+\sin^2\xi'-2\sin\xi\sin\xi'\cos(\varphi-\varphi'))^{\frac{1}{2}}} = \frac{i}{8\pi^2}\int_0^{2\pi}d\psi\int_0^{\infty}\frac{\kappa d\kappa}{((ka)^2-\kappa^2)^{\frac{1}{2}}}\exp[i\kappa\sin\xi\cos(\varphi-\psi) - i\kappa\sin\xi'\cos(\varphi'-\psi)].$$

From the plane wave expansion in normalized Legendre functions,

$$\exp(ix\cos\Theta)=\sum_{l=0}^{\infty}i^l(2l+1)j_l(x)P_l(\cos\Theta)$$

$$=2\sum_{l=0}^{\infty}\sum_{m=-l}^{l}i^l j_l(x)P_l^m(\cos\xi) \times P_l^m(\cos\xi')\exp[im(\varphi-\varphi')],$$

$$\cos\Theta=\cos\xi\cos\xi'+\sin\xi\sin\xi'\cos(\varphi-\varphi'),$$
$$j_l(x)=(\pi/2x)^{\frac{1}{2}}J_{l+\frac{1}{2}}(x)$$

$$\int_0^{\pi}P_l^m(\cos\xi)P_{l'}^m(\cos\xi)\sin\xi d\xi=\delta_{ll'},$$

we obtain, with $\xi'=\pi/2$,

$$\exp[ix\sin\xi\cos(\varphi-\varphi')]=2\sum_{l=0}^{\infty}\sum_{m=-l}^{l}i^l j_l(x)P_l^m(0) \times P_l^m(\cos\xi)\exp[im(\varphi-\varphi')]. \quad (A.7)$$

Inserting a pair of the latter type expansions in (6), and performing the integration with respect to ψ, it follows that

$$\frac{\exp[ika(\sin^2\xi+\sin^2\xi'-2\sin\xi\sin\xi'\cos(\varphi-\varphi'))^{\frac{1}{2}}]}{4\pi(\sin^2\xi-\sin^2\xi'-2\sin\xi\sin\xi'\cos(\varphi-\varphi'))^{\frac{1}{2}}}$$

$$=\frac{i}{\pi}\sum_{l,l'=0}^{\infty}\sum_{m=-l}^{l}(i)^{l-l'}P_l^m(0)P_{l'}^m(0)P_l^m(\cos\xi) \times P_{l'}^m(\cos\xi')\exp[im(\varphi-\varphi')] \cdot\int_0^{\infty}\kappa((ka)^2-\kappa^2)^{-\frac{1}{2}}j_l(\kappa)j_{l'}(\kappa)d\kappa, \quad (A.8)$$

and finally

$$\bar{G}(\xi,\xi')=\frac{2i}{a}\sum_{l,l'=0}^{\infty}(-)^{l-l'}A_{ll'}P_{2l}(0)P_{2l'}(0) \times P_{2l}(\cos\xi)P_{2l'}(\cos\xi'),$$

$$A_{ll'}=\int_0^{\infty}\kappa((ka)^2-\kappa^2)^{-\frac{1}{2}}j_{2l}(\kappa)j_{2l'}(\kappa)d\kappa. \quad (A.9)$$

By contour integration, it may be shown that

$$A_{ll'}=\int_0^{ka}\kappa((ka)^2-\kappa^2)^{\frac{1}{2}}j_{2l}(\kappa)h_{2l'}^{(1)}(\kappa)d\kappa, \quad l'\leqslant l,$$

$$h_l^{(1)}(x)=(\pi/2x)^{\frac{1}{2}}(j_l(x)+in_l(x));$$

the latter form is suitable for the development of $A_{ll'}$ in powers of ka. In particular, as $ka\to 0$,

$$A_{ll'}\doteq-[\pi i/2][\delta_{ll'}/(4l+1)],$$

and (9) reduces to a summation with a single index.

The representation (9) in terms of an orthogonal set of Legendre polynomials for the interval $0\leqslant\xi\leqslant\pi/2$,

$$\int_0^{\pi/2}P_{2l}(\cos\xi)P_{2l'}(\cos\xi)\sin\xi d\xi=\tfrac{1}{2}\delta_{ll'} \quad (A.10)$$

permits the solution of (5) by an expansion in these functions, provided a similar expansion of the inhomogeneous term $J_0(ka\sin\xi)$ is known. Thus, we write

$$\phi(a\sin\xi)\cos\xi=\sum_{l=0}^{\infty}B_l P_{2l}(\cos\xi)/P_{2l}(0), \quad (A.11)$$

where the relation ($\xi=\pi/2$)

$$\sum_{l=0}^{\infty} B_l=0 \tag{A.12}$$

eliminates a singularity of the field on the rim of the screen. Placing $\varphi'=0$ in (7), and integrating with respect to φ,

$$\int_0^{2\pi} \exp[ix\sin\xi\cos\varphi]d\varphi=2\pi J_0(x\sin\xi)$$

$$=4\pi\sum_{l=0}^{\infty}(-)^l j_{2l}(x)P_{2l}(0)P_{2l}(\cos\xi),$$

which provides the desired expansion,

$$J_0(x\sin\xi)=\sum_{l=0}^{\infty} C_l P_{2l}(0)P_{2l}(\cos\xi),\quad C_l=2(-)^l j_{2l}(x). \tag{A.13}$$

Inserting (9), (11), (13) in (5), and using (10), we obtain

$$\sum_{l,l'=0}^{\infty}(-)^{l-l'}A_{ll'}B_{l'}P_{2l}(0)P_{2l}(\cos\xi)$$

$$=(1/ka)-(iA/a)J_0(ka\sin\xi)$$

$$=\sum_{l=0}^{\infty}[(2/ka)\delta_{l0}-(iA/a)C_l]P_{2l}(0)P_{2l}(\cos\xi),$$

and by identifying the coefficients of $P_{2l}(\cos\xi)$,

$$\sum_{l'=0}^{\infty}(-)^{l-l'}A_{ll'}B_{l'}=(2/ka)\delta_{l0}-(iA/a)C_l. \tag{A.14}$$

From (4),

$$A=-(i/k)+(a/2)\int_0^{\pi/2}\phi(a\sin\xi)\cos\xi\exp(ika\sin\xi)d\xi,$$

whence, using (11),

$$A=-\frac{i}{k}+a\sum_{l=0}^{\infty}B_l D_l, \tag{A.15}$$

$$D_l=(1/2P_{2l}(0))\int_0^{\pi/2}P_{2l}(\cos\xi)\exp(ika\sin\xi)d\xi.$$

Substituting (15) in (14), we arrive at the set of inhomogeneous linear equations to determine the expansion coefficients B_l in (11):

$$\sum_{l'=0}^{\infty}B_{l'}[(-)^{l-l'}A_{ll'}+iC_lD_{l'}]=(2/ka)\delta_{l0}-(1/ka)C_l,$$

$$l=0,1,\cdots. \tag{A.16}$$

Finally, the relation (12) can be used to eliminate B_0 from (16), with the result

$$\sum_{l'=1}^{\infty}B_{l'}[(-)^l\{(-)^{l'}A_{ll'}-A_{l0}\}+iC_l\{D_{l'}-D_0\}]$$

$$=(2/ka)\delta_{l0}-(1/ka)C_l,\quad l=0,1,\cdots. \tag{A.17}$$

The preceding analysis thus furnishes a complete set of functions for the expansion of the aperture field, as in (11), or equivalently, in the original coordinate

$$\phi(\rho)=\sum_{l=1}^{\infty}\bar{B}_l(1-\rho^2/a^2)^{l-\frac{1}{2}}. \tag{A.18}$$

A study of the coefficients reveals that the leading term in the expansion of B_l is of order $(ka)^{2l-1}$, $l\geqslant 1$. Thus (11), (18) represent expansions of the aperture field in ascending powers of the frequency; clearly, these contain the most suitable trial functions for use in the variational principle.

If we solve (17) for the coefficient B_1 (taking $B_2=B_3=\cdots=0$), it turns out that

$$B_1\doteq i(4ka/3\pi),\quad ka\to 0,$$

and thus, since $B_0=-B_1$, we obtain from (11),

$$\phi^{(1)}(\rho)=-(4ika/\pi)(1-\rho^2/a^2)^{\frac{1}{2}}.$$

Inserting this aperture field in (2.21) and neglecting the phase variations of the exponential factor, we obtain the asymptotic form of the diffracted field,

$$\phi^{(+)}(\mathbf{r})\sim-(2/3\pi)k^2a^3\cos\vartheta(e^{ikr}/r),\quad r\to\infty,\quad ka\to 0 \tag{A.19}$$

in agreement with Rayleigh's solution.[2] The transmission coefficient computed from (19) is equal to the leading term of (4.24) (see reference 11).

APPENDIX 2.

Evaluation of the Integrals I_{mn}, R_{mn}, Eqs. (4.18), (4.19)

We consider first the integral

$$I_{mn}(\alpha)=\int_0^1 v^{-(m+n)}(1-v^2)^{\frac{1}{2}}J_{m+\frac{1}{2}}(\alpha v)J_{n+\frac{1}{2}}(\alpha v)dv;$$

on introducing the product representation

$$J_\mu(z)J_\nu(z)=(2/\pi)\int_0^{\pi/2}J_{\mu+\nu}(2z\cos\vartheta)\cos(\mu-\nu)\vartheta d\vartheta,$$

$$Re(\mu+\nu)>-1, \tag{A.20}$$

we find

$$I_{mn}(\alpha)=(2/\pi)\int_0^1 v^{-(m+n)}(1-v^2)^{\frac{1}{2}}dv\int_0^{\pi/2}J_{m+n+1}$$

$$\times(2\alpha v\cos\vartheta)\cos(m-n)\vartheta d\vartheta.$$

Writing $v=\sin\varphi$ and interchanging the orders of integration,

$$I_{mn}(\alpha)=(2/\pi)\int_0^{\pi/2}\cos(m-n)\vartheta d\vartheta\int_0^{\pi/2}J_{m+n+1}$$

$$\times(2\alpha\cos\vartheta\sin\varphi)\sin^{-(m+n)}\varphi\cos^2\varphi d\varphi.$$

The integral with respect to φ can be performed by means of the general result[12]

$$\int_0^{\pi/2}J_\alpha(z\sin\varphi)\sin^{1-\alpha}\varphi\cos^{2\beta+1}\varphi d\varphi=2^{1-\alpha}z^{-(1+\beta)}$$

$$\times(1/\Gamma(\alpha))s_{\alpha+\beta,\beta-\alpha+1}(z),\quad Re\beta>-1, \tag{A.21}$$

where $s_{\mu,\nu}(z)$ is a Lommel function. Taking $\mu=m+n+1$, $\nu=\frac{1}{2}$, it follows that

$$I_{mn}(\alpha)=(2/\pi)2^{-(m+n)}(1/\Gamma(m+n+1))$$

$$\times\int_0^{\pi/2}\cos(m-n)\vartheta\cdot(2\alpha\cos\vartheta)^{-\frac{1}{2}}$$

$$\times s_{m+n+(3/2),\,-(m+n-\frac{1}{2})}(2\alpha\cos\vartheta)d\vartheta.$$

[12] See reference 9, p. 374.

From the recurrence formula

$$s_{\mu+2,\nu}(z)=z^{\mu+1}-[(\mu+1)^2-\nu^2]s_{\mu,\nu}(z),$$

we obtain the more useful expression

$$I_{mn}(\alpha)=2^{1-m-n}(1/\pi\Gamma(m+n+1))\left[\int_0^{\pi/2}(2\alpha\cos\vartheta)^{m+n-1}\cos(m-n)\vartheta d\vartheta\right.$$
$$-2(m+n)\int_0^{\pi/2}\cos(m-n)\vartheta\cdot(2\alpha\cos\vartheta)^{-\frac{1}{2}}$$
$$\left.\times s_{m+n-\frac{1}{2},-(m+n-\frac{1}{2})}(2\alpha\cos\vartheta)d\vartheta\right]. \quad (A.22)$$

The Lommel functions with half integral indices, occurring in (22), are defined by

$$s_{\mu,-\mu}(z)=(\pi/2\sin\mu\pi)\left[J_\mu(z)\int_0^z z^\mu J_{-\mu}(z)dz\right.$$
$$\left.-J_{-\mu}(z)\int_0^z z^\mu J_\mu(z)dz\right]$$

and are related to the Struve functions, in accordance with the equation

$$s_{\mu,-\mu}(z)=2^\mu\Gamma(1/2)\Gamma(\mu+\tfrac{1}{2})S_\mu(z).$$

Explicit forms for a few of the Lommel functions are as follows

$$s_{1/2,-1/2}(z)=z^{-\frac{1}{2}}[1-\cos z],$$
$$s_{3/2,-3/2}(z)=z^{-\frac{1}{2}}[z-2\sin z+(2/z)(1-\cos z)],$$
$$s_{5/2,-5/2}(z)=z^{-\frac{1}{2}}[z^2+4+8\cos z-(24/z)\sin z$$
$$+(24/z)(1-\cos z)].$$
$$s_{7/2,-7/2}(z)=z^{-\frac{1}{2}}[z^3+6z+48\sin z+(72/z)+(288/z)\cos z$$
$$-(720/z^2)\sin z+(720/z^3)(1-\cos z)],$$

Thus, returning to (22), we find, with $m=n=1$,

$$I_{11}(\alpha)=(\alpha/2\pi)-(1/2\pi\alpha^2)\int_0^{\pi/2}[\alpha\cos\vartheta-\sin(2\alpha\cos\vartheta)$$
$$+(1/\alpha\cos\vartheta)\sin^2(\alpha\cos\vartheta)]\cos^{-2}\vartheta d\vartheta.$$

Writing

$$P(\alpha)=\int_0^{\pi/2}[\alpha\cos\vartheta-\sin(2\alpha\cos\vartheta)$$
$$+(1/\alpha\cos\vartheta)\sin^2(\alpha\cos\vartheta)]\cos^{-2}\vartheta d\vartheta,$$

we obtain on integration by parts,

$$P(\alpha)=\int_0^{\pi/2}\left[\alpha\sin\vartheta-2\alpha\sin\vartheta\cos(2\alpha\cos\vartheta)\right.$$
$$+(\sin\vartheta/\cos\vartheta)\sin(2\alpha\cos\vartheta)$$
$$\left.-\frac{\sin\vartheta\sin^2(\alpha\cos\vartheta)}{\alpha\cos^2\vartheta}\right]\frac{\sin\vartheta}{\cos\vartheta}d\vartheta,$$

whence

$$\widetilde{2P(\alpha)}=\int_0^{\pi/2}\left[\alpha\cos\vartheta-\sin(2\alpha\cos\vartheta)+\frac{\sin^2(\alpha\cos\vartheta)}{\alpha\cos\vartheta}\right]d\vartheta$$
$$+2\alpha\int_0^{\pi/2}[1-\cos(2\alpha\cos\vartheta)]\sin^2\vartheta\cos^{-1}\vartheta d\vartheta.$$

In terms of the Struve function $S_\nu(z)$, which has the integral representation

$$S_\nu(z)=\frac{2(\tfrac{1}{2}z)^\nu}{\Gamma(\nu+\frac{1}{2})\Gamma(\frac{1}{2})}\int_0^{\pi/2}\sin(z\cos\vartheta)\sin^{2\nu}\vartheta d\vartheta,$$

we readily find

$$P(\alpha)=(\alpha/2)-(\pi/4)S_0(2\alpha)+(\pi/8\alpha)\int_0^{2\alpha}S_0(t)dt$$
$$+(\pi\alpha/2)\int_0^{2\alpha}t^{-1}S_1(t)dt$$

and

$$I_{11}(\alpha)=(\alpha/2\pi)-(1/4\pi\alpha)+(1/8\alpha^2)S_0(2\alpha)$$
$$-(1/16\alpha^2)\int_0^{2\alpha}S_0(t)dt-(1/4\alpha)\int_0^{2\alpha}t^{-1}S_1(t)dt.$$

The integrals which occur in this expression for I_{11} can be evaluated numerically with the existing tables of Struve functions. Other values of I_{mn} are obtained in similar fashion.

A series expansion for I_{mn} is easily derived from the product representation

$$J_\mu(z)J_\nu(z)=\sum_{p=0}^{\infty}\frac{(-)^p(z/2)^{\mu+\nu+2p}\Gamma(\mu+\nu+2p+1)}{p!\Gamma(\mu+\nu+p+1)\Gamma(\mu+p+1)\Gamma(\nu+p+1)}$$

with the result

$$I_{mn}(\alpha)=(\pi^{\frac{1}{2}}/4)\sum_{p=0}^{\infty}$$
$$\times\frac{(-)^p(\alpha/2)^{m+n+2p+1}(m+n+2p+1)!}{(m+n+p+1)!\Gamma(m+p+\frac{3}{2})\Gamma(n+p+\frac{3}{2})\Gamma(p+\frac{5}{2})}. \quad (A.23)$$

This expansion has been used to verify the forms of I_{11}, I_{12}, and I_{22} given in Section 4.

The asymptotic behavior of I_{mn} for large values of the argument is obtained by noting that

$$I_{mn}(\alpha)=\alpha^{m+n-1}\int_0^\alpha(1-z^2/\alpha^2)^{\frac{1}{2}}z^{-(m+n)}J_{m+\frac{1}{2}}(z)J_{n+\frac{1}{2}}(z)dz$$
$$\sim\alpha^{m+n-1}\int_0^\infty z^{-(m+n)}J_{m+\frac{1}{2}}(z)J_{n+\frac{1}{2}}(z)dz,\quad \alpha\to\infty,$$

and using the result

$$\int_0^\infty t^{-\lambda}J_\mu(t)J_\nu(t)dt$$
$$=\frac{\Gamma(\lambda)\Gamma\left(\frac{\mu+\nu-\lambda+1}{2}\right)}{2^\lambda\Gamma\left(\frac{\lambda+\nu-\mu+1}{2}\right)\Gamma\left(\frac{\lambda+\mu+\nu+1}{2}\right)\Gamma\left(\frac{\lambda+\mu-\nu+1}{2}\right)},$$

whence

$$I_{mn}(\alpha)\backsim\frac{\alpha^{m+n-1}}{2^{m+n}(m+n)\Gamma(m+\frac{1}{2})\Gamma(n+\frac{1}{2})},\quad \alpha\to\infty. \quad (A.24)$$

For the integral

$$R_{mn}(\alpha)=\int_1^\infty v^{-(m+n)}(v^2-1)^{\frac{1}{2}}J_{m+\frac{1}{2}}(\alpha v)J_{n+\frac{1}{2}}(\alpha v)dv,$$

the representation (20) leads to

$$R_{mn}(\alpha)=(2/\pi)\int_0^{\pi/2}\cos(m-n)\vartheta d\vartheta\int_1^\infty v^{-(m+n)}$$
$$\times(v^2-1)^{\frac{1}{2}}J_{m+n+1}(2\alpha v\cos\vartheta)dv.$$

Using the integral[13]

$$\int_s^\infty\frac{J_\nu(ax)}{x^{\nu-1}}(x^2-z^2)^\mu dx=\frac{2^\mu\Gamma(\mu+1)}{a^{\mu+1}z^{\nu-\mu-1}}J_{\nu-\mu-1}(az),\quad a\geq 0,$$
$$Re(\nu/2-\tfrac{1}{4})>Re\,\mu>-1, \quad (A.25)$$

[13] See reference 9, p. 417.

we find

$$R_{mn}(\alpha)=(2/\pi)^{\frac{1}{2}}\int_0^{\pi/2}\cos(m-n)\vartheta\cdot(2\alpha\cos\vartheta)^{-\frac{1}{2}}\times J_{m+n-\frac{1}{2}}(2\alpha\cos\vartheta)d\vartheta. \quad (A.26)$$

The Bessel function occurring in (26), whose order is half of an odd integer, is expressible in finite terms by means of algebraic and trigonometric functions of the argument. For example,

$$R_{11}(\alpha)=(1/2\pi\alpha^2)\int_0^{\pi/2}\left[\frac{\sin(2\alpha\cos\vartheta)}{2\alpha\cos\vartheta}-\cos(2\alpha\cos\vartheta)\right]\cos^{-2}\vartheta d\vartheta d\vartheta.$$

Writing

$$P(\beta)=\int_0^{\pi/2}[(1/\beta\cos\vartheta)\sin(\beta\cos\vartheta)-\cos(\beta\cos\vartheta)]\cos^{-2}\vartheta d\vartheta,$$

we find, on integration by parts,

$$P(\beta)=\int_0^{\pi/2}\left[\sin(\beta\cos\vartheta)\beta\sin\vartheta+\frac{\cos(\beta\cos\vartheta)\sin\vartheta}{\cos\vartheta}-\frac{\sin(\beta\cos\vartheta)\sin\vartheta}{\beta\cos^2\vartheta}\right]\sin\vartheta\cos^{-1}\vartheta d\vartheta,$$

whence

$$2P(\beta)=(\beta+1/\beta)\int_0^{\pi/2}\sin(\beta\cos\vartheta)\cos^{-1}\vartheta d\vartheta-\int_0^{\pi/2}\cos(\beta\cos\vartheta)d\vartheta-\beta\int_0^{\pi/2}\sin(\beta\cos\vartheta)\cos\vartheta d\vartheta$$
$$=\pi/2\left[(\beta+1/\beta)\int_0^{\beta}J_0(t)dt-J_0(\beta)-\beta J_1(\beta)\right]$$

and

$$R_{11}(\alpha)=P(2\alpha)/2\pi\alpha^2=\frac{1}{4\alpha}\left(1+\frac{1}{4\alpha^2}\right)\int_0^{2\alpha}J_0(t)dt-\frac{1}{8\alpha^2}J_0(2\alpha)-\frac{1}{4\alpha}J_1(2\alpha).$$

Integrals of the zero-order Bessel function are available in the literature.[14] Additional values of R_{mn} are derived by similar procedures.

An expansion for R_{mn} is obtained by inserting the Bessel function series

$$J_\nu(z)=\sum_{p=0}^{\infty}\frac{(-)^p(z/2)^{\nu+2p}}{p!\Gamma(\nu+p+1)}$$

in (26), and employing the integral

$$\int_0^{\pi/2}\cos^{m+n-2}\vartheta\cos(m-n)\vartheta d\vartheta=\frac{\pi\Gamma(m+n)}{(m+n-1)2^{m+n-1}\Gamma(m)\Gamma(n)},\quad m+n>1;$$

the result is

$$R_{mn}(\alpha)=(\pi^{\frac{1}{2}}/4)\sum_{p=0}^{\infty}\times\frac{(-)^p(\alpha/2)^{m+n+2p-2}(m+n+2p-2)!}{p!(m+p-1)!(n+p-1)!\Gamma(m+n+p+\frac{1}{2})}. \quad (A.27)$$

It follows from the asymptotic behavior of the Bessel function in (26) that R_{mn} vanishes for infinitely large argument.

[14] A. N. Lowan and M. Abramowitz, J. Math. and Phys. **22**, 1 (1943).

Letters to the Editor

PUBLICATION of brief reports of important discoveries in physics may be secured by addressing them to this department. The closing date for this department is five weeks prior to the date of issue. No proof will be sent to the authors. The Board of Editors does not hold itself responsible for the opinions expressed by the correspondents. Communications should not exceed 600 words in length.

On the Multiple Production of Mesons

G. WATAGHIN
Departamento de Física, da Universidade de São Paulo, São Paulo, Brasil
July 6, 1948

SOME years ago we proposed a description of the multiple creation of mesons by the high energy collisions of nucleons on the basis of few assumptions.[1] Today we can compare this description with the observations and supplement it with few a remarks. From the experimental data we can deduce: (a) The cross section for the meson production by a primary proton (or by a secondary nucleon) is $\sim 5\times 10^{-25}$ cm² per air nucleus (4×10^{-26} cm² per nucleon), varying only slowly with the energy. (b) In every collision the incident particle loses a large fraction of its energy. (c) The multiple production of mesons (π, μ, neutrettos, etc.), is a fundamental process characteristic of high energy collisions of two nucleons or two nuclei.[2] The average multiplicity is given by the following rule: in the center of mass system, the mesons and the nucleons have, after the collision, kinetic energies $\sim\mu c^2\sim 10^8$ ev.[1] (d) The variation with atmospheric depth of the number of fast nucleons, producing the local penetrating showers, obeys an exponential law.[3] If b denotes the coefficient of absorption of a fast nucleon due to the creation of mesons, and b^* is the average coefficient of production of fast secondary nucleons, then the intensity of the flux of fast nucleons as function of the depth x (in g/cm²) is $I=I_0\exp[-(b-b^*)x]$, where $(b-b^*)=0.01$ g/cm². Measurements of the transition effect[4] and of the saturation point give us directly the value of b (because locally produced nucleons give rise to showers simultaneous to the incident nucleon and thus are not registered separately). We find $b^{-1}\sim 50$ and $(b^*)^{-1}\sim 100$ g/cm². Thus primary protons are very rare at sea level, and most of the fast nucleons at sea level are produced by the mechanism of "cascades of nucleons and meson showers."

Let us consider the collision of two nucleons in the center of mass system, and let their energies before the collision be $E_{01}=E_{02}>Mc^2$. Let $E_{f1}E_{f2}$ be the energies of the nucleons after the collision, and let n_i denote the number of mesons of mass μ_i and of average energy ϵ_i created in the collision. Putting $E_{f1}\sim E_{f2}\sim 1.1\times Mc^2$ and neglecting the eventual emission of other particles, we have

$$E_{01}+E_{02}-2.2\times Mc^2=\Sigma n_i\epsilon_i=n\epsilon.$$

Now we assume that the distribution of the momenta of created mesons and of nucleons is spherically symmetrical and that the average kinetic energy ϵ per particle is $\sim\mu c^2$. Performing a Lorentz transformation from the center of mass system to the terrestrial frame, where one of the nuclei is at rest and the other has an energy E_P, we obtain:

$$E_p=2Mc^2(an^2+bn+d),$$

where $a\sim 0.03$, $b\sim 0.4$, and $d\sim 1.1$. This formula gives the dependence of n from E_P. In Table I are indicated some typical values of E_P, n and of the average energy of the mesons E_μ.[5] The observations seem to support the correctness of the picture of the meson showers given above. Indeed, if, e.g., $n\gtrsim 100$, we have $n\sim(E_P)^{\frac{1}{4}}$ in accord with the recent results of G. F. Chew,[6] who derived this relation from the study of fast mesons made by Gill, Schein, and Yngve.[7] [Energetic mesons are created in showers with high n.] For primaries, sensitive to the earth's magnetic field ($E_p\sim 10^{10}$ ev), we obtain plausible values for the E_μ. It seems also noteworthy that Schein and Steinberger obtained remarkable accord between observed and theoretical spectrum of mesons starting from assumptions which, for $E_p\sim 10^{10}$, are similar to ours.[8] The best proof can be derived in the following way: let us indicate with $dN=kE_P^{-\gamma}dE_P$ and $dn=k'\epsilon^{-s}d\epsilon$ the spectral distributions of the primary protons and of the μ-mesons, respectively. If the average multiplicity n of a meson shower is proportional to $E_P{}^r$, then, assuming $E_P\sim n\epsilon$ (in accord with our description if $n>100$), one has $r=(s-\gamma)/(s-2)$.[9] Experimentally one finds[10] $\gamma=2.45$, from the azimuthal effect for high energy mesons, and one has $s=2.9$, from the meson intensity at great depths. Then, substituting these values in r, we obtain $r=0.5$ for high values of E_P, in accord with our theory.

Let us consider the assemblage of n-created mesons and of two nucleons after the collision (in the center of mass system) at the moment when they still occupy a volume of linear dimensions $l\sim h/\mu c$. We assume that the interaction between these particles at this moment is still sufficiently strong in order to give rise to a statistical distribution of energy and momenta. Then the most probable distribution is $n_i=g_i/(\exp(\alpha+\beta E_i)\pm 1)$, where $g_i=8\pi l^3h^{-3}p_i^2dp_i$ and other symbols have their usual meaning. From the uncertainty reaction the momenta must be $\gtrsim h/l$, and thus $\beta^{-1}\geqslant\mu c^2$. Now, either we assume $\beta^{-1}=\mu c^2$, or we introduce a convenient cut-off factor; in both cases we obtain the properties of the showers specified above. Very similar calculations can be made in the case of the collision of a proton with a nucleus of mass number A. We can suppose that r nucleons ($r\leqslant A$) suffer simultaneous collision with the incident proton, the remaining $(A-r)$ nucleons suffering only a negligible exchange of energy during the collision.

TABLE I. Average multiplicity n and average energy of mesons E_μ are given in function of the primary energy E_P (in ev).

E_P	$A=1$ n	$A=1$ E_μ	$A=r=14$ n	$A=r=14$ E_μ
5.0×10^9	3	5×10^8	9	3×10^8
1.8×10^{10}	12	9×10^8	27	4×10^8
1.3×10^{12}	1.6×10^2	8×10^9	6×10^2	2×10^9
1.3×10^{14}	1.6×10^3	8×10^{10}	6×10^3	2×10^{10}
1.9×10^{17}	6×10^4	3×10^{12}	2×10^4	8×10^{11}

Some results of these calculations (for $r=A=14$) are given in Table I. The high energy mesons must also be produced in groups. If $E_P \sim 10^{17}$ ev, we find multiplicities $\sim 10^5$ mesons, and meson energies $\sim 10^{12}$ ev sufficient to explain the penetration of mesons at great depths.[11]

[1] Symposium on Cosmic Rays, Acad. Bras. Ciencias 129 (1941); G. Wataghin, Phys. Rev. **70**, 787 (1946); Comptes Rendus **207**, 358 (1938).
[2] In accord with Heisenberg's general idea of explosion showers.
[3] G. Wataghin, Phys. Rev. **71**, 453 (1947); E. P. George and A. C. Jason, Nature **161**, 248 (1948); J. Tinlot, Phys. Rev. **73**, 1476 (1948).
[4] L. Janossy, Proc. Roy. Soc. **A179**, 361 (1941); L. Janossy and Rochester, Proc. Roy. Soc. **A183**, 181 (1944); V. H. Regener, Phys. Rev. **64**, 252 (1943).
[5] More data about these showers can be found in our paper (see reference 1).
[6] G. F. Chew, Phys. Rev. **73**, 1128 (1948).
[7] P. S. Gill, M. Schein, and V. Yngve, Phys. Rev. **72**, 733 (1948).
[8] M. Schein and J. Steinberger, Phys. Rev. **72**, 734 (1948).
[9] H. W. Lewis, J. R. Oppenheimer, and S. A. Wouthuysen, Phys. Rev. **73**, 140 (1948).
[10] P. S. Gill and G. H. Vaze, Phys. Rev. **73**, 1395 (1948).
[11] See Professor A. H. Compton's remarks at the Symposium (reference 1).

Non-Rectifying Germanium

W. C. Dunlap, Jr. and E. F. Hennelly
Research Laboratory, General Electric Company, Schenectady, New York
September 3, 1948

RECENTLY germanium of rather unique properties has been prepared in this laboratory. Most unique of the properties observed is an almost complete absence of surface rectification at the germanium-metal contact. Several ingots of this type were prepared by melting germanium powder at a pressure of less than 10^{-4} mm Hg. The powder was prepared by reduction of germanium dioxide in a hydrogen furnace. Ten-point, plane-welded contact rectifiers were made from one ingot. Their average rectification ratio for 20 volts and at room temperature was 3.54. At −196°C the average ratio was 1.22. These units were weakly *N*-type at room temperature, *P*-type at −196°C. Hall effect measurements on larger samples showed that the material was *P*-type at low temperatures, reversing to *N*-type at 70°C. Potential distribution studies indicated a uniform resistivity of 17.8 ohm cm. The mobility averaged 2890 cm²/volt sec. and the Hall coefficient 514,000 e.m.u.

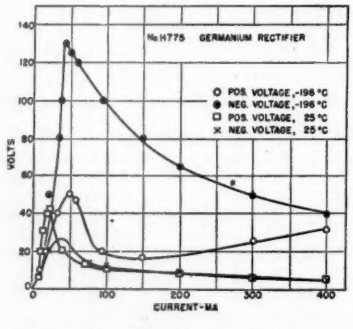

FIG. 1. Residual rectification characteristics for a welded contact rectifier made from "non-rectifying" germanium. At voltages below 10 the rectification ratio is less than 1.5, both at 25°C and −196°C, but at voltages of the order 50 there is a slight rectification with ratio ~2 at both temperatures. "Breakdown" occurs at 25 volts for 25°C, at 125 for −196°C. It is the result of heating at the point of contact.

The room temperature resistivity was increased by 22 percent by application of a magnetic field of 13,750 gauss. The Hall coefficient decreased by 29 percent on changing the magnetic field from 3600 to 13,750 gauss. Resistance of the point-contact rectifiers increased by about 18 percent in a field of 13,750 gauss, for both directions of current. Since this result is almost as large as the magnetoresistance of the bulk, one is compelled to conclude that practically all the resistance at the contact was "spreading resistance," with little contribution from contact barriers. The contact resistance averaged 2900 ohms. This is roughly ten times the forward resistance of *N*-type units made from material of comparable resistivity. Thus the "electric field-sensitive" conductivity studied by Bray, Lark-Horovitz, and Smith,[1] and by Brattain and Bardeen[2] may not appear in *P*-type germanium.

Figure 1 illustrates the residual rectification of a typical non-rectifying unit, No. H775. For small voltages the rectification was negligible, at both 25°C and −196°C, but the rectification factor increased to a value of the order 2 at 20–100 volts. It seems probable that the observed rectification was due to heating and consequent inhomogeneity in the germanium rather than to a true rectification between the germanium and the Pt-10 percent Ru whisker. Pressure contacts utilizing brass, stainless steel, and dural were found to yield negligible rectification. A study is now being made of the relation of the above results to the theory of the contact properties of a *P*-type semi-conductor.

A second point of interest is that, in spite of the apparently high degree of homogeneity in this *P*-type germanium, the magnetoresistance was large, as was the variation of Hall coefficient with magnetic field. Since the magnetoresistance of the ten test units was determined largely by a very small region of germanium around the point of contact, it seems that either the magnetoresistance (and probably also the variation of Hall coefficient with field) is intrinsic (not a result of inhomogeneity) or else the inhomogeneity is on a scale small compared to the dimensions of the point contact (~0.0002 in.). Although we cannot decide definitely as yet between these possibilities, a plausible picture retaining the second hypothesis is that the inhomogeneity consists of a rather uniform distribution of sub-microscopic lattice defects, which may also be responsible for the *P*-type conduction. Work is continuing to test these ideas.

[1] R. Bray, K. Lark-Horovitz, and R. N. Smith, Phys. Rev. **72**, 530 (1947).
[2] W. H. Brattain and J. Bardeen, Phys. Rev. **74**, 231 (1948).

γ-Radiation from Be^8

S. Devons and M. G. N. Hine
University of Cambridge, Cambridge, England
August 19, 1948

THE cross section for the capture of a proton by the Li^7 nucleus, resulting in a state of Be^8 having an excitation energy of 17 Mev, shows a strong resonance

maximum at a proton energy, E_r, of 439 kev; and the form of the maximum agrees, at least approximately, with that to be expected from the Breit-Wigner dispersion formula ($\Gamma_r = 12$ kev).[1] For proton energies very different from E_r, the cross section does not fall away as rapidly as would be expected from the dispersion formula; in fact, there appears superposed on the resonance peak a much smaller cross section which varies only slowly for proton energies up to 1.0 Mev.[2] The energy of the γ-radiation following proton capture has been measured by several investigators, the general indication of the results being that at the resonance the γ-radiation is predominantly of quantum energy 17.0 Mev[1,3] (i.e., a transition to the ground state of Be^8). But for proton energies substantially different from E_r, the γ-energy is somewhat smaller[4] (probably mostly 14.0 Mev, i.e., transition to the well-known excited state of Be^8 at 3 Mev).[5] These facts are usually explained by assuming that the resonance corresponds to a state of Be^8 with odd total angular momentum, J, or odd parity (or both), and that the slowly varying cross section corresponds to one or more broad levels of Be^8 with even parity and J. Be^8 nuclei formed in the former states cannot break up into two α-particles; those formed in the latter states can—hence the marked difference in the widths of the two states. The approximate isotropy[6] of the γ-radiation at resonance (i.e., formation by S-protons) and the large radiation width (10 ev) together suggest that the resonance corresponds to a state of Be^8 with odd parity and $J=1$ (assuming Li^7 to have odd parity). The "non-resonant" radiation arises from states of Be^8 with even parity and $J=2, 4, \cdots$. This latter radiation should therefore show marked anisotropy. Furthermore, if the γ-transitions from the two states are not *always* of different energies and, if in addition both narrow and broad states can be formed by the same arrangement of Li^7 and proton spins (i.e., Li^7 and proton spins antiparallel, if $J=1$ is the correct assignment for the resonance level), then interference between the radiation from the two states can occur. A difference in parity in the two states will then be revealed as an asymmetry in the intensity of the γ-radiation with respect to the plane perpendicular to the incident proton beam.

We have made careful investigations, in particular of the angular distribution, of the γ-radiation from this process for proton energies of 300–800 kev, and have been able to verify most of the features of the above interpretation. The main results of our investigation are:

(1) With a "thick" Li target and protons of 500-kev energy, the γ-radiation is not exactly isotropic but is of the form:

$$1+0.05\cos\theta.$$

(θ is the angle between proton beam and direction of γ-radiation. Allowance is made for center of gravity motion.)

(2) With a "thin" target and varying proton energy the angular distribution near resonance is of the form $1+\alpha\cos\theta$, where α is positive for proton energies greater than about 435 kev and negative for smaller proton energies.

(3) The forward-backward asymmetry is a maximum ($|\alpha| \sim 0.3$) for proton energies of about 350 kev and 620 kev.

The experimental results are not sufficiently precise to exclude the possibility of small higher terms of the type $\cos 2\theta$, etc. The measured variation of $I(30°)/I(150°)$ is shown in Fig. 1. These results are consistent with the interpretation of the radiation as a superposition of electric-dipole radiation (from the 439-kev level) and electric-quadrupole radiation (from the broad level). The change in sign of α on passing through resonance is just that to be expected from the change in phase of the resonant state on passing through the resonance energy. The occurrence of maxima in α at energies so far from the resonance energy is at first sight surprising, but is in accordance with slow variation in the *amplitude* of the resonance state predicted by the dispersion formula (namely, as $(E-E_r+\frac{1}{2}i\Gamma_r)^{-1}$). With some simplifying assumptions the value of $R=I(0°)/I(180°)$ is given by:

$$R=\frac{a^2+\sin^2\gamma+2\sqrt{2}a\cos(\chi-\gamma)\sin\gamma}{a^2+\sin^2\gamma},$$

where $a^2(\ll 1)$ represents the relative intensities of resonant and "non-resonant" γ-radiation, $\tan\gamma=2\Gamma_r/(E-E_r)$ and χ is an angle related to phase difference of the two nuclear states at a particular energy. The asymmetry will clearly be a maximum when $\gamma \sim a \sim 2\Gamma_r/(E-E_r)$, or, physically, the interference term causing asymmetry will have maximum *relative* magnitude when the amplitudes of the radiation from the two states of Be^8 are of comparable magnitude. From the experimental results $2\Gamma/(E-E_r)$ is about 0.2 for E corresponding to maximum asymmetry; hence $a^2 \sim 0.04$, a result consistent with the observed ratio of γ-intensities from the narrow and broad levels, as deduced from observations at angle of 90° to the proton beam where the interference term vanishes.

The above results require, *inter alia*, that the γ-radiation from the broad and narrow levels contain components of the same energy. We have made some qualitative measurements of the variation of γ-energy in the neighborhood of the resonance, and find that the component of energy

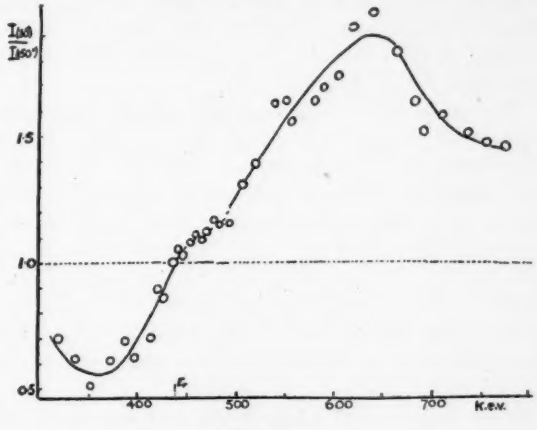

FIG. 1. Variation of asymmetry with proton energy. This curve is strongly distorted in the region near E_r owing to the finite target thickness (~30 kev).

17-Mev is present at all energies although its intensity relative to the total γ-intensity does vary by a factor of about two. Measurements of the γ-radiation asymmetry near resonance, as a function of γ-energy, indicate that the 17-Mev γ-component is responsible for most of the asymmetry, which confirms the conclusion that γ-radiation from the broad level contains an appreciable 17-Mev component. This result would be expected from the known properties of the ground state and 3-Mev level of Be^8.

In making measurements of the angular distribution, particularly near resonance where the asymmetry is small, due regard must be paid not only to the effect of the recoil of the Be^8 nucleus on the angular distribution, but also to the effect of the Doppler frequency shift on the efficiency of detection of the γ-radiation. By deliberately increasing dependence of γ-detection on γ-energy, we have observed a change in apparent angular distribution agreeing with that to be expected for a Be^8 nucleus recoiling with full energy. This is consistent with a short lifetime ($<10^{-14}$ sec.) for the compound Be^8 nucleus.

Details of the above measurements, and their interpretation, and of investigations of other (p, γ) reactions will be published elsewhere.

[1] Fowler, Lauritsen, Lauritsen, Rev. Mod. Phys. **20**, 236 (1948); T. W. Bonner and J. E. Evans, Phys. Rev. **73**, 666 (1948).
[2] Hudson, Herb, and Plain, Phys. Rev. **57**, 587 (1940).
[3] McDaniel, von Dardel, and Walker, Phys. Rev. **72**, 985 (1947).
[4] Tangen, quoted in reference (1).
[5] J. A. Wheeler, Phys. Rev. **59**, 16 (1940).
[6] Ageno, Amaldi, Bocciarelli, and Trabacchi, Ricerca Scient. **12**, 139 (1941).

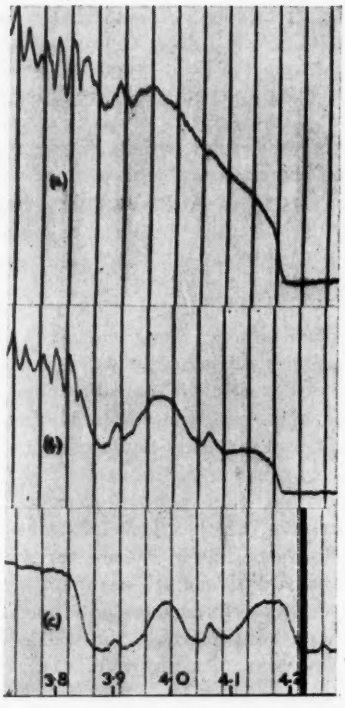

FIG. 1. (a) The solar spectrum from 3.7μ to 4.2μ. Complete absorption beyond about 4.2μ is due to CO_2. (b) Spectrum of sunlight, in the same region, after passage through an absorption tube containing 7 atmos./cm of N_2O. (c) Spectrum of the radiation from a Nernst filament, in the same region, after passage through 25 atmos./cm of N_2O and about 4 meters of air. Absorption bands due to N_2O at 3.90μ and 4.06μ and due to CO_2 at 4.26μ.

Nitrous Oxide in the Earth's Atmosphere

J. H. SHAW, G. B. B. M. SUTHERLAND, AND T. W. WORMELL
Solar Physics Observatory, Cambridge, England
August 30, 1948

A SERIES of solar spectra in the wave-length range from 2.5μ to 5.0μ have been obtained at the Solar Physics Observatory, Cambridge, England (30 m above M.S.L.) during the last week of July, 1948, using a spectrometer with a lithium fluoride prism and a Hilger-Schwarz thermocouple as detector. They show convincing evidence of the existence of nitrous oxide (N_2O) in the atmosphere above the observatory.

This region of the solar spectrum contains numerous bands, many of which are intense absorptions due to carbon dioxide and water vapor, but bands at 3.90μ, 4.06μ, and 4.50μ agree in wave-length with known absorptions of nitrous oxide[1] and give satisfactory agreement in position, relative intensity, and contour with bands delineated in the laboratory with the same spectrometer, using a Nernst filament as source and an absorption cell filled with N_2O. Nitrous oxide also has other weaker bands at 3.57μ, 2.97μ, and 2.87μ; these are concealed, in the solar spectrum, by the water vapor bands in this region.

In the region around 4.0μ in the solar spectrum, one remarks immediately a doublet of moderate intensity centered at 3.9μ (Fig. 1a). Spectra taken at different solar altitudes show a marked intensification of this band at low solar elevations and, if the beam of sunlight is passed through an absorption tube containing N_2O, the band is intensified but unchanged in position and general appearance (Fig. 1b). A comparison with this band, as obtained from a laboratory source and known amounts of nitrous oxide, indicates that the amount of N_2O present in the atmosphere above Cambridge is of the order of 1.0 atmos./cm, which is in good agreement with the value estimated by Sutherland and Callendar[2] from Adel's[3] work at Flagstaff.

The 4.5μ N_2O doublet is a very intense band, but in the solar spectrum it is partially masked by the CO_2 band at 4.3μ which gives complete absorption over a wide region of the spectrum. The central hump and longer wave-length half of the N_2O band are, however, clearly present and confirm the evidence of the 3.9μ-band (Fig. 2). The band at 4.06μ is a much weaker absorption, but its presence too can be observed in the solar spectrum when the sun's altitude is low.

Bands at 7.8μ and 8.6μ, on which Adel[3] based his first suggestion of nitrous oxide in the earth's atmosphere, had previously been sought by us, using a rocksalt prism, but their presence in the solar spectrum could not be definitely established. The region around 7.8μ is largely masked, when observing from such a low altitude station, by the edge of the great 6.3μ-water-vapor band. The 8.6μ-band is a weak one, and even in this region the solar spectrum shows a

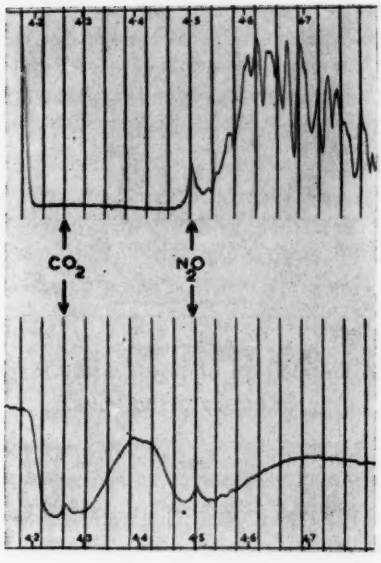

FIG. 2. The upper tracing is a portion of the solar spectrum from 4.2μ to 4.7μ, showing the nitrous oxide band at 4.5μ at the edge of the wide CO_2 band. The lower tracing is a comparison spectrum of the same region using a Nernst filament and an absorption tube containing 2 atmos./cm of N_2O, the beam also traversing about 4 meters of air.

number of intense narrow absorptions which would hide the contour of a weak band.

The results of the present work may be considered to confirm Adel's[3,4] identification of nitrous oxide in the atmosphere and also to show that the amount present is of the same order both in England and in America. It is thus reasonably certain that its presence is a world-wide and not merely a local phenomenon, and it becomes a matter of some urgency to determine, if possible, its vertical distribution. If the maximum concentration is in the upper atmosphere, it may play an appreciable role in the atmosphere's radiative equilibrium.

[1] G. Herzberg, *Infrared and Raman Spectra* (D. Van Nostrand Company, New York, 1945), p. 278.
[2] G. B. B. M. Sutherland and G. S. Callendar, *Reports on Progress in Physics* (The Physical Society, London, 1942–43), Vol. IX, p. 24.
[3] A. Adel, Astrophys. J. **90**, 627 (1939).
[4] A. Adel, Astrophys. J. **93**, 509 (1941).

Theory of Internal Conversion

H. A. MEYER
Departamento de Física, da Universidade de São Paulo, São Paulo, Brazil
August 24, 1948

THE theory of internal conversion has been given by Mott and Taylor[1] and by Hulme,[2] making use of a retarded interaction between the nuclear particle and the electron.

Recently Schönberg developed a formalism of quantum electrodynamics,[3] eliminating all the divergences. The interaction between the particles consists of two parts: an unquantized relativistic generalization of the Coulomb forces and a field of photons with positive and negative energies. The unquantized part consists of an interaction in which each particle acts on the others by means of a force corresponding classically to one-half the sum of its retarded and advanced fields. Schönberg gave tentatively a physical interpretation for his formalism. In the special case of internal conversion, this rule leads to the result that the interaction between the nuclear particle and the electron is half-retarded—half-advanced.

We computed the internal conversion coefficient for an electron on the K-shell as a function of $\theta = mc^2/hV$, assuming a dipolar transition. The details of the calculations will be given elsewhere. The results for an atom with $Z = 84$ are shown on curve I on Fig. 1, curve II representing the internal conversion coefficient computed by Hulme. For the highest energy we considered, the difference between the two curves is about 30 percent. At the actual state of experimental technique a decision between the two interactions seems to be difficult. If the half-retarded—half-advanced interaction does not agree with experiment, Schönberg's physical interpretation rule should be modified in order to obtain a correct result.

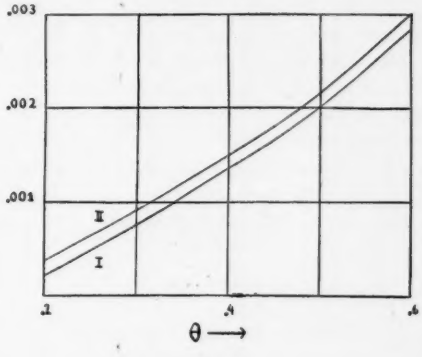

FIG. 1.

We are computing now the quadripole transitions.

We thank Professor M. Schönberg for the suggestion of the problem and for the helpful discussions, and Professor G. Beck for his kind interest.

[1] N. F. Mott and H. M. Taylor, Proc. Roy. Soc. **138**, 665 (1932).
[2] H. R. Hulme, Proc. Roy. Soc. **138**, 643 (1932).
[3] M. Schönberg, Phys. Rev., in print.

Nuclear Relaxation in Ice at −180°C

G. E. PAKE*†
Lyman Laboratory of Physics, Harvard University, Cambridge, Massachusetts
AND
H. S. GUTOWSKY**
Gibbs Chemical Laboratory, Harvard University, Cambridge, Massachusetts
September 7, 1948

THE spin-lattice relaxation time for protons in ice has been measured at −180°C, using a sample of conductivity water which had been redistilled in quartz.

The sample was contained in a radiofrequency coil which occupied a cavity within a $2\frac{1}{2}''\times 2''\times\frac{11}{16}''$ copper block, and cooling was effected by liquid nitrogen supplied to an adjacent cavity of the block from a double-walled reservoir. Temperatures were measured by means of a copper constantan thermocouple, one junction of which was set directly in the sample. The assembly was used in conjunction with the permanent magnet apparatus described elsewhere.[1]

Measurements were made at a radiofrequency of 29.0 mc per sec., which was fixed throughout the experiment. With the r-f magnetic field sufficiently large (about 10^{-2} gauss) to produce saturation, the external magnetic field was maintained at the resonant value until the signal decreased to its saturated value for that power level. The external field was then moved about 35 gauss from the center of the 16-gauss wide resonance, allowing the Boltzmann distribution of spin states to begin to re-establish. After t minutes, the magnetic field was quickly returned to resonance and the signal strength was measured by recording the peak height Y of the central maximum of the dispersion curve derivative. Figure 1 plots the experimental values of Y against re-establishment time t. The smooth curve has the form $Y=390-360\exp(-t/T_1)$, with $T_1=10.0$ minutes. It is estimated that the relaxation time T_1 is 10 ± 1 minutes.

This relaxation time, although appreciably longer than those thus far measured for many substances at both lower and higher temperatures,[2,3] falls far short of correlation with the Debye dielectric relaxation time τ_1. Bloembergen, Purcell, and Pound[2] have successfully correlated, on the basis of their theory, measured values of T_1 in ice between -2°C and -40°C with dielectric data. From dielectric

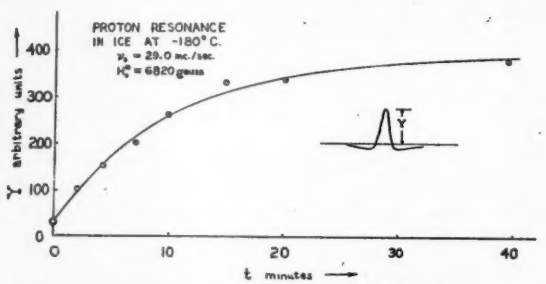

FIG. 1. The maximum Y of the dispersion curve derivative, dx'/dH_0, is plotted against the time during which the Boltzmann distribution of proton spin states has begun to re-establish from a given saturated condition.

measurements on ice extended to -139°C, Murphy[4] deduces a formula which would yield a value of several minutes for τ_1 at -180°C. The graph on p. 709 of reference 2 shows that, in this temperature range, $T_1\cong 6\times10^5\tau_1$, if both dielectric and paramagnetic relaxation are attributable to the same reorienting motions. The measured T_1 is thus too small by a factor 10^5, and it appears that ice, at sufficiently low temperatures, joins most ionic crystals[2] in possessing an unexpectedly short relaxation time.

More detailed experiments on nuclear relaxation in ice are in progress at this laboratory.

Facilities for these experiments were provided in part through a Frederick Gardner Cottrell Special Grant-in-Aid from the Research Corporation.

* Predoctoral Fellow of the National Research Council.
† Now at Washington University, St. Louis, Missouri.
** Now at the University of Illinois, Urbana, Illinois.

[1] G. E. Pake, J. Chem. Phys. 16, 327 (1948).
[2] N. Bloembergen, E. M. Purcell, and R. V. Pound, Phys. Rev. 73, 679 (1948).
[3] B. V. Rollin and J. Hatton, Nature 159, 201 (1947); B. V. Rollin, J. Hatton, A. H. Cooke, and R. J. Benzie, Nature 160, 436 (1947); B. V. Rollin and J. Hatton, Phys. Rev. 74, 346 (1948).
[4] E. J. Murphy, Trans. Electrochem. Soc. 65, 133 (1934).

Mass Deposition of Completely Resolved Samarium Isotopes

A. E. SHAW
Argonne National Laboratory, Chicago, Illinois
August 27, 1948

A CONTINUATION of the experiments with the new positive ion source,[1] which employs a tungsten crucible surrounded by a tungsten loop filament for heating and ionizing the material within the crucible, has shown that it is suitable for producing microgram quantities of completely resolved isotopes. Electronic stabilizer circuits have been added to control both the electron bombarding voltage between the tungsten filament and the crucible and the electron emission current from the filament to the crucible.

It was found that uniform deposits could not be built up on ordinary metallic surfaces because of the tendency to sputter under ion impact. Successful deposits were obtained with a system of rectangular metallic cups, of about the same open area as the individual isotope beams, and deep enough to suppress the loss by sputtering. As an example of a typical deposit laid down in such a cup system, about 60 milligrams of Sm_2O_3 were melted in a tungsten crucible having a tantalum cap with a 1-mm hole in the axis. The melted Sm_2O_3 formed a glass-hard mass. The crucible thus prepared was placed in the source in the spectrograph which was provided with a 0.250-mm slit formed by two jaws of pure tungsten, 0.125 mm thick. This slit withstood for several hours the intense bombardment of a positive ion beam of 8500 volts emerging from the source.

The ion beam was monitored by a collector at the Sm^{154} line. With a bombarding voltage of 700 volts, an emission current of 0.175 ampere, and an ion accelerating voltage of 8500 volts, the average intensity at Sm^{154} was 3×10^{-8} ampere and 12.9×10^{-8} ampere in all the isotopes. These currents may be raised by a factor of 10 by increasing the

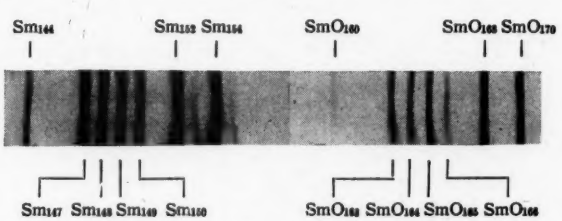

FIG. 1. Mass deposits of the first-order isotopes of Sm and SmO.

electron power put into the crucible. The total elapsed time for this deposit was 215 minutes. This corresponds to a mass of 2.65 micrograms. By recharging the crucible it was found possible to build up a total deposit of about 5 micrograms of completely resolved isotopes of Sm.

Although poor deposits were collected on ordinary metal surfaces, it was found possible to collect good deposits on a plate of pure aluminum whose surface had been microblasted with a water suspension of 325-mesh vermiculite under a pressure of 70 lbs/in.². A photograph of such a deposit whose mass is approximately 0.9 microgram for the Sm isotopes is shown in Fig. 1. This was obtained under essentially the same conditions as the previous deposit except that the exposure time was 108 minutes and the ion accelerating voltage was 8000 volts. Figure 1 shows that, in the case of samarium, the oxide as well as the metal ions are deposited.

[1] A. E. Shaw, Phys. Rev. **73**, 1222 (1948).

Long-Lived Metastable State of Te^{125}

G. FRIEDLANDER, M. GOLDHABER,* AND G. SCHARFF-GOLDHABER*
Brookhaven National Laboratory, Upton, Long Island
September 7, 1948

WITH the emission of beta-rays, gamma-rays, and Te K x-rays, Sb^{125} (2.7 yr.) decays.[1] It seemed worth while to investigate whether the Te x-rays are emitted from a metastable state of Te^{125}. We, therefore, separated Te chemically from a source of Sb^{125} which had been produced in Oak Ridge by bombardment of Sn with slow neutrons through the reaction $Sn^{124}(n, \gamma)Sn^{125} \xrightarrow{\beta} Sb^{125}$.

The Te fraction was found to be active. Figure 1 shows the absorption curve in Al of the electrons taken with a mica end window counter. The range of ~18 mg/cm² Al corresponds to an energy of 120 kev with an uncertainty of about 10 percent. The absorption of the remaining photon component is shown in Fig. 2. In these experiments a stronger source was used. One can conclude that the radiation is largely K radiation of Te and that, if any unconverted γ-rays of an energy of about 120 kev are present, their intensity is <1 percent of the transitions converted in the K-shell. We have so far only determined an approximate value of about two months for the half-life of Te^{125*}.

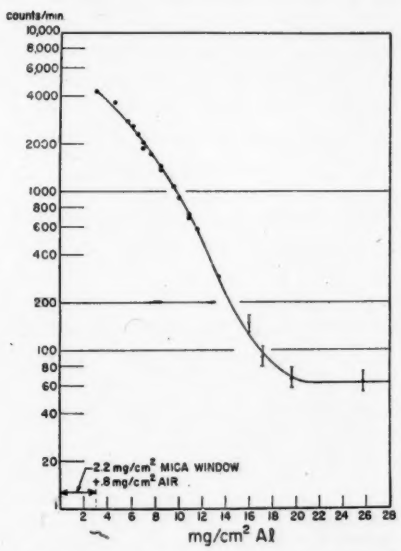

FIG. 1. Absorption of Te^{125*} internal conversion electrons in Al.

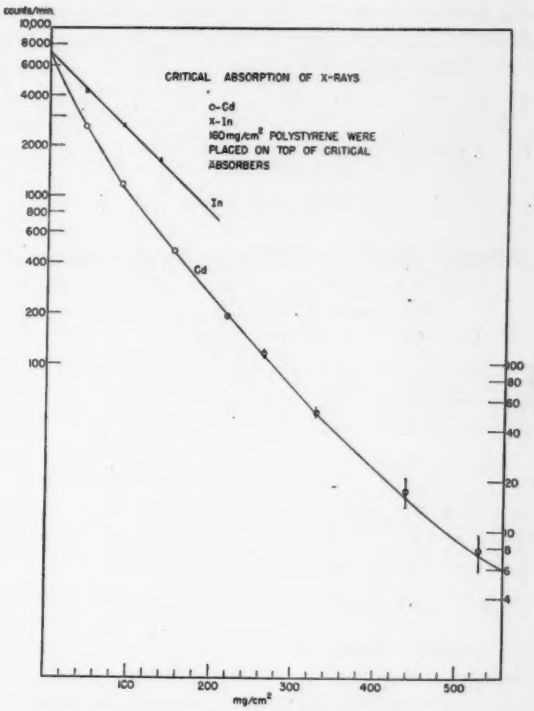

FIG. 2. Absorption of photons from Te^{125*} in Cd and In.

Reid and Keston[2] discovered a 56-day isotope of iodine, which has been assigned by Glendenin and Edwards[3] on plausible grounds to I^{125}. Reid and Keston noted a Te activity growing out of this iodine activity, but with radiations which did not seem compatible with those of Te^{125*}. Dr. Keston kindly sent us an aged sample of I^{125} from which we separated Te. A weak activity was observed, and an absorption curve in Al measured. Within the limits of error this curve agreed with the electron absorption curve shown in Fig. 1.

From our measurements it appears that Te^{125*} decays by an isomeric transition which is probably "2^5-pole." Because of the fact that this metastable state is by far the longest-lived known for a nucleus with a stable ground state and because Te^{125*} can be obtained carrier free and in weighable amounts, it appears to be a particularly suitable example for a test of the theory of nuclear isomerism by a direct measurement of the spins of the two isomers. Such an attempt is at present underway in this laboratory.

We wish to thank Mr. M. McKeown for his valuable assistance. This work was carried out under the auspices of the Atomic Energy Commission.

* Now at University of Illinois.
[1] Plutonium Project, "Nuclei produced in fission," Rev. Mod. Phys. 18, 513 (1946).
[2] A. F. Reid and A. S. Keston, Phys. Rev. 70, 987 (1946).
[3] L. E. Glendenin and R. R. Edwards, Phys. Rev. 71, 742 (1947).

Analytic Behavior of Heisenberg's *S*-Matrix

R. J. EDEN
Peterhouse, Cambridge, England
May 13, 1948

IF scattering of a photon on a hydrogen atom is studied by usual quantum perturbation theory, the wave matrix takes the form[1]

$$(p\alpha'|\psi_1|p^0\alpha^0)=(p\alpha'|p^0\alpha^0)+\delta_+(\nu-\nu')(p\alpha'|r_1|p^0\alpha^0), \quad (1)$$

where p is the momentum, ν is the energy of outgoing photon, and $\nu'=E^0-H_S(\alpha')$ is determined by energy conservation. The "partial" S-matrix is defined by

$$(p\alpha'|S_1|p^0\alpha^0)=(p\alpha'|p^0\alpha^0)+\delta(\nu-\nu')(p\alpha'|r_1|p^0\alpha^0). \quad (2)$$

This should be distinguished from the "complete" S-matrix, which is defined only for energies large enough to ionize the atom and contains elements for electron photon scattering on a proton center. The form of r_1 will depend on the approximation used. For total energy E^0 near to $H_S(\alpha'')$, the energy of an excited state, it can be shown that the matrix element $(p\alpha'|r_1|p^0\alpha^0)$ taken on the energy shell is an analytic function of E^0 if $H_S(\alpha')<H_S(\alpha'')$, and has a singularity at $E^0=H_S(\alpha'')+a-ib$, where b is positive. As remarked by Wentzel,[2] b is related to the total emission probability from state (α'').

If $\alpha^0\alpha'\alpha''$ denote ground level, first excited level, etc., the matrix element $(p\alpha^0|r_1|p^0\alpha^0)$ for elastic scattering is an analytic function of E^0 even at the critical values $H_S(\alpha')$, but the matrix element $(p\alpha'|r_1|p^0\alpha^0)$ for inelastic scattering is zero for $E^0<H_S(\alpha')$ but non-zero and analytic for $E^0>H_S(\alpha')$. This has two consequences: the partial S-matrix goes into the complete S-matrix for high enough energies, and the partial S-matrix is not an analytic function of energy. If the complete S-matrix is analytically continued into the low energy region, it will satisfy the unitary condition $SS\dagger=I$; hence the partial S-matrix is not unitary.

It is desirable that a consistent physical picture be given by the complete S-matrix, and this requires an interpretation of the analytic continuation of matrix elements $(p\alpha'|r|p^0\alpha^0)$ in region $E^0<H_S(\alpha')$ where inelastic scattering is not possible, i.e., where $(p\alpha'|r_1|p^0\alpha^0)=0$. This is obtained by defining probability as $(p\alpha'|r|p^0\alpha^0)(p^0\alpha^0|r\dagger|p\alpha')$, where $r\dagger$ is the analytic continuation in the E^0 plane of the Hermitian conjugate to r taken for E^0 greater than ionization energy. Thus the probability is $|(p\alpha'|r|p^0\alpha^0)|^2$ for $E^0>H_S(\alpha')$, but because of a factor $(\nu')^{-1}$ in $(p\alpha'|r|p^0\alpha^0)$ is $-|(p\alpha'|r|p^0\alpha^0)|$ for $E^0<H_S(\alpha')$. In S-matrix theory we require the interpretation that a negative probability corresponds to a physically impossible process.

Since this work was completed a note by T. S. Chang[3] has appeared, mentioning negative probabilities in connection with the unitary condition on S, but without further details it is not possible to tell if his conclusions are the same as ours. A fuller account of the calculations reported here will be published later. I wish to thank Dr. N. Kemmer for advice and encouragement.

[1] P. A. M. Dirac, *Quantum Mechanics*, third edition, Chapter 8.
[2] G. Wentzel, Helv. Phys. Acta 21, 49 (1948).
[3] Chang, Am. Phys. Soc. (April 29, 1948).

Neutron Deficient Isotopes of Cerium and Lanthanum

J. B. CHUBBUCK AND I. PERLMAN
Radiation Laboratory and Department of Chemistry, University of California, Berkeley, California
August 30, 1948

FAST particle fission of bismuth in this laboratory has produced neutron deficient isotopes in the region of cerium.[1] The studies described herein were undertaken partly to identify some of these.

On the neutron deficient side of stability, two radioactive isotopes of lanthanum assigned to La^{137} [2,3] and La^{138} [4] have been reported, but recent measurements[5] show La^{138} to be stable or extremely long-lived and present in naturally occurring lanthanum to the extent of 0.089 percent. Evidence is presented below for assigning the reported radioactive properties of La^{137} to La^{135} and those of La^{138} to La^{136}.

To prepare the lanthanum activities cesium in the form of $CsNO_3$ was irradiated with 30-Mev helium ions in the 60-inch cyclotron. The lanthanum fraction was separated and the decay curve resolved into two components of 2.1-hour and 19.5-hour half-lives. Both of these activities, therefore, must belong to isotopes of lanthanum of mass number 136 or lower.

A low resolution beta-ray spectrometer showed a positron of 0.82 Mev, decaying with the 2-hour half-life, the energy estimated from the visual end point of the spectrometer curve. No negative particles were detected. A Feather analysis of a beryllium absorption curve, taken soon after

TABLE I.

Isotope	Type of radiation	Half-life	Energy of radiation in Mev: Particle	Energy of radiation in Mev: Electromagnetic	Produced by	Cross section $\times 10^{24}$ cm^2
La^{137}		>400 yr.			decay of Ce^{137}	
La^{136}	β^+	2.1 hr.	0.84	None	$Cs^{133}(\alpha, n)$	0.0003*
La^{135}	K, γ	19.5 hr.	None	0.76	$Cs^{133}(\alpha, 2n)$	0.03*
Ce^{139}	K, γ, e^-	140 days	0.15	0.18 1.8	$La^{139}(d, 2n)$	0.09**
Ce^{137}	K, γ, e^-	36 hr.	0.18	0.28 0.75	$La^{139}(d, 4n)$	0.06† 0.002** 0.04††
Ce^{135}	β^+	16 hr.			$La^{139}(d, 6n)$	

* 30-Mev helium ions.
** 20-Mev deuterons.
† 40-Mev deuterons.
†† 60-Mev deuterons.

the bombardment, gave a range in beryllium of 310 mg/cm², corresponding to an energy of 0.84 Mev.

A beryllium absorption curve was taken about twenty-four hours after the bombardment, when the 2.1-hour activity had decayed out. This curve showed no particle radiation, but a 5.2-kev L x-ray component could be resolved from the harder electromagnetic radiation. The positron activity determined earlier therefore belongs entirely to the 2.1-hour activity. Earlier absorption curves taken with aluminum showed the presence of a 34-kev x-ray while a 0.76-Mev gamma-ray in low intensity was determined by lead absorption. All of the electromagnetic radiation noted soon after bombardment could be attributed to the 19.5-hour activity that was present; thus the 2.1-hour activity probably has no electromagnetic radiation. In the 19.5-hour activity x-rays were more abundant than gamma-rays by a factor of about 50, indicating that most of the electron capture decay goes directly to the ground state.

As indicated in Table I, the 2.1-hour activity was formed in about 1/100 the yield of the 19.5-hour activity. With the energy of helium ions employed (30 Mev), the $(\alpha, 2n)$ reaction is more prolific than the (α, n) reaction.[6] The order of the decay energies is also compatible with the assignment of the 2.1-hour period to La^{136} and the 19.5-hour period to La^{135}.

The radioactive isotope of cerium decaying by K-electron capture and assigned to mass number 137 is discussed below. The lanthanum daughter of this isotope was not definitely observed, and a minimum half-life could be set at 400 years, based on x-ray counting rates.

Cerium activities were produced by irradiating La_2O_3 with 20-Mev deuterons in the 60-inch cyclotron. A sample of the chemically separated cerium resolved into two components: 140-day Ce^{139} and a 36-hour activity assigned below to Ce^{137}. Pool and Krisberg[7] have recently reported work with Ce^{139} in which they found conversion electrons and gamma-radiation of 0.184 and 0.8 Mev, respectively. In the present study, the conversion electrons were confirmed, the low energy gamma-ray was determined as 0.18 Mev, but a value of 1.8 Mev was found for the hard component. The conversion electrons were determined as 0.15 Mev, both with the beta-ray spectrometer and by absorption in beryllium.

In another bombardment of La_2O_3, 40-Mev deuterons from the 184-inch cyclotron were employed. This bombardment produced the 36-hour activity in far greater yield compared to the 140-day activity than did the 20-Mev deuteron bombardment. These two cerium activities are therefore probably not isomers, and the most likely assignment for the 36-hour activity is Ce^{137}.

A sample containing the 36-hour activity showed a well defined conversion electron peak, with an energy of about 0.23 Mev. There was no positron activity with this isotope. A beryllium absorption curve indicated a range of about 45 mg/cm², corresponding to an energy of about 0.22 Mev. An aluminum absorption curve showed the presence of 34-kev x-rays while gamma-rays of 0.28 and 0.75 Mev were measured with lead absorbers.

A third bombardment of La_2O_3 was made, this time with 60-Mev deuterons, in an attempt to prepare the parent of La^{135} by the $d, 6n$ reaction. The 36-hour Ce^{137} activity was formed in such high yield that the Ce^{135} activity was completely masked in the gross decay curve, but a sample of the cerium activity placed on the beta-ray spectrometer showed positron activity. Because of the great background from scattered radiation, the positron energy could only be estimated as 0.4 Mev. Integration of the area under the positron peaks of successive beta-ray spectrometer curves taken for two days indicated a half-life of about 16 hours. It was impossible to determine any other characteristics of this isotope. The activity is assigned to Ce^{135} because it had not appeared in bombardments at lower energies, and 19.5-hour La^{135} could be shown to grow into the cerium fraction at a rate corresponding to a half-life for its parent of about 16 hours.

The cooperation of Dr. J. G. Hamilton, Mr. D. C. Sewell, Mr. J. T. Vale, Mr. T. Putnam, Mr. B. Rossi, and other members of the 60-inch and 184-inch cyclotron groups is gratefully acknowledged. This research was sponsored by the Atomic Energy Commission under Contract No. W-7405-eng-48 with the Radiation Laboratory, University of California, Berkeley, California.

[1] R. H. Goeckermann and I. Perlman, Phys. Rev. **73**, 1127 (1948).
[2] K. E. Mounce, M. L. Pool, and J. D. Kurbatov, Phys. Rev. **61**, 389 (1942).
[3] K. E. Weimer, M. L. Pool, and J. D. Kurbatov, Phys. Rev. **63**, 67 (1943).
[4] M. L. Pool, J. M. Cork, and R. L. Thornton, Phys. Rev. **52**, 239 (1937).
[5] M. G. Inghram, R. J. Hayden, and D. C. Hess, Jr., Phys. Rev. **72**, 967 (1947).
[6] G. Wilkinson, private communication.
[7] M. L. Pool and N. L. Krisberg, Phys. Rev. **73**, 1035 (1948).

Anomalous Values of the Thermionic Emission Constant

HENRY F. IVEY
Research Department, Lamp Division, Western Electric Corporation, Bloomfield, New Jersey
July 19, 1948

THE theoretical value for the thermionic emission constant, A, in the Richardson-Dushman equation, $I=AT^2\exp(-e\phi/kT)$, is 120 amp./cm² deg.² In general, measured values are smaller than this figure. Recently two papers[1,2] have appeared in which an attempt is made to explain theoretically the anomalously large values of A reported for some metals, and in particular for nickel. Both of these authors have accepted the experimental value of Fox and Bowie[3] for nickel, $A=1380$ amp./cm² deg.² $\times(\phi=5.03$ ev). As is well known and indeed is stressed by Wohlfarth,[2] the emission constants are very sensitive to surface impurities. Later, measurements by Wahlin[4] under very exacting experimental conditions have resulted in values of $A=30$ amp./cm² deg.² and $\phi=4.61\pm0.05$ ev for nickel. If these values are assumed correct, then the emission constant for nickel is not greater than the theoretical value.

A similar situation exists in the case of platinum. The often quoted DuBridge[5] measurements gave $A=17{,}000$ amp./cm² deg.² and $\phi=6.27$ ev. Later measurements by

Van Velzer[6] resulted in $A=170\pm20$ amp./cm^2 deg.^{2} and $\phi=5.40\pm0.03$ ev after severe heat treatment. The more recent investigations of Whitney[7] have given values of $A=32$ amp./cm^2 deg.^{2} and $\phi=5.32$ ev. In the words of Whitney, "Special explanations to justify the exceptional behavior of platinum now seem unnecessary."

The only other metal for which an A value greater than 120 amp./cm^2 deg.^{2} has been reported is zirconium, for which Zwikker[8] obtained $A=330$ amp./cm^2 deg.^{2}, $\phi=4.12$ ev. Recent experiments[9] in this laboratory seem to indicate that there is no anomaly for this material either, the values being at least as low as $A=120$ amp./cm^2 deg.^{2} and $\phi=4.00$ ev.

The latest measurements therefore seem to indicate that there is no *clean* metal with an emission constant larger than the theoretical value, and complicated theoretical arguments to explain such values are unnecessary. A satisfactory explanation of the fact that the experimental values for clean metals in general are smaller than the theoretical value, while those for metals which are not clean may be larger than this value, is of course still very desirable.

[1] Sun Nien T'ai and W. Band, Proc. Camb. Phil. Soc. **42**, 72 (1946).
[2] E. P. Wohlfarth, Proc. Phys. Soc. **60**, 360 (1948).
[3] G. W. Fox and R. M. Bowie, Phys. Rev. **44**, 345 (1933).
[4] H. B. Wahlin, Phys. Rev. **61**, 509 (1942).
[5] L. A. DuBridge, Phys. Rev. **32**, 961 (1928).
[6] H. L. Van Velzer, Phys. Rev. **44**, 831 (1933).
[7] L. V. Whitney, Phys. Rev. **50**, 1154 (1936).
[8] C. Zwikker, Physik. Zeits. **30**, 378 (1929).
[9] Sponsored by the Signal Corps Engineering Laboratories, U. S. Army, under Contract No. W-36-039-sc-33643.

Anomalous Values of the Thermionic Emission Constant

E. P. WOHLFARTH
Department of Physics, Leeds University, Leeds, England
July 26, 1948

IN a recent paper[1] the writer has given a theoretical treatment of the temperature variation of thermionic emission constants of metals, with particular reference to nickel. In this treatment the effect of the overlap of the d and s electronic energy bands is considered, following earlier work by Sun Nien T'ai and Band.[2] It is shown that for nickel, for which the unoccupied energy width of the d band is relatively small, there is a marked decrease of the work function, χ, with temperature. By writing the Richardson-Dushman equation in the form

$$I=A(1-\dagger)T^2\exp(-\chi_0/kT),$$

with χ_0 constant, the current constant A, defined by

$$A/A_0=\exp(\chi_0-\chi)/kT,$$

increases with temperature, A_0 being the "standard" constant, 120 amp. cm^{-2} deg.$^{-2}$. It is shown, by employing precise values of Fermi-Dirac functions, that the increase is such as to make A/A_0 equal to about 2 at 1400°K. The treatment given is necessarily rather complicated, if the effect of band overlap on thermionic emission is to be accurately assessed. The experimental value of A for nickel due to Fox and Bowie,[3] $A=1380$ amp. cm^{-2} deg.$^{-2}$, which was thought to be the most recent and reliable, is about six times larger than that calculated. It has been pointed out to the writer by Dr. H. F. Ivey that the more recent values of A due to Wahlin[4] are much smaller than the calculated one. Various possible reasons for anomalous values of the current constant, either larger or smaller than the theoretical A, have already been given[1] and are briefly summarized below.

In the first place, the theoretical value derived from a consideration of electronic energy bands does not allow for the effects of surface charging, thermal expansion, etc. These have been fully recognized and discussed by Herzfeld,[5] Becker and Brattain,[6] Wigner,[7] Reimann,[8] and others, who have shown that the effects introduce a multiplying factor which may be greater or less than unity. (The effect of thermal expansion on the number of electrons per unit volume, for example, was shown by Reimann[8] to be a decrease of the current constant by a factor which may be as much as 5.) Secondly, the representation of the thermionic current by a Richardson line leads to a value of log$A$ as determined by extrapolation of the line to $1/T=0$. The experimental results are usually obtained at temperatures corresponding to $1/T\times10^4$ lying between 5 and 10, and the long-range extrapolation may often be uncertain, leading to slight errors in log$A$ and correspondingly larger ones in A. In addition, with a temperature dependent work function, the value of A derived by this means usually varies with the temperature of observation, and is thus of less direct theoretical significance than was previously supposed. Finally, as pointed out by Wahlin[4] and others, the effect of the heat treatment of the specimen, prior to measurement, is of predominant importance. The earlier measurements on nickel[3] were made after severe outgassing, and the specimens were considered pure. Wahlin heat-treated his specimens even more rigorously and obtained current constants which decreased from values of the same order as those observed by Fox and Bowie[3] to much lower ones of about 30 to 70 amp. cm^{-2} deg.$^{-2}$. As Wahlin points out, one effect of prolonged heating may be the diffusion of impurity atoms to the emitter surface. This might lead to the formation of a monatomic surface film, as in the case of thoriated tungsten, for which very small values of A have been observed,[9] due, possibly, to an increase in the reflection coefficient. Although Wahlin's specimens were stated to be free from cobalt and platinum, minute traces of other impurities, of sufficient amount to form a monatomic film, might well have been present.

In view of the many factors which are difficult to control and which may influence the thermionic emission to an unpredictable extent, it is not surprising that there are such marked differences among the experimental values of A. The theoretical calculations are believed to be essentially correct for the ideal metal, but they make no allowance for the various disturbing secondary effects. Until these are more fully understood, no really satisfactory comparison of theoretical and experimental results can be made. It is perhaps not irrelevant to point out that the more recent work raises the question as to whether the

apparent agreement of the experimental values of A, reported earlier for many metals,[9] with the standard value of 120 amp. cm^{-2} deg.$^{-2}$ is more than fortuitous.

[1] E. P. Wohlfarth, Proc. Phys. Soc. **60**, 360 (1948).
[2] Sun Nien T'ai and W. Band, Proc. Camb. Phil. Soc. **42**, 72 (1946).
[3] G. W. Fox and R. M. Bowie, Phys. Rev. **44**, 345 (1933).
[4] H. B. Wahlin, Phys. Rev. **61**, 509 (1942).
[5] K. H. Herzfeld, Phys. Rev. **35**, 248 (1930).
[6] J. A. Becker and W. H. B. Brattain, Phys. Rev. **45**, 694 (1934).
[7] E. P. Wigner, Phys. Rev. **49**, 696 (1936).
[8] A. L. Reimann, Nature **133**, 833 (1934).
[9] A. L. Reimann, *Thermionic Emission* (Chapman and Hall, Ltd., London, 1934).

Erratum: The Magnetic Threshold Curves of Superconductors

[Phys. Rev. **72**, 89 (1947)]

J. G. DAUNT
Mendenhall Laboratory, Ohio State University, Columbus, Ohio

August 24, 1948

IN a letter with the above title a misprint occurred in Eq. (2), giving the temperature dependency of the number of superconductive electrons. This should read:

$$n_s = n_0[1-(T/T_c)^4].$$

This is in agreement with the experimental results obtained so far by penetration depth measurements.[1] It also can be deduced, as pointed out by the author earlier, from the two-fluid theory of superconductivity of Gorter and Casimir,[2] provided a parabolic form[3-5] is assumed for the magnetic threshold curves. A further discussion of this has been given by Miller.[6] It should be remembered that this result quoted above treats only the thermodynamic properties of the superconductor and any subsequent evaluation of electrodynamic properties must involve further assumptions.

[1] J. G. Daunt, A. R. Miller, A. B. Pippard, and D. Shoenberg, Phys. Rev. **74**, 842 (1948).
[2] C. J. Gorter and H. Casimir, Zeits. f. tech. Physik **15**, 539 (1934).
[3] J. A. Kok, Physica **1**, 1103 (1934).
[4] J. G. Daunt, A. Horseman, and K. Mendelssohn, Phil. Mag. **27**, 754 (1939).
[5] J. G. Daunt, Phys. Rev. **72**, 89 (1947).
[6] A. R. Miller, Aust. J. Sci. (June, 1948).

Divergence Difficulty and Mixed Meson Theory

GENTARO ARAKI
Department of Industrial Chemistry, Kyoto University, Kyoto, Japan

July 7, 1948

THE divergence of the magnetic moment of the nucleon is one of the grave difficulties of Yukawa's theory of mesons. Another difficulty is that the nuclear potential involves also divergent integrals according to the one-meson theory, although this fact has not yet been fully noticed. These difficulties can be removed by mixing a pseudoscalar field with a pseudovector one. The pseudoscalar theory[1] gives the proton a positive surplus magnetic moment, whereas the pseudovector theory has a negative one. They are given by the following divergent integrals:

$$\mu_P = +(e/\hbar c)(f^2/\kappa^2)(2/3\pi)\int_0^\infty [k^4dk/(k^2+\kappa^2)^2] \quad \text{(pseudoscalar)}, \quad (1)$$

$$\mu_P = -(e/\hbar c)(g^2/K^2)(2/3\pi)\int_0^\infty [k^4dk/(k^2+K^2)^2] \quad \text{(pseudovector)}, \quad (2)$$

where f and g are, respectively, the constants of pseudovector and six-vector couplings of pseudoscalar and pseudovector mesons with nucleons, and $\hbar\kappa/c$ and $\hbar K/c$ are, respectively, the masses of pseudoscalar and pseudovector mesons. If we consider a mixture of both fields and, further, if we assume $(f/\kappa)^2=(g/K)^2$ and $\kappa<K$, the surplus magnetic moment of the proton becomes a following positive finite value:

$$\mu_P = (e/2\kappa)(f^2/\hbar c)[(K/\kappa)-1]. \quad (3)$$

This amounts to 1.86 nuclear magnetons, i.e., the observed value, if $K=4.7\kappa$, $f^2=0.05\hbar c$, and $M=10\mu$, where μ and M denote the masses of the pseudoscalar meson and the proton. Various experimental evidences are in favor of the pseudoscalar theory.[2] The scalar theory does not explain the magnetic moment of nucleons (in the Schrödinger approximation), and the vector theory gives the proton a positive surplus moment. Therefore, there is no remedy for the difficulty but the above-mentioned mixture. Schwinger's mixture[3] must be ruled out in this respect.

The present mixture removes also the divergent and r^{-3} difficulties from the nuclear potential. The nuclear potential in the symmetrical pseudoscalar meson theory has the same form as that given by (4) below, but ϕ and χ involve divergent integrals. The divergent part of ϕ represents a direct interaction and it can be eliminated in the relativistically invariant way by introducing its negative in the Hamiltonian.[2,4] In the case of the pseudovector theory the sign of (4) is to be reversed and f and κ are to be replaced by g and K. In this case ϕ and χ involve the divergent terms also. The former can be eliminated in the same way. On the contrary, the divergent part of χ cannot be excluded in such a way in both cases. However, this divergent term also disappears in the present mixture. The nuclear potential becomes the following finite expression:

$$U = f^2(\tau^{(1)}\tau^{(2)}/2)\{(\sigma^{(1)}\sigma^{(2)}/3)\phi+\Lambda\chi\}, \quad (4)$$

where $\Lambda=3(\sigma^{(1)}\mathbf{x})(\sigma^{(2)}\mathbf{x})/r^2-\sigma^{(1)}\sigma^{(2)}$, and ϕ and χ are now given by convergent integrals. The function $\chi(r)$ has only a r^{-1} singularity as Schwinger's mixture.[4] The term including ϕ is repulsive for small r, attractive for large r, and it has consequently a shallow minimum in the even state. This feature of ϕ distinguishes the present mixture from Schwinger's. This weakness of the attraction due to ϕ may give a favorable effect to the electric quadrupole moment of deuteron caused by $\Lambda\chi$-term.[2]

The energy spectrum of the nuclear β-decay in the present mixed theory is somewhat different from the result of the pseudoscalar theory. It is given by

$$a(1+b^2-2b/\epsilon)(\epsilon^2-1)^{\frac{1}{2}}(\epsilon_0-\epsilon)^2\epsilon d\epsilon, \quad (5)$$

where $b=(g'/f')(\kappa/K)$. This reduces to the result of the pseudoscalar theory if we put $b=0$. From this and the experiment of Bjerge and Brostrøm[5] we obtain the lifetime of the pseudoscalar meson as follows:[6]

$$\tau_0 = 10^{-5}|J|^2 \quad \text{or} \quad 1.6\times10^{-5}|J|^2 \text{ sec.}, \quad (6)$$

according to $b=0.3$ or 1, where J is the overlapping integral of wave functions (space part) of ^{6}He ^{1}S and ^{6}Li ^{3}S. If we assume $J=0.5$ we have $\tau_0=2.5\times10^{-6}$ or 4×10^{-6} sec., which agrees with experiment. This value of J is quite reasonable. Such an agreement can only be obtained in the pseudoscalar theory, as I pointed out already.[6] Other bearing on experimental facts was well discussed for the two-meson theory by Wentzel.[2]

The detailed report will be published in Progress of Theoretical Physics.

[1] G. Araki, Prog. Theor. Phys. 1, 1 (1946).
[2] G. Wentzel, Rev. Mod. Phys. 19, 1 (1947).
[3] J. Schwinger, Phys. Rev. 61, 387 (1942).
[4] G. Araki, discussion in the meeting of meson theory held in Tokyo, Sept. 26, 1943.
[5] T. Bjerge and K. J. Brostrøm, Nature 138, 400 (1936).
[6] G. Araki, Sci. Pap. I. P. C. R. 40, 311 (1943).

On the Magnetic Moment of Nucleons According to the Pseudovector Meson Theory

GENTARO ARAKI
Department of Industrial Chemistry, Kyoto University, Kyoto, Japan
September 2, 1948

RECENTLY I have been able to eliminate the divergency of the magnetic moment of nucleons as well as that of the two-nucleon potential by assuming a pseudoscalar-pseudovector mixed theory of mesons.[1] In this calculation I assumed that the interaction between pseudovector mesons and nucleons is the 6-vector coupling (g being its constant).

On the other hand, we can equally assume that the interaction is the pseudovector coupling (F being its constant). On the basis of an assumption of both the couplings we have still the negative surplus magnetic moment of the proton. It consists of two terms proportional to F^2 and g^2, respectively, but it does not include a term proportional to Fg. The g^2 term was given previously. The F^2 term is as follows:

$$\mu_P=-(e/2K)(F^2/\hbar c)(2/\pi K)\int_0^\infty[(k^4-K^2k^2)/(k^2+K^2)^2]dk,$$

where $\hbar K/c$ is the mass of the pseudovector meson. This result provides us with criteria for various mixed meson theories.

We consider three kinds of the pseudovector mesons. The first is in interaction with nucleons by the 6-vector (antisymmetric tensor of the second rank) coupling, the second by the pseudovector coupling, and the third by both couplings. These will be referred to as *pvt*, *pvv*, and *pv*, respectively. Further, we refer to the vector and the pseudoscalar mesons as *v* and *ps*, respectively. If we consider a mixture of two fields in order to eliminate divergencies from the magnetic moment of nucleons and the two-nucleon potential, we have eight possibilities as follows: (a) *ps* and *v*, (b) *ps* and *pvt*, (c) *v* and *pvt*, (d) *pvv* and *v*, (e) *pvv* and *ps*, (f) *pvv* and *pvt*, (g) *pv* and *ps*, (h) *pv* and *v*. Cases (a) and (b) were already discussed. In the cases (a) and (f) we can eliminate the divergency from the two-nucleon potential but not from the magnetic moment.[2] In the cases (c) and (e) we can eliminate the divergency from the latter but not from the former. In the case (d) we can eliminate separately from each but not simultaneously from both. The case (g) reduces to (b) in order to satisfy the above-mentioned requirement.

In the last case (h) the conditions are $(G/K_1)^2=5(g/K)^2$ and $F^2=6g^2$ for that requirement, where $\hbar K_1/c$ is the mass of v, and G is a constant of the 6-vector coupling between v and nucleons. Further, K_1 must be smaller than $1.3K$ in order that the surplus magnetic moment of the proton is positive and K_1 must be larger than K in order that the electric quadrupole moment of the deuteron is positive. Then the spherically symmetric part of the two-nucleon potential is repulsive for large r. If we require that it becomes attractive for small r, we must restrict K_1 more severely so that $1.14K<K_1<1.3K$.

We have thus examined all cases of possible mixtures of two meson fields and we see that only two cases (b) and (h) enable us to eliminate the divergencies in question. If we want to know which assumption is in accordance with experiments, the more detailed study is necessary.

[1] G. Araki, Phys. Rev., preceding letter.
[2] The case (f) has been suggested by S. Watanabe in his private communication for me.

Erratum: A Convergent Expression for the Magnetic Moment of the Neutron

[Phys. Rev. 74, 2 (1948)]
D. RIVIER AND E. C. G. STUECKLBERG
University of Geneva, Geneva, Switzerland

IN our previous letter two misprints have occurred which make the text impossible to understand: The formulas defining T^2 and $\theta(T^2)$ are

$$T^2=t^2-r^2,$$
$$\theta(T^2)=0, \quad T^2<0,$$
$$\theta(T^2)=1, \quad T^2>0.$$

Dielectric Behavior of Single Domain Crystals of BaTiO$_3$

GORDON C. DANIELSON, BERND T. MATTHIAS, AND JOHN M. RICHARDSON
Bell Telephone Laboratories, Inc., Murray Hill, New Jersey
August 26, 1948

AN accurate determination of the dielectric anisotropy of $BaTiO_3$ was, till now, partly hindered by the domain structure of the crystals. More detailed studies of the domain structure of crystals grown from C.P. ingredients indicated that the splitting up into domains is largely due to impurities. Two ways of obtaining single domain crystals seemed possible: increase of purity or the use of mineralizers. The latter way proved to be successful. The resultant single domain crystals were large (0.5 cm) flat plates with the optic (c) axis normal to the major plane.

The dielectric measurements were made by conventional methods except for the precaution of using painted electrodes in order to avoid the splitting up into domains

readily arising from small mechanical stresses. In agreement with previous statements[1] the ϵ_a for small fields was larger than ϵ_c. However, the ratio was found to be orders of magnitude larger than previously. At room temperature ϵ_c and ϵ_a were found to be approximately 3×10^2 and 2×10^5, respectively, and near the Curie point (122°C) they both reached flat peaks having maxima about twice the values at room temperature.

These dielectric constants show a marked decrease with frequency[2] in the range of about 1 to 10 mc. The relaxation time of ϵ_a was found to be about 10^{-7} sec. and that of ϵ_c seemed to be about 10^{-8} sec., although there were experimental difficulties in the latter case.

Having a single domain, we could now verify by x-rays the displacement of the Ti or O ions from their symmetric positions. Weissenberg pictures showed this displacement to be ~0.16A in agreement with experimental values of the spontaneous polarization.[3]

Detailed results will be presented in a forthcoming paper.

[1] B. T. Matthias, Nature **161**, 325 (1948).
[2] The authors are indebted to W. A. Yager of Bell Telephone Laboratories for performing these measurements.
[3] H. F. Kay and R. G. Rhodes, Nature **160**, 126 (1947).

Theory of the Dielectric Behavior of $BaTiO_3$

JOHN M. RICHARDSON AND BERND T. MATTHIAS
Bell Telephone Laboratories, Inc., Murray Hill, New Jersey
August 26, 1948

IN the preceding letter we have presented measurements of the real part ϵ' of the complex dielectric constant of a single domain crystal of $BaTiO_3$ as a function of the temperature and of the frequency ω along the a and c axes ($\perp$ and $\parallel$ to the direction of spontaneous polarization). Here we will advance a theory for the spontaneous polarization and for the relative magnitudes of ϵ' along the a and c axes. We will also discuss in a qualitative way the frequency dependence. We will consider possible reasons for the anisotropy of the experimental dielectric measurements above the Curie point (122°C) which are in contradiction to x-ray studies.[1,2]

Let the $BaTiO_3$ crystal be represented by the idealized system consisting of a cubic lattice of cubically symmetrical potential wells (representing short-range interactions with the oxygen nearest neighbors), each containing one Ti ion subject to Coulomb interactions with the other Ti ions. Let $\mathbf{r}_n$ be the displacement of the nth Ti ion from the central position in its potential well and suppose that the distribution of charge in the neighborhood of the Ti ion be such that there is no net charge and such that when $\mathbf{r}_n=0$ there is no net electric moment. The moment of the nth Ti ion is $\boldsymbol{\mu}_n=q\mathbf{r}_n$, where q is the effective charge. It is now our task to calculate the average moment of a Ti ion when the applied field is $\mathbf{E}$ (average field in the material).

The quantum-mechanical density matrix ρ for the system if given by maximizing the entropy $S=-ktr(\rho\log\rho)$, subject to the restrictions that the average energy is fixed and that the density matrix is normalized. By approximating the density ρ by $\Pi_n\rho_n$, where ρ_n is the density matrix for $\mathbf{r}_n$ and where all of the ρ_n's are of the same form, the above variational process yields the following equation forming the basis of a simple cooperative theory:

$$\langle\bar{\mu}\rangle_{Av}=tr(\boldsymbol{\mu}_1\exp[-(H_1-\boldsymbol{\mu}_1\cdot\mathbf{F})/kT])/tr\exp[-(H_1-\boldsymbol{\mu}_1\cdot\mathbf{F})/kT], \quad (1)$$

where H_1 is the Hamiltonian operator for a Ti ion in its own potential well acted upon by no other forces, and where $\mathbf{F}$ is the so-called local field approximating the Coulomb interactions with neighboring Ti ions. Including *now* the polarizability α per unit cell associated with everything but the displacement of Ti ions, we find the local field to be given approximately by

$$\mathbf{F}=[\mathbf{E}+(4\pi/3v)\langle\bar{\mu}\rangle_{Av}]/[1-(4\pi\alpha/3v)], \quad (2)$$

when v is the volume of a unit cell. Eliminating $\mathbf{F}$ from Eqs. (1) and (2) and solving for $\langle\bar{\mu}\rangle_{Av}$, we have the final solution of our problem. In the case in which $\langle\bar{\mu}_1\rangle_{Av}=0$ and $\mathbf{E}=0$ we find the dielectric constant (at zero frequency) to be

$$\epsilon_0=1\epsilon_0,$$
$$(\epsilon_0-1)/(\epsilon_0+2)=(4\pi/3v)(\alpha+\alpha_{\mathrm{Ti}}), \quad (3)$$

where

$$\alpha_{\mathrm{Ti}}=\tfrac{1}{3}\Sigma_{ij}(\mu_{1,ij}\cdot\boldsymbol{\mu}_{1,ji}\times[\exp[-H_{1,i}/kT]-\exp[-H_{1,j}/kT]/(H_{1,j}-H_{1,i})])/\Sigma_i\exp[-H_{1,i}/kT] \quad (4)$$

is the ionic polarizability of the Ti ion. ($\boldsymbol{\mu}_{1,ij}$ are the matrix elements of $\boldsymbol{\mu}_1$ in a representation in which H_1 is diagonal, that is, $H_{1,ij}=H_{1,i}\cdot\delta_{ij}$.) It is found that with $\mathbf{E}=0$ Eqs. (1) and (2) have a unique solution $\langle\bar{\mu}_1\rangle_{Av}=0$ when

$$(4\pi/3v)(\alpha+\alpha_{\mathrm{Ti}})<1, \quad (5)$$

and that when the inequality is reversed there are several non-vanishing solutions in addition to the solution $\langle\bar{\mu}_1\rangle_{Av}=0$ which is then unstable ($4\pi/3$ catastrophe). Using $\langle\bar{\mu}_1\rangle_{Av}=\langle\bar{\mu}_1\rangle_{Av}/q$ as a parameter of external force, we find the free energy, A, of a Ti ion in the first case to have one minimum at $\langle\mathbf{r}_1\rangle_{Av}=0$ and no other extrema, and in the second case to have one maximum at $\langle\mathbf{r}_1\rangle_{Av}=0$ and several minima at points $\langle\mathbf{r}_1\rangle_{Av}\neq0$. Thus the existence of spontaneous polarization in $BaTiO_3$ can be explained on the basis of this simple picture in which an excessively large polarizability[3] per unit volume causes the cubic structure to become unstable.

The simple facts regarding ϵ and the direction of spontaneous polarization can be understood by assuming A to be a cubically symmetrical 4th degree polynominal in $\langle\mathbf{r}_1\rangle_{Av}$. In this case it is found that spontaneous polarization can occur only in a (100) or (111) direction. If a system is on the border line between these two types of polarization, the dielectric constant $\perp$ to the direction of spontaneous polarization will be infinite. The large ratio ϵ_a/ϵ_c of the dielectric constants $\perp$ and $\parallel$ to the direction of spontaneous polarization in $BaTiO_3$ can be explained by assuming that the crystal is spontaneously polarized in a (100) direction but is on the verge of going over to a (111) direction.

The frequency dependence of ϵ_a and ϵ_c can be fitted fairly well by curves based upon one relaxation time each: τ_a and τ_c. It is found experimentally that $\tau_a/\tau_c \sim 10$. Presumably there are no domains and consequently no hysteretic losses associated with domain boundary movements. The losses might be assumed to arise from the anharmonic interactions between the motion of the Ti ions and the other normal modes of nuclear motion. The anharmonicity of the motion of Ti in the *a* direction will be much larger than that of the motion in the *c* direction because of the much lower harmonic force constant in the former case. Hence there will be a much larger interaction between the motion of Ti in the *a* direction and the other normal modes than in the case of the *c* direction. Consequently we would have $\tau_a/\tau_c \gg 1$.

The observed dielectric anisotropy above the Curie point (122°C) in these experiments is still unexplained. It must be remembered that the sample is macroscopically very anisotropic, the thickness (in the *c* direction) being only a few hundredths of the length and breadth (in the *a* and *b* directions). A marked anisotropy of ϵ in the normally cubic crystal may be caused by strains produced in the growth process. Since the thickness is only a few micros, it is not impossible that some surface effects are coming in.

The subjects discussed here will be treated more fully in a forthcoming paper.

[1] H. D. Megaw, Proc. Roy. Soc. **A189**, 261–83 (1947).
[2] G. C. Danielson, private communication.
[3] It is possible that an abnormally high electronic polarizability of $O^=$ is largely responsible. See W. Shockley, Phys. Rev. **73**, 1273 (1948).

Natural and Induced Ferromagnetic Resonance

J. B. Birks
Department of Natural Philosophy, The University, Glasgow, Scotland
August 23, 1948

THE complex permeabilities of several ferromagnetic compounds have been measured over the frequency range 500–28,000 Mc/sec. by the dual impedance waveguide method.[1] In each case, the magnetic dispersion and absorption have similar resonance characteristics to those observed in γ-ferric oxide,[1,2] with the real component of permeability falling below unity, and the magnetic loss tangent passing through a maximum, at frequencies of 3000–10,000 Mc/sec. The observations agree well with the theoretical formula for a damped resonance

$$(\mu-1)/(\mu_0-1)=\nu_n^2/(\nu_n^2-\nu^2+2i\nu\nu'), \qquad (1)$$

where μ_0, μ are the permeabilities at low frequencies and at frequency ν, respectively, ν_n is the natural resonant frequency, and ν' is the damping frequency.

This *natural ferromagnetic resonance* is attributable to Larmor spin resonance in the internal anisotropy and/or strain field H_n of the material.[3] Using the relation

$$h\nu_n=g\mu_B H_n, \qquad (2)$$

where μ_B is the Bohr magneton, and taking $g=2$ for an electron spin, the effective values of H_n can be derived from the experimental values of ν_n. Data for typical specimens of three of the compounds investigated are tabulated below.

The *induced ferromagnetic resonance* has also been investigated in these compounds. Kittel[3] has considered the theory of this resonance absorption, which occurs when a large magnetostatic field is applied perpendicular to the microwave field in the ferromagnetic, and he has shown that the simple resonance condition

$$h\nu_i=g\mu_B H_i \qquad (3)$$

is valid only for spherical specimens, the relation being modified in other cases by the shape demagnetization coefficients.

Spherical samples, 0.125″ diameter, moulded from mixtures of the powdered compounds with paraffin wax, were located centrally in an H_{01} wave-guide section, $\lambda_{g/2}$ in front of a terminating short. The frequency of operation ν_i was 9721 Mc/sec. A perpendicular magnetostatic field was applied parallel to the narrow side of the guide, and the Q of the wave-guide section was determined, by standing wave measurements, as a function of the applied field. The field H_p at which maximum absorption occurred is given in the table. H_p was found to be independent of the mixture concentration, so that the results may be taken as valid for the solid.

If H_p is substituted for H_i in (3), anomalous values of greater than 2.0 are obtained, similar to those found by other observers on supermalloy[4] and Zn-Mn ferrite,[5] who offered no explanation of the cause of the anomaly. In the table the theoretical values for a free spin are included for comparison, and it will be noted that there is a definite correlation between the magnitude of the internal field H_n, and the deviation of H_p from the free spin value.

Material	ν_n(Mc/sec.)	H_n(Oe)	H_p(Oe)	H_i	g
Ni-Zn ferrite	6250	2240	2630	3456	2.01
Fe_3O_4	5200	1850	2940	3474	2.00
γ-Fe_2O_3	3850	1370	3170	3454	2.01
Free spin (Theoretical)	0	0	3470	3470	2.00

It is evident, therefore, that the anomalous g values arise from neglecting the effect of H_n. A theoretical relation has been derived for H_i:

$$H_i=(H_p^2+H_i^2)^{\frac{1}{2}}, \qquad (4)$$

which is in close agreement with the experimental data. The values of H_i and g derived from (4) and (3) are tabulated.

It is likely that the anomalous g values reported for supermalloy and Zn-Mn ferrite[4,5] are due to internal fields. Although supermalloy is stated to have a low natural anisotropy, the preparation of the thin-sheet specimen used by Yager and Bozorth may have introduced an artificial strain anistropy.

A fuller account of this work will be published later.

[1] J. B. Birks, Proc. Phys. Soc. **60**, 282 (1948).
[2] J. B. Birks, Nature **159**, 775; **160**, 535 (1947).
[3] C. Kittel, Phys. Rev. **73**, 155 (1948).
[4] W. A. Yager and R. M. Bozorth, Phys. Rev. **72**, 80 (1947).
[5] W. H. Hewitt, Jr., Phys. Rev. **73**, 1118 (1948).

The Radioactive Decay of K^{40}*

L. B. Borst and J. J. Floyd
Brookhaven National Laboratory, Upton, New York
September 10, 1948

FOR some time we have been interested in the radioactive decay of K^{40} and its geochemical significance. This note reports preliminary observations made on the β-ray from a sample of potassium enriched 14-fold in K^{40}, obtained from the Stable Isotopes Division of the U. S. Atomic Energy Commission,[1] and, in addition, a test for argon extractable from Permian sylvite obtained from the Department of Mineralogy, Harvard University.

Current interest in this problem is high because of the difficulty in establishing the partial disintegration constant for electron capture λ_e, because of the uncertainty in the partial disintegration constant for β-emission λ_β, and because of the uncertainty in the energy changes involved in electron capture and the β-processes and their relation to γ-emission.

Gleditsch and Gráf[2] and Birch[3] have pointed out that too low a half-life for decay will be difficult to accept in view of the existence of rocks of ages up to 2×10^9 yr.,[2b,4] which could not crystallize if the K^{40} heat output exceeds some roughly known upper limit. In particular the low value recently reported by Bleuler and Gabriel[5] for the total half-life of K^{40}, $T_{\frac{1}{2}}=(2.4\pm0.5)\times10^8$ yr., has been the subject of discussion[2,3] and of detailed criticism by Ahrens and Evans.[6] These last authors report a revised half-life of $(4.5\pm0.5)\times10^8$ yr. based on a reinterpretation of older counting data and an interpretation of the trends in the calcium to potassium ratio of old and young lepidolite samples.

The results reported below lead to a still higher value for the half-life for decay of K^{40} of $4\text{–}12\times10^8$ yr.

1. *Specific beta-activity.* A sample of KCl weighing 18.9 mg, and containing 0.15 ± 0.02 percent K^{40}, was studied in thin layer (2.5 mg/cm²) mounted on thin aluminum (7 mg/cm²), using a mica window counter and aluminum absorbers[7] (Fig. 1). The data plotted are individual counting rates after subtracting the counter background. The broken line indicates the γ-ray contribution evaluated from a sample of normal potassium metal. Using a geometry of 21 ± 1 percent, calibrated by UX_2 and RaE-RaF counting, the measured activity at zero total absorber was found to be 33 ± 1 counts/min., with back-scattering negligible. 19.4-mg normal KCl, measured under similar circumstances, showed an activity of 3.0 ± 0.6 counts/min., entirely consistent with the value for the enriched sample.

From the observed activity of the enriched sample the partial disintegration constant for β-emission is

$$\lambda_\beta=(3.9\pm0.4)\times10^{-10}\ \text{yr.}^{-1};$$

this value is slightly smaller than that of Mülhoff,[8] smaller than that derived in a complicated manner by Ahrens and Evans,[6] and also much smaller than that of Bleuler and Gabriel.[5] The difference in the last case may well be due to back-scattering.[6]

2. *Beta-energy.* Using standard techniques[7,9] the Al absorption curve of the β-rays from the enriched sample was compared with the β-rays UX_2 and RaE. Comparison with the latter by the Feather method up to 60 percent of the range led to an extrapolated range of 900 mg/cm². The Feather analysis is shown in the insert in Fig. 1. This range corresponds to a maximum β-energy of 1.9 ± 0.2 Mev, slightly higher than the new value of 1.70 ± 0.15 Mev reported by Franchetti and Giovanozzi,[10] and substantially higher than older values[2,6,11,12] of 1.3–1.4 Mev.

Within the limits of experimental accuracy, the absorption curve of K^{40} is of identical shape to that of RaE. In contrast it is of markedly different shape from that of UX_2, having many more low energy electrons. The K^{40} to Ca^{40} transition involves a spin change of four and is usually assumed to be three or fourfold forbidden.[13] Since high resolution β-ray spectra will not be available until much more highly enriched K^{40} samples are available, the present comparison between the RaE spectrum, usually considered singly or doubly forbidden,[14] and K^{40} provides the best key to the shape of highly forbidden spectra.

3. *Assignment of the gamma-transition.* Ahrens and Evans[6] have determined that the γ-ray energy output from normal potassium is 4.9 ± 0.1 Mev/g-sec. Using the energy 1.55 ± 0.05 Mev,[2a] the disintegration constant for emission of a hard γ-ray is

$$\lambda_\gamma=(0.62\pm0.02)\times10^{-10}\ \text{yr.}^{-1}.$$

Previous authors[2,6,11] have considered that this gamma-ray is associated with the electron capture decay rather than with electron emission because of the supposed deficiency of mass difference between K^{40} and Ca^{40}. Our energy experiments reopen the question.

Dr. C. D. Coryell has pointed out to us that a consideration of the packing fractions in the series Si^{28}, S^{32}, A^{36}, and Ca^{40} suggests that Ca^{40} is more stable than A^{40} (*M*

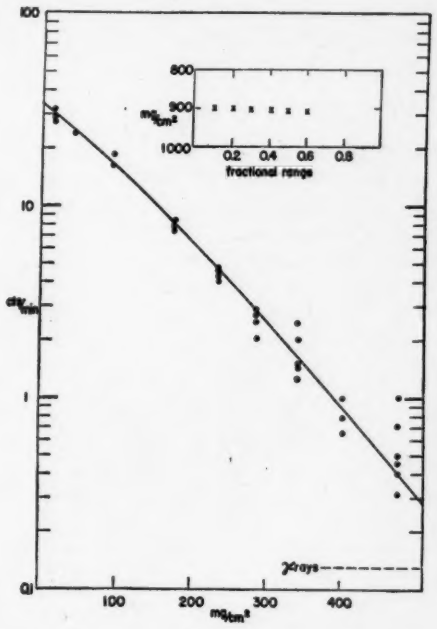

FIG. 1.

$=39.9755$),[15] making it more likely that γ-emission is associated with the emission of a very soft β-ray than with electron capture. This is also suggested by the twenty-shell argument given by Mayer.[16] The soft β-ray is probably not counted in the experiments in Part 1, nor in the coincidence studies of Meyer, Schwachheim, and deSouza Santos.[17] If this is true, λ_γ must be added to the experimental λ_β recorded in Part 1, whereas if the γ-emission is associated with a form of electron capture, λ_γ is included in λ_e calibrated by x-ray emission[5] or by argon production.[18]

4. *The yield of* A^{40}. Qualitative arguments and semi-quantitative calibrations[5, 6] have shown that the partial disintegration constant for electron capture is of the same order of magnitude as that for electron emission, and that positron emission is less than 1 percent of electron emission.[5] Bleuler and Gabriel report $\lambda_e:\lambda_\beta=1.9\pm0.4$, and Ahrens and Evans report[7] 1.4 ± 0.2. Our modification of the value of λ_β would tend to support a higher ratio than the Ahrens and Evans analysis.

The argon content of a sample of Permian sylvite (KCl) of estimated age 2×10^8 yr. was determined by collection of the total permanent gas obtained on dissolving in air-free water. The total gas evolved was 0.0046 cm^3/g of K at S.T.P. No attempt was made to assay the argon content of the gas sample. If it be assumed that no A^{40} was lost from the sylvite, and that no other permanent gases were occluded in the mineral or introduced in the manipulations, the partial disintegration constant for electron capture would be

$$\lambda_e \simeq 2.8\times10^{-10}\ \text{yr.}^{-1},$$

if $\lambda_\beta+\lambda_\gamma=4.5\times10^{-10}$ is used for total β-emission. Essentially the same result is obtained if $\lambda_\beta=3.9\times10^{-10}$ is used, associating γ-emission with electron capture.

Contaminates in the extracted gases would make this value high whereas, more important, loss of A^{40} from the mineral would make this value low. Indeed, Suess[18] has reported much lower limits on the quantity of A^{40} in sylvine and carnallite, corresponding to $\lambda_e=3\times10^{-11}$ yr.$^{-1}$. It seems reasonable to suppose that λ_e lies between 2 and 12×10^{-10} yr.$^{-1}$ (between two-thirds and three times our observed value), corresponding to a range of $\lambda_e:\lambda_\beta$ from 0.5 to 3.

5. *Gross decay.* The summation of the decay constants λ_β, λ_γ, and λ_e gives the range $(5.9\text{–}16.5)\times10^{-10}$ yr.$^{-1}$ for the total disintegration constant, corresponding to a range in half-life $(4\text{–}12)\times10^9$ yr.; we have a subjective preference for a half-life of 6×10^9 yr. based on $\lambda_e=7\times10^{-10}$ yr.$^{-1}$ and $(\lambda_\beta+\lambda_\gamma)=4.5\times10^{-10}$ yr^{-1}. The estimated isotopic abundance of K^{40} at the time of nucleogenesis ($\sim3\times10^9$ B.C.) is, therefore, about 0.5 percent. The estimated current heat output of natural potassium from λ_β and an average β-energy of 0.6 Mev and the known γ-energy output[6] is now considered to be 20 microcal./yr. per gram of potassium, and the value at the time of petrogenesis ($\sim2.4\times10^9$ B.C.) was roughly sixteen times as great—300 microcal./yr. per gram of potassium.

* Research work done at Brookhaven National Laboratory under the auspices of the Atomic Energy Commission.

[1] The enriched K^{40} was produced by the Electromagnetic Separation Division, Carbide and Carbon Chemicals Company, Oak Ridge, Tennessee.

[2] (a) E. Gleditsch and T. Gráf, Phys. Rev. **72**, 640 (1947); (b) E. Gleditsch and T. Gráf, Phys. Rev. **72**, 641 (1947).
[3] F. Birch, Phys. Rev. **72**, 1128 (1947).
[4] C. Goodman and R. D. Evans, Bull. Geol. Soc. Am. **52**, 491 (1941).
[5] E. Bleuler and M. Gabriel, Helv. Phys. Acta **20**, 67 (1947).
[6] L. H. Ahrens and R. D. Evans, Phys. Rev. **74**, 279 (1948).
[7] C. D. Coryell, *"Use of Isotopes in Biology and Medicine"* (Univ. of Wisconsin Press, Madison, Wisconsin, 1948), Ch. VII, pp. 121, 128.
[8] W. Mühloff, Ann. d. Physik **7**, 205 (1930).
[9] L. E. Glendenin, Nucleonics **2**, 12 (1948).
[10] S. Franchetti and M. Giovanozzi, Rend. Acc. Linc. **1**, 1078 (1946); Phys. Rev. **74**, 102 (1948).
[11] O. Hirzel and H. Wäffler, Helv. Phys. Acta **19**, 216 (1946).
[12] B. Dzelepow, M. Kopjova, and E. Vorobjov, Comptes Rendus (U.S.S.R.) **52**, 121 (1946); Phys. Rev. **69**, 538 (1946).
[13] R. Marshak, Phys. Rev. **61**, 431 (1942).
[14] E. Greuling, Phys. Rev. **61**, 568 (1942).
[15] J. Mattauch, *Nuclear Physics Tables (1941)* (Interscience Publishers, Inc., New York, 1946).
[16] M. C. Mayer, Phys. Rev. **74**, 235 (1948).
[17] H. A. Meyer, G. Schwachheim, and M. D. deSouza Santos, Phys. Rev. **71**, 908 (1947).
[18] H. E. Suess, Phys. Rev. **73**, 1209 (1948).

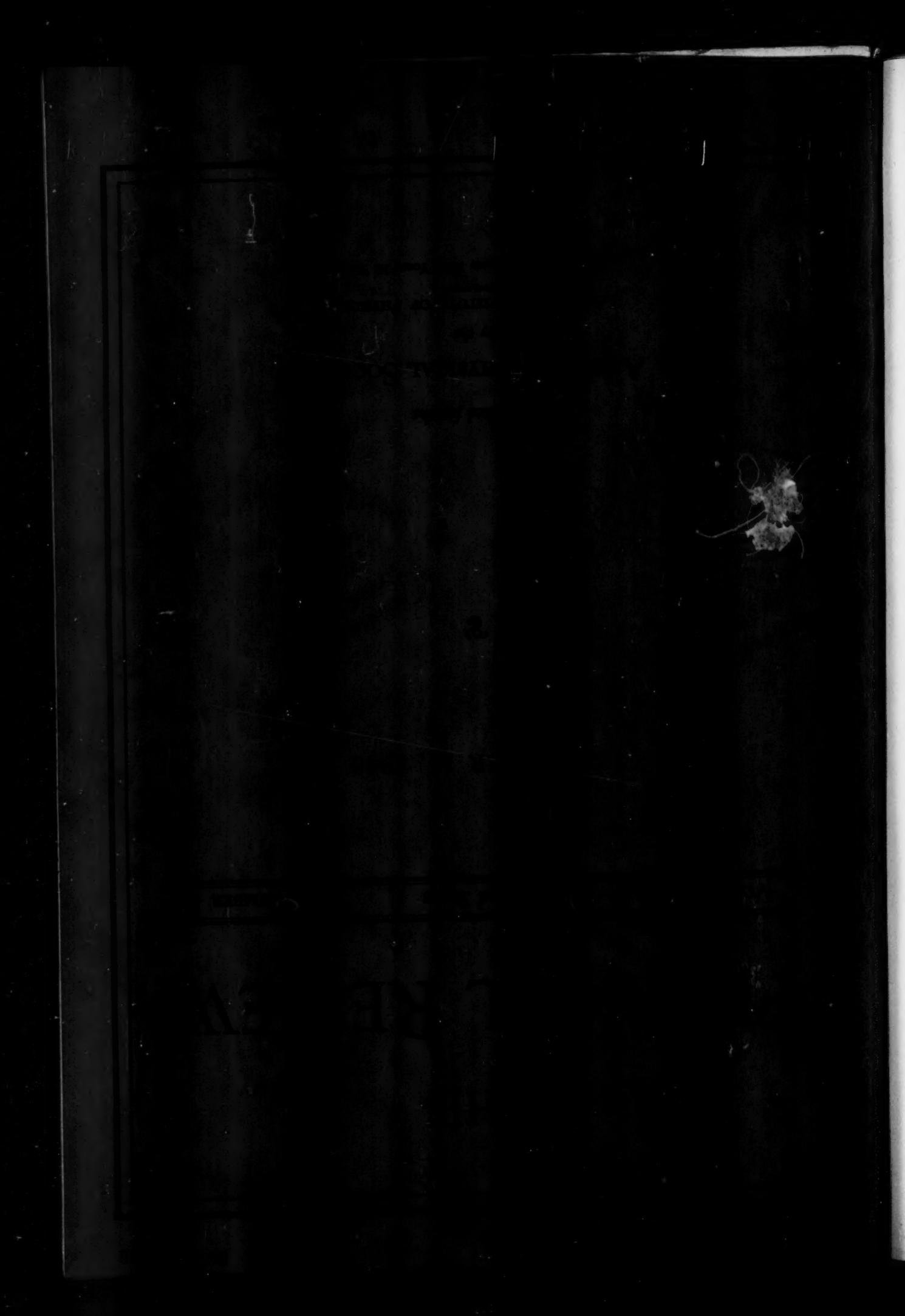

THE PHYSICAL REVIEW

A journal of experimental and theoretical physics established by E. L. Nichols in 1893

Published by the American Institute of Physics for the

AMERICAN PHYSICAL SOCIETY

Officers

President

J. R. OPPENHEIMER
Institute for Advanced Study
Princeton, New Jersey

Vice-President

F. W. LOOMIS
University of Illinois
Urbana, Illinois

Secretary

K. K. DARROW
Bell Telephone Laboratories
Office:
Columbia University
New York 27, New York

Treasurer

G. B. PEGRAM
Columbia University
New York 27, New York

Local Secretary for the Pacific Coast

J. KAPLAN
University of California at Los Angeles
Los Angeles, California

Editor

JOHN T. TATE
University of Minnesota
Minneapolis, Minnesota

BOARD OF EDITORS

Editor		*Assistant Editor*
JOHN T. TATE		J. W. BUCHTA

Associate Editors

E. J. KONOPINSKI	H. A. BETHE	S. A. GOUDSMIT
H. H. NIELSEN	L. A. RIDENOUR	E. M. PURCELL
E. C. FULLARD	W. H. ZACHARIASEN	V. F. WEISSKOPF

Manuscripts for publication should be submitted to John T. Tate, University of Minnesota, Minneapolis, Minnesota.

Proof and all correspondence concerning papers in the process of publication should be addressed to the Publication Manager, American Institute of Physics, 57 East 55 Street, New York 22, New York.

Subscription Price

United States and Canada.....$15.00
Elsewhere.....$16.50

Back Numbers

Complete set: Series 2,[1] Vol. 1, 1913–Vol. 72, 1947—$630.00
Yearly rate: $20.00
Single copies: $2.00 each, prior to July, 1929;
$1.00 each, July, 1929–December, 1941;
$2.00 each, January, 1942–December, 1946.
Current issues: $1.00 each.

Subscriptions and orders for back numbers should be addressed to Prince and Lemon Streets, Lancaster, Pennsylvania, or to the American Institute of Physics, 57 East 55 Street, New York 22, New York.

Changes of address in the case of members of the American Physical Society should be addressed to the Treasurer; in the case of other subscribers to the Business Manager, American Institute of Physics.

[1] For Series 1 inquire of Physics Department, Cornell University, Ithaca, New York.

The Physical Review is published semi-monthly at Prince and Lemon Streets, Lancaster, Pennsylvania.

Entered as second-class matter March 6, 1918, at the Post Office at Lancaster, Pennsylvania, under the Act of March 3, 1879.

Acceptance for mailing at special rate of postage provided for in paragraph 4, section 538, P. L. & R., authorized January 23, 1925.

THE AMERICAN INSTITUTE OF PHYSICS

INCORPORATED

57 East 55 Street New York 22, N.Y.

MEMBER SOCIETIES:

American Physical Society
KARL K. DARROW, *Secretary*, Columbia University, New York 27, New York.

Optical Society of America
ARTHUR C. HARDY, *Secretary*, Massachusetts Institute of Technology, Cambridge 39, Massachusetts.

Acoustical Society of America
WALLACE WATERFALL, *Secretary*, 57 East 55th Street, New York 22, New York.

Society of Rheology
EARL K. FISCHER, *Secretary*, Institute of Textile Technology, Charlottesville, Virginia.

American Association of Physics Teachers
C. J. OVERBECK, *Secretary*, Northwestern University, Evanston, Illinois.

AFFILIATED SOCIETIES:

American Society for X-Ray and Electron Diffraction
Electron Microscope Society of America
Physical Society of Pittsburgh
Physics Club of Chicago
Physics Club of Philadelphia
Cleveland Physics Society
Physics Club of the Lehigh Valley

ASSOCIATES:

Over seventy-five leading industrial enterprises and other institutions which contribute to the support of the Institute.

JOURNALS:

The Physical Review
Reviews of Modern Physics
JOHN T. TATE, *Editor*—J. W. DUFFIELD, *Assistant Editor*, University of Minnesota, Minneapolis, Minnesota.

Journal of the Optical Society of America
GEORGE R. HARRISON, *Editor*, Massachusetts Institute of Technology, Cambridge, Massachusetts.

The Journal of the Acoustical Society of America
FLOYD A. FIRESTONE, *Editor*, 3328 Tennyson Street, N.W., Washington, D. C.

American Journal of Physics
THOMAS H. OSGOOD, *Editor*, Michigan State College, East Lansing, Michigan.

The Review of Scientific Instruments
GAYLORD P. HARNWELL, *Editor*, Randal Morgan Laboratory of Physics, University of Pennsylvania, Philadelphia, Pennsylvania.

The Journal of Chemical Physics
JOSEPH E. MAYER, *Editor*, Kent Chemical Laboratory, University of Chicago, Chicago 37, Illinois.

Journal of Applied Physics
ELMER HUTCHISSON, *Editor*, Case Institute of Technology, Cleveland 6, Ohio.

Physics Today
DAVID A. KANTZER, *Editor*, American Institute of Physics, 57 East 55 Street, New York 22, New York.

OFFICERS

GEORGE R. HARRISON, *Chairman*
Massachusetts Institute of Technology
WALLACE WATERFALL, *Secretary*
The Celotex Corporation
GEORGE B. PEGRAM, *Treasurer*
Columbia University
JOHN T. TATE,
Adviser on Publications
University of Minnesota

GOVERNING BOARD

LUIS W. ALVAREZ
ROBERT B. BRODE
E. U. CONDON
A. J. DEMPSTER
W. F. FAIR, JR.
HARVEY FLETCHER
R. C. GIBBS
GEORGE R. HARRISON
W. V. HOUSTON
PAUL E. KLOPSTEG
F. W. LOOMIS
PHILIP M. MORSE
GEORGE B. PEGRAM
A. H. PFUND
JOHN T. TATE
WALLACE WATERFALL
M. W. WHITE
A. G. WORTHING

ADMINISTRATIVE STAFF

HARRY A. BARTON, *Director*
CLEVELAND NORCROSS,
Assistant Director
RUTH F. BEYAMS,
Publication Manager
THEODORE VOORHEES,
Business Manager

THE American Institute of Physics was founded in 1931 as a federation of leading societies in the field of Physics. It combines into one operating agency those functions on behalf of physics which can best be done by the Societies jointly. Its purpose is the advancement and diffusion of physics and its applications to human welfare. To this end it publishes for itself or the Societies the eight journals listed on this page; promotes unity and effectiveness of effort among all who are interested in physics; renders numerous direct services to physicists and to the public; and cooperates with government agencies, national associations, educational institutions, technical industries, and others in such manner as to realize the opportunities and fulfill the responsibilities of physics as an important and constructive human activity.

CONTENTS

THE PHYSICAL REVIEW [illegible] Series, Vol. 78, No. 8 OCTOBER 15, 1950

Theory of Oscillating Absorber [illegible] . . . . A. M. WOLSKY AND H. C. SCHWEIDLER 847

Measurement of Neutron Absorption Cross Sections with a Pile Oscillator . . J. I. HOOVER, W. H. JORDAN, C. D. MOAK, [illegible] H. POMERANCE, J. D. STRONG, AND E. O. WOLLAN 854

Radioactive Br Isotopes . . . . . L. L. WOOSTER, D. A. MCCOWAN, AND M. L. POOL 870

Argon 40 in Potassium Minerals . . . . . T. AHRENS AND ALFRED O. NIER 874

On the Momentum Distribution of [illegible] Electrons from Negative Mesons . H. PRIMAKOFF 878

Motion of an Electron in the Field [illegible] Magnetic Pole . . . . . HARISH-CHANDRA 883

Study of the Radiation from Cobalt [illegible], Rhenium (185), Gallium (191), and Osmium (193) . . . . . C. [illegible] MAINVILLE, M. V. SCHERB, AND W. B. KRIGHTON 888

Note on the Magnetic Moment of [illegible] . . . . . J. M. LUTTINGER 893

On the Life of Self-Quenching [illegible] . . . . . S. S. FRIEDLAND 895

Study of the Deterioration of [illegible] Geiger-Müller Counters . . . . . CARLE C. FARMER AND SANBORN C. BROWN 901

Factorization Method, Hydrogen [illegible] and Related Problems . . . . . T. E. HULL AND L. INFELD 906

Electrical Breakdown of a Gas [illegible] Coaxial Cylinders at Microwave Frequencies . . . . . MELVIN A. HERLIN AND SANBORN C. BROWN 912

Internal Friction and Precipitation [illegible] Solid Solution of N in Tantalum . . T'ING-SUI KÊ 916

Beta-Ray Spectra of Europium [illegible] . . . . . FRANKLIN B. SHORR 917

Large-Angle Scattering of [illegible] . . . . . HERBERT POLLARD AND DAVID E. ALBURGER 924

Structure of the ^2D Terms of [illegible] Spectrum of Lithium . . . . . W. MEISSNER, L. G. MUNDIE, AND P. H. STELSON 932

Relativistic Cut-Off for Classical [illegible] . . . . . R. P. FEYNMAN 939

Concentration of He^3 by Thermal [illegible] . . . . . [illegible]CHTER, L. T. ALDRICH, AND ALFRED O. NIER 943

Phenomenological Quantum-[illegible] . . . . . J. M. JAUCH AND K. M. WATSON 949

On the Theory of Diffraction [illegible] Plane Wave by an Infinite Plane Screen. I . . . . . HAROLD LEVINE AND JULIAN SCHWINGER 955

Letters to the Editor:

On the Multiple Production [illegible] . . . . . G. WATAGHIN 973

Non-Rectifying Germanium [illegible] . . . . . W. C. DUNLAP, JR. AND R. F. HERZOG 974

γ-Radiation from Be^9 . . . . . S. DEVONS AND M. G. N. HINE 975

Nitrous Oxide in the Earth's [illegible] . . . . . SHAW, G. E. M. JAUNCEY, AND T. W. WORMELL 976

Theory of Internal Conversion [illegible] . . . . . H. A. MEYER 978

Nuclear Relaxation in [illegible] . . . . . G. E. PAKE AND H. S. GUTOWSKY 979

Mass Deposition of Cosmic [illegible] Spectrum Neutrons . . . . . A. E. SHAW 980

Long-Lived Metastable [illegible] . . . . . M. GOLDHABER, AND G. SCHARFF-GOLDHABER 981

Analytic Behavior of [illegible] . . . . . R. J. EDEN 982

Neutron Deficient Isotopes [illegible] . . . . . J. R. CHURBUCK AND I. PERLMAN 983

Anomalous Values of Gas [illegible] Constants . . . . . HENRY F. IVEY 985

Anomalous Values of [illegible] Constants . . . . . E. P. WOHLFARTH 986

Erratum: The Magnetic [illegible] . . . . . J. G. DAIBER 986

Divergence Difficulty [illegible] . . . . . GENTARO ARAKI 986

On the Magnetic Moment [illegible] . . . . . GENTARO ARAKI 987

Erratum: A Cesium Beam [illegible] . . . . . P. KUSCH AND E. C. G. SUDARSHAN 987

Dielectric Behavior of [illegible] . . . . . T. MATSUMA, AND JOHN G. RICHARDSON 987

Theory of the Dielectric [illegible] . . . . . JOHN G. RICHARDSON AND BERND T. MATTHIAS 988

Natural and Induced [illegible] . . . . . J. B. BIRKS 989

Radioactivity Decay of [illegible] . . . . . L. B. BORST AND J. J. FLOYD 990

LANCASTER PRESS, INC., LANCASTER, PA.